The Design of Hybrid Cooling Tower Heat Pump Systems

By

Amanda Pertzborn

A dissertation submitted in partial fulfillment of

the requirements for the degree of

Doctor of Philosophy

(Mechanical Engineering)

At the

UNIVERSITY OF WISCONSIN-MADISON

2013

Date of final oral examination: 06/07/13

The dissertation is approved by the following members of the Final Oral Committee:

Sandy Klein, Professor, Mechanical Engineering
Franklin Miller, Assistant Professor, Mechanical Engineering
Greg Nellis, Associate Professor, Mechanical Engineering
Doug Reindl, Professor, Mechanical Engineering
Scott Sanders, Associate Professor, Mechanical Engineering

This page intentionally left blank

Abstract

The objective of this research is to address the cost and technical barriers that currently prevent widespread use of ground source heat pumps (GSHP) in the U.S. Unlike an air-source heat pump, in a GSHP system the ground provides a heat source/sink temperature that is relatively uniform throughout the year, which improves the efficiency of the overall heat pump system. There are several advantages associated with GSHP systems; these include reduced parasitic (pump and fan) power, longer life expectancy (due to nearly constant operating conditions), and increased COP and capacity. The disadvantages of GSHP systems include the relatively high first cost of the ground-coupled heat exchangers as well as issues related to thermal annealing of the ground in regions where the cooling and heating needs are not well-balanced over a year. The use of Hybrid GSHP systems (HyGSHPs) addresses both of these disadvantages.

This thesis documents a variety of studies related to the design and performance of a cooling tower HyGSHP. The ultimate deliverable from this work is a design tool, FHyGSHP, which can be used to optimize the design of a cooling tower HyGSHP. This tool can, perhaps more significantly, be used to explore various aspects of a HyGSHP and compare it to GSHP and conventional designs. This tool is freely available for use by researchers and designers alike.

Acknowledgements

Over the course of the last four years a significant number of people have supported me both in my work and in keeping my sanity. I first want to acknowledge Greg Nellis and Sandy Klein, who have been great advisors and instructors. Although frustrating at times, they questioned every aspect of my work and have been vital in ensuring its quality. They never failed to steer me back on track when I wandered into a tangent. My skills in conducting and writing about my research have improved dramatically under their supervision.

Lee DeBaillie, Keith Swartz, and Scott Hackel at the Energy Center of Wisconsin helped me transition into my research topic, introducing me to building simulation programs and technologies that have aided me throughout. Scott Hackel tirelessly shared his knowledge and experience with ground source heat pump technology; rather than starting from scratch, I was able to build on his work, for which I am grateful.

My lab mates in the SEL have also been a source of knowledge. I would especially like to thank John Dyreby for sharing his programming knowledge and skills. Some of the others who have been there to help distract or advise me throughout my time here are: Mike Cheadle, Harrison Skye, Amir Jahromi, Ty Neises, Will Seidel, Lukas Feierabend, Greg Marsicek, Russell Knudson, and many more that I won't list here, but they know who they are.

I was fortunate to find Graduate Women in Science early in my return to graduate school. This organization has been a source of support and friendship throughout my time here. I spent many hours with Tina Hill and Tess Killpack in "writing club," a time during which we encouraged each other to work on those projects we kept putting off.

Finally, there are the friends and family off campus who supported me in my decision to return to school. During the last four years my nieces have lost teeth, started school, and learned

to ride a bike, while my nephew has learned to walk and talk. These three have helped me maintain perspective about what is ultimately important. The oldest, disappointed that I couldn't answer a question, challenged me with "but you've been through all the grades." Now that I have truly been through all the grades I still don't have all the answers.

This work is dedicated to those I lost in the course of completing my PhD: Rosella Hesseling (grandmother), Fred Pertzborn (father), Margaret Pertzborn (grandmother), and Julius Pertzborn (grandfather). I was fortunate to have had the opportunity to spend time with them before they passed.

Table of Contents

Table of Figures

List of Tables

Nomenclature

Upper case

ASHRAE - American Society of Heating, Refrigerating, and Air-Conditioning Engineers

BC - Boundary Condition

BHE - Borehole Heat Exchanger

Blow - Water consumption in the CT due to blow down

C - Specific heat, heat capacity, or cost

CDD - Cooling Degree Days

CF - Correction Factor

CFD - Computational Fluid Dynamics

Cont - Continuous

COP - Coefficient of Performance

CS - Control Strategies

CSM - Cylindrical Source Model

CT - Cooling Tower

CT1 - Cooling Tower set point 1

CT2 - Cooling Tower set point 2

CT_down - Cooling Tower Hybrid with the cooling tower downstream of the ground heat exchanger

CT_down_f - Cooling Tower Hybrid with the cooling tower downstream of the ground heat exchanger and a furnace

CT_up - Cooling Tower Hybrid with the cooling tower upstream of the ground heat exchanger

CT_up_f - Cooling Tower Hybrid with the cooling tower upstream of the ground heat exchanger and a furnace

Drift - water consumption in the CT due to drift

DST - Duct STorage Model

DTPC - Pre-Cooling set point temperature

E - Energy

EES - Engineering Equation Solver

EFT - Entering Fluid Temperature

Evap - evaporative water consumption of the CT

EWT - Entering Water Temperature

DF - Density function

DT - Temperature change

FDM - Finite Difference Model

FEM - Finite Element Model

FHyGSHP - Fast Hybrid Ground Source Heat Pump

FLSM - Finite Line Source Model

Fo - Fourier number

GHX - Ground Heat Exchanger

GSHP - Ground Source Heat Pump

GSHP_f - Ground Source Heat Pump with a furnace

GUI - Graphical User Interface

HDD - Heating Degree Days

HyGSHP - Hybrid Ground Source Heat Pump

IC - Initial Condition

L - Length or Location

LCC - Life Cycle Cost

LSM - Line Source Model

M - Multiplier

MBE - Mean Bias Error

MFGSHP - Multi-Function Ground Source Heat Pump

MLAA - Multiple Load Aggregation Algorithm

N - Number of years or data points

NMS - Nelder Mead Simplex

P - Power consumption

P_1 - Used in economic calculations

P_2 - Used in economic calculations

PC - Peak Cooling or Pre-Cooling

PH - Peak Heating

PLF - Part Load Factor

PLR - Part Load Ratio

PWF - Present Worth Factor

Q - Heat transfer or capacity

R - thermal resistance

RMS - Root Mean Square

Size - Size of a component T - Temperature

SPF - Seasonal Performance Factor

TMY - Typical Meteorological Year

TPC - Pre-Cooling set point temperature

TRNSYS - Transient System Simulation

TRT - Thermal Response Test

V - Volumetric flow rate or volume

VHE - Vertical Heat Exchanger

$\dot{W}$ - Work/power

Lower case

b - intercept of curve fit

c - specific heat or flag to indicate commercial entity (economic factor)

d - discount rate

f - actual flow rate divided by the rated pump flow rate or a factor

h - enthalpy

i - inflation or interest rate

k - thermal conductivity

m - slope of curve fit

$\dot{m}$ - mass flow rate

occup - occupancy

p - probability

q - Heat transfer or capacity

r - restart

s - ratio of CT size to nominal size

$\bar{t}$ - effective tax rate

tol - tolerance

u - uncertainty

x - x axis data

y - constant in cooling tower calculation (value is 0.6) or y-axis data

subscripts

0 - initial condition

CT - Cooling Tower

GHX - Ground Heat Exchanger

HP - heat pump

PG - propylene glycol

Q - building load

T - temperature

a - annual time frame

abs - absorbed

air - air

b - borehole

base - base for comparison

best - current best design

c - cooling

cap - capacity

cool - related to the cooling load

d - daily time frame

data - measured data

day - value on a daily basis

db - dry bulb

design - design conditions

diff - differential

e - economic

f - fuel or working fluid

fan - cooling tower fan

first - first cost

fit - curve fit

freeze - freezing point

furnace - related to the furnace

g - ground

gas - natural gas

guess - guess value

h - heating

hour - value on a hourly basis

hyb - hybrid

i - index

in - inlet

input - data entered into the program

load - building load

m - motor or monthly time frame

maint - maintenance

month - value on a monthly basis

nom - nominal

on - the item is operating

out - outlet

p - power, pump, or penalty

peak - peak load

rated - manufacturer specification of the variable

rej - rejected

rel - relative

sat - saturated

sc - short circuit

set - set point

size - size of the component

sp - related to water spray in the CT

spray - related to water spray in the CT

st - stored

sump - relating to the sump pump in the CT

syn - synthetic

treatment - relating to water treatment in the CT

wb - wet bulb

wi - inlet

wo - outlet

Greek letters

α - thermal diffusivity

η - efficiency

λ - factor in cooling tower calculations

μ - mean or SUBPLEX optimization parameter

ρ - density

σ - standard deviation

τ - time period

ψ - Simplex reduction coefficient

ω - Step reduction coefficient

This page intentionally left blank

Chapter 1 Introduction

1.1 Overview

The objective of this research is to address the cost and technical barriers that currently prevent widespread use of ground source heat pumps (GSHP) in the U.S. Unlike an air-source heat pump, in a GSHP system the ground provides a heat source/sink temperature that is relatively uniform throughout the year, which improves the efficiency of the overall heat pump system. There are several advantages associated with GSHP systems as compared to conventional systems; these include reduced parasitic (pump and fan) power, longer life expectancy (due to nearly constant operating conditions), and increased COP and capacity. The disadvantages of GSHP systems include the relatively high first cost of the ground-coupled heat exchangers as well as issues related to thermal annealing of the ground in regions where the cooling and heating needs are not well-balanced over a year. The use of Hybrid GSHP systems (HyGSHPs) addresses both of these disadvantages.

1.2 Background

GSHPs provide an efficient method to both heat and cool a building. A length of pipe is buried in the ground, which then acts as a source of heat for the heat pump in heating mode or as a sink for heat in cooling mode. Although there are a number of possible designs for the ground heat exchanger (GHX), the design considered in this study consists of a series of boreholes drilled vertically into the ground to depths on the order of 100 m; this design is called a vertical heat exchanger (VHE) or borehole heat exchanger (BHE).

As heat is added to or removed from the GHX, the ground temperature changes. If the total annual heating load does not balance the total annual cooling load, then there is a net change in the ground temperature after each year of operation. The ground temperature will

increase if the building is cooling dominated and decrease if the building is heating dominated. Over many years of operation, the ground will become a poorer source or sink for energy in an unbalanced system and therefore the overall system efficiency will decrease. In some cases, the system will eventually be unable to meet the building loads. In order to avoid this situation, the ground loop can be made very large, but this comes with a greater first cost. According to Kavanaugh [1], this increase in first cost frequently leads to removing a GSHP system from consideration in the building design. Reducing system first cost is one of the primary reasons to consider a HyGSHP design over a GSHP system. The addition of a supplemental device offsets the ground load and eliminates the need to increase the size of the GHX. If the building is heating dominated and a ventilation system already exists or is being planned, it can be economical to add a relatively inexpensive boiler (or furnace) on the building side of the system to create a boiler (or furnace) hybrid. If the building is cooling dominated then a cooling tower can be added to create a cooling tower (CT) hybrid.

One of the primary challenges of a HyGSHP design is determining how large the supplemental component should be, where it should be placed, and how it should be sized. The standard design procedure for a GSHP system [2] includes a brief section on designing a HyGSHP, as does the *Commercial/Institutional Ground Source Heat Pumps Engineering Manual* [3]. Kavanaugh [1] revised these existing HyGSHP design concepts by studying a cooling dominated HyGSHP systems. The cooling tower/fluid cooler hybrid performance was evaluated and a method was developed to determine how best to integrate the heat rejecter into the GSHP design. Kavanaugh recommends using the peak block load at the design condition to size the cooling tower and the GSHP length; some of the other key components of the revised design procedure are:

- use the conventional method to determine the required length of a GSHP design,
- estimate the heat rejection to the ground, and
- size the supplemental cooling component to balance the annual net heat load to the ground.

An economic analysis of the HyGSHP system accounting for the costs related to the cooling tower or fluid cooler showed that the economic benefits are greatest in locations with significant cooling loads and the benefits are questionable in cooler climates. Kavanaugh also notes that although the first costs of the system decrease, there are additional maintenance requirements for the heat rejecter, adding operational costs that should be considered. Hackel et al. developed design guidelines for both cooling and heating dominated hybrid systems [4].

One frequently cited study of an operational HyGSHP system is reported by Phetteplace and Sullivan [5]. They analyzed the performance of a cooling tower HyGSHP over 22 months in Fort Polk, Louisiana. In this case, there was a significant load imbalance and there were space constraints which led the builders to use a hybrid system. The design procedure is very similar to that recommended by Kavanaugh:

- design the GSHP loop to meet the peak heating loads,
- calculate the heat rejection capacity of the ground, and
- subtract the peak cooling load from the prior result to obtain the cooling tower capacity.

The cooling tower was placed upstream of the GSHP and approximately 1/3 of the flow passed through the cooling tower at all times, regardless of the fan operation. The authors note that this has been an effective design for balancing the load on the ground, but careful design and monitoring are required in order to determine the optimal component sizes and layout.

Two additional real world case studies are presented by Singh and Foster [6]. In the first case, a GSHP system was initially intended for the building, but geological conditions at the site limited the depth of the boreholes so a cooling tower was added in order to supplement the smaller than required GSHP. In the second case, space was insufficient for a GSHP bore field, so a cooling tower hybrid system was implemented. In both cases, the hybrid system was more economical than a GSHP only system.

A more recent study of HyGSHP systems was completed by Hackel and Pertzborn [7]. The authors examined data from two CT hybrid installations and one boiler hybrid, using that data to validate models of the systems. These validated models were then used to evaluate how the designs and operation could be improved in order to minimize life cycle cost. In all three cases the hybrid designs were compared to a conventional system design and a standard GSHP design. The hybrid designs were more cost effective in all cases, though this economic advantage came at the expense of a slight increase in energy consumption over the GSHP design. Both the hybrid and GSHP designs led to a significant reduction in carbon emissions relative to the conventional design.

A pond can be used as the supplemental heat rejecter instead of a cooling tower [8]. The performance of non-hybrid and pond hybrid systems in hot/humid and moderate climates was evaluated using a simulated small office building. As the pond size increased (more heat rejection), the total system energy consumption decreased. However, based on an economic analysis, although a hybrid system is favorable, the most economical option is not necessarily the one with the largest pond. Similarly to Kavanaugh, the authors concluded that a hybrid system is most economical when there is significant imbalance in the cooling and heating loads.

A different approach to hybrid design was presented by Li et al. [9]. The authors developed a multi-function ground source heat pump (MFGSHP), in which hot water is supplied to a building by a GSHP in addition to meeting heating and cooling loads. This is an example of a hybrid GSHP system in which the supplemental component, a water heater, does not decrease the load on the GSHP, but rather improves the GSHP efficiency by reducing the load imbalance on the ground. Based on a 3D CFD simulation, the authors found that using the MFGSHP, the ground temperature increase after seven years was reduced by 3°C; the ground was actually 1°C cooler than the initial state.

1.3 Research Objectives

The literature review provides evidence that a HyGSHP can be an economical alternative to a GSHP system and they can be implemented in a variety of ways, but there are still many questions left unanswered. The current work focuses in three areas:

- the effect of year-to-year weather variability on the design of HyGSHP systems,
- the optimal control strategy for a CT HyGSHP, and
- the development of a design tool for these systems.

Additional work, such as the experimental validation of a model of the ground heat exchanger, was also completed in support of these efforts.

1.3.1 Year-to-Year Weather Variability

In general, heating and cooling loads are calculated for building designs based on a typical weather year which is calculated based on the weighting of individual actual weather years. This typical weather year can not represent the variation inherent in actual weather, which can lead to a system design which is under-sized for severe weather conditions. Designers typically use safety factors in order to account for unknown conditions, but as further emphasis is

placed on reducing building energy use, it is more important to size the heating and cooling plant more exactly. The study of the effect of weather variation on the plant design is presented in Chapter 5 and Reference [10].

1.3.2 CT HyGSHP Control Strategies

The control strategies for a CT HyGSHP are primarily focused on determining how to optimally control the CT in order to minimize costs (which typically also minimizes energy consumption). One strategy that has not received much analysis is pre-cooling. In the pre-cooling strategy, as defined in this research, the cooling tower operates at night (when electricity rates are lower), in order to cool the ground to improve the system efficiency the next day by reducing the temperature of the fluid entering the heat pump. The goal is to reduce energy usage and cost. The effectiveness of pre-cooling is not well established, so one of the objectives of this work is to determine if pre-cooling is beneficial. This work found that pre-cooling is not an optimal control strategy; rather it is best to operate the CT with continuously variable fan speed based on temperature set points. This work is documented in Chapter 6.

1.3.3 A Design Tool

In ASHRAE Technical Research Project 1384, a distributable modeling tool, HyGCHP (Hybrid Ground Coupled Heat Pump), was developed [11] in order to model: boiler–GSHP hybrids, cooling tower-GSHP hybrids, and GHSP only systems. HyGCHP can be used to optimize the size of the components in the specified system (boiler and GSHP, CT and GSHP, or GSHP only) and the set point temperatures used to control the components in order to minimize the life cycle cost (*LCC*) associated with owning and operating the system for twenty years. *LCC* accounts for the estimated first costs, operating costs, and maintenance costs associated with the system.

A new software program, FHyGSHP, inspired by HyGCHP, is developed in this project. The FHyGSHP program focuses on the design of a CT HyGSHP, but also has the option to design a conventional system (defined as a CT and furnace) or a standard ground source heat pump. FHyGSHP is an executable FORTRAN program which can be run from a graphical user interface (GUI) built in EES (Engineering Equation Solver [12]) or in batch mode. The calculation speed is substantially faster than HyGCHP and several key features have been added, including:

- continuously variable CT fan speed operation,
- the inclusion of pre-cooling as a control strategy,
- the ability to include year-to-year weather variability in the design,
- a built in sensitivity study,
- the ability to specify an upper limit on the total change in ground temperature, and
- the ability to specify a lower limit on energy savings relative to a conventional system.

These latter two features allow the user to change from an optimal design based solely on economic factors to an optimal design that also considers energy consumption and the impact on the ground used for the ground heat exchanger. Similar to HyGCHP, FHyGSHP can be used to optimize component sizes and control set points, and multiple system configurations (i.e. CT upstream or downstream of the GHX) can be modeled.

1.4 Organization of the Thesis

This thesis is organized into 9 chapters, including this Introduction. Chapters 2 through 4 provide much of the background information needed for the remaining chapters. Chapter 2 provides a detailed discussion of the components, such as heat pumps, cooling tower, ground

heat exchanger, etc., which are used in the software tools. Chapter 3 is a discussion of the experimental validation of the ground heat exchanger model used in the software. Chapter 4 is a detailed discussion of the optimization methods available in the software and the complexities involved in optimization.

Chapters 5 through 8 discuss the three major deliverables from this work. Chapter 5 is a detailed discussion of how real world weather variability matters in designing a ground source heat pump and how it is accounted for in FHyGSHP. Chapter 6 presents the evaluation of different control strategies for a cooling tower hybrid ground source heat pump, including a detailed examination of pre-cooling. Chapter 7 is an overview of the FHyGSHP program and Chapter 8 provides examples of the application of FHyGSHP to design questions related to HyGSHP systems. The final chapter, Chapter 9, is a discussion of future work related to these topics.

Chapter 2 Model Components

This section contains some of the details of the component models used in the simulations referenced throughout this report as well as some other information that will be useful to the reader. The available system configurations that can be modeled in FHyGSHP are also presented. The means of inputting data and selecting configurations in FHyGSHP are discussed in Chapter 7.

2.1 Configurations

The FHyGSHP program can be used to model a conventional, ground source heat pump, or cooling tower hybrid system for heating and cooling. The conventional system is comprised of a cooling tower with a heat pump (aka air conditioner) for meeting cooling loads and a furnace on the air side of the building for meeting heating loads. If there is a cooling load, the cooling tower must operate and if there is a heating load the furnace must operate. In the ground source heat pump system the only source/sink for heating and cooling is the ground, so whenever there is a building load there is flow through the ground heat exchanger.

The cooling tower hybrid system can take two different forms. First, it can contain the ground heat exchanger (GHX), which meets the entire heating load and a portion of the cooling load, and a cooling tower (CT) which meets the cooling load that is not met by the GHX. In this system if the CT is not in use but there is a cooling load, then the GHX must be used; the GHX is always used when there is a heating load. In the second form the system can contain the GHX and CT as before, but a furnace can also be added to the air side of the system. The purpose of adding the furnace is to help meet peak heating loads; rather than sizing the GHX to meet the occasional extreme heating event, a furnace can be added to meet a portion of the heating load.

This prevents the GHX from being over-sized for typical heating loads; this consideration is discussed further in Chapter 5.

In the CT hybrid system the CT can be placed either upstream (Figure 2-1) or downstream (Figure 2-2) of the ground heat exchanger; note that the furnace is not shown in either of these figures because it is on the air side of the building, but it could be included in either configuration. The figures show how the fluid streams are mixed or split depending on the control decisions. The GHX and CT can be bypassed if there is no load or if there is a control decision not to use one of the components. When there is a load, at least one component (GHX, furnace, or CT) must be in use.

There is one control set point for the ground heat exchanger, *GHX1*. If the temperature of the fluid entering the GHX (T_{GHX}) exceeds *GHX1*, then the ground heat exchanger is used in cooling. If the furnace is not included in the system, then the GHX is always used when there is a heating load. If there is a furnace present, then when the heating load exceeds a set point, Q_{set}, the furnace is used to supplement the GHX, but the GHX is still the primary source of heating. This control methodology is adequate for determining the capacity of the furnace, but it does not dictate the real world operation of the furnace. In reality, the heating load is not measured, so the furnace does not turn on based on the heating load but instead it operates when the fluid temperature at a certain point drops below a set point; this location could be, for example, the outlet from the GHX. In order to maintain the performance of the program it was decided that it should be left to the designer to determine the temperature set point for the furnace. Modification of the program to allow for temperature control of the furnace is one area that may be addressed in future versions of the program (see Chapter 9). If the GHX size is optimized to zero the furnace is always used when there is a heating load.

Depending on the control strategy selected, discussed in detail in Chapter 6, the CT may have one or two control set points. If the CT fan has one speed or operates over a continuous range of speeds, then the only set point is *CT1*; if the temperature of the fluid entering the CT (T_{CT}) is greater than *CT1*, then the CT is used in cooling. If the CT has two speeds then both *CT1* and *CT2* are relevant. If the difference between the temperature of the fluid entering the CT and the wet bulb temperature, T_{wb}, exceeds *CT2*, then the CT is used at low speed. If this set point is not exceeded but the *CT1* set point is, then the CT will operate at high speed. The following sections of this chapter describe how the various components in these systems are modeled.

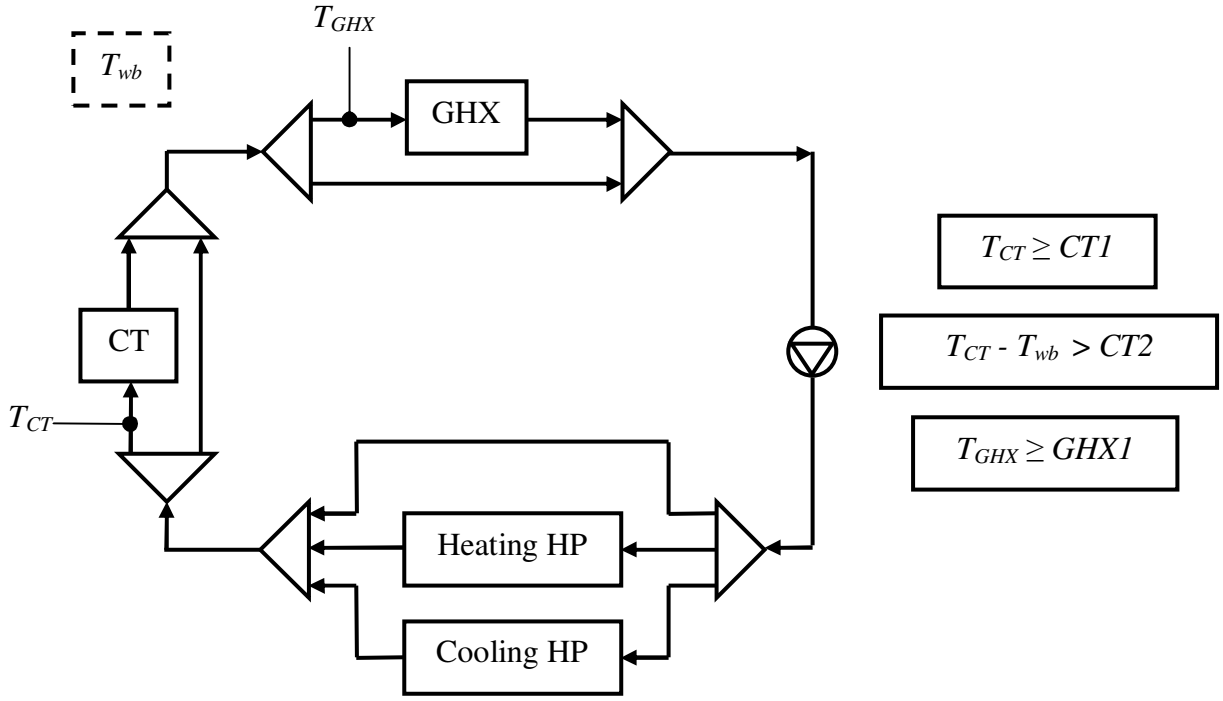

Figure 2-1 Upstream configuration.

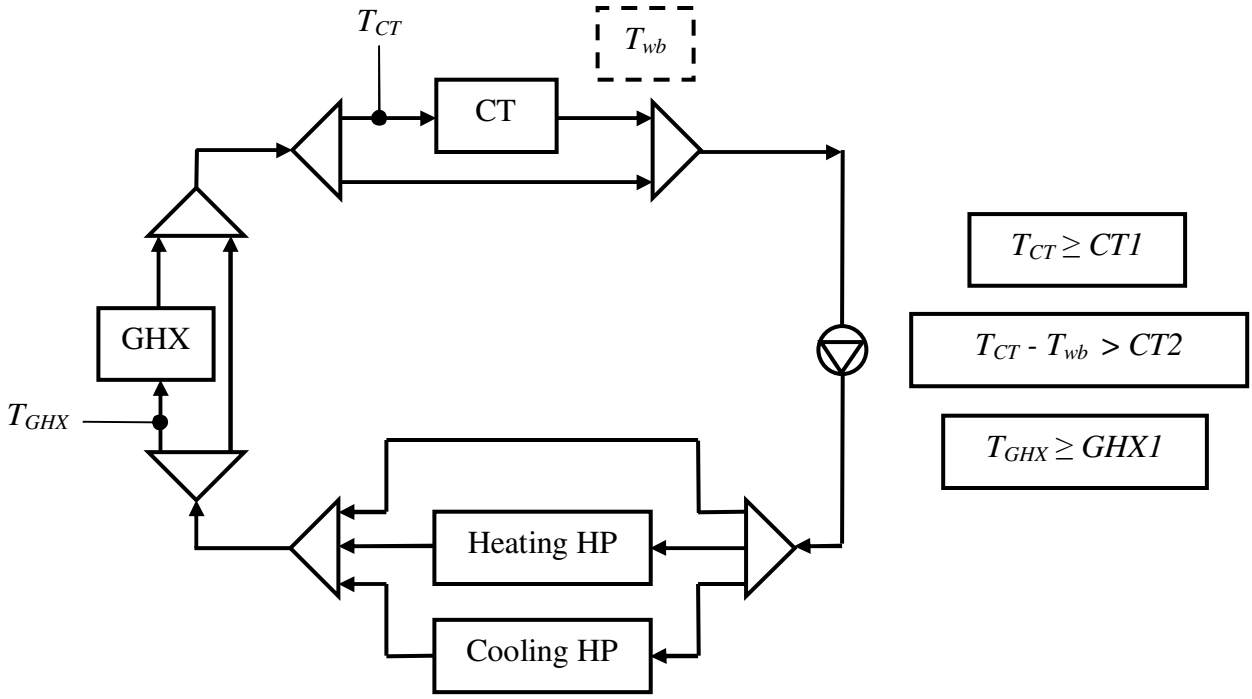

Figure 2-2 Downstream configuration.

2.2 Heat Pump Model

In a real building there can be dozens or even hundreds of individual heat pumps; modeling each of these heat pumps would be prohibitive for multi-year simulations with optimization. Instead, a gang of heat pumps model is used to represent the aggregate performance of the heat pumps as one device, which is why there is a Heating HP and Cooling HP in Figure 2-1 and Figure 2-2 rather than many individual heat pumps. The gang of heat pumps model is described and justified in the references [4,13]. In the model used in this work, the performance of the heat pump is calculated using correlations that are based on data provided by the manufacturer of the heat pump. For example, the plot of the *COP* of a heat pump operating in heating mode is shown in Figure 2-3 as a function of the temperature of the fluid entering the heat pump. This plot was generated from manufacturer data for a specific heat pump model [14] and a line is fit to the data. This curve fit is what is used in the calculation. For the

gang of heat pump model, the correlations were built using data obtained from multiple manufacturers [4], but the correlations can be modified by the user in FHyGSHP by changing the slope and intercept which are input to the curve fit. A similar relationship is required for the heat pump capacity.

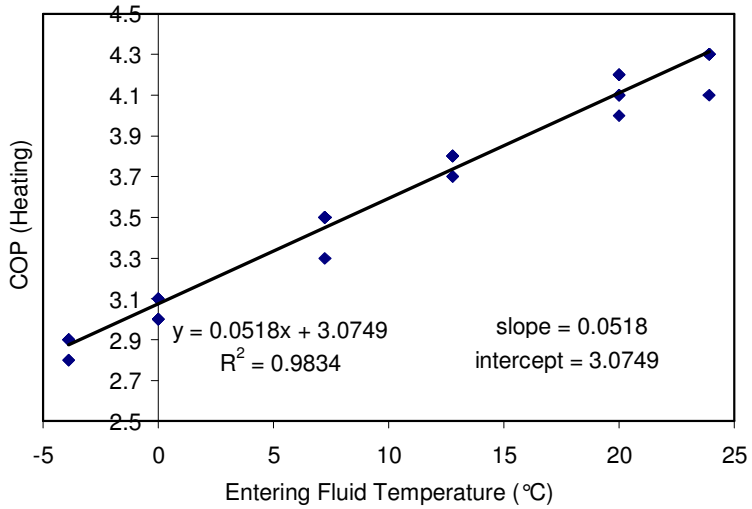

Figure 2-3 COP in heating versus the temperature of the fluid entering the heat pump for a specific heat pump model [14]**.**

The heat pump power consumption is based on two factors, the fan power and the compressor power. The compressor power is the ratio of the heat pump capacity at the inlet fluid temperature, *q*, to the heat pump efficiency defined by the coefficient of performance, *COP*, as shown in Eq.(2.1).

$$P_{hp} = \frac{q}{COP} \tag{2.1}$$

As explained above, the *COP* is a function of the fluid temperature. In FHyGSHP, the correlation between *COP* and inlet fluid temperature (developed for the gang of heat pumps model [4]) is used to correct a nominal *COP* for the actual fluid temperature. The correlation for cooling using the gang of heat pumps model is shown in Eq.(2.2) and the correlation for heating is shown in

Eq.(2.3). The nominal *COP*, COP_{nom}, and the slope and intercept of each of these equations can be entered in FHyGSHP; the default values for $COP_{c,nom}$ and $COP_{h,nom}$ are 4.57 and 3.42, respectively.

$$COP_c = COP_{c,nom}\left(-0.02521T_f + 1.6298\right) \tag{2.2}$$

$$COP_h = COP_{h,nom}\left(0.01437T_f + 1\right) \tag{2.3}$$

The correlation to correct the heat pump capacity for the inlet fluid temperature is given in Eq.(2.4) for cooling and Eq.(2.5) for heating; the units are kJ/hr. The nominal heat pump capacity, $q_{c,nom}$ and $q_{h,nom}$, is set to a value of one because as implemented in the gang of heat pumps model, this value cancels out of the calculation. The default values of the slope and intercept are shown here, but these values can be set by the user in FHyGSHP.

$$q_c = \left(-0.00856T_f + 1.2130\right)q_{c,nom} \tag{2.4}$$

$$q_h = \left(0.02251T_f + 1\right)q_{h,nom} \tag{2.5}$$

The compressor power is also corrected for the actual air outdoor temperature. This correction assumes that the supply air is ventilation air from outside; the correction for air temperature is minor, so this assumption does not significantly impact the results. The manufacturer provides correction factors for power consumption based on dry bulb temperature. FHyGSHP interpolates the value of the correction factor, CF_p, from an input file; a default file is included with the program, but the user could modify this file if desired. The final equations for

the compressor power in cooling and heating are Eq.(2.6) and Eq.(2.7), respectively, where CF_p is the correction factor for the dry bulb temperature.

$$P_{hp,c} = \frac{q_c}{COP_c\left(-0.02521T_f + 1.6298\right)} CF_P \tag{2.6}$$

$$P_{hp,h} = \frac{q_h}{COP_h\left(0.01437T_f + 1\right)} CF_P \tag{2.7}$$

The fan power consumption is calculated from Eq.(2.8), where the part load ratio (*PLR*) is defined in Eq.(2.9); if the heating load ($q_{load,h}$) during a time step exceeds the cooling load ($q_{load,c}$), the first equation for P_{fan} is used, otherwise the second equation is used. *Cont* is a flag that indicates that the fan is on if the building is occupied; *occup* is a flag that specifies if the building is occupied during a given time step; $q_{peak,c}$ and $q_{peak,h}$ are the peak cooling and heating loads, respectively.

$$P_{fan} = \begin{cases} 0.15\left(1-PLR\right) Cont\ Occup \dfrac{q_{peak,h}}{COP_h}, & q_{load,h} > q_{load,c} \\ 0.15\left(1-PLR\right) Cont\ Occup \dfrac{q_{peak,c}}{COP_c}, & otherwise \end{cases} \tag{2.8}$$

$$PLR = \frac{q_{load,c} + q_{load,h}}{\min\left(q_{peak,c}, q_{peak,h}\right)} \tag{2.9}$$

The total heat pump power consumption is the sum of P_{hp} and P_{fan}. Typical values of parameters used in the heat pump model are given in Table 2-1.

Table 2-1 Inputs to the heat pump models.

Description	Value
Continuous fan operation during occupied hours	1
Blower power	671.1 kJ/hr
Room temperature in the summer	24°C
Room temperature in the winter	21°C
Cooling COP	4.57
Heating COP	3.42
Controller power	36 kJ/hr
Slope for heating capacity curve	0.022507 kJ/hr-°C
Intercept for heating capacity curve	1 kJ/hr
Slope for cooling capacity curve	-0.00856 kJ/hr-°C
Intercept for cooling capacity curve	1.213 kJ/hr
Slope for heating COP curve	0.014366 1/°C
Intercept for heating COP curve	1
Slope for cooling COP curve	-0.02521 1/°C
Intercept for cooling COP curve	1.6298
Fraction of outdoor air	0
Percent PG	0%
Relative humidity in the space	42%
Humidity ratio in the space	0.008 kg(vapor)/kg(dry air)

2.3 Cooling Tower Model

An existing TRNSYS [15] model of a closed circuit CT, Type 510 [16], is used to model the thermodynamic and heat transfer characteristics of the CT; this model is based on the model presented in Zweifel, et al. [17]. In a closed circuit CT, the working fluid passes through a set of tubes; water is sprayed into air from the environment which passes across the tubes. The fluid in the tubes is primarily cooled by water evaporating from the tube surface. The relevant temperature for this heat transfer process is the wet bulb temperature.

One of the major assumptions in the model is that the temperature of the working fluid as it leaves the CT, $T_{fluid,out}$, is equal to the saturated wet bulb air temperature; using this assumption, Zweifel et al. derived Eq. (2.10) for the saturated air enthalpy, h_{sat}. In this equation $h_{air,in}$ is the enthalpy of the air from the environment which is drawn into the CT, $\dot{Q}_{fluid}$ is the

heat transfer from the working fluid, $\dot{m}_{air}$ is the mass flow rate of the air through the CT, λ_{design} is given in Eq. (2.11), and *y* is a constant with a value of 0.6. The design values of the air mass flow rate, $\dot{m}_{air,design}$, fluid outlet temperature, $T_{fluid,out,design}$, and air inlet and outlet temperatures, $T_{air,in,design}$ and $T_{air,out,design}$, respectively, are obtained from manufacturer specifications.

$$h_{sat}\left(T_{fluid,out}\right) = h_{air,in}\left(T_{air,in}\right) + \frac{\dot{Q}_{fluid}}{\dot{m}_{air}\left\{1-\exp\left[-\lambda_{design}\left(\frac{\dot{m}_{air}}{\dot{m}_{air,design}}\right)^{y-1}\right]\right\}} \quad (2.10)$$

$$\lambda_{design} = \ln\left[\frac{h_{sat}\left(T_{fluid,out,design}\right) - h_{air,in}\left(T_{air,in,design}\right)}{h_{sat}\left(T_{fluid,out,design}\right) - h_{air,out}\left(T_{air,out,design}\right)}\right] \quad (2.11)$$

The energy balance in Eq. (2.12) is applied in order to find the outlet air enthalpy at design conditions, $h_{air}\left(T_{air,out,design}\right)$. Eq. (2.10) can be rewritten as Eq.(2.13) using Eq.(2.12).

$$\dot{Q}_{design} = \dot{m}_{fluid,design} c_p \left(T_{fluid,in,design} - T_{fluid,out,design}\right) = \ldots \\ \dot{m}_{air,design}\left[h_{air}\left(T_{air,out,design}\right) - h_{air}\left(T_{air,in,design}\right)\right] \quad (2.12)$$

$$h_{sat}\left(T_{fluid,out}\right) = h_{air,in}\left(T_{air,in}\right) + \frac{\dot{m}_{fluid} c_p \left(T_{fluid,in} - T_{fluid,out}\right)}{\dot{m}_{air}\left(1-\exp\left[-\lambda_{design}\left(\frac{\dot{m}_{air}}{\dot{m}_{air,design}}\right)^{-0.4}\right]\right)} \quad (2.13)$$

In practice, the saturation enthalpy of the air at the fluid outlet temperature is found in an iterative process. First, the outlet fluid temperature is guessed and the heat transfer is calculated as shown in Eq. (2.14).

$$\dot{Q}_{fluid,guess} = \dot{m}_{fluid} c_p \left(T_{fluid,in} - T_{fluid,out,guess}\right) \quad (2.14)$$

Next, the outlet air enthalpy is calculated as shown in Eq.(2.15).

$$h_{sat,guess} = h_{air,in}\left(T_{air,in}\right) + \frac{Q_{fluid,guess}}{\dot{m}_{air}\left(1-\exp\left[-\lambda_{design}\left(\frac{\dot{m}_{air}}{\dot{m}_{air,design}}\right)^{-0.4}\right]\right)} \quad (2.15)$$

The difference between the saturation enthalpy found from a psychrometric analysis of the air at the guess temperature, $h_{sat}\left(T_{fluid,out,guess}\right)$, and the saturation enthalpy calculated from the heat transfer in the CT, $h_{sat,guess}$, is shown in Eq.(2.16). If this difference is within the specified convergence tolerance, then the fluid outlet temperature is the guess temperature and the simulation can continue. If this difference is not within the convergence tolerance, then a new guess temperature is chosen and another iteration is performed.

$$\Delta h = h_{sat}\left(T_{fluid,out,guess}\right) - h_{sat,guess} \quad (2.16)$$

The next sections discuss the calculation of power and water consumption and the method for determining the CT fan speed in a given time step.

2.3.1 Cooling Tower Power and Water Consumption

The CT power consumption for a closed circuit CT is composed of the fan power and the power required by the spray pump. (The circulating pump power is combined into the total system circulating pump power.) This model is general and during optimization the CT size may vary, so the power is scaled with the size of the CT. The most relevant factors for scaling the power consumption are discussed here, but further details can be found in reference [4].

The parameters are scaled based on a nominal unit, the Baltimore Air Coil [18] Series V unit number VF1-009; this unit has a 2 hp fan, a 1/3 hp spray pump, and a nominal cooling capacity of 10 tons. The use of these parameters in scaling will be seen in the following discussion. Unless otherwise shown, it is assumed that these parameters are converted to the appropriate unit system.

$$\dot{W}_{fan,nom} = 2[hp]$$
$$\dot{W}_{nom} = 10[tons]$$
$$\dot{W}_{spray} = \frac{1}{3}[hp] \tag{2.17}$$
$$s = \frac{Size_{CT}}{\dot{W}_{nom}}$$

Using various Baltimore Air Coil Series V units, the fan power was plotted as a function of normalized CT size (normalized by $\dot{W}_{nom}$) resulting in the curve fit presented in Eq.(2.18), where s is the normalized size as defined in Eq. (2.17).

$$CT_{ratio} = \begin{cases} 0.0183\, s^2 + 1.4886\, s & s \le 18.64 \\ -0.014\, s^2 + 2.0907\, s & s > 18.64 \end{cases} \tag{2.18}$$

The rated fan power is then defined in Eq.(2.19), where M is a multiplier that can be used to further adjust the power consumption in order to fit another manufacturer's specifications.

$$P_{fan,rated} = M\ CT_{ratio}\ \dot{W}_{fan,nom} \tag{2.19}$$

Using fan laws, the fan power is then calculated as the rated power times the cube of the fan speed.

$$P_{fan,CT} = P_{fan,rated}\gamma^3 \tag{2.20}$$

The spray pump power is also estimated from a curve fit; the nominal spray pump power is scaled as shown in Eqs.(2.21) and (2.22). The parameter CT_{on} is a flag that has a value of one if the CT is on.

$$CT_{ratio,sp} = 0.9884\, s \tag{2.21}$$

$$P_{spray} = \dot{W}_{spray}\ CT_{ratio,sp}\ CT_{on} \tag{2.22}$$

The total CT power (excluding the circulating pump) is the sum of Eqs. (2.20) and (2.22).

As in the case of the power consumption, the nominal mass flow rates of the air and fluid are based on the Baltimore Air Coil Series V CT. The nominal mass flow rate of the air ($\dot{m}_{air,design}$ in the previous section) is given in Eq.(2.23), where the volumetric air flow rate is multiplied by the density of air, ρ_{air}. The mass flow rate of air is then scaled as shown in Eq.(2.24) to account for the actual size of the CT; the multiplier M_{air} can be used to scale the flow rate to fit other manufacturer specifications. Similarly, Eq. (2.25) shows the nominal mass flow rate of the fluid in the CT and Eq.(2.26) shows how this nominal mass flow rate is scaled to the actual size of the CT and other manufacturer's specifications [4].

$$\dot{m}_{air,nom} = \left(4970\,[cfm]\right)\rho_{air} \tag{2.23}$$

$$\dot{m}_{air} = M_{air}\left(1.0808s\right)\ \dot{m}_{air,nom} \tag{2.24}$$

$$\dot{m}_{fluid,nom} = \left(25\,[gpm]\right)\rho_{fluid} \tag{2.25}$$

$$\dot{m}_{fluid} = M_{fluid}\ \dot{m}_{fluid,nom}\ s \tag{2.26}$$

In the CT makeup water is required to replace evaporated water, water transported from the CT by air flows (drift), and water used in blow-down (replacing sump water to reduce the concentration of contaminants) [19]. The volume of water evaporated per time step is calculated in Eq. (2.28) assuming that 87% of the heat transfer is due to evaporation (based on research detailed in [19]); Q_{fluid} is the heat transfer from the CT, Δh_{water} is the change in the enthalpy of the water, and ρ_{water} is the density of water. The blow down water consumption is equal to the evaporative water consumption and the drift water consumption, given in Eq.(2.30), is 0.01% of the spray pump flow rate, given in Eq.(2.29), when the CT is operating [19]. Note that the spray pump flow rate is scaled based on the size of the CT.

$$m_{water} = \frac{Q_{fluid}}{\Delta h_{water}} \tag{2.27}$$

$$Evap = 0.87 \frac{Q_{fluid}}{\Delta h_{water} \rho_{water}} \tag{2.28}$$

$$V_{spray} = 35\,[gpm] \tag{2.29}$$

$$Drift = 0.0001 V_{spray}\ s\ CT_{on} \tag{2.30}$$

The total water consumption is given in Eq.(2.31).

$$m_{water,total} = Evap + Blow + Drift = \left[2\left(0.87 \frac{Q_{fluid}}{\Delta h_{water} \rho_{water}} \right) + 0.0001 V_{spray}\ s \right] CT_{on} \tag{2.31}$$

Key inputs to the CT model are listed in Table 2-2.

Table 2-2 Inputs to the cooling tower model.

Description	Value
Cooling tower fan power multiplier (M)	0.75
Cooling tower fan air flow multiplier (M_{air})	0.61
Cooling tower fluid flow multiplier (M_{fluid})	0.96
Design inlet fluid temperature ($T_{fluid,in,design}$)	39.25°C
Design outlet fluid temperature ($T_{fluid,out,design}$)	34.25°C
Design ambient air temperature ($T_{air,in,design}$)	35°C
Design wet bulb temperature	25°C
Power coefficients	0, 0, 0, 1

2.3.2 Cooling Tower Fan Speed

The HyGCHP (Hybrid Ground Coupled Heat Pump) program and the early versions of FHyGSHP had two primary control strategies for the CT in the CT hybrid ground source heat pump: set point temperature control and differential temperature control. These are two of the strategies frequently referenced in the literature and are discussed in more detail in Chapter 6. Set point control operates the CT as a single speed device; if the temperature of the fluid entering the

CT exceeds a set point temperature (*CT1*) then the CT will operate at the user defined fan speed (a value of 50% or 100% is typical). Differential temperature control operates the CT as a two speed device and is based in part on the temperature difference between the fluid and the wet bulb temperature. The higher fan speed (typically 100%) is used when the fluid temperature entering the CT exceeds a set point (*CT1*); the lower fan speed (typically 50%) is used when the fluid temperature exceeds the wet bulb temperature by a set point (*CT2*). CT power consumption is proportional to the cube of the CT fan speed and the square of the CT size, so the optimal CT hybrid design is typically one with a large CT that operates at a fan speed below 100%.

In order to more accurately capture the real world operation of a CT and capture the efficiency associated with operating at lower fan speeds, a continuous control scheme was added to the two existing schemes. In FHyGSHP there is the option to select single speed, two speed, or continuously variable speed operation. If single speed or two speed operation are selected, then the CT speed(s) is also specified by the user. The development of the continuous scheme is detailed here; the speed ranges from 10% to 100%.

In order to model a continuously changing fan speed, a relationship needs to be developed between the fan speed and a control parameter. The fan speed is proportional to the CT size and the cooling load. In an actual system, the total cooling load could be estimated from Eq.(2.32), where $\dot{m}$ is the flow rate of the working fluid through all of the heat pumps, c is the specific heat of the working fluid, T_{in} is the temperature at the inlet to all of the heat pumps and T_{out} is the temperature at the outlet. The portion of the cooling load met by the CT can also be estimated from this equation where $\dot{m}$ is the flow rate of the working fluid through the CT and T_{out} and T_{in} are the outlet and inlet temperatures to the CT, respectively.

$$Q_{cool} = \dot{m}\, c \left(T_{out} - T_{in} \right) \tag{2.32}$$

Simulations were completed in different climates in order to determine the optimal CT fan speed for a given CT size and cooling load. Figure 2-4 shows the optimal fan speed as a function of the ratio of CT size to cooling load in St. Louis; the results in other climates were very similar to these results.

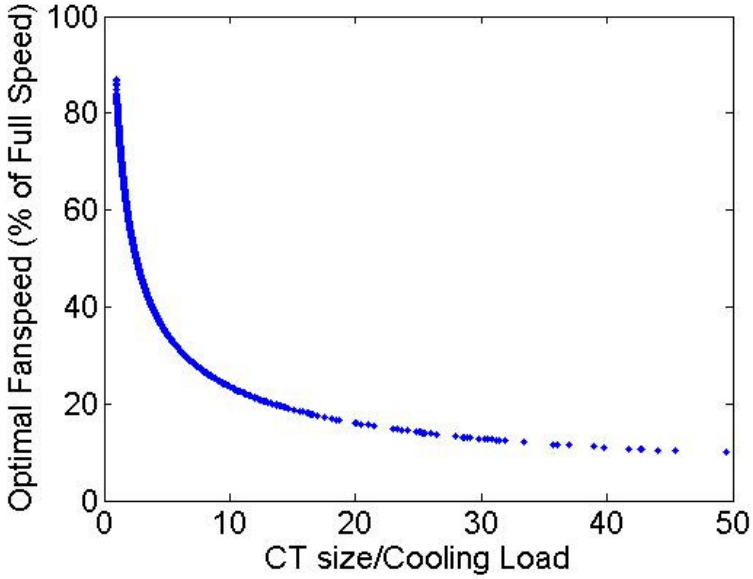

Figure 2-4 Optimal fan speed as a function of the ratio of cooling tower size to cooling load.

This relationship is best represented by the power law equation given in Eq.(2.33); CT_{size} is the size of the CT and *Load* is the building cooling load.

$$FanSpeed = 0.838\left(\frac{CT_{size}}{Load}\right)^{-0.552} \tag{2.33}$$

Although the inlet and outlet temperatures are typically measured in existing systems, the flow rate often is not; therefore an alternate relationship was developed which depends only on temperature measurements.

The most relevant temperature difference for the operation of the CT is between the temperature entering the CT, $T_{ct,in,}$ and the wet bulb temperature, T_{wb}. Simulations were run in

which the fan speed was calculated using the relationship defined in Eq.(2.33) and this fan speed was then related to the relevant system temperatures. Figure 2-5 shows the fan speed as a function of the difference between the fluid temperature entering the CT and the wet bulb temperature in St. Louis, Atlanta, and Phoenix. Although the general behavior is the same in each situation, there is significant scatter.

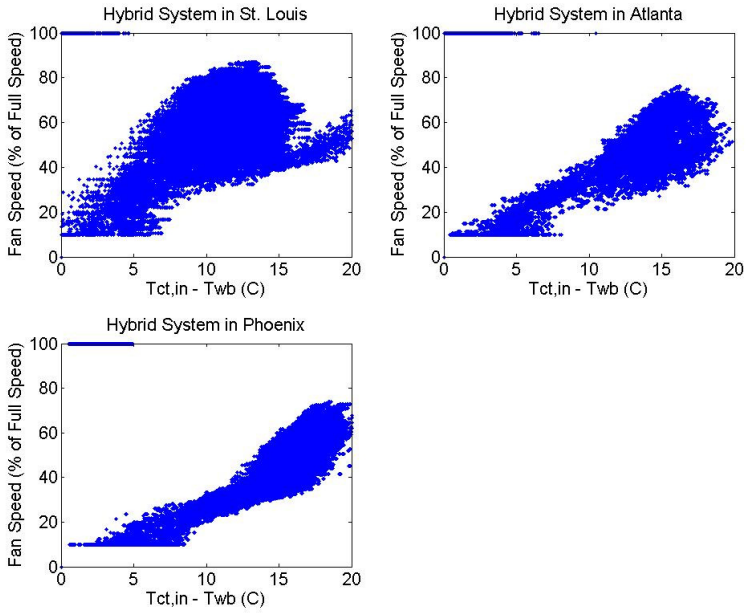

Figure 2-5 Relationship between cooling tower fan speed and the difference between the temperature entering the cooling tower ($T_{ct,in}$) and the wet bulb temperature (T_{wb}).

A simple linear relationship was developed using the data shown in Figure 2-5. This relationship does not fit any of the individual locations perfectly, but provides a reasonable approximation for all three sets of data, as shown in Figure 2-6.

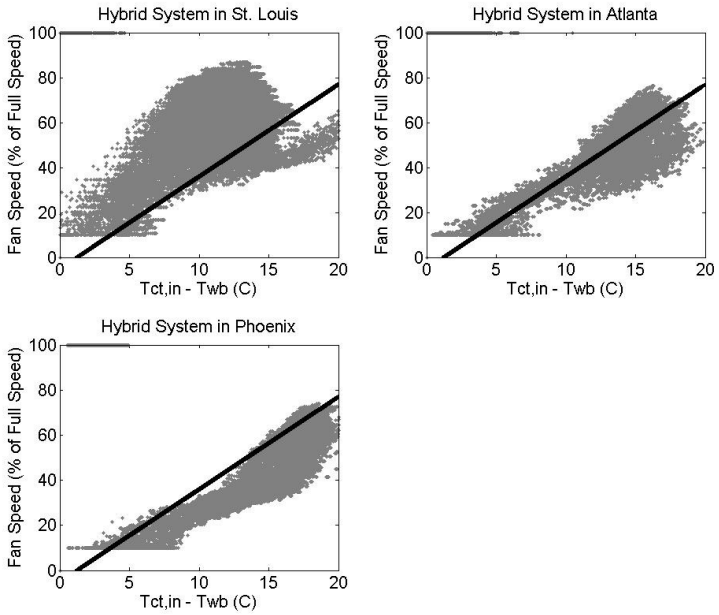

Figure 2-6 The relationship between CT fan speed and the difference in temperature between the temperature of the fluid entering the CT ($T_{ct,in}$) and the wet bulb temperature (T_{wb}).

This relationship is given in Eq.(2.34). If the difference between $T_{ct,in}$ and T_{wb} exceeds the control set point *CT1*, then the CT will be used. If the temperature difference exceeds the set point *CT2*, then the CT fan will operate at full speed (1 = 100%), otherwise the fan speed is calculated using the equation shown (this is the line shown in Figure 2-6). This fan speed is further limited to values between 0.1 (10%) and 1 (100%). This is the relationship included in FHyGSHP. System designs using this relationship for continuous fan speed operation are compared to those using single speed or two speed operation in Chapter 6. Note that this calculation does not account for drive losses.

$$FanSpeed = \begin{cases} 1 & T_{ct,in} - T_{wb} > CT2 \\ 0.041\left(T_{ct,in} - T_{wb}\right) - 0.05 & otherwise \end{cases} \tag{2.34}$$

2.4 Ground Heat Exchanger Model

This section provides a brief review of models of the ground heat exchanger with a focus on the model used in this work, the Duct Storage or DST model. This model was ultimately

selected because it has been widely used, was readily available in a form that could be easily incorporated into the FHyGSHP program, and is a good compromise between calculation speed and accuracy.

There are numerous models of GHX performance, only some of which are presented in this section. The interested reader is referred to Xu and Yang et al. [13,20] for an additional discussion of GHX models. In general, GHX models can be divided into two categories (with some overlap), numerical and analytical. In general, numerical solutions are more detailed and more accurate, but they are also more computationally expensive and require substantial time for the analysis. The analytical solutions are generally less computationally expensive and faster, but the accuracy can be lower because of assumptions made in the model to allow an analytical solution. The following paragraphs discuss some of the existing models of the GHX though this is by no means an exhaustive review.

Two often referenced analytical models are the line source model (LSM) and the related cylindrical source model (CSM). The LSM consists of an infinitely long line source or sink in an infinite medium of initial temperature T_0; the temperature can then be calculated at any radial location, assuming only radial heat transfer from the line and a constant heat transfer rate during the period of interest [21,22]. A superposition method can be applied to calculate the temperature over different time periods. According to the authors, this model does not account for the interaction between multiple pipes and is inaccurate for short time periods (less than a few days) and larger diameter pipes.

Zeng et al. developed a finite line source model (FLSM) as a more realistic representation of boreholes [23]. They used this model to examine the effect of load imbalance on the long-term performance of the GHX, stating that maintaining performance over system life is best achieved

by keeping the steady state borehole wall temperature within a certain range. Zeng et al. further developed a quasi 3D analytical model using FLSM [24]. This model incorporated detailed geometric and physical data, including pipe sizes and flow rates and was used to calculate the borehole thermal resistance. Bandos et al. created a FLSM which includes the thermal gradient along the borehole and variation in the ground surface temperature [25].

In the cylindrical source model (CSM) a single, infinitely long, isolated borehole is surrounded by an infinite medium [22,26]. The CSM is similar in concept to the LSM, but the function for calculating the temperature at a point in the medium is more complex and is more accurate for a wider range of time scales and geometries. Deerman and Kavanaugh [27] performed a detailed study of the CSM in order to evaluate its usefulness as an alternative to more computationally expensive numerical methods. The authors modified the CSM to include: a correction to account for the presence of two pipes (i.e. a u-tube) in the bore rather than one, convective resistance between the working fluid and the pipe wall, a correction factor to account for the non-uniformity of the heat flux on the surface of the pipe, and a correction for short-circuiting between the u-tube pipes within the bore. The authors state that the CSM model can provide sufficiently accurate results, but the accuracy is highly dependent on knowledge of the thermal properties of the medium.

Dobson et al. [28] also modified the CSM. They discretized the pipe length in order to more closely approximate the assumption of constant surface heat flux, directly modeled the thermal interaction between the two pipes in the u-tube using superposition, and used a sufficiently small time step to capture transient behaviors. The authors compared simulation results using this model to experimental measurements, finding that the prediction of entering

water temperature to the heat pump was incorrect on average by 0.3°C. They also note that knowledge of soil properties is important for obtaining accurate results.

A more complex model of the temperature distribution around a borehole was developed by Eskilson [29]. This is a two dimensional transient finite-difference model of a single borehole which can account for the interaction between multiple boreholes. A step heat pulse is applied to the single borehole and the response of the ground to this pulse is calculated. The response to any magnitude heat pulse can be calculated, and the responses can be superposed over time to calculate a long term response. These non-dimensional response factors are referred to as g-functions and can be calculated for a variety of multi-bore configurations. Yavuzturk and Spitler extended the method to time periods of less than an hour [30] by developing g-functions that are valid for shorter time periods. Additional work on the short time step extension of Eskilson's model was performed by Young [31].

LSM and CSM neglect the thermal mass of the fluid in the building and GSHP loops. Bandyopadhyay et al. developed an analytical solution that includes the temperature response of the fluid by modeling the fluid as a "virtual solid" (Gopal Bandyopadhyay et al. 2008). The authors conclude that the GSHP design length will be shorter than that obtained from LSM or CSM solutions. A semi-analytical tool has also been developed to incorporate the u-tube geometry within the grouted borehole into the model [33].

Load aggregation has been applied to several different model types as a means to decrease computational requirements and, in some cases, account for the interaction between multiple boreholes ([30,34]). Load aggregation is based on the idea that in calculating the performance of GSHPs at a moment in time, the short term thermal history is more important than the long term thermal history. The simulation is divided into time periods, where a single

representative load is applied throughout the time period. The time periods may be hourly, daily, weekly, monthly, or yearly, depending on the specific model. The GSHP performance is calculated using the aggregated loads. Based on comparisons of the multiple load aggregation algorithm (MLAA) to the duct storage model (DST, see below), hourly simulations of the GSHP are sufficiently accurate using MLAA [34].

Many finite difference models (FDM) have also been applied to the analysis of GSHPs. Mei and Fischer detail the early study of a GSHP system and the development and validation of a finite difference model for the analysis [35]. This model was modified for a two pipe u-tube system and experimentally validated, but the authors noted that the model was overly simple [36]. Bi et al. developed a FDM to analyze a vertical double spiral coil GSHP configuration [37]. Rottmayer developed an explicit Euler FDM in order to incorporate more complexity than can be accounted for in the LSM [38]. One limitation of this model is that it used a non-circular geometry for the borehole due to the constraints of the finite difference geometry. The author found that the model could produce results within 8% of experimental values, but he notes that it would be beneficial to be able to model more complex geometries.

Several finite element methods (FEM) have been developed to allow more detailed analyses of the physics in a GSHP. A model developed by Muraya is transient and accounts for thermal interference between the u-tube legs [39,40]. Kohl et al. developed the finite element program FRACTure for studying fluid flow and heat transfer in geological formations [41]. This program allows calculations with 1D, 2D, and/or 3D elements, with the 1D elements typically applied to the borehole. The FRACTure program has been applied to the analysis of an existing single deep borehole system and a more traditional multi-bore field [42,43]. A similar multi-dimensional element technique is used by Al-Khoury et al. [44] to create a more computationally

efficient FEM. Cui et al. used an FEM model to evaluate transient GSHP behavior on short time scales [45]. The authors compared the FEM results to the results of a FLSM model in order to evaluate the accuracy of FLSM on short time scales. They found that the initial relative error is large, but after a few hours of simulation the error decreases to 4%, so FLSM may be appropriate for long time scale design.

The model used in the present work is the Duct Storage Model (DST), developed by Hellström [46]. The DST is a numerical model which calculates the ground temperature using the superposition of three separate heat transfer calculations:

- the steady flux solution accounts for the slow redistribution of heat through the sub-regions near the borehole,
- the global solution accounts for heat flow over long time scales (months or years),
- and the local solution accounts for heat flow on short time scales near the bore hole.

The local and global solutions require implementation of a finite difference model while the steady flux solution is an analytical model. In the local solution, a single borehole is modeled and assumed to be representative of all boreholes. A 1D finite difference solution is applied in the radial dimension near the borehole. The vertical dimension is divided into a number of sub-regions and the 1D solution is applied to each sub-region. The outer radius boundary condition is a zero flux boundary and the inner radius boundary condition is a constant temperature boundary; the temperature of the boundary is based on the temperature and flow rate of the fluid passing through the tube as well as the convective and conductive resistance to heat flow in the pipe and the borehole fill material. The steady-flux solution accounts for heat pulses that vary slowly in time and this solution controls the redistribution of energy through the storage volume and links to the local and global solutions. The combination of these three calculations accounts

for the heat transfer between the fluid in the pipe and the ground near the pipe as well as the interaction between neighboring boreholes.

Prior validation and calibration performed on the DST model have demonstrated its effectiveness [47–49]. In these studies the soil thermal conductivity, specific heat, density, and the deep earth temperature were calibrated in order to achieve the best match between the modeled heat pump entering water temperature and the measured heat pump entering water temperature. The calibrated values differed from the measured values, but were similar to the thermal properties for sand and clay tabulated in other references.

Several studies have been performed comparing the results of different GSHP modeling programs. Partenay et al. [50] discuss the importance of understanding the short time scale performance of a bore field on the calculation of GSHP efficiency. One goal was to develop a model which includes the fluid delays associated with flow through the pipes and the convective resistance between the fluid and the pipe. The outlet temperature from the GSHP of an experimental test bed was compared to the outlet temperature from the authors' new model (3DM) and the DST model; although the DST model is accurate after a certain time period (RMS of 0.053°C), it did not match the measured results for the first seven hours of the test. The 3DM model provides a better match to the measurements in this initial time frame.

In a second test, 1500 W was injected into the system for 1 hour over a three hour period for 48 hours for a total of 16 cycles. In this case, although the DST model does eventually show the correct trend, it does not match the measured temperature (RMS of 0.68°C) at either the beginning or end of the cycle. The 3DM model provides a better match to the measured temperature (RMS of 0.34°C) after 35-40 minutes. In the macroscopic view, as compared to the

actual experiment, over 48 hours the DST model yielded 40.8% less energy injected into the system and the 3DM model yielded 13.3% less energy injected into the system.

Following this initial model evaluation, a closed loop test was conducted over a one week period with 5 s time steps. In this case, a simulated building was constructed and the loads from this building were subsequently applied to the existing test bed. Three figures of merit were used to compare the DST and 3DM models to the experiment: energy delivered to the building, seasonal performance factor (SPF), and number/duration of heat pump cycles. The DST model estimated the energy delivered to the building to within 0.7%, while the 3DM model was within 1.3%. However, the DST model underestimated the SPF by 13.6% while the 3DM model underestimated by 3.2%. The DST and 3DM models had heat pump cycle durations of 3.1 hours and 2.9 hours, respectively, while the actual cycle duration was 2.8 hours. One year simulations with 30 s time steps were run using each model in several different European climates; in heating the relative difference between the models was approximately 5% and in cooling it was approximately 11%. The comparison indicates that over short time periods (hours or days), the DST model can be inaccurate, but over longer time periods, such as those used in the proposed research, it can predict energy transfer and fluid temperature with sufficient accuracy.

Shonder et al. used five commercially available programs to calculate the design length of the GSHP; the variation between the programs was ±7% and ±16% for cooling and heating dominated sites, respectively [47]. The authors used the DST model, which they had validated in a prior study, as the baseline for comparison. More recently, Spitler et al. performed a comparison of six commercially available programs [51]. In this study, each model was evaluated by comparing the average heat flow rate to the bore field and the exiting fluid temperature from the bore field obtained from each model to experimental results. The authors

found that the prediction of the fluid temperature exiting the GSHP varied significantly between the models and suggested additional investigations to determine the cause. The DST model performed as well or better than other models when comparing to experimental data.

The goal of this research is not to develop a new ground store model, but rather to use an existing model which is widely recognized and sufficiently validated to evaluate the behavior of the GHX and compare the performance of different strategies for controlling and designing a HyGSHP system. A detailed transient analysis was desired for evaluating design configurations and control strategies, so the DST model as implemented in TRNSYS is an ideal tool. The DST model has been used in numerous studies, including the analysis of existing systems and comparison with experimental data [34,47–49,51], so it is a widely recognized and validated model. It also generates a temperature distribution over a user defined grid that can be used for detailed study of the ground store. The model is limited in that it does not incorporate ground water flow, assumes bore field symmetry, and has limited accuracy over time scales on the order of hours, but the proposed research will look at long range performance, for which the DST model is accurate [48,49,52]. For the comparative studies in the present work, the DST model will provide the needed accuracy. Typical values of parameters input to the DST model are given in Table 2-3. For simplicity the simulations described throughout this report use only a single ground layer in the DST, thereby assuming that the ground properties are constant for the entire depth of the borehole. Validation of the DST model beyond that which has already been discussed was performed as part of the work documented in this report and is presented in Chapter 3.

Table 2-3 Inputs to the DST model.

Description	Value
Maximum drill depth	91.4 m
Space between boreholes	6.1 m
Thermal conductivity of the ground	2.423 W/m-K
Heat capacity of the ground	2093 kJ/m^3-K
Header depth	1.8 m
Borehole radius	0.057 m
Outer pipe radius	0.0167 m
Inner pipe radius	0.01365 m
Center to center half distance	0.038 m
Thermal conductivity of the grout	1.385 W/m-K
Thermal conductivity of the pipe	0.42 W/m-K
Thermal conductivity of the gap	0.52 W/m-K
Gap thickness	0
Reference temperature	30°C
Number of ground layers	1

2.5 Circulating Pump Model

Although in a real system there may be several circulating pumps (at least one for the GHX and one for the CT), in this model the total power consumption of the pumps is calculated using a single variable speed pump model (adapted from TRNSYS Type 743). The pump power is calculated from Eq.(2.35) where P_{rated} is the rated pump power and f is the actual flow rate divided by the rated flow rate. Y_{power} is a polynomial curve fit representing a typical pump power curve. For the simulations in this report it is assumed that 55% of the system pressure drop occurs in the GHX; the GHX generally contains a great deal of small diameter piping, so it is assumed that more than half of the pressure drop occurs in the GHX. Assigning a percentage of the pressure drop to the GHX avoids the necessity to perform extensive pressure drop calculations which take into account the pressure drop in all pipes and components of the system.

The remainder of the system pressure drop occurs in the building piping, cooling tower, heat exchangers, pumps, etc. The portion of the pressure drop assigned to the GHX is included as a user input in FHyGSHP.

$$P_{pump} = \begin{cases} 0.45 P_{rated} Y_{power} & GHX\ bypassed \\ P_{rated} Y_{power} & GHX\ used \end{cases}$$
$$Y_{power} = \left(0.1 + 0.05 f + 0.88 f^2\right) \quad (2.35)$$
$$P_{rated} = P_{W,ton} q_{peak,c}$$

For the generic system design used in this analysis, there is no rated pump power because there is no specified pump; however, it can be estimated using benchmarks for circulating pump power consumption as a function of peak cooling, $P_{W,ton}$, as shown in Table 2-4, which was adapted from Kavanaugh and Rafferty [53]. This table presents a grade for pump design based on the power consumption of the pump and can provide a guide for selecting an appropriate rated pump power. Typical values used in the simulations in this work are given in Table 2-5.

Table 2-4 Benchmarks for pumping power vs. peak cooling load; adapted from Kavanaugh and Rafferty [53]**.**

W/ton	hp/100 ton	Grade
<= 50	<= 5	Excellent
50 to 75	5 to 7.5	Good
75 to 100	7.5 to 10	Mediocre
100 to 150	10 to 15	Poor
> 150	> 15	Bad

The final pumping power also incorporates the pump efficiency and is calculated as shown in Eq.(2.36). The two efficiencies in the denominator are the shaft efficiency, η_p, and the motor efficiency, η_m. The shaft efficiency is calculated by dividing the total pump efficiency, which is an input to the program, by the motor efficiency, which is also an input to the program.

$$P_{pump,total} = \frac{P_{pump}}{\eta_p \eta_m} \tag{2.36}$$

Table 2-5 Inputs to the circulating pump model.

Rated	50 W/ton
% Pressure Drop in GHX	55
Total pump efficiency	0.65
Motor efficiency, constant speed	0.8
Motor efficiency, variable speed	0.9

2.6 Supplemental Furnace

There is an option to add a furnace to the air side of the building so that rather than sizing the GHX to meet the maximum heating load, the GHX can be sized to meet the majority of the heating load and the furnace can be used to assist during times of peak heating. The model of the furnace is straightforward. If the building load as read from the input file, Q_H, is greater than a set point load, Q_{set}, then the furnace will be used to meet the portion of the building load that exceeds Q_{set} as shown in Eq.(2.37). If Q_{set} is zero, then the entire heating load is met by the GHX; if $Q_{set} = Q_H$, then the entire heating load is met by the furnace.

$$Q_{furnace} = Q_H - Q_{set} \tag{2.37}$$

The capacity of the furnace, $Q_{f,cap}$, is estimated as the maximum value of $Q_{furnace}$ over all time steps of the simulation divided by the efficiency of the furnace. The cost of operating the furnace is given in Eq.(2.38), where η_f is the user specified efficiency of the furnace; in this work the efficiency was set to 0.95.

$$Cost_{furnace} = \text{cost}_{gas} \frac{Q_{furnace}}{\eta_f} \tag{2.38}$$

2.7 Working Fluid

The working fluid can be either water or an anti-freeze mix of water and propylene glycol. Most systems will use propylene glycol if at some point during annual operation the fluid temperature could be below or near the freezing point of water. The anti-freeze mixture has different physical properties than water. The amount of propylene glycol in the working fluid, V_{PG} [%], is calculated based on the minimum expected fluid temperature, T_{freeze} [°C], as shown in Eq.(2.39); T_{freeze} is a user input to FHyGSHP. The density and specific heat of the propylene glycol mixture are also required; these properties are functions of both the fluid temperature and the concentration of propylene glycol. However, the dependence on fluid temperature is minimal in comparison to the dependence on concentration, so correlations were developed as a function of concentration only. The correlation for density, ρ_{PG} [kg/m^3], is given in Eq.(2.40) and the correlation for specific heat, c_{PG} [kJ/kg-K], is given in Eq.(2.41) [54].

$$V_{PG} = 4.9158 - 2.0814\,T_{freeze} - 0.0207\,T_{freeze}^2 \tag{2.39}$$

$$\rho_{PG} = 998.35 + 0.8173\,V_{PG} \tag{2.40}$$

$$c_{PG} = 4.2454 - 0.013\,V_{PG} \tag{2.41}$$

2.8 Economic Model

In this work the primary metric for evaluating and comparing system designs is life cycle cost; the P_1-P_2 method is used to estimate this metric [55]. This method divides the calculation into two parts, one part associated with the operational fuel costs and a second part associated with the investment costs. P_1 is the ratio of the life cycle fuel savings to the first year fuel savings and P_2 is the ratio of capital expenditures over the life of the system to the initial system cost. P_1 and P_2 are defined in Eqs.(2.42) and (2.43), where PWF is the present worth factor, which relates the long term cost to present dollars. The equation for P_2 includes only the factors which are non-

zero for the current calculation; the actual equation contains additional terms relating to loan costs and salvage. Terms in these equations are defined in Table 2-6. The values used for the current analysis are based on values adapted from the references [56,57].

$$P_1 = \left(1 - c\bar{t}\right) PWF\left(N_e, i_f, d\right) \tag{2.42}$$

$$P_2 = D + t\left(1 - \bar{t}\right) PWF\left(N_e, i, d\right) - \frac{c\bar{t}}{N_d} PWF\left(N_{\min}, 0, d\right) \tag{2.43}$$

$$PWF = \begin{cases} \dfrac{1}{d-i}\left[1 - \left(\dfrac{1+i}{1+d}\right)^N\right] & i \neq d \\ \dfrac{N}{N+1} & i = d \end{cases} \tag{2.44}$$

The life cycle cost, *LCC*, is given in Eq.(2.45), where C_{fuel} is the cost of fuel (combined cost of both electricity and gas) in the first year and C_{first} is the first cost of the system.

$$LCC = P_1 C_{fuel} + P_2 C_{first} \tag{2.45}$$

The first cost of the GHX is the total length, L_{GHX}, times the cost per unit length, C_{GHX} (Eq.(2.46)). The first cost of the CT is defined in Eq.(2.47), where the cost of a 10 ton CT is $4500 and there is an additional cost associated with a storage tank for storing sump water when the CT is drained; the multiplier M_{cost} can be used to scale the first cost of the CT based on current rates or a different model. These cost relationships are taken from RS Means cost data [58]. Recall that the variable *s* is used to scale the cost to the actual size of the CT (10 tons is the nominal CT size).

$$GHX_{first} = L_{GHX} C_{GHX} \tag{2.46}$$

$$CT_{first} = \$4500\, M_{\cos t}\left(-0.0021\, s^2 + 0.2878\, s + 0.868\right) + C_{sump} \qquad (2.47)$$

$$C_{sump} = \$960\left(0.6909\, s + 0.3162\right)$$

$$C_{first} = CT_{first} + GHX_{first} \qquad (2.48)$$

C_{fuel} generally includes only the electrical costs related to operating the system, but in this case additional parameters are included to account for demand charges, ratchet charges, water cost, and maintenance charges.

The base cost of electricity is calculated using time of day and time of year rates. The cost of electricity is greater during the afternoon hours in the summer, so the penalty associated with operating during these times is accounted for in the calculation. The rates used in the current study are shown in Table 2-6 [57]. A demand charge is a monthly charge based on the maximum electrical power draw during a certain time interval during the month; in this study that time interval is 30 minutes, but different utilities have different definitions. A ratchet charge is the annual demand charge; it is based on the maximum electrical power draw during a certain time interval for the prior 11 months. For this study that time interval was again taken as 30 minutes, but as with the demand charge the details can vary depending on the utility. Both of these charges would be based on the total building power consumption, so there is an assumption that building heating and cooling is the most significant use of electrical power; these economic factors are a small part of the total fuel cost, so this is a safe assumption. The cost of the water used by the CT as calculated in Eq.(2.31) is included in the fuel cost.

The maintenance costs of the CT include an annual maintenance cost, Eq.(2.49) [58], and an annual cost of treating the water, Eq.(2.50), where C_{water} is the volumetric cost of water and V_{water} is the volume of water used annually (from Eq.(2.31)).

$$CT_{ma\text{int}} = \$290.5\left(-10^{-5} s^2 + 0.055\, s + 1.059\right) \qquad (2.49)$$

$$CT_{treatment} = 0.556\, C_{water} V_{water} \tag{2.50}$$

Table 2-6 Economic Inputs.

Symbol	Description	Value
	Loan duration	20 years
c	Commercial building (1 yes, 0 no)	1
i_f	Fuel inflation rate	1.6%
d	Discount rate	7%
$\overline{t}$	Effective income tax rate	35%
	Inflation rate	1.6%
t	Property tax rate	3%
	Loan interest rate	6%
N_d	Depreciation life	4.55 years
D	Down payment	100%
	Rebate	0
	Salvage value	0
N_e	Economic analysis duration	20 years
	Cost of GHX	36.1 $/m
	Cost of PG	0.82 $/m
	Cost of water	0.35 $/m^3
	First cost of the CT	4500 $/10 tons
	Multiplier on first cost of CT	2.75
	Maintenance cost of PG	50
	CT maintenance cost	290.5 $/10 tons
	Multiplier on CT maintenance cost	1.2
	Peak electrical cost	0.094 $/kWh
	Off-peak electrical cost	0.063 $/kWh
	Peak winter electrical cost	0.081 $/kWh
	Off-peak winter electrical cost	0.05 $/kWh
	Demand charge, summer	4.22 $/kW
	Demand charge, winter	1 $/kW
	Ratchet charge	1.05 $/kW

Chapter 3 Experimental Validation of a Ground Heat Exchanger Model

This chapter provides an overview of short time scale validation of the Duct Storage Model [46] (described in Chapter 2) for the simulation of ground source heat pump performance using experimental data acquired from two operational systems. The error in the temperature change across the ground heat exchanger in the first system was within measurement error, but was larger than measurement error in the second system due to uncertainty in the thermal properties of the ground. A sensitivity study determined that the thermal conductivity and heat capacity have the greatest impact on the model accuracy. An assessment of the error in the model using ASHRAE handbook [59] values for thermal conductivity and heat capacity provided a measure of acceptable error. The difficulties of using real world operational systems for model validation are also discussed.

3.1 Introduction

The DST model is used in all of the simulations detailed in this thesis to model the ground heat exchanger; this chapter discusses the effort to validate the DST model in order to ensure that it is sufficiently accurate for use in this work. The validation utilizes data obtained from two operational systems. One system that uses a cooling tower (CT) with a 360 bore ground-storage heat pump system is installed in a mixed use facility near Las Vegas, NV. The other system is installed in multifamily buildings located in Madison, WI; this system has a small boiler that is rarely used, so the system is considered a 39 bore ground source heat pump (GSHP) only system for the purposes of the study detailed here. In addition to evaluating the ability of the DST model to simulate the existing systems, the limitations and difficulties associated with using data from operational systems to validate a model are discussed.

3.2 Model

There are a variety of ways to implement a ground heat exchanger (GHX) in a GSHP, but this work is focused on the vertical heat exchanger design. A vertical heat exchanger consists of bore holes drilled into the ground to a depth that depends on the local geology. A high density polyethylene pipe is placed in the hole. This pipe has a u-bend at the bottom so that the working fluid flows down one leg of the pipe and then back up through the other leg. The number of bore holes is based on the expected load of the building (or buildings) and the entire array of bore holes is the GHX. The bore holes are tied together with a header manifold and connected to the building. Heat is transferred between the building and the ground via a working fluid. The working fluid is often water; however in cold regions antifreeze mixtures are often used.

One commonly used model of a system of bore holes and the surrounding ground is the Duct Storage Model (referred to as the DST model), developed by Hellström [46]. The DST model calculates the ground temperature using the superposition of three separate heat transfer calculations:

- the steady flux solution accounts for the slow redistribution of heat through the sub-regions near the bore hole,
- the global solution accounts for heat flow over long time scales (months or years), and
- the local solution accounts for heat flow on short time scales near the bore hole.

The local and global solutions require implementation of a finite difference method while the steady flux solution is based on an analytical model. In the local solution, a single bore hole is modeled and assumed to be representative of all bore holes. A one-dimensional (1-D) finite difference solution is applied in the radial dimension near the bore hole. The vertical dimension is divided into a number of sub-regions and the 1-D solution is applied to each sub-region. The outer radius boundary condition is a zero flux boundary and the inner radius boundary condition

is a constant temperature boundary; the temperature of the boundary is based on the temperature and flow rate of the fluid passing through the tube as well as the convective and conductive resistance to heat flow in the pipe and the bore hole fill material. The steady-flux solution accounts for heat pulses that vary slowly in time and this solution controls the redistribution of energy through the storage volume and links to the local and global solutions. The combination of these three calculations accounts for the heat transfer between the fluid in the pipe and the ground near the pipe as well as the effect of neighboring bore holes on each other. Inputs to the model include the thermodynamic state and flow rate of the entering fluid, the geometry of the heat exchanger, and the conditions of the surroundings. Outputs from the model include the thermodynamic state of the fluid leaving the heat exchanger and the rate of heat transfer from the fluid to the ground.

Although this work uses the DST model, implemented in TRNSYS [15], there are other models of the GHX behavior that have been developed and validated by other researchers. One model which has become the basis for a variety of others is the g-function model developed by Eskilson [29]. This model was extended to shorter time-steps and experimentally validated by Yavuzturk and Spitler [30,60]. Xu and Spitler later combined Eskilson's model with a numerical model of the short time-step behavior of the bore field [61]. Gentry et al. [62] detail the experimental validation of this model using a three-bore cooling-tower hybrid ground source heat pump system [63]. In addition, the results of simulations using several different models have been compared by Spitler, et al [51].

Prior validation and calibration performed on the DST model have demonstrated its effectiveness [47–49]. In these studies, the soil thermal conductivity, specific heat, density, and the deep earth temperature were chosen to achieve the best match between the modeled heat

pump entering water temperature and the measured heat pump entering water temperature. The chosen values differed from the measured values, but were similar to the thermal properties for sand and clay tabulated in other references.

The experimental data acquired in this study are similar to those used by Yavuzturk and Spitler, but the results are applied to the validation of the DST model. Unlike some of the prior validation efforts for the DST model, this paper focuses on the simulation results obtained using the measured thermal properties and values obtained from the ASHRAE Handbook [54], which is a common resource for GSHP design. A comparison of the results of these simulations provides an indication of the capability of the DST model to predict actual short term performance and adds to the prior body of work on GHX model validation.

3.3 Experimental Measurements

Measurements of temperature and flow rate were acquired from a cooling tower HyGSHP system near Las Vegas, NV (Site 1) and from a system in Madison, WI (Site 2). At Site 1 the measurements are acquired instantaneously at 15 minute intervals; at Site 2 the measurements are acquired continuously with a sample rate of 1 Hz and averaged over each 15 minute time period.

Site 1 became operational in January of 2009, but the data used in the validation begin approximately six months later. The first six months of data were included in the analysis at one point, but it was determined that their inclusion did not significantly alter the conclusions of this research. Since the system was undergoing commissioning during this period (and control set points were changing), it was decided to exclude these data from the final study. Site 2 became operational in June of 2004 but the measurements were acquired in 2009 and 2010. The five year

period between initial system operation and the collection of validation data may have contributed to some of the inconsistencies in the data that will be presented later.

Figure 3-1 is a schematic of the system at Site 1; the dots show the location of key temperature measurements and the squares show the location of key flow rate measurements. The temperature measurements referenced in the following sections are given in Table 3-1.

Table 3-1 Temperatures Referenced in the Site 1 Model.

T1	the temperature downstream of the GHX fields
T2	the temperature downstream of the GHX fields and cooling tower
T3	the temperature entering the GHX fields

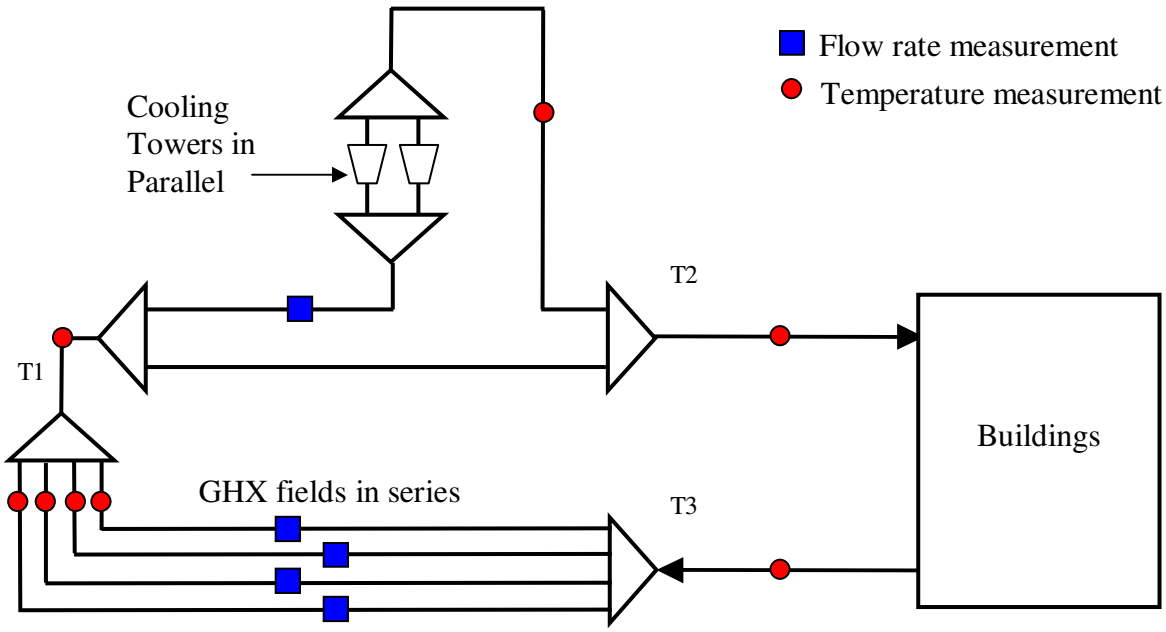

Figure 3-1 Schematic of the hybrid system at Site 1.

Figure 3-2 is a schematic of the system at Site 2. There is an open bypass leg in this system because the flow through the GHX is greater than the flow through the building for all cases observed in this study. The pump for the GHX loop is constant speed and currently operates continuously even when there is no building load; the inefficiency of this design was discussed in an independent study [7]. The temperature measurements that are referenced in the

following sections are listed in Table 3-2. T2 and T3 should read the same temperature and, unless significant heat is added to the flow by the pump, the temperature reading at T4 should be the same as at T3. T5 and T1 generally will not read the same temperature due to the addition of flow from the bypass leg in between the two sensor locations.

Table 3-2 Temperatures Referenced in the Site 2 Model.

T1	the temperature entering the GHX
T2	the temperature downstream of the GHX
T3	the temperature downstream of the GHX and bypass
T4	the temperature downstream of the entire plant
T5	the temperature exiting the building and entering the bypass

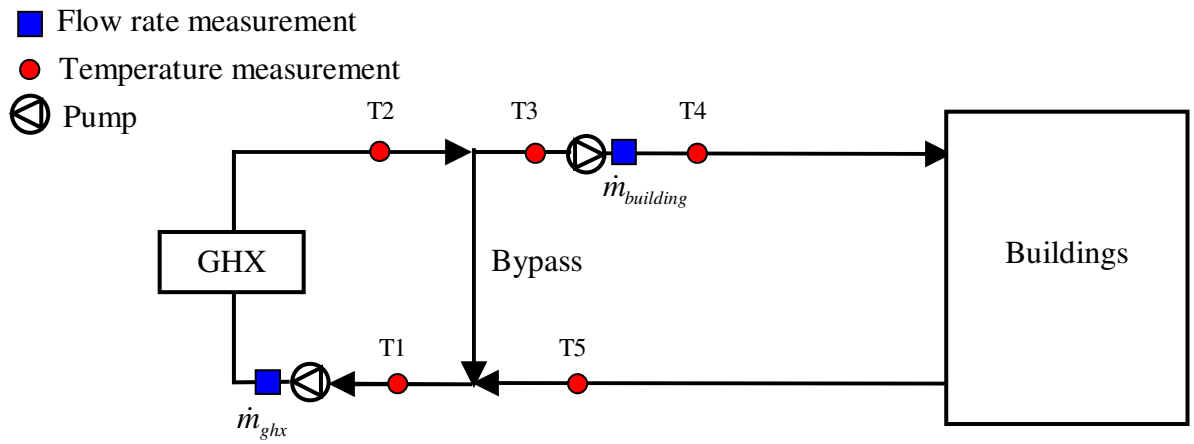

Figure 3-2 Schematic of the system at Site 2.

The instrumentation at Site 1 was installed during system installation, prior to the initiation of this study; therefore, the uncertainty in these data is based on typical manufacturer information. The instrumentation at Site 2 was installed by the authors and calibrated prior to installation. The temperature measurements at Site 1 are assumed to have an uncertainty of ±0.5℃ while the measurements at Site 2 are assumed to have a lower uncertainty of ±0.2 ℃, based on calibration. One important measured parameter is the temperature change that is induced as the fluid flows through the GHX, ΔT, which is defined as:

$$\Delta T = \left(T_{in} - T_{out}\right) \tag{3.1}$$

where T_{in} and T_{out} are the measured inlet and outlet temperatures, respectively. The uncertainty associated with the measured temperature change, $u_{\Delta T}$, is given in Eq. (3.2), which is derived from Taylor series uncertainty propagation:

$$u_{\Delta T} = \sqrt{u_{T_{in}}^2 + u_{T_{out}}^2} = u_T\sqrt{2} \sim \begin{cases} \pm 0.7\Delta°C & Site\ 1 \\ \pm 0.28\Delta°C & Site\ 2 \end{cases} \tag{3.2}$$

where u_T is the uncertainty in the measured temperature.

A second important measured parameter is the flow rate passing through the GHX. Both sites use constant speed pumps. At Site 1 the measurements are instantaneous, so the flow rate is sometimes acquired at a time when the flow is ramping up or down. Measurements acquired during these times are misrepresentative of the average flow rate during the measurement time period and the removal of these data points from the analysis is discussed subsequently. Flow rates are acquired by turbine flow meters (Onicon F-1210 and F-1110) with a manufacturer specified uncertainty of at most 2% of full scale.

At Site 2, flow rates are continuously monitored using pressure transducers (Dwyer 629-01-CH-P2-E5-S4) to measure the pressure differential that is induced across an orifice. The orifice is part of a multi-purpose valve (TACO Plus One MPV030) used for balancing the hydronic system; there is an orifice for each of the flow rate measurements shown in Figure 3-2. A flow curve for the orifice, obtained from the manufacturer, was used to correlate pressure drop across the valve to flow rate. Using this flow rate and the measured temperatures T1, T2, T3, and T5 (see Figure 3-2) an energy balance was performed on the bypass leg. The normalized energy balance is defined by Eqs. (3.3) - (3.5). The imbalance between the flow energy entering the bypass (E_{in}) and the flow energy exiting the bypass (E_{out}), normalized by the maximum cooling

load ($Q_{max,cooling}$), is shown in Figure 3-3 and labeled "Original". The measurements indicate a significant energy imbalance. The cause of this error must lie in either the temperature measurements or in the flow rate measurements (or both).

$$E_{in} = \dot{m}_{ghx} T_2 + \dot{m}_{building} T_5 \tag{3.3}$$

$$E_{out} = \dot{m}_{ghx} T_1 + \dot{m}_{building} T_3 \tag{3.4}$$

$$\text{Imbalance} = \frac{|E_{out} - E_{in}|}{Q_{\max,cooling}} \tag{3.5}$$

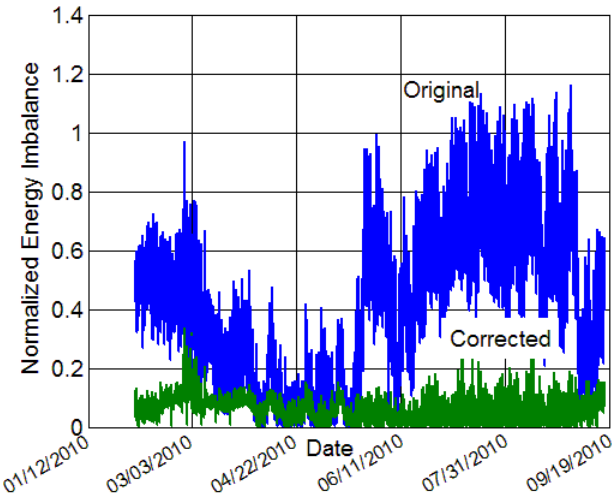

Figure 3-3 Energy imbalance on the bypass leg for the original and corrected flow rate data.

Error in the temperature measurements was ruled out as the major factor causing the imbalance after verifying the correct placement of all thermocouples and comparing the readings from T2 and T3. In addition, a Taylor series uncertainty propagation shows that, when there is flow through the system, the uncertainty due to the temperature measurements is at most 25% of the total uncertainty, and typically on the order of 10%; the remaining component of the uncertainty is due to the uncertainty in the flow rate measurement. Since the orifices used to measure the flow rate were not intended for research use, but rather are standard devices

included in the pumps, it was determined that the error was likely related to the flow rate measurement. To obtain an additional, redundant and more accurate measurement of the flow rate, a transit-time ultrasonic flow meter was used (Fuji FSCS10A1-00) to acquire spot measurements of the flow in the ground loop; this meter has a manufacturer specified accuracy of ± 1%. The continuously monitored flow rates measured using the orifice were calibrated to match the flow rates measured from the ultrasonic flow meter. This calibrated flow rate resulted in a dramatic reduction in the energy imbalance between the ground loop and building loop; this is shown in Figure 3-3 and labeled "Corrected." As a third point of validation (though not quite as strong as the first two), the flow rate and temperatures across the building were compared with a calibrated building model and showed a reasonable match. Based on the energy imbalance still remaining after flow calibration an uncertainty of ± 20% is assigned to the flow rate measurement.

3.3.1 DST Validation at Site 1

A schematic of the entire cooling tower HyGSHP system is shown in Figure 3-1. This system services several multi-use buildings and utilizes water as the working fluid. The system is composed of four GHX fields; at any given time, one of these is designated as the lead field, which is the first to be switched on. The remaining fields are turned on or off depending on how well the load is being met by the currently operating fields. The lead field is varied every few days in order to distribute the load through the entire GHX system. If the four fields can not meet the cooling load, then one or both of the cooling towers are activated in addition to all of the GHX fields.

Experimental data from the four GHX fields were used to validate the DST model. A schematic of the modeled system and the locations of the temperature and flow rate

measurements are shown in Figure 3-4, where T18, T17, T16, and T15 are temperatures measured at the exit of each of the four fields. A constant speed pump is located in each individual field and a turbine flow meter is used to measure the flow through each field. The total field flow is not independently measured, but it is estimated as the sum of these four flow measurements.

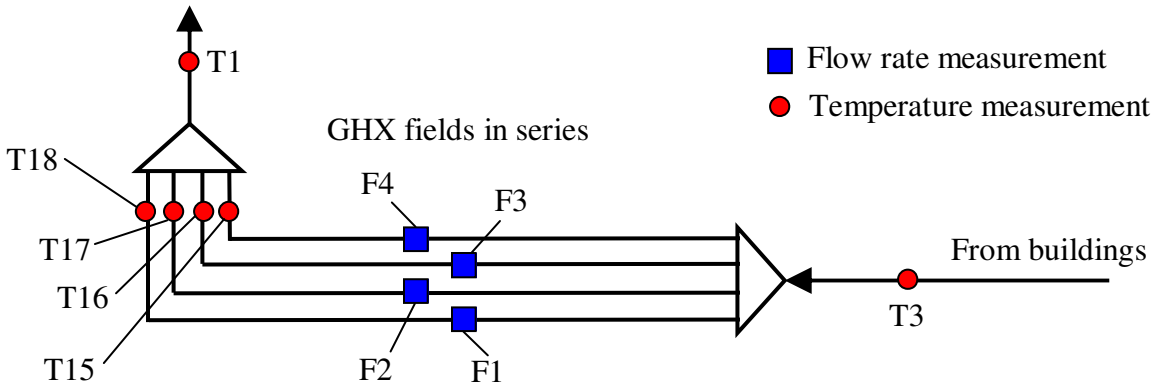

Figure 3-4 Sketch of the modeled system and the key measurement locations.

The DST model requires numerous inputs related to the system design and characteristics of the ground, as summarized in Table 3-3; these values are input to each of the four separate DST models for Site 1. The thermal properties of the ground and undisturbed ground temperature are the average of those calculated from two in-situ thermal response tests (TRT) [64]. Note that a relatively large uncertainty has been estimated for the ground thermal conductivity. Commercial TRTs do not cite an uncertainty, but based on the multitude of assumptions made concerning both the installed system and the theory behind the calculation of thermal conductivity from the data measured in the test, the uncertainty can be large (sources of error are discussed in more detail subsequently) [65]. The primary outputs from the DST model are the temperature of the working fluid exiting the model and the total rate of heat transfer between the fluid and the ground.

Table 3-3 Inputs to the DST Model at Site 1.

Parameter	Value	Source	Author Estimated Uncertainty
# of bore holes/field	90	Building specification	
Bore hole depth	122 m (400 ft)	Building specification	
Header depth	1.52 m (5 ft)	Building specification	
Bore hole radius	6.51 cm (2.56 in)	Building specification	
u-tube inner radius	1.74 cm (0.69 in)	Building specification	
u-tube outer radius	2.13 cm (0.84 in)	Building specification	
Bore hole spacing	7.62 m (25 ft)	Building specification	
# of bore holes in series	1	Building specification	
# of vertical sub-regions	120		
Ground thermal conductivity	1.94 W/m-K (1.12 Btu/h-ft-F)	Thermal response test	±40%
Ground heat capacity	2616 kJ/ m^3-K (39.1 Btu/h- ft^3-F)	Thermal response test	±15%
Grout thermal conductivity	2.08 W/m-K (1.2 Btu/h-ft-F)	Building specification	±5%
Undisturbed ground temperature	25.6°C (78°F)	Thermal response test	±2 Δ°C

3.1.3.1 Individual field validation

Additional inputs to the model include the experimentally measured fluid inlet temperature, T3, and the measured flow rates: F1, F2, F3, and F4, as defined in Figure 3-4. Each field is individually modeled and analyzed; i.e. a single DST model is placed in the simulation file (although the results are the same if all four fields are modeled together). Figure 3-5 shows a comparison of the measured and modeled temperature change across field 4 as calculated by Eq. (3.6), where T3 is the fluid temperature at the inlet to field 4 and T15 is the fluid temperature at the outlet of field 4 as shown in Figure 3-4.

$$\Delta T = T_3 - T_{15} \tag{3.6}$$

The line shows the case when the modeled results perfectly match the measured results; although some data fall along this line, a significant number of data points lie above or below the line, indicating that the model over-predicts the temperature change across the field.

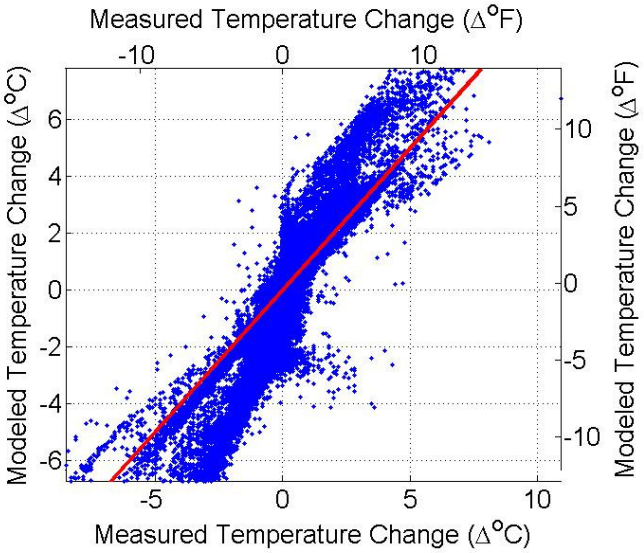

Figure 3-5 Measured and modeled temperature change across field 4.

At Site 1, constant speed pumps are used in each of the GHX fields. Therefore, the flow is either on, ramping up or down to or from its full on value, or completely off. The field pumps are located downstream of the flow meters but upstream of the fields, as shown in Figure 3-6; this arrangement has the disadvantage that even if the pump for field 4 (for example) is off, the flow meter installed in field 4 may register a small, non-zero flow rate if there is flow through any of the other fields. Since all of the fields are connected to the same header pipe, flow through that pipe can cause a disturbance in the pipe leading to a field even if that field is not in use. The flow rate is one input to the DST model; if this small, non-zero flow rate is input to the model, the model will predict heat transfer associated with that field when, in reality, there is none. Although the predicted heat transfer will be small, it will still lead to an over-prediction of the temperature change across the field as compared to the measured result. The model accuracy should only be assessed when there is full flow through the field; this is the only condition of interest in operation and the only condition where the model inputs are known with sufficient accuracy.

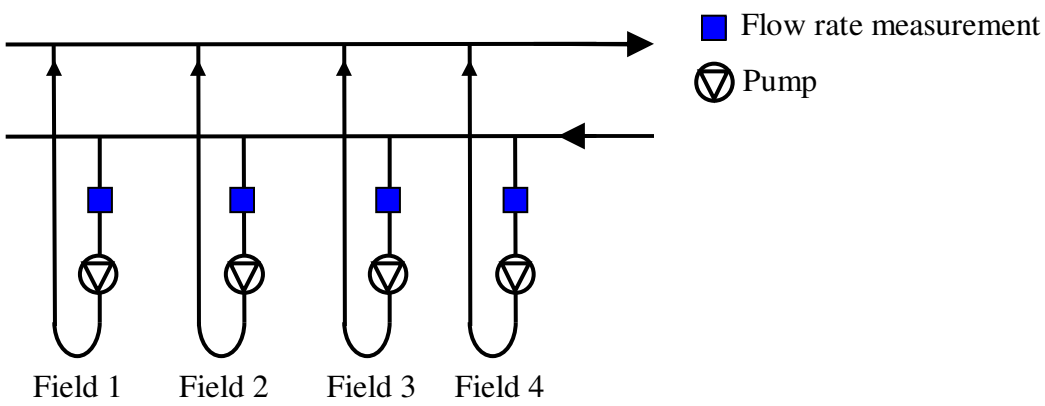

Figure 3-6 Arrangement of the flow meters and pumps for the four GHX fields.

An additional source of complexity is that the flow measurements at Site 1 are instantaneous rather than time-averaged. Therefore, if the measurement is acquired at a time near the activation or deactivation of the pump, then the measured flow may not accurately reflect the actual average value of the flow during the measurement period.

Figure 3-7 provides a visual demonstration of the flow rate regimes described above for field 4. Figure 7(a) shows the flow rate measured in field 4 as a function of the flow rate through all of the fields. There are three distinct regions exhibited in this figure:

- full flow corresponds to the steady state flow through the loop associated with the constant speed pump operating at its full speed value (the large clumps of data towards the top of the figure correspond to pump 4 being on full speed with 0, 1, or 2 additional pumps being activated, moving from left to right),
- transitional flow corresponds to the increase or decrease in the flow rate as the pump transitions from on to off or off to on, and
- no flow corresponds to the flow rate measured when the loop pump is not on, but there is flow through one or more of the other GHX fields causing a small nonzero flow measurement.

In the full flow region (~42% of the data), the scatter in the data are due to variation in the pressure drop through the system and the repeatability of the pump operation. In the no flow region (~58% of the data), the level of flow recorded by the flow meter is proportional to the number of other fields on; i.e. if two other fields are on then the measured flow rate is greater than when only one other field is on.

Figure 7(b) shows the flow rate measured in field 4 as a function of time. This figure demonstrates that the transitional flow points are scattered and represent less than 1% of the total number of data points. These figures are representative of the behavior of the flow rate measurement in the other three fields.

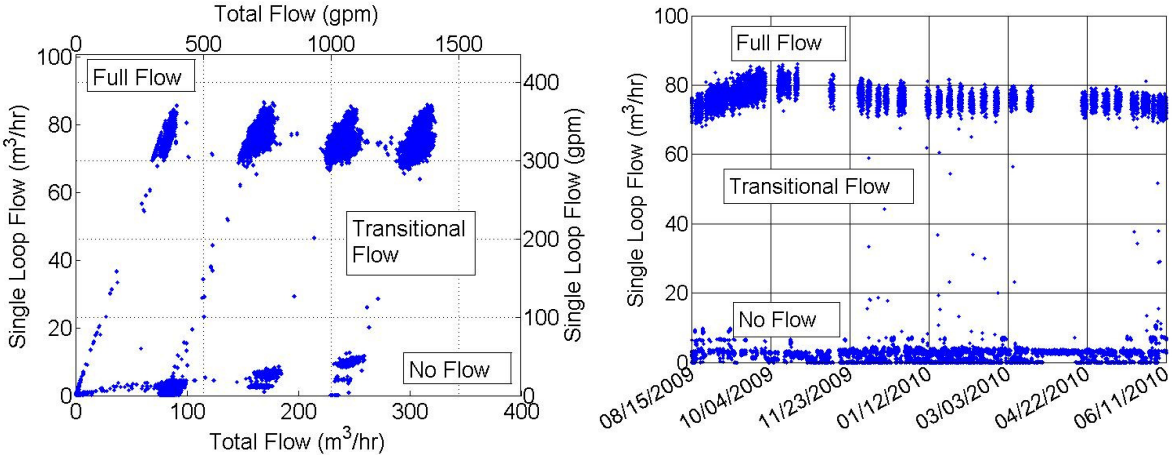

Figure 3-7 Flow rate through field 4 as a function of the total flow rate through all four fields (a) and time (b).

In order to arrive at an assessment of the model accuracy, only the data points corresponding to full flow are used. These data points are selected based on the criteria that the flow is greater than 60 m^3/hr and the assumption that this is the flow for the full time step. Figure 3-8 shows the data from Figure 3-5 excluding the low/no flow data; the match is very good.

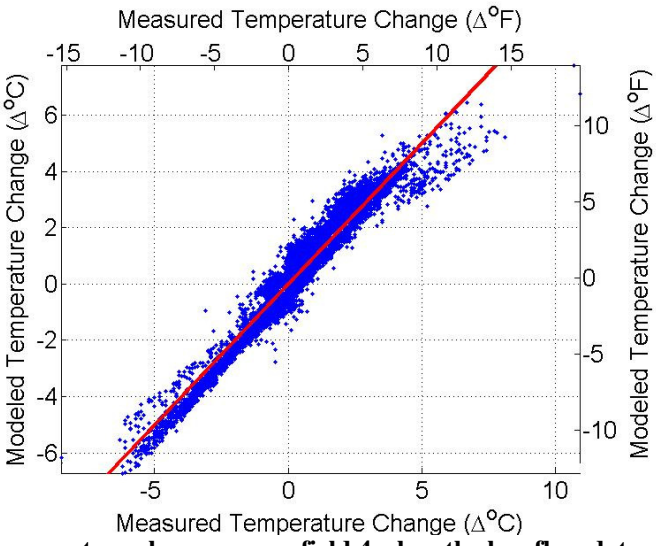

Figure 3-8 Temperature change across field 4 when the low flow data are removed.

Two metrics that characterize the accuracy of data are the mean bias error (MBE) and the root mean square (RMS) error. The mean bias error is used to assess the magnitude of the difference between the values that are being compared; it is a measure of the presence of bias in the model. For example, a large positive value indicates that the model consistently overestimates the temperature change across the field. A result such as this can help pinpoint how the model is in error. The root mean square error is essentially the standard deviation; it is representative of the scatter in the data because values of opposite sign do not cancel. A large RMS value indicates that each individual point of comparison is significantly removed from the mean of the comparison. In this study the MBE is removed from the simulation results in the calculation of the RMS error so that the RMS error represents the scatter in the agreement between the model and the measurements absent any systematic bias. Table 3-4 contains a summary of the error terms for the temperature drop as defined in Eqs. (3.7) and (3.8).

$$MBE = \frac{\sum (Modeled - Measured)}{N} \tag{3.7}$$

$$RMS = \sqrt{\frac{\sum\left[\left(Modeled - MBE\right) - Measured\right]^2}{N}} \tag{3.8}$$

Table 3-4 Error Results for Individual GHX Fields.

	MBE (Δ°C)	RMS (Δ°C)	Max ΔT (Δ°C)
Field 1	0.18	0.38	10.28
Field 2	0.09	0.38	10.23
Field 3	0.16	0.42	10.26
Field 4	0.06	0.42	10.88

The MBE is within the measurement uncertainty specified for Site 1 in Eq. (3.2) and shows a tendency for the model to slightly over-predict the temperature change. The RMS error is within measurement uncertainty.

3.3.2 DST Validation at Site 2

A building site located in Madison, WI, consisting of 61 apartment units in two buildings, was also instrumented for use in this study. The system is composed of one GHX field containing 39 bore holes of a depth of approximately 91 m (300 ft). Measurements of the flow rate through the GHX, and the temperatures at the inlet and outlet of the GHX were acquired as averages over 15 minute intervals. The constant speed pump for the GHX loop is always operational; even when there is no building load there is flow through the loop. The working fluid is a 25% propylene glycol – water mixture. The inputs relating to the system design and characteristics of the ground are summarized in Table 3-5. The thermal properties and the undisturbed ground temperature were calculated from a single in-situ TRT [66]. As previously mentioned, there was a five year operational period prior to the acquisition of the measurements used in this study, but for the purposes of the base case, the thermal history is neglected and the values obtained from the TRT are used for simulation.

Table 3-5 Inputs to the DST Model.

Parameter	Value	Source	Author Estimated Uncertainty
# of bore holes	39	Building specification	
Bore hole depth	85 m (280 ft)	Building specification	
Header depth	1.22 m (4 ft)	Building specification	
Bore hole radius	7.62 cm (3 in)	Building specification	
u-tube inner radius	1.37 cm (0.54 in)	Building specification	
u-tube outer radius	1.67 cm (0.66 in)	Building specification	
Bore hole spacing	4.57 m (15 ft)	Building specification	
# of bore holes in series	1	Building specification	
# over vertical sub-regions	120		
Ground thermal conductivity	3.5 W/m-K (2.02 Btu/h-ft-F)	Thermal response test	±40%
Ground heat capacity	2622.28 kJ/ m^3-K (39 Btu/h- ft^3-F)	Thermal response test	±15%
Grout thermal conductivity	1.73 W/m-K (1 Btu/h-ft-F)	Building specification	±5%
Undisturbed ground temperature	12.2°C (54°F)	Thermal response test	±1 Δ°C

The predicted temperature change of the fluid as it passes through the GHX is compared to the measured temperature change in Figure 9 (a); the solid line represents a perfect match. There is relatively little scatter in the data, but the model tends to over-predict the temperature change of the fluid (i.e., over-predict the performance of the heat exchanger) most of the time. The MBE is 0.49Δ°C and RMS is 0.85Δ°C, both of which exceed measurement error; see Table 3-6 for additional results.

It is clear from this result that the field is performing worse than expected based on the thermal properties and undisturbed ground temperature acquired from the TRT; a closer look at the TRT will help identify some of the reasons why this may occur. The TRT is performed by injecting a set about of heat into a flow stream that passes through an existing borehole. The temperature of the fluid entering and leaving the borehole is measured as well as the energy injected to the fluid and the flow rate [65]. The thermal conductivity is calculated using the infinite line source model [21]; the heat transfer from the borehole to the field is assumed to

occur uniformly along the entire length of the borehole. Some additional assumptions of the TRT include [65]:

- heat transfer is only by conduction – ground water flow is not taken into account,
- there is no axial heat transfer,
- the thermal conductivity is isotropic – measurements from one borehole are representative of the entire field, and
- the thermal conductivity does not vary with time or season.

One of the major assumptions is that there is no ground water flow which could transport heat away from the borehole. Ground water flow, or simply ground moisture, can vary with location in a bore field as well season, making the assumption of conductive heat transfer only and a constant bore field conductivity suspect; this not an issue in Las Vegas, where conditions are dry. In addition, the heat transfer is unlikely to be uniform along the length of the borehole, especially when the geology varies from the top to the bottom.

There are also factors in the installation of the system that can lead to degraded performance such as voids in the grout, partial collapse of the borehole, and flow imbalances that lead to reduced heat transfer. Finally, since this system was in operation for approximately five years, the undisturbed ground temperature has been disturbed and is not uniform throughout the field. Temperature measurements at the outlet of the ground loop when there is no building load (i.e., the fluid just circulates through the ground) indicate that a better approximation to the undisturbed ground temperature may be 10.6 °C rather than 12.22 °C; however, this value does not account for the non-uniformity of the ground temperature and the error increased in a simulation conducted using this lower value for undisturbed ground temperature.

In order to better understand the effect of thermal conductivity, heat capacity, and undisturbed ground temperature on the accuracy of the DST model a sensitivity study was performed; the results are shown in Figure 9. The case shown in (a) is the baseline case using the measured values. Figure 9 (b) shows that when heat capacity is halved, the slope of the data approaches the perfect case (shown by the line) and there is additional scatter in the data. Figure 9 (c) shows that when thermal conductivity is halved the slope of the data approaches the perfect case and there is a reduction in the data scatter. Finally, Figure 9 (d) shows that when the undisturbed ground temperature is decreased by 6.1°C (11°F) the slope of the data decreases slightly, the data scatter decreases slightly at the lower left while increasing at the center, and, most significantly, the data translate vertically away from (0,0). In summary, the effect of heat capacity and thermal conductivity is to modify the slope and data scatter while the effect of undisturbed ground temperature is to translate the data along the y-axis (i.e. to or away from the origin). This is the reason why the simulation error increased when the undisturbed ground temperature was decreased to 10.6 °C; the entire data set translated away from the origin and, without modifying thermal conductivity as well, the error increased. These results indicate that although undisturbed ground temperature does influence accuracy, thermal conductivity and, to a lesser extent, heat capacity, are far more important in minimizing simulation error.

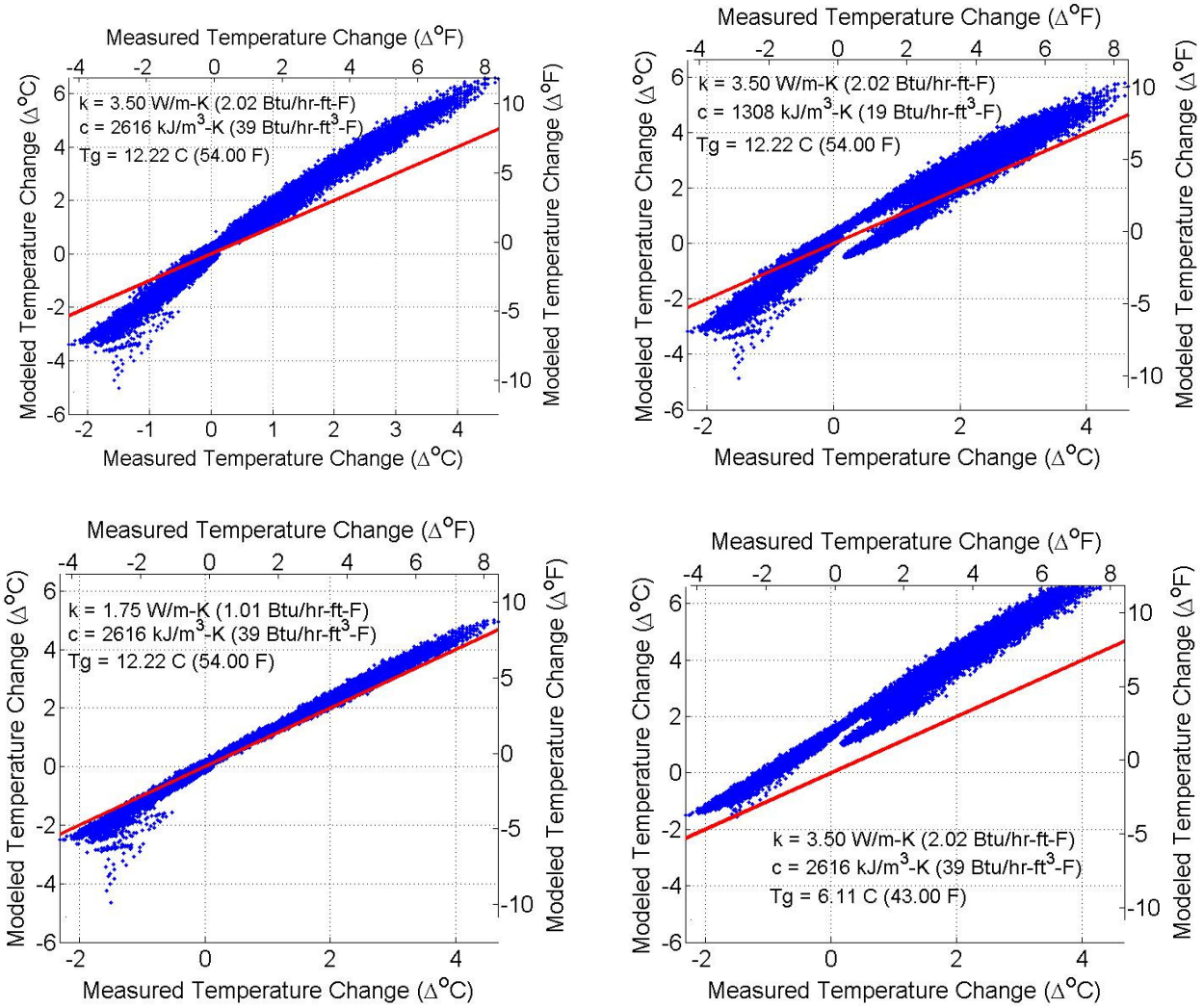

Figure 3-9 Effect of ground thermal properties and undisturbed ground temperature on the accuracy of the model results.

This leads to the question, how accurate do the thermal conductivity and heat capacity need to be? In other words, what is an acceptable level of error? This question has two answers, in a validation setting the error should be less than measurement error; this is the case at Site 1, but not at Site 2. In a design setting, an acceptable error can be larger. In practice, thermal conductivity and heat capacity are not always measured prior to system design, so a designer may rely on values obtained from the ASHRAE handbook [59]. So, what would be the error between the modeled and measured values of temperature change across the GHX field if

ASHRAE handbook values were input to the DST model? The results of four simulations using the range of thermal conductivity and heat capacity values from the handbook for sandstone, which is the dominant geology at Site 2, are shown in Table 3-6. The error using values from the thermal response test falls within the range of errors obtained using the thermal properties from the handbook, with the minimum error corresponding to the smallest values for heat capacity and thermal conductivity. If a designer used the mean thermal conductivity and heat capacity listed in the handbook, the error would be slightly less than the error using the measured values. These results support the conclusion that, at least in a design setting, the error at Site 2 is within an acceptable level of error.

Table 3-6 Errors in the Nominal and Optimized Model Results.

Source of Data	Thermal conductivity (W/m-K)	Heat Capacity (kJ/m^3-K)	MBE (Δ°C)	RMS (Δ°C)	Max ΔT (Δ°C)
Measured Values	3.50	2615.50	0.49	0.85	4.67
ASHRAE Suggested Values	2.08	2759.29	0.21	0.41	
	3.46	4598.82	0.61	1.07	
	2.08	1609.59	0.10	0.28	
	3.46	2682.64	0.49	0.85	
Mean ASHRAE	2.77	2710.88	0.36	0.66	

3.4 Conclusions

For this work, the most important result of this study is confidence in the ability of the DST model to accurately model the performance of a ground heat exchanger, lending credibility to the decision to use the DST in the simulations detailed throughout this thesis. Prior validation of the DST model has focused on the model performance using calibrated soil properties [47–49]. This work has expanded on the prior work focusing on the performance of the model using only apriori inputs obtained from design documents and thermal response tests. At Site 1, data are available from the point of system startup and groundwater flow is not significant, so the ground properties are unlikely to differ significantly from those measured during the thermal

response tests (although there can be variation throughout a field). At Site 1, calibration was unnecessary because simulation results using apriori inputs to the DST model compared to measured results within measurement uncertainty.

At Site 2, data are available from a point approximately five years after system startup and groundwater flow is significant, so the ground thermal properties and undisturbed ground temperature have changed as compared to the values obtained from the thermal response test. In other words, the thermal history of the ground store is significant. Based on calibration, the undisturbed ground temperature at the beginning of this study is about 1.6 Δ°C lower than it was during the thermal response test; however, a sensitivity study showed that this variation is not a major cause of the simulation error. The thermal conductivity and heat capacity are the major factors determining the model accuracy, and these values can vary throughout a GHX field due to inhomogenieties. In addition, ground water flow can have a significant impact on thermal properties, leading to variation in thermal conductivity with time.

In order to evaluate the significance of the error at Site 2, simulations were run for thermal conductivity and heat capacity values obtained from the ASHRAE handbook. The error in the temperature change across the GHX at Site 2 falls in the range of errors obtained using handbook values, indicating that it is a reasonable design error. In general, however, a location such as Site 2 is not ideal for model validation because of the uncertain thermal history and limited instrumentation. It is also apparent that the best simulation results will be obtained when operational data are available so that the thermal properties and ground temperature input to the model of the GHX can be calibrated to the actual installation.

For this research, it was desirable to include the complexities inherent in a large scale, real world facility, to test the robustness of the DST model as a design tool. However, as

documented throughout this paper, those complexities can lead to unexpected difficulties in data analysis. At Site 1 the data are obtained instantaneously, which, while potentially valuable for assessing building operation, can cause difficulties for research purposes. A turbine meter inserted into the flow will register a signal when the flow is in the process of increasing or decreasing toward a steady state of either on or off. Data are acquired at 15 minute intervals, but the instantaneous measurement of flow rate may not be useful for determining the integrated heat transfer that occurred during the 15 minute interval; for example, if the flow rate measurement occurs as the flow is ramping up, then the heat transfer will be calculated based a low flow rate, leading to an underestimate of the total heat transfer for that time step. An accurate assessment of the model requires that the instantaneous flow rate not change significantly during the time step. In addition, the turbine meter can register flow when there is flow through the header pipe but not through the pipe leading to the field. These are misleading readings that must be removed from the data analysis. Instantaneous measurements can be useful to a researcher if they are acquired at a high data rate (on the order of a minute), but that is generally un-necessary for building owners.

There are several potential solutions to this problem. The data acquisition system could potentially be modified to monitor both instantaneous and average flows or it may be possible to modify the system to obtain more frequent (every minute) instantaneous measurements during the period of interest to the researcher. These options, however, require some modification to an existing system which a building owner may not agree to.

At Site 2 the two primary difficulties were a lack of knowledge about the thermal history of the system and the lack of an existing inline flow rate measurement. Both of these situations reflect the fact that when the facility was designed, only instrumentation that directly influenced

the control of the system, such as a few key temperature measurements, was installed. Although temperature measurements were acquired from the moment of system startup, those data were no longer accessible five years later because it was unnecessary to keep it for system operation. In this case the system was designed for operation but without a need to understand every aspect of the system performance.

This latter situation is likely to be encountered in many smaller systems, where there are fewer operational complexities and therefore a simpler control scheme requiring less monitoring can be implemented. In this system, it would have been difficult to remove sections of pipe to install flow meters or to modify the existing control system. If possible, a situation such as this one, with limited data and an unknown thermal history, should be avoided as a source for providing model verification data. At the very least, if a site such as this is used, it should be understood that there will likely be substantial complications in using the data and calibration will probably be required.

Chapter 4 Optimization

There are three parts to an optimization problem: the objective function, the decision variables, and constraints. The objective function is the relationship that is to be minimized (or maximized depending on the problem) as a function of the decision variables; in this work, the life cycle cost (LCC) is the objective function. The decision variables are the parameters that are varied in order to minimize the objective function; in this work the decision variables include the ground heat exchanger (GHX) length, cooling tower (CT) size, furnace capacity, and control set points. The EFT (Entering Fluid Temperature) to the heat pump is constrained to be less than 35°C and greater than 1.7°C (though these values can be adjusted by the user in FHyGSHP); if either of these constraints is violated, a penalty function is added to the LCC so that the optimizer will know that the design violates the temperature constraints and should be rejected. There are additional constraints on the decision variables in order to limit the potential values to physically realistic values (e.g., the GHX will not have negative length).

An example of the formulation of the optimization problem is given in Eq.(4.1), where x is a vector of the decision variables for the problem and *lower bound* and *upper bound* are vectors of the lower and upper limits on the decision variables. The solution space, i.e. the region in which the optimal value of the objective function will be found, is defined by the limits placed on the decision variables. *Penalty1* is a penalty added to the LCC if the EFT violates either of its bounds. In FHyGSHP the user has the option of including a load imbalance constraint; if the imbalance on the ground between heating and cooling loads (based on the change in the ground temperature over time) exceeds a specified value, then *Penalty2* is added to the objective function. The user also has the option of requiring that the HyGSHP design reduce energy

consumption by a specified amount relative to a conventional design; if the design violates this requirement then *Penalty3* is added to the objective function.

$$\begin{aligned} \min \quad & LCC + Penalty1 + Penalty2 + Penalty3 \\ \text{subject to} \quad & 1.7°C \le EFT \le 35°C \\ & lower\,bound \le x \le upper\,bound \end{aligned} \tag{4.1}$$

The LCC is treated as a black box objective function that is based on the combined effects of a number of transient variables such as building load, air temperature, ground temperature, etc. The decision variables are inter-dependent. For example, if the GHX size is increased, then the CT can be made smaller, but the exact relationship can not be represented in a simple analytical formulation. As implemented, the objective function does not have a simple formulation and the problem is not easily differentiable either analytically or numerically. Gradient-based methods of optimization are therefore not appropriate. Instead, the direct search algorithms SUBPLEX (Nelder-Mead Simplex) and DIRECT are used in FHyGSHP. These algorithms find an optimal solution by evaluating the objective function at various points in the solution space (defined by the boundaries on the decision variables). New search locations are found based on the value of the objective function during prior iterations. The SUBPLEX and DIRECT methods are described in this chapter as applied to a minimization problem, though detailed descriptions are not included in this chapter (see Appendix B). The implementation of optimization in FHyGSHP and the recommended optimization settings are also discussed.

4.1 Overview of Optimization Methods

This section provides a brief description of the SUBPLEX [67] and DIRECT [68] methods of optimization, but more detail on these algorithms can be found in Appendix B.

4.1.1 SUBPLEX

The SUBPLEX method uses the Nelder-Mead simplex algorithm (NMS) [69]. Each step of the method contains a simplex of points that approximate the optimal solution. A triangle is an example of a simplex in two dimensions; a tetrahedron is an example in three dimensions. The objective function is evaluated at each vertex of the simplex (e.g. vertices of a triangle) and the vertices are ranked based on the value of the objective function at each vertex, x, from 1 to $N+1$, where N is the number of decision variables. The goal is to replace the worst vertex (i.e. the one with the largest value of the objective function), x_{N+1}, with a new point; the procedure for accomplishing this is complex and the explanation is included in Appendix B. A new simplex is generated during each iteration. One vertex of the old simplex is replaced to form the new simplex; however, there is no guarantee that the new vertex has a lower value for the objective function than the old vertex.

The process repeats until the NMS termination criteria are satisfied. There are two criteria, either the maximum number of iterations has been reached or the difference between the best and worst objective function evaluations in the current simplex is less than the specified tolerance, τ. NMS is not guaranteed to find a global minimum. The size of the steps taken in the search for a new vertex may be too large and the global minimum might be stepped over. If the steps are too small, the method can become bogged down, or stagnate, around a local or non-optimal solution [69].

According to Rowan [67], NMS:

- can be used on noisy functions,
- is inefficient for $N > 5$,
- works poorly if infeasible points are rejected rather than penalized with a penalty function,

- and requires $O(N^2)$ storage ($N+1$ vertices each of size N).

Rowan designed the SUBPLEX method to improve upon the NMS method. Many optimization techniques locate the optimum by defining an improved search direction in each iteration (e.g. increasing one variable while decreasing another); the SUBPLEX method expands this concept by defining improved subspaces at each iteration and using NMS to search those subspaces.

One of the disadvantages of NMS is that it is inefficient for problems with a large number of decision variables ($N > 5$). The SUBPLEX method combats this problem by creating several mutually orthogonal subspaces of small dimension that, when combined, consider all of the decision variables. For example, there may be a problem with five decision variables. The SUBPLEX method could divide this problem into a two dimensional subspace and a three dimensional subspace. In the 2D subspace, two of the five variables are optimized using NMS while the other three variables are held constant. Once the 2D subspace has reached the NMS termination criterion, the "optimal" values of the first two variables are held constant and the 3D subspace is analyzed using NMS by varying the remaining three variables. This process is repeated until the NMS termination criterion is met for the entire simplex, which is composed of all five vertices. The SUBPLEX method terminates once the simplex becomes sufficiently small or the maximum number of function evaluations has been reached. Until this point, when the NMS criterion is met but the SUBPLEX criterion is not, the subspaces are re-calculated and the evaluation starts again.

Although the SUBPLEX method overcomes some of the limitations of NMS, it still has the limitation that global convergence is not guaranteed. In practice, the SUBPLEX method has been found to converge to different optima based on the value of the initial guess. Another limitation is that it is designed for unconstrained decision variables; therefore, bounds on the

variables are not taken into account when the sample points are selected (they are enforced after the fact) and the search may be inefficient for constrained problems.

The original SUBPLEX method terminates when the simplex becomes small or when the maximum number of function evaluations has been reached. Two additional termination criteria were added to the method for FHyGSHP. One: if the current best value of the function does not change for a specified number of function evaluations, then the optimization process is terminated. Two: if the current best value of the function changes by a specified small amount, then the optimization process is terminated. These criteria are meant to prevent the program from spending significant time trying to find a modestly better solution.

4.1.2 DIRECT

The SUBPLEX method is a practical direct search method, but there is no proof of convergence to a global solution and, in practice, SUBPLEX does not always find a global optimum, so an alternative optimization scheme was sought. The DIRECT scheme (DIviding RECTangles) is also a direct sampling method; the solution space, defined by the boundaries on the decision variables, is sampled in order to locate a global optimum. Finkel and Kelley [70] show that "certain subsequences of the sample points converge to points that satisfy the necessary conditions for optimality… DIRECT is, in the limit, an exhaustive search and will, if [the function] is continuous, find an arbitrarily accurate approximation to the global minimum." Global convergence is guaranteed in the limit, but in practice the optimization is stopped after a finite number of function evaluations, so care is still required to ensure that the optimal returned is satisfactorily close to the global optimum.

The modified version of the DIRECT method as developed by Gablonsky, et al. [71], is used in FHyGSHP by default, although the original version [68] can also be selected. The basic

concept is this: take the entire solution space as defined by the boundaries on the decision variables and divide it into thirds in each dimension, where there is the same number of dimensions as there are decision variables. There are now three intervals in each dimension and the value of the decision variable at the center of each interval is selected. For example, if there are two decision variables, x_1 and x_2, then there are two dimensions, so the solution space is a rectangle. The space is divided in thirds in each dimension and a point is placed at the center of each interval, resulting in 5 points (there is one coincident point), as shown in Figure 4-1.

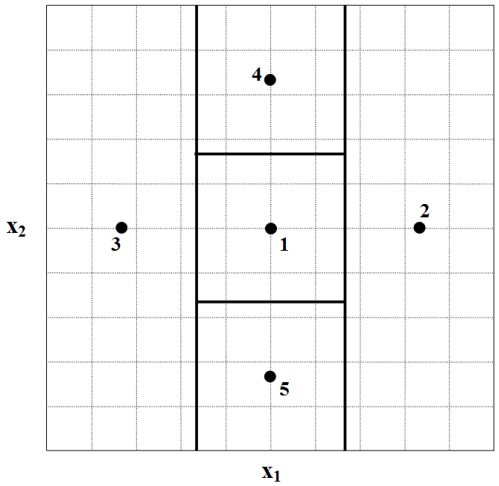

Figure 4-1 Example of a two dimensional problem subdivided using the DIRECT algorithm.

The objective function is evaluated at each point and the solution space is further subdivided based on the value of the objective function until the convergence criterion is satisfied. The solution space decreases in size as the calculations continue and the algorithm narrows in on the optimal solution. The DIRECT method converges if the maximum number of iterations or function evaluations is reached or the size of the solution space is reduced by a specified amount during the subdivision process.

Some modifications have been made to the DIRECT program for FHyGSHP based on observations of how the method behaves when used with this specific problem. The greatest limitation of the DIRECT method is speed; because the method considers the entire solution

space, there can be a significant number of function evaluations. If the maximum number of function evaluations is set low so that the program will terminate early, then the run time can be reduced but the global optimum may not be found. In order to combat this issue, a restart option has been added. If the best function value improves for a specified number of iterations, then the program restarts with different boundaries on the GHX length and CT size variables. The new boundaries are defined by a multiplier on the current best point which defines a lower and upper boundary (which must still be contained within the original boundaries).

The multiplier is applied only to the GHX length and CT size; the range in set point temperatures has less impact on the run time. If a two stage optimization method as described in the next section is used, then the change in the GHX and CT upper and lower bounds for the first stage optimization is defined by Eq. (4.2). In this equation GHX_{best} and CT_{best} are the current GHX length and CT size for the current best optimization point. The upper bound on the GHX becomes tighter as the number of restarts, *r*, increases, while the upper bound on the CT remains unchanged.

$$\begin{aligned} &GHX: \\ &upper\ bound \quad \min\left[\left(1+\frac{0.9}{r}\right)GHX_{best}, original\right] \\ &lower\ bound \quad \max\left[0.5\,GHX_{best}, original\right] \\ &CT: \\ &upper\ bound \quad original \\ &lower\ bound \quad \max\left[0.9\,CT_{best}, original\right] \end{aligned} \tag{4.2}$$

The change in the GHX and CT upper and lower bounds for the second stage optimization or for the *Nominal* optimization (see the next section) is defined by Eq.(4.3).

$$
\begin{aligned}
&GHX: \\
&upper\ bound \quad \min\left[\left(1+\frac{0.9}{r}\right)GHX_{best}, original\right] \\
&lower\ bound \quad \max\left[0.85\,GHX_{best}, original\right] \\
&CT: \\
&upper\ bound \quad \min\left[\left(1+\frac{0.9}{r}\right)CT_{best}, original\right] \\
&lower\ bound \quad \max\left[0.85\,CT_{best}, original\right]
\end{aligned}
\tag{4.3}
$$

These equations were developed based on observations of the optimization process, but future work may include a more detailed examination of what these equations should be (see Chapter 9).

Use of the restart method reduces the solution space and the optimal value can be found more quickly. This method, however, is not foolproof; it is possible to reduce the size of the solution space too quickly and thereby miss the global optimum. Another modification is the addition of a limit on the number of iterations that the current best function value can be repeated before the program exits (this is a user input). This is the same as the first modification to the SUBPLEX method and is used to prevent the program from spending an inordinate amount of time finding a slightly better optimum.

4.1.3 Implementation in FHyGSHP

Optimization is a balance between computational efficiency and accuracy; it is possible to use the DIRECT method to find the global minimum to a great degree of accuracy, but it may require days to achieve that goal. Often, “close enough” is good enough, especially when FHyGSHP is being used solely to compare systems. If each system uses the same optimization settings, the results can typically be compared with confidence although none of the results may be the actual optimal design. FHyGSHP has three optimization methods that can be selected

based on the needs of the user. The default settings can be used for the majority of basic calculations, but if the user has concerns that the reported optimal design is not the actual optimal design, or if they desire a very accurate optimization then the settings can be modified accordingly.

The *Nominal* optimization method uses either the SUBPLEX or DIRECT method to conduct an optimization for the design configuration specified by the user. The *Starter* method is a two-stage optimization. The first stage is a coarse optimization; the time step is set to one hour even if the user has selected a sub-hour time step and the simulation duration may be set to a shorter time period than the user has selected for the main optimization (one year is recommended). The first stage provides a starting point for the second stage, or main, optimization. This optimization uses the time step and simulation duration specified by the user. The first and second stage can use either the SUBPLEX or DIRECT method. For example, the user could specify that the first stage should use the DIRECT method and perform an optimization using a one year simulation of the system operation (the time step is one hour by default). The second stage could use the SUBPLEX method with the user defined time step of ½ hour and a simulation time of 20 years starting from the optimal design arrived at in the first stage. The purpose of this method is to provide a good starting point for the main optimization.

The *Mix* method is similar to the starter method, but the first stage does not run a coarse optimization. Instead, the first stage completes a full optimization using the user specified time step and simulation duration to find a starting point for the second stage, which also uses the user specified time step and simulation duration. The purpose of this method is to generate a potentially better starting point for the second stage optimization. In theory this method has the potential to be the most accurate, but it may also take the most time to arrive at an optimal result.

Sometimes the optimization does not converge to an optimum; in these situations the LCC is generally greater than 1e8 because the design has violated some constraint, leading to a non-zero penalty function. A result such as this requires the user to modify the optimization settings or perhaps loosen the constraints in order to find an optimum. In order to reduce the chances of the optimization failing, if the optimization fails then the starting point for the optimization is perturbed and it is re-run; this can occur up to four times. Notes are written in the log file "optimization_summary.txt" to indicate that this has occurred. For the *Starter* and *Mix* methods, only the second stage optimization is re-run with the perturbed starting point.

4.2 Evaluation and Comparison of Optimization Options

Multiple optimization options are available in FHyGSHP for two reasons: 1) a knowledgeable user has the option of changing the settings in order to find the most appropriate method for their specific purpose and 2) some problems are difficult to optimize, so in the event that an optimization fails alternative methods can be tried. However, an optimization method must be selected for general use so that the typical user with a typical problem can design a system without needing any expertise in optimization. This section provides a detailed study of the seven optimization techniques available in FHyGSHP and listed in Table 4-1.

Table 4-1 The seven optimization methods studied.

Method	Optimization Method	Main Algorithm	Starter Algorithm
1	Nominal	SUBPLEX	
2	Nominal	DIRECT	
3	Starter	SUBPLEX	SUBPLEX
4	Starter	SUBPLEX	DIRECT
5	Starter	DIRECT	SUBPLEX
6	Starter	DIRECT	DIRECT
7	Mix	SUBPLEX	DIRECT

Optimization was performed using each of these seven methods in Phoenix, Atlanta, St. Louis, and Salt Lake City. Note that Phoenix provides a particularly difficult optimization

problem due to the extreme imbalance between cooling and heating loads; therefore, it is an ideal case for testing the robustness of an optimization method. The design that results in the minimum LCC for all seven methods is considered the optimal design, although it is possible that this LCC is not actually the global optimum. The design and LCC found by each method are compared to the optimal design and LCC. The methods are evaluated for the ability to find an optimal or near optimal design in multiple locations (i.e. robustness) and the time to convergence. Using these criteria, method 4, the *Starter* method with DIRECT for the first stage optimization and SUBPLEX for the second stage optimization, is the recommended optimization method.

The following sections discuss the study conducted in detail and present a full list of the optimization parameters.

4.2.1 Discussion

Figure 4-2 through Figure 4-5 show the GHX length, CT size, furnace capacity, and LCC for each optimization method (see Table 4-1) in each location, normalized by the optimal design in that location. For example, in St. Louis the design with the minimum LCC was obtained by using method 4 – the *Starter* method with DIRECT for the first stage optimization and SUBPLEX for the second stage optimization. All other cases were compared to this case. The furnace capacity in Phoenix is not shown in Figure 4-4 because it is at or near zero for all cases. In cases where the optimization failed the LCC was > 1e8, so those points are not shown in Figure 4-5.

There is variability in the size of the GHX, CT, and furnace as a function of the optimization method, but this variability does not carry through to the LCC, which varies from within a few percent of the minimum value to 17% greater than the minimum value. A 17% more expensive design is certainly not desirable, but this 17% increase is associated with a 40%

smaller GHX and a 90% larger CT, so extreme differences in component sizes do not lead to as extreme differences in LCC.

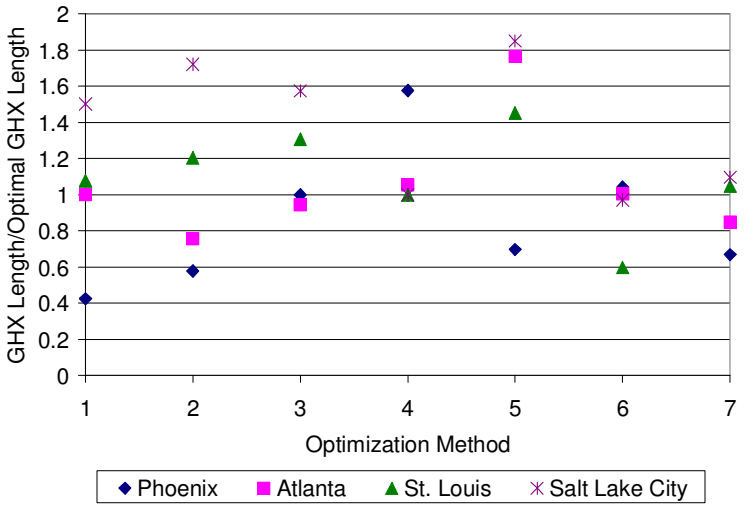

Figure 4-2 GHX length for each case normalized by the optimal length of all cases.

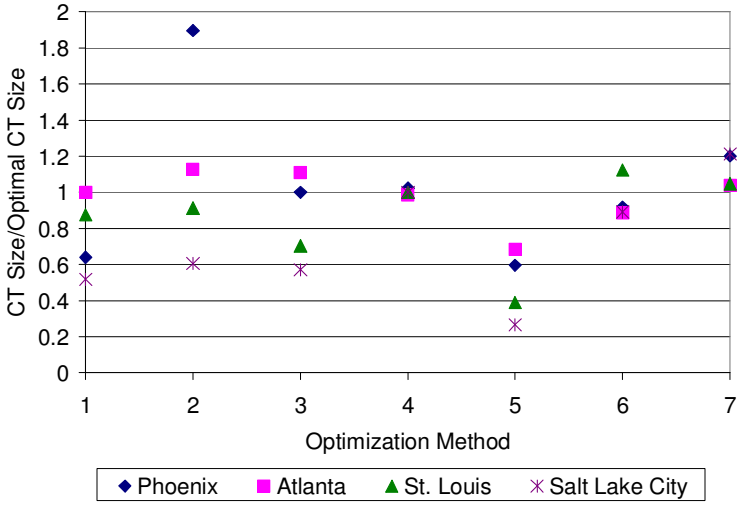

Figure 4-3 CT size for each case normalized by the optimal length of all cases.

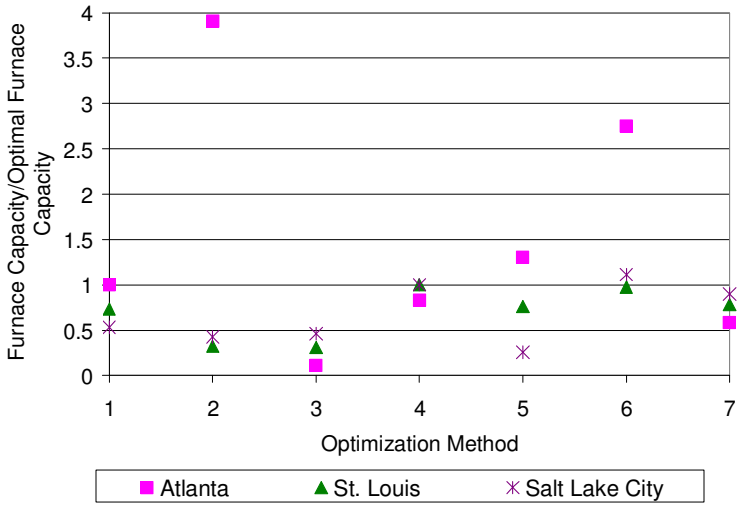

Figure 4-4 Furnace capacity for each case normalized by the optimal length of all cases.

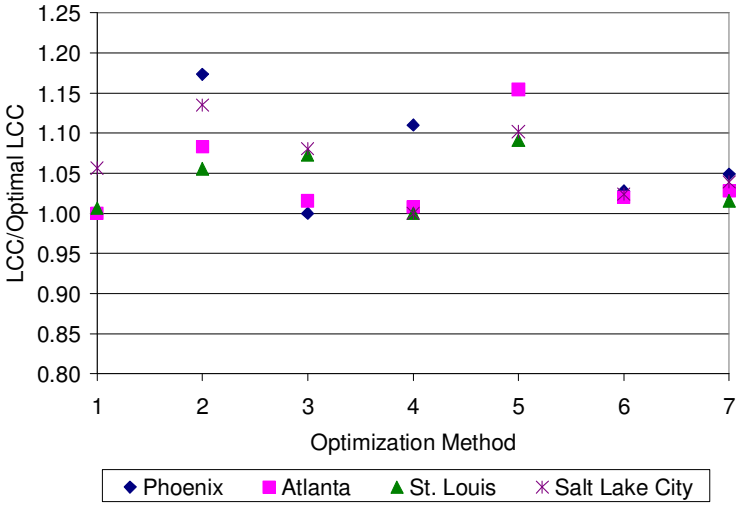

Figure 4-5 LCC for each case normalized by the optimal length of all cases.

None of the optimization methods led to the optimal design in all four locations. In Phoenix, method 3 was optimal, in Atlanta, method 1 was optimal, and in St. Louis and Salt Lake City, method 4 was optimal. Some of the methods can be removed from consideration as the recommended general method. Methods 1 and 5 failed to converge in Phoenix and method 6 failed to converge in St. Louis, so these three methods are not sufficiently robust to be recommended for general use. Although these methods failed, the components sizes found using these methods are shown in the figures because they can provide some information about why

the optimization failed. For example, using method 5 in Phoenix, the GHX length (see Figure 4-2) and CT size (see Figure 4-3) are smaller than optimal, indicating that this method was unable to move away from a non-optimal location.

As previously mentioned, a design with a LCC 17% greater than optimal is undesirable. This result was obtained using method 2 in Phoenix, so this method is also removed from further discussion. There are now three methods remaining for consideration: 3, 4, and 7. The least variability in LCC across location was found using method 7; the LCC was within 5% of optimal in all four locations. However, another factor to consider is the time required to complete the optimization. Figure 4-6 shows the time required for the calculation by each method normalized by the time required by the optimal method in each location. Method 3 converges to an optimal value in less than or equal time to the optimal method, method 4 converges to an optimal value in equal time to the optimal method, and method 7 requires substantially more time. There may be situations when this additional time is justified, but in general method 3 or 4 will lead to a sufficiently good near optimal solution in less time, so method 7 is also removed from consideration as the generally recommended method.

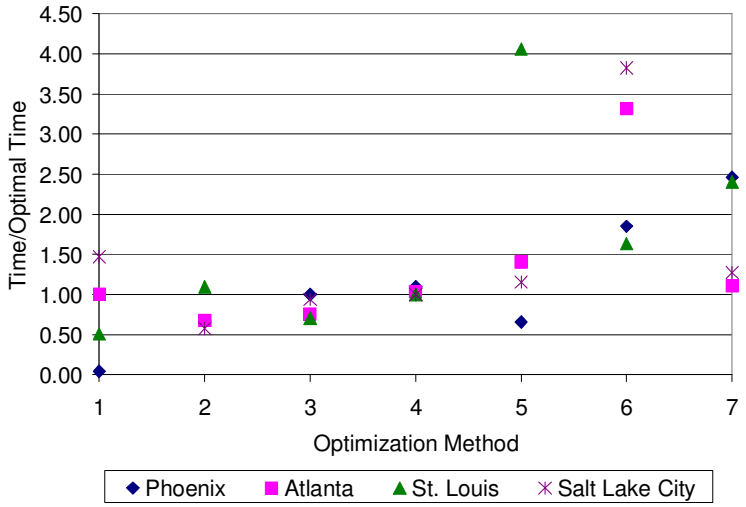

Figure 4-6 Solution time for each case normalized by the time to find the optimal design.

Methods 3 and 4 produce similar results, but method 4 shows less variation in the size of the GHX and CT, especially if the results from Phoenix are removed from the analysis. Method 4 was also the optimal method in two locations and is theoretically more robust than method 3. The DIRECT method is preferred for the first stage optimization because it examines a larger portion of the solution space than SUBPLEX and is less likely to overlook an optimal region. For these reasons, the *Starter* method with DIRECT for the first stage optimization and SUBPLEX for the second stage optimization is recommended as the general optimization method.

4.2.2 Optimization Parameters

This section contains a summary of the optimization parameters and recommended settings. Additional information on these parameters can be found throughout this document, but Chapter 7 and Appendix B provide the most extensive information.

Table 4-2 Optimization parameters (*Advanced parameters).

Method		Valid values	Recommended value
Optimize	Should an optimization be performed?	Yes/No	
Optimization method	Should the optimization use the starter method to set the initial guess value?	Starter/Nominal	Starter
User supplied guess value	If the user has a good estimate of the optimal design they can choose to use that as the guess instead of the ASHRAE sizing method [59].	Yes/No	
*Optimization algorithm	Which of the two methods should be used for the optimization? This parameter is set for both the starter and main methods.	DIRECT/SUBPLEX	Starter: DIRECT Main: SUBPLEX

General		Valid values	Recommended value
Maximum number of function evaluations	The maximum number of function evaluations before the optimization will terminate.	$(0,\infty)$	1000
Variable bounds	Set the lower and upper bounds on each variable; note that the bounds may change based.	$(-\infty,\infty)$	100 < GHX length < 100000 30 < CT size < 3000 -5 < CT2 < 20 -2 < CT1 < 50 -2 < GHX1 < 50 -2 < TPC < 50 -5 < DTPC < 20
Initial guess	Initial guess value for each variable; when the "User supplied guess value" is set to yes, these values are used as the initial guess.	$(-\infty,\infty)$	Variable

DIRECT		Valid values	Recommended value
Maximum number of iterations	The maximum number of iterations before the optimization will terminate; if the maximum number of function evaluations is reached first, then the optimization will terminate based on that criterion.	$(0,\infty)$	200
*DIRECT algorithm	Choose to use either the original or modified version of the algorithm [71].	Original/Modified	Modified

DIRECT		Valid values	Recommended value
*ε	Constant used to ensure that the best function value decreases with each new potentially optimal hyper-rectangle; the solution is relatively insensitive to this parameter.	$[10^{-3}, 10^{-7}]$	10^{-4}
*Terminate based on the percent reduction in the volume of the hypercube	Terminate if the volume of the hypercube is reduced by a specified percentage; unused if the value is set to 0. Larger values will lead to earlier termination.	$[0,\infty)$	0
*Terminate based on the size of the hyper-rectangle	Terminate if the size of the hypercube is less than the specified amount; unused if the value is set to 0. Larger values will lead to earlier termination.	$[0,\infty)$	0
*FHyGSHP version	Should the modifications to DIRECT made for the FHyGSHP program be used?	Yes/No	Yes
*Multiplier on ASHRAE based sizes	Specify the lower and upper bounds on the GHX length and CT size by specifying an amount to multiply the ASHRAE (or user supplied guess) by. For this problem it is usually more important to have a larger upper bound.	$[0,\infty)$	Lower bound: 0.3 Upper bound: 4
*Number of iterations before restart	Set the number of nominal DIRECT iterations to complete before using restart. A lower number will result in more changes in the size of the solution space.	$(0,\infty)$	Starter: 2 Main: 4
*Maximum number of restarts	The maximum number of times that the restart can be used.	$[0,\infty)$	100
Unchanging optimal value	Maximum number of iterations the optimal value can remain unchanged before terminating. Lower values lead to earlier termination but may miss the global optimum.	$(0,\infty)$	15
*Specified change in optimal value	If the best function evaluation changes by less than the specified amount between iterations, the program will terminate.	$[0,\infty)$	0.000001

SUBPLEX		Valid values	Recommended value
*Reflection coefficient, α	Magnitude of the reflection move.	$(0,\infty)$	1
*Contraction coefficient, β	Magnitude of the contraction move.	$(1,\infty)$	2
*Expansion coefficient, γ	Magnitude of the expansion move.	$(0,1)$	0.5
*Shrinkage coefficient, δ	Magnitude of the shrinkage move.	$(-1,0)$	-0.5
*Simplex reduction coefficient, ψ	Accuracy of the subspace search; smaller values lead to greater accuracy but also more iterations.	$(0,1)$	0.5
*Step reduction coefficient, ω	Scaling of the step size.	$(0,1)$	0.25
Scale	Sets the initial step size on each variable.	$(0,\infty)$	Variable
*Convergence tolerance	Termination criteria; see Appendix B for details.	$(0, \infty)$	Starter: 1 Main: 0.25
Unchanging optimal value	Maximum number of iterations the optimal value can remain unchanged before terminating. Lower values lead to earlier termination but may miss the global optimum.	$(0, \infty)$	Starter: 15 Main: 15
*Specified change in optimal value	If the best function evaluation changes by less than the specified amount between iterations, the program will terminate.	[0, 1]	10^{-7}

Chapter 5 Weather Variability and Generation

In general, building simulation programs use a typical meteorological year (TMY) of weather data as one of the inputs for the models. If a multi-year simulation is performed, this single TMY file is used for every year in the simulation, so the year-to-year variability that occurs in reality is not considered in the simulation; this is the default method used in the FHyGSHP program. This chapter first assesses the impact of this simplification on the design of a hybrid ground source heat pump (HyGSHP) and then explains how synthetic weather and load data can be developed based on an input file containing a single year of hourly dry and wet bulb temperatures and cooling and heating loads. The designs of a HyGSHP using measured temperatures and synthetic temperatures are compared.

5.1 The Significance of Variability

This section presents a study of the impact of year-to-year weather variability on the design of a HyGSHP. It was completed using the HyGCHP program [4,7,11,72] and is adapted from a published paper [10].

5.1.1 Introduction

The HyGCHP (Hybrid Ground Coupled Heat Pump) program was originally developed for ASHRAE Technical Research Project 1384 [4] using TRNSYS [15]. The user provides an input file containing hourly cooling load, heating load, dry bulb temperature and wet bulb temperature for a single year; the default operation of the program is to re-use this single year for every year of a multi-year simulation. The program then optimizes the size of the components in the system (boiler and GHX, CT and GHX, or GHX only) as well as the set point temperatures used to control each component in order to minimize the life cycle cost (LCC) associated with installing and operating the system over its life (typically 20 years).

In the standard methodology, the building loads are calculated using a weather file that is based on a Typical Meteorological Year (TMY2), generated from observations of a 30 year period from 1961 to 1990 [73]. This representation does not incorporate the year-to-year variation in weather that actually occurs; the design obtained using TMY2 weather data may be under-sized for severe weather years. Therefore, an optimal GSHP design based on weather data that include year-to-year variations and therefore include unusually severe weather years is different from a design based on a TMY2 weather file.

5.1.2 Calculation of Building Loads

The baseline optimized boiler hybrid design for a 455 m^2 office building in Madison, WI and CT hybrid design for a 8856 m^2 office building in Atlanta, GA were created using a standard TMY2 weather file derived from the 1961-1990 National Solar Radiation Data Base (NSRDB) [73]. A TMY3 weather file derived from the years 1991-2005 is available, but the TMY2 file has been more widely used to date, so it was chosen for this study. However, some cases were analyzed using the TMY3 file and the results were similar to those obtained from the TMY2 weather file. Optimal hybrid designs for these buildings were also created using individual annual weather data for the years 1991-2005 from an update to the NSRDB [74]; these measurements were acquired from approximately the same latitude and longitude as the TMY2 data, so the comparison should be valid. The simulation optimization of the hybrid design is based on a 20 year operating period; however, only 15 individual years of weather data are available. Therefore, the first 15 years of the simulation utilized weather data from 1991-2005 in sequential order and the final 5 years were simulated by returning to the beginning of the file (i.e., using 1991-1995 weather data).

The building loads for the 15 years were calculated using the Equivalent Full Load Hours (EFLH) program developed for ASHRAE Technical Research Project 1120 [75] with the settings shown in Table 5-1 and these building loads were input to HyGCHP in the same order as the weather data. Parameters not shown in the table were set to their default values [75].

Table 5-1 Input parameters input to the EFLH program for a 455 m^2 in Madison and a 8856 m^2 building in Atlanta.

Parameter	Value	Value
Location	Madison, WI	Atlanta, GA
Area of building	455 m^2	8856 m^2
# of floors	1 floor	1 floor
Wall height	3 m	3 m
Fraction of building in core zone	0.33	0.934
Average perimeter loss coefficient	2337 W/K	3517 W/K
Average core loss coefficient (roof & floor)	467 W/K	704 W/K
Fraction of horizontal solar that is heat gain	0.1015	0.010
Period in session (for school)	N/A	N/A
Weekday occupancy (# people)	30 people	1200 people
Weekday occupancy times	8am - 5pm	9am – 9pm
Weekend occupancy (# people)	2 people	1200 people
Weekend occupancy times	8am - 5pm	9am – 9pm
Occupied lighting and equipment gains	6.8 W/m^2	13.9 W/m^2
Fraction of occupied gains during unoccupied times	0.042	0.27
Infiltration (air changes/hr)	0.4 air changes/hr	0.4 air change/hr
Fraction of infiltration during unoccupied times	0.5	0.5
Fresh air required during occupied times	0.54 cfm/m^2	1.6 cfm/m^2
Cooling set point	24.4°C	24.4°C
Heating set point	21.1°C	21.1°C

The peak heating and cooling load for each year and the mean of these loads over the simulation period were calculated. The ratio of the annual heating to annual cooling loads was calculated as well. Figure 5-1 shows the results of these calculations for each building; these results are normalized by the corresponding result calculated using TMY2 weather data and the value of the TMY2 result is shown. The range of values calculated during the 15 years is indicated by the error bars. Notice that the peak heating and cooling loads calculated from the 15 years of actual weather data are slightly lower than the peak values calculated from the TMY2 data. The error bars show the variation in the building loads; the loads are strongly influenced by

weather and change substantially from year-to-year even for a large building. The Heating Degree Days (HDD) and Cooling Degree Days (CDD), calculated on a base of 18.3°C, for both sets of weather data are compared in Figure 5-1, with the Madison data on the left and the Atlanta data on the right. In both locations there is a noticeable difference between the degree days for TMY2 and annual data.

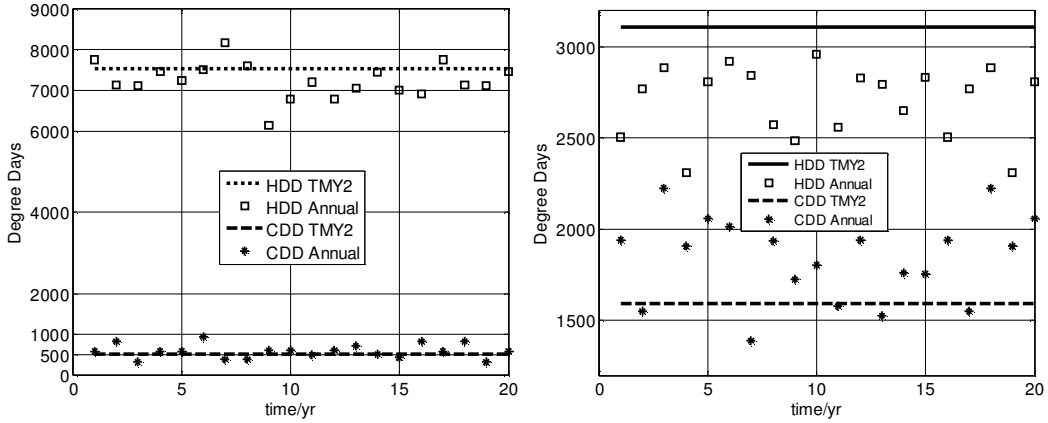

Figure 5-1 HDD and CDD for Madison, WI (left) and Atlanta, GA (right). The lines show the values for the TMY2 data.

$$CDD = \sum_{i=1}^{N} \left(\overline{T}_{day,i} - T_{base} \right)^{+}$$
$$HDD = \sum_{i=1}^{N} \left(T_{base} - \overline{T}_{day,i} \right)^{+} \qquad (5.1)$$

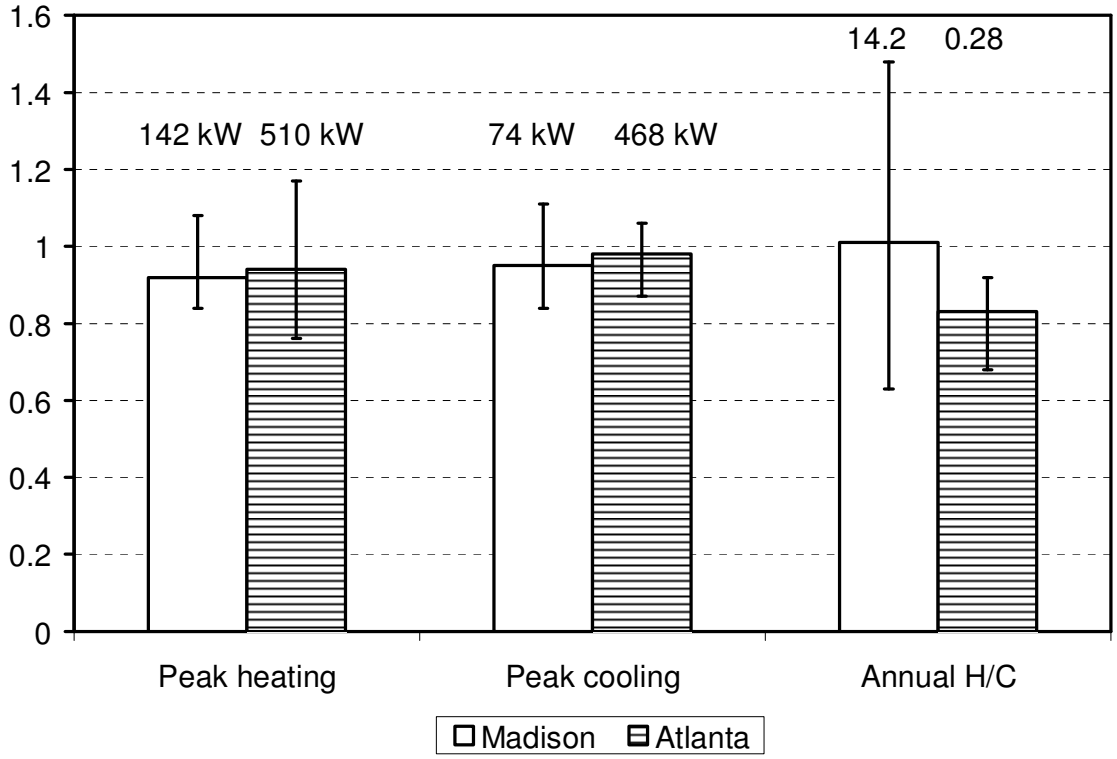

Figure 5-2 The average peak heating and peak cooling loads and the ratio of the annual heating to cooling load based on 15 years of individual weather files normalized by the same values calculated based on the TMY2 weather data. The error bars indicate the range of each value over the 15 years. The value of each parameter based on TMY2 weather data is shown.

5.1.3 Results for the Office in Madison

The office building in Madison is heating dominated, with a mean annual heating to cooling ratio over 15 years of approximately 14. Figure 3 shows the characteristics of a HyGCHP boiler hybrid designed for this building using 15 years of actual weather data. As in Figure 5-2, the results are normalized by the same quantities obtained using TMY2 weather data in order to clearly show the effect of actual year-to-year weather variation on the design and the value of the TMY2 result is shown. The parameters shown in Figure 5-3 and Figure 5-4 include:

- *LCC* – Life Cycle Cost over 20 year simulation
- *LGHX* – Ground Heat Exchanger length
- $Q_{cap,boiler}$ – Size of boiler
- *DELTA* T_g – Change in ground temperature after 20 years

- Q_{rej} – Heat rejected to the ground over 20 years
- Q_{abs} – Heat removed from the ground over 20 years
- $Q_{cap,CT}$ – Size of he cooling tower

Figure 5-3 shows that the optimal size of the GHX is the same for both models. The most dramatic effect of considering the actual weather variation in the design is to increase the size of the boiler by approximately 11% relative to a design obtained from TMY2 weather data. In this heating dominated case, the ground temperature decreases over time due to the large unbalance between the heat removed from the ground during the heating season and added to the ground during the cooling season. However, the ground temperature decrease over the course of 20 years is 5.6% less when 15 years of actual data are used, indicating that the boiler is used for heating more often than in the nominal case. The LCC decreases slightly when 15 years of actual data are used for design. An examination of the components of the LCC shows that although the first cost increases slightly due to the increase in boiler capacity, the LCC decreases because the annual fuel cost decreases. The boiler is used more often in the design based on actual data, increasing gas consumption; therefore the GHX is used less, reducing electricity and resulting in a net decrease in LCC.

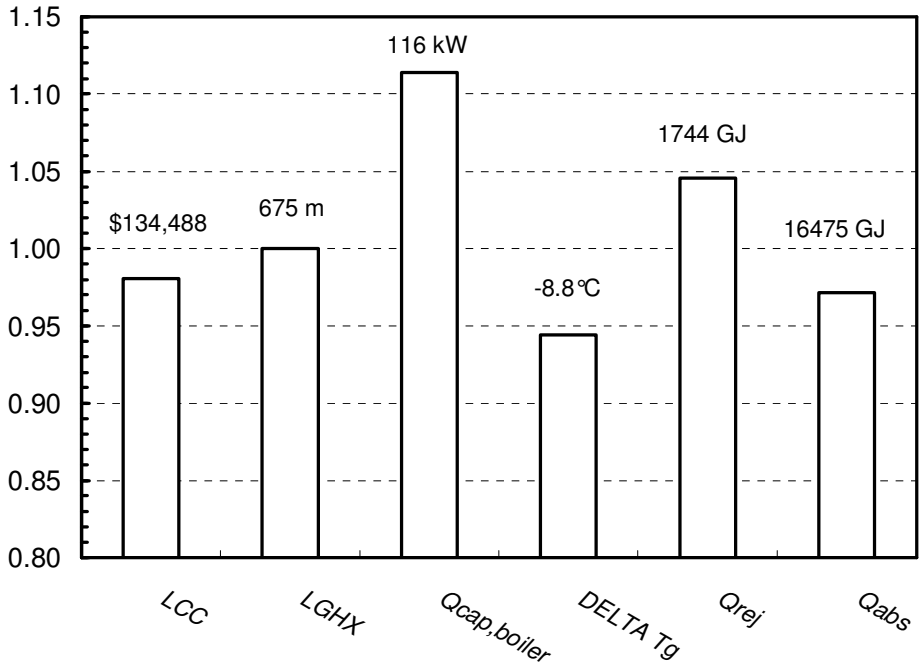

Figure 5-3 Characteristics of a boiler hybrid designed for the building in Madison using 15 years of actual annual weather data. The values are normalized by the values for the TMY2 weather data. The value of each parameter based on TMY2 weather data is shown.

In order to assess the consequence of this difference, the optimal design using TMY2 data was tested using 15 years of actual data. In this design, there were only 34 hours of operation over 20 years where the entering fluid temperature (EFT) to the heat pump was below the 1.7°C lower operating limit and only ten hours when it was above the 35°C operating limit. The consequence of using the TMY2 weather file for design is that the system is slightly under-sized, but the reality is that the consequences are minimal. When the optimizer is provided with actual yearly weather data, it elects to increase the size of the supplemental heating system (the boiler) in order to accommodate severe weather years.

5.1.4 Results for the Office in Atlanta

The office in Atlanta is cooling dominated with a mean annual heating to cooling ratio of approximately 0.3. The characteristics of a hybrid cooling tower design (without boiler backup) are shown in Figure 5-4. Each value is normalized by the same characteristics obtained using

TMY2 data and that value is shown. In addition to the parameters listed above, $Q_{cap,CT}$ is the cooling tower size and Q_{CT} is the heat rejected by the cooling tower. The most significant effects of using the 15 years of actual weather data are that $Q_{cap,CT}$ increases by approximately 19% and L_{GHX} decreases by 8%. The *LCC* increases slightly when 15 years of actual weather data are used because the cooling load associated with the annual weather data is nearly identical to the load calculated with the TMY2 data (see Figure 5-2) and yet the system must deal with particularly severe weather years. Notice that the optimizer has elected to increase the size of the supplemental cooling system in order to handle particularly severe weather years, just as in the case of a boiler hybrid in Madison. This choice tends to reduce the variation in the ground temperature over the course of the simulation.

In this situation the consequence of using the TMY2 data is a little more severe; using the TMY2 design with the annual weather data results in 310 hours in which the 35°C operating limit is exceeded. This is 0.18% of the hours over the course of 20 years as compared to 0.02% of the hours over 20 years for TMY2 weather data. This is still a small percentage, but when the number of hours of unmet load is evaluated on a yearly basis as shown in Table 5-2, it becomes apparent that there are some years in which there are a relatively large number of hours when the loads are not met. For example, in the last year of operation 1.23%, or 108 hours, of unmet load occur. In addition, the unmet loads tend to occur during the afternoon, starting around 1 pm and peaking around 4 pm, hours in which the building is likely to be occupied; the severity of this under-sizing is highly dependant on building use and the actual weather conditions. Another consequence of this undersizing is that the system efficiency is reduced when operating near the design limits. The design using TMY2 data is under-sized and in this case, the optimizer chose to

increase $Q_{cap,CT}$ in order to accommodate the actual conditions. This result indicates that TMY2 weather files should be used with caution.

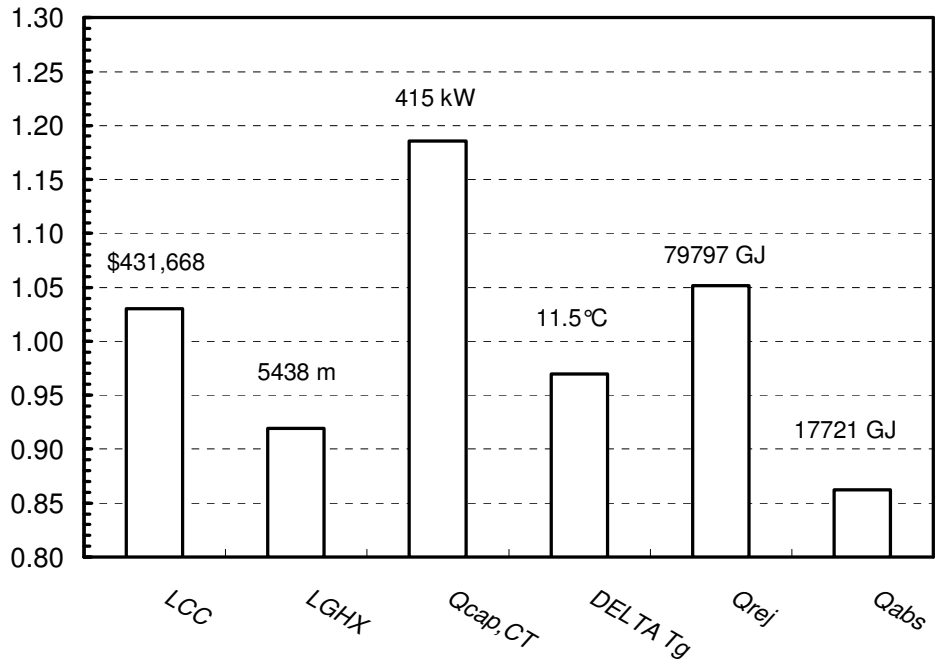

Figure 5-4 Characteristics of a cooling tower hybrid designed for the building in Atlanta using 15 years of actual weather data. The values are normalized by the results from the TMY2 weather data. The value of each parameter based on TMY2 weather data is shown.

Table 5-2 Number of Hours of Unmet Load each Year

Year	5	9	10	12	15	16	17	18	20
% hours over 35°C	0.48	0.26	0.14	0.01	0.06	0.39	0.05	0.92	1.23
# of hours	42	23	12	1	5	34	4	81	108

Previous studies have shown that L_{GHX} is based on the peak heating load in a cooling dominated hybrid system [1,4]. Therefore, the reduction in L_{GHX} is somewhat counter-intuitive because the peak heating load is not less for the 15 years of actual weather data than it is for the TMY2 data. Figure 5-2 shows that there is at least one year in which the peak heating load associated with the 15 years of actual data exceeds the peak heating load based on a TMY2 weather file and yet the optimizer has elected to reduce L_{GHX}. In order to understand this result,

it is necessary to understand the impact of weather sequencing on the design; i.e. how does the design change if the most severe year is the first year in a 20 year simulation (or the last year)?

5.1.5 Weather Sequencing

For a cooling dominated, cooling tower (CT) hybrid system (without boiler backup), the GHX must provide all of the heating required by the building. Previous studies have found that the lowest cost system will size the GHX so that it just meets the peak heating load and allow the cooling tower to meet any cooling load that cannot be met with the GHX. The ground temperature tends to rise for this type of system. A similar design rule has been identified for a heating dominated boiler hybrid system. The GHX is the only source of cooling and therefore the lowest cost system sizes the GHX so that it just meets the peak cooling load and allows the boiler to meet any heating load that is unmet by the GHX. The ground temperature tends to fall for this type of system.

With this in mind, the worst weather sequence that may be encountered by a cooling dominated CT hybrid occurs when the most severe heating year is placed at the start of the 20 year simulation and the most severe cooling year is placed at the end of the simulation. In the first year the ground temperature is lowest and therefore the GHX is least effective in heating mode. In the final year of the simulation the ground temperature is highest and therefore the GHX is least effective in cooling mode. This sequence leads to the most conservative system design because it is forced to deal with the worst possible weather pattern observed in the 15 years of data. The opposite occurs for a boiler hybrid system optimized for a heating dominated building. The most conservative design is obtained when the most severe cooling year is placed first and the most severe heating year is placed last.

Two weather sequences were used for the optimization for the studies presented in this section. One sequence placed the peak heating year first and the peak cooling year last (labeled *PH, PC*), and the other placed the peak cooling year first and the peak heating year last (labeled *PC, PH*). In the standard sequence the optimal design is calculated using the actual weather sequence (i.e. 1991-2005, 1991-1995); this design is used as a basis for comparison in the following sections.

5.1.1.5 Boiler Hybrid

The characteristics of the optimized designs for the PC, PH and PH, PC sequences applied to the office in Madison are normalized by the standard sequence and shown in Figure 5-5. The results of the standard sequence design are also shown in this figure. When the peak heating year is first, the GHX size is unchanged, as expected because the heating load is met by both the boiler and GHX. When the peak cooling year is first, the GHX size increases by 13% because it is the only means of meeting the cooling load. The ground temperature is highest in the first year, which compromises the ability of the system to meet the abnormally severe cooling load in the first year.

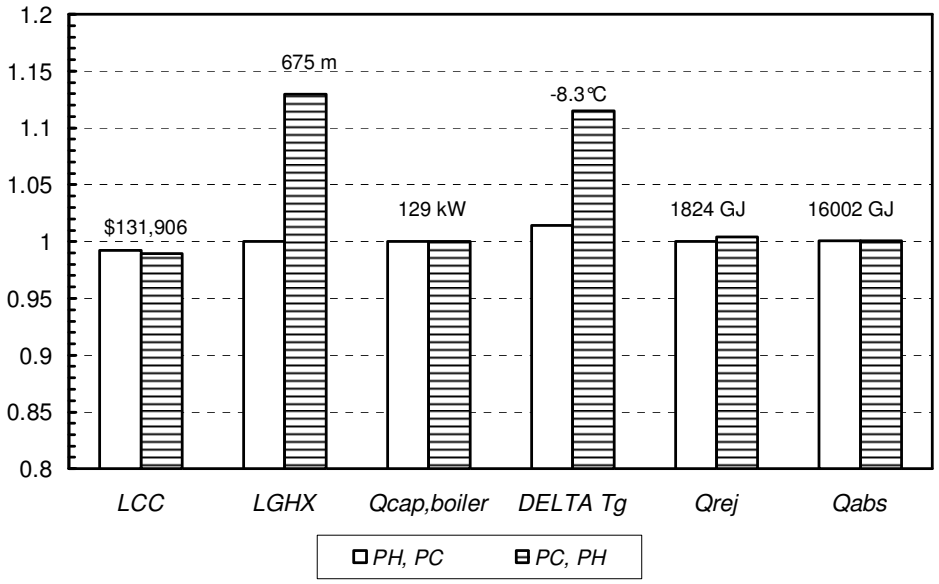

Figure 5-5 Characteristics of a boiler hybrid system designed for the building in Madison using weather data where the peak heating year is first and the peak cooling year is last (PH, PC) and vice versa (PC, PH). The results are normalized by the design obtained using the standard weather sequence. No matter where the peak load years are sequenced, the boiler size is unchanged. However, the GHX size increases by 13% when the peak cooling year is first. The value of each parameter based on the standard sequence is shown.

5.2.1.5 Cooling Tower Hybrid

The characteristics of the optimized designs for the PC, PH and PH, PC sequences applied to the office in Atlanta are normalized by the standard sequence and shown in Figure 5-6. The results of the standard sequence design are also shown in this figure. It is worthwhile to note the extreme differences in the design obtained based on the sequence of the weather years. When the peak cooling year is first, $Q_{cap,CT}$ increases nearly 10% and L_{GHX} decreases approximately 14%. This is the expected behavior. The GHX size is based on the heating load and the most severe heating load is encountered in the last year when the ground temperature is highest. As a result, a smaller GHX will suffice. The smaller GHX is not meeting as much of the cooling load and therefore $Q_{cap,CT}$ increases. When the peak heating year is first, L_{GHX} increases nearly 39% and $Q_{cap,CT}$ decreases just over 15%. The GHX is the only source of heating. Therefore, when the peak heating year is encountered in the first year when the ground temperature is lowest, L_{GHX} must increase dramatically to meet this abnormally high heating

load. In this case, $Q_{cap,CT}$ decreases because more of the cooling load can be met by the large GHX.

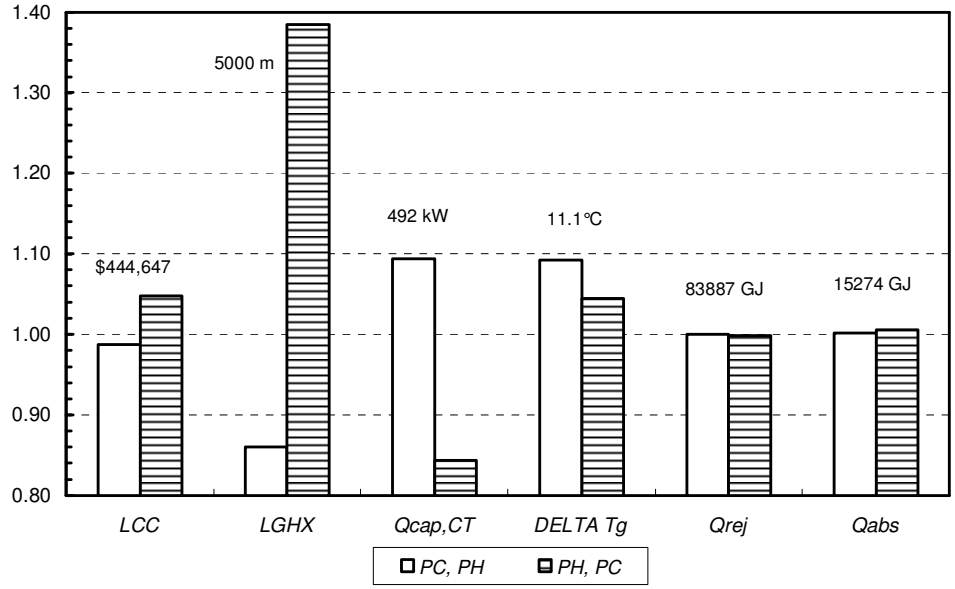

Figure 5-6 Characteristics of the CT hybrid designed for the building in Atlanta using weather data where the peak cooling year is first and the peak heating year is last (PC, PH) and vice versa (PH, PC). The results are normalized by the design obtained using the standard sequence. The value of each parameter based on the standard sequence is shown.

In both hybrid systems, changing the sequence of the building loads changes the optimal design even more versus a design based on a TMY2 weather file. This study emphasizes that the system should be designed so that it can meet load even in the face of severe weather encountered at any point during the system life. If a boiler hybrid system is being designed then a severe cooling year should be placed at the start of the 20 year simulation. If a CT hybrid is being designed then a severe heating year should be placed at the start of the 20 year simulation.

5.3.1.5 Supplemental Heating

The results of the last section suggest that the system design of a CT hybrid for a cooling dominated building is most challenged when the most severe heating year occurs early in the system's life. In this case, the GHX must become very large and expensive to assure that the

system can meet the exceptionally large heat load while the ground temperature is low when there is no boiler. The majority of commercial office buildings in the US are cooling dominated. Therefore, a method to improve the CT hybrid design in order to accommodate severe heating loads associated with severe weather years has been evaluated. Rather than increasing L_{GHX} to meet severe heating loads encountered only occasionally during the life of the system, it may be more economical to supplement a CT hybrid with another source of heating. A simple model was created that allows a portion of the heating load to be shifted from the GHX to a supplemental source. The model of the TRNSYS controller used in the HyGCHP simulation was modified so that when the total heating load exceeds a control set point, Q_{set}, then the GHX will meet a load equal to Q_{set} and the supplemental source will meet the remaining load. If the control parameter Q_{set} is greater than the total heating load then the entire load is met by the GHX and the supplemental source is not used. The control parameter Q_{set} is varied by the optimizer (together with the other design parameters) in order to minimize the life cycle cost of the system. It is assumed that this supplemental source uses natural gas which is consistent with a gas-fired boiler backup system placed on the building (rather than the loop) side of the system. The total cost of the gas is estimated by multiplying the cost per GJ by the heat supplied by the supplemental source. The cost was varied in this study, but the design did not change (although the LCC did), so only one set of results is presented. The first cost and any maintenance costs associated with the supplemental source were neglected.

Figure 5-7 shows the design parameters for PH, PC and Supplemental normalized by the design parameters obtained based on the standard sequence of years and not including a boiler backup system. The PH, PC results are the same as those shown in Figure 6 and the results of the model with no boiler backup are shown. The Supplemental results are those obtained including a

boiler backup using the PH, PC sequence. In the standard CT hybrid design with the peak heating year first, the LCC increased by about 5% due to a 39% increase in L_{GHX} and a 16% decrease in $Q_{cap,CT}$. In the modified CT design with a supplemental heat source, the LCC decreased by 2.5%, due primarily to a 28% reduction in L_{GHX}, and $Q_{cap,CT}$ increased by 13%. $Q_{GHX,heat}$ is the total heat load carried by the GHX over the 20 year simulation; it decreases when a supplemental source is added. The effect of adding a supplemental heat source was also evaluated using the TMY2 weather data and is presented in Figure 5-8 normalized by the design using a standard CT hybrid also designed using TMY2 weather data. The results of the model using TMY2 weather data and no boiler backup are shown. The same general trend holds; LCC decreased due to a decrease in L_{GHX}, but $Q_{cap,CT}$ increased in order to meet the cooling load that is no longer being met by the GHX.

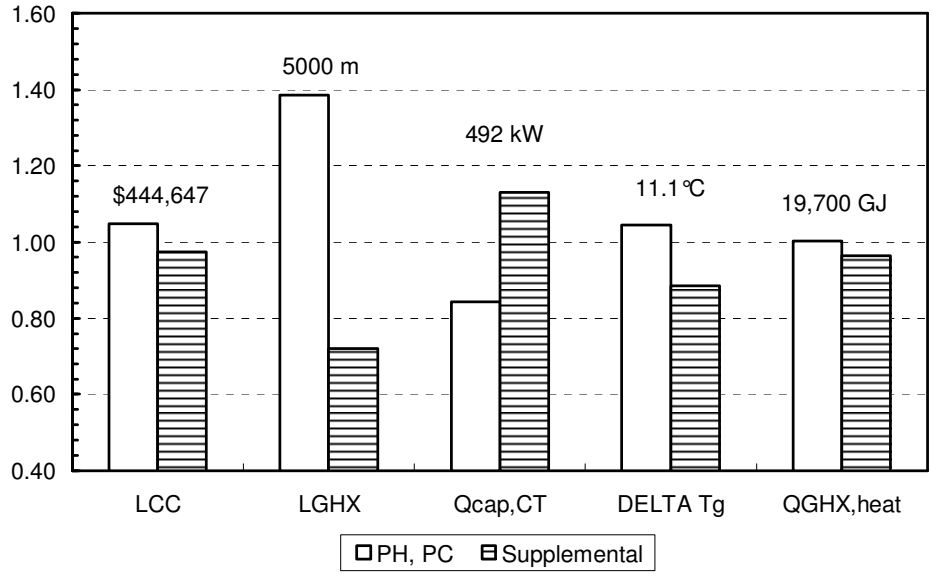

Figure 5-7 Characteristics of two designs of a cooling tower hybrid for the office in Atlanta. The PH, PC design is the same as shown in Figure 5-5. The Supplemental design is the result associated with a design that includes boiler backup and 15 years of actual weather data, normalized by the results from a system without boiler backup. The value of each parameter based on the design with no boiler backup is shown.

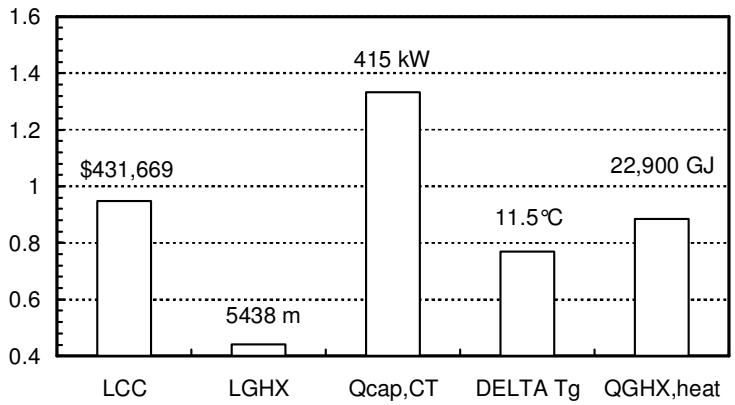

Figure 5-8 Characteristics of a design based on a system using TMY2 weather data and a boiler backup normalized by a design using TMY2 weather data and no boiler backup. The value of each parameter based on the design with no boiler backup and TMY2 weather data is shown.

The percentage of the heat load met by the GHX for each hour of the 20 year simulation is shown in Figure 5-9. A histogram of these same data is shown in Figure 5-10; the y-axis is the number of hours in each 2.5% bin presented on a logarithmic scale and the x-axis is the percentage of the load met by the GHX in 2.5% bins. Figure 5-10 illustrates that, during hours of particularly severe weather, the GHX supplies as little as 36% of the total heat and the supplemental source meets the remaining need. Figure 5-9 shows that the vast majority of the time the GHX is capable of meeting the entire heating load. Over the entire 20 year simulation, the GHX meets 96% of the total heat load. However, by using the supplemental source at peak load times, as represented by the data points in Figure 5-9 below 100%, the GHX size can be reduced and the LCC decreased.

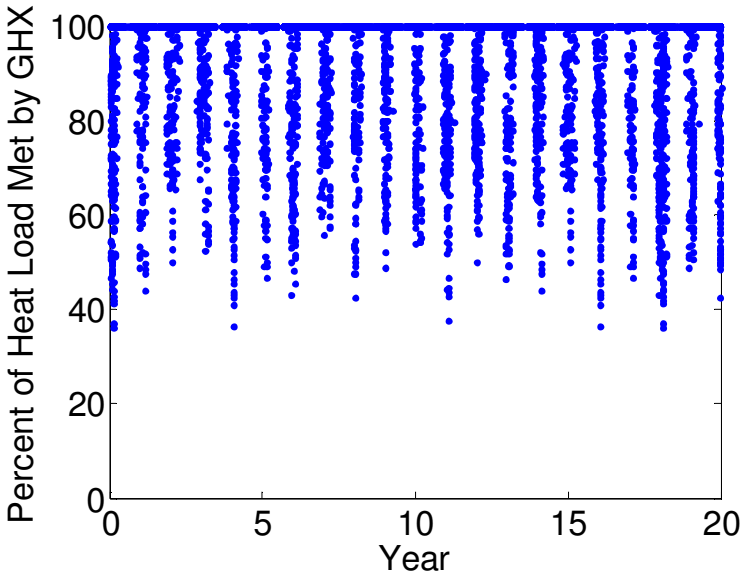

Figure 5-9 The percent of the heat load met by the GHX is shown for the entire 20 year simulation. Each data point represents an hour of severe weather.

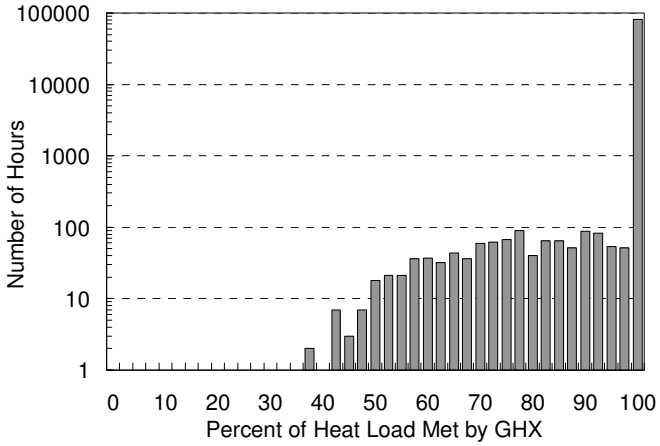

Figure 5-10 A histogram of the percent of the heat load met by the GHX over the entire 20 year simulation. The y-axis is the # of hours associated with each 2.5% bin; notice that the y-axis is logarithmic and the vast majority of the time the entire heat load is met by the GHX.

5.1.6 Conclusions

When year-to-year weather variability is accounted for in designing a GHX system, hybrid or otherwise, the results can significantly change from those based on the use of a typical meteorological year for every year of the simulation. A system designed based on a TMY2 file may be unable to meet the loads during a severe weather year. Over the course of the system life, it is likely that at least one year will deviate substantially from the average. In addition, the

location of a severe weather year within the sequence of years used in the simulation can significantly change the design. The most conservative design of a boiler hybrid is one in which the most severe cooling load occurs in the first year of the simulation. The most conservative design of a CT hybrid is one in which a severe heating load occurs in the first year of the simulation.

Adding a separate supplemental heat source to a CT hybrid (i.e., the use of a boiler backup system) appears to be an effective method of meeting unusually severe heating loads without requiring a large GHX which leads to a higher system cost. The GHX is used to meet the majority of the heat load but the supplemental heat source operates during peak load periods. The CT size must increase in order to compensate for the loss of cooling available from the GHX. In situations where a ventilation system already exists or is being planned, it can be economical to add a relatively inexpensive boiler on the building side of the system. In addition, building owners may be more comfortable with a system that includes a familiar back-up system of this kind. Each situation should be evaluated to determine the applicability of a CT-GSHP or boiler-GSHP hybrid.

5.2 Synthetic Temperatures and Loads

One of the primary inputs to the FHyGSHP simulation model is a file containing annual hourly cooling and heating loads and dry and wet bulb temperatures. The building loads are calculated by the user using a building simulation program, typically based on TMY weather conditions. Nominally, this input file is used for every year of a system simulation (e.g. a 20 year simulation uses the input file for each of the 20 years), but the FHyGSHP program also gives the user the option of generating synthetic load and temperature data in order to introduce realistic annual weather variation into the simulation. Rather than repeating the same weather and load

profile for every year of the simulation, a different weather and load profile can be used for every year of the simulation. The requirements of the procedure for developing synthetic weather and load data are to:

- capture real world weather variability as measured by standard deviation,
- use minimal location-dependent information such as a
    - single year of hourly wet and dry bulb temperature and a
    - single year of hourly cooling and heating loads, and
- be valid for climate zones in the lower 48 states of the United States.

This section describes and evaluates the procedure; the simulations in this section were performed in FHyGSHP.

5.2.1 Generation of Synthetic Dry Bulb Temperature

The first and most important step is to derive a synthetic dry bulb temperature, which is used to calculate synthetic wet bulb temperature and building loads. The overall concept is described in two steps:

1) Determine the magnitude of a perturbation of dry bulb temperature for each month of the year
2) Perturb the dry bulb temperature of each hour of a given month by the amount determined in step 1 for that month

The underlying question in the first step is: by how much should the dry bulb temperature be perturbed? This question is discussed in the next section.

5.1.2.1 Probability Distribution of Temperature

The magnitude of the perturbation needs to result in a dry bulb temperature which reflects what could actually occur, so the logical procedure is to develop a probability distribution of

actual weather data. In order to make this distribution relevant for a variety of locations, it is developed using data from the 14 locations listed in Table 5-3.

Table 5-3 Locations used to generate probability distributions.

Location		Climate Zone	
Phoenix, AZ	PHO	2	Hot-Dry
Houston, TX	HOU	2	Hot-Humid
Orlando, FL	ORL	2	Hot-Humid
Atlanta, GA	ATL	3	Mixed-Humid
Las Vegas, NV	LV	3	Hot-Dry
San Francisco, CA	SAF	3	Marine
Memphis, TN	MEM	3	Mixed-Humid
St. Louis, MO	STL	4	Mixed-Humid
Seattle, WA	SEA	4	Marine
Salt Lake City, UT	SLC	5	Cold
Indianapolis, IN	IND	5	Cold
Erie, PA	ERI	5	Cold
Albany, NY	ALB	5	Cold
Madison, WI	MSN	6	Cold

The temperature is perturbed on a monthly basis. A daily or weekly time frame would result in more temperature discontinuities between adjacent days than a monthly time frame; a seasonal time frame might lead to exaggerated weather extremes (e.g. the temperature could be abnormally high for 3 months rather than just 1). The mean monthly dry bulb temperature, $\overline{T}_{db,month}$, is defined in Eq. (5.2) and is a function of the maximum and minimum temperature [54].

$$\overline{T}_{db,month} = \frac{T_{\max,db,month} + T_{\min,db,month}}{2} \tag{5.2}$$

This quantity was calculated for each month of 20 years of measured temperature data in each of the 14 locations, resulting in a total of 3360 data points. In practice, the hourly dry bulb temperature, $T_{db,hour,in}$, for a given month is perturbed by a value, ΔT_{month}, defined in Eq. (5.3) as the difference between the mean monthly dry bulb temperature and the mean monthly dry bulb temperature of TMY3 data (or any other "typical" dry bulb temperature). $T_{db,hour,in}$ is the hourly dry bulb temperature supplied by the user and $T_{db,hour,syn}$ is the synthetic hourly dry bulb

temperature. The value of ΔT_{month}, rather than the mean monthly temperature, is what is required in the calculations.

$$\Delta T_{month} = \bar{T}_{db,month} - \bar{T}_{db,month,TMY}$$
$$T_{db,hour,syn} = T_{db,hour,in} + \Delta T_{month} \quad (5.3)$$

A histogram of these data is shown in Figure 5-11 with a normal distribution (left) and logistic distribution (right) fit to these data. Although the data are reasonably well represented by a normal distribution, the logistic distribution is a better representation of the data because it better captures the peak and the longer tails.

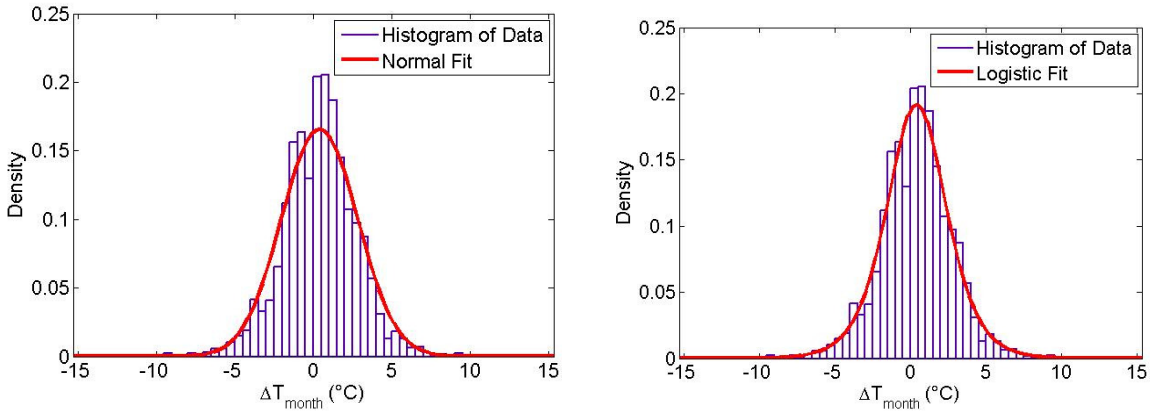

Figure 5-11 Histogram of mean monthly dry bulb temperature minus the mean monthly dry bulb temperature of TMY data in 14 locations with a logistic curve fit. Left: A normal distribution fit to the histogram. Right: A logistic distribution fit to the histogram.

The logistic distribution is given in Eq.(5.4), where μ is the mean and σ is the standard deviation, given in Eqs. (5.5) and (5.6), respectively; note that $\bar{y}$ is used as a generic variable for the mean of data set y in Eq. (5.5). For the data in Figure 5-11, the mean (μ or y) is 0.401 and the standard deviation is 1.303. For computational efficiency, rather than using the histogram directly in FHyGSHP in order to determine the magnitude of the perturbation for each month, the logistic distribution is used with mean and standard deviation set to default values or specified by the user.

$$f(x)=\frac{e^{-\left(\frac{x-\mu}{\sigma}\right)}}{\sigma\left[1+e^{-\left(\frac{x-\mu}{\sigma}\right)}\right]^2},\quad x=\Delta T_{month} \tag{5.4}$$

$$\overline{y}=\frac{\sum_{i=1}^{n} y_i}{n}=\mu \tag{5.5}$$

$$\sigma=\sqrt{\frac{\sum_{i=1}^{n}\left(y_i-\overline{y}\right)^2}{n-1}} \tag{5.6}$$

The perturbation for a given month is determined by randomly selecting a point that falls within the logistic distribution; the inversion method is used to generate these points [76]. In the inversion method, the random variate, x or ΔT_{month}, is generated by finding the inverse of the density function of the logistic distribution. The density function (also known as the cumulative distribution function) for the logistic distribution is given in Eq. (5.7) and the inverse is given in Eq. (5.8). The variable p is a random number from the uniform distribution. Using the derived value of ΔT_{month}, the density is found using the logistic function in Eq.(5.4); a plot of the density versus ΔT_{month} as generated from Eq. (5.8) shows that the inversion method reproduces the logistic distribution; see Figure 5-12.

$$F(x)=\frac{1}{1+e^{-\frac{x-\mu}{\sigma}}} \tag{5.7}$$

$$F^{-1}(p)=x=\mu+\sigma\log\left(\frac{1-p}{p}\right)=\Delta T_{month} \tag{5.8}$$

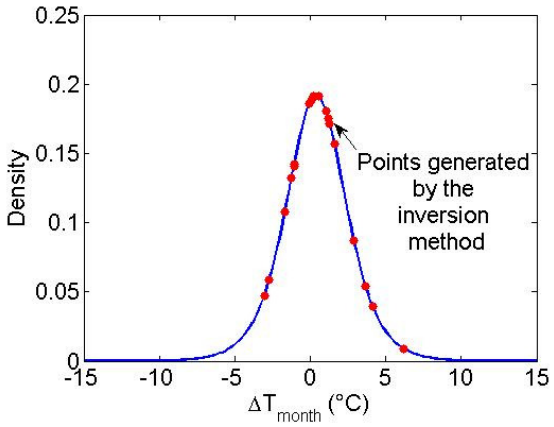

Figure 5-12 Logistic curve and random variates from the logistic distribution generated by the inversion method.

5.2.2.1 Application of the Synthetic Temperature Method

A simple metric for evaluating how well the synthetic data capture the behavior of the real weather data is to compare the standard deviation of the degree days for the two sets of data as shown in Eq. (5.9), where σ_{rel} is the relative standard deviation. In this equation n is the number of years, which is 20, and y is either heating degree days (HDD) or cooling degree days (CDD).

$$\sigma_{rel} = \frac{\sigma}{\bar{y}} \bullet 100 \tag{5.9}$$

HDD and CDD are defined in Eq. (5.10) and are calculated using a base temperature, T_{base}, of 18.3°C [54] and the mean daily dry bulb temperature, $\bar{T}_{db,day}$, of either the actual or synthetic data. Although building loads are sometimes generated from degree day information, the purpose of CDD and HDD in this situation is solely as a means for computing an integrated statistic of temperature.

$$HDD = \sum_{i=1}^{365} \max\left(T_{base} - \bar{T}_{db,day,i}, 0\right)$$
$$CDD = \sum_{i=1}^{365} \max\left(\bar{T}_{db,day,i} - T_{base}, 0\right) \quad (5.10)$$

20 years of actual dry bulb temperatures were available and 20 years of synthetic dry bulb temperatures were calculated. The annual CDD and HDD were calculated for each of the 20 years of actual and synthetic dry bulb temperature; comparisons between these data sets are shown in Figure 5-13 and Figure 5-14. The two plots on the left show the relative standard deviation of CDD and HDD for both the actual and synthetic data as defined in Eq. (5.9) (with n = 20 years). The two plots on the right show the range in the CDD and HDD over the course of 20 years, as calculated in Eq. (5.11) (where DD is either CDD or HDD). For example, in Atlanta from 1991 through 2010 there was a maximum of 1309 CDD and a minimum of 782 CDD, making the range in CDD for Atlanta over those 20 years: 1309 – 782 = 527. The corresponding synthetic data result in a range over 20 years in CDD of: 1420 – 784 = 636.

$$range = \max\left(DD_{20\,years}\right) - \min\left(DD_{20\,years}\right) \quad (5.11)$$

In these figures the x-axis is the location number as indicated in Table 5-4 (e.g. 1 corresponds to Atlanta).

Table 5-4 Cities as numbered in Figure 5-13 and Figure 5-14.

Number	City	Number	City
1	Atlanta, GA	8	Houston, TX
2	St. Louis, MO	9	San Francisco, CA
3	Salt Lake City, UT	10	Indianapolis, IN
4	Phoenix, AZ	11	Memphis, TN
5	Las Vegas, NV	12	Orlando, FL
6	Madison, WI	13	Erie, PA
7	Seattle, WA	14	Albany, NY

Figure 5-13 compares actual data to synthetic data derived using a logistic distribution with mean 0.401 and standard deviation 1.303, which are based on the fit of a logistic curve to the histogram as shown in Figure 5-11. Figure 5-14 compares the data using a logistic distribution with mean 0.385 and standard deviation 1.186. These values are based on an optimization of the synthetic temperature generation program in which the value of *f* in Eq. (5.12) is minimized (for 20 years of temperatures in 14 locations).

$$f = \sqrt{\sum_{j=1}^{14}\left(\sum_{i=1}^{20} CDD_{actual,i,j} - \sum_{i=1}^{20} CDD_{syn,i,j}\right)^2 + \sum_{j=1}^{14}\left(\sum_{i=1}^{20} HDD_{actual,i,j} - \sum_{i=1}^{20} HDD_{syn,i,j}\right)^2} \quad (5.12)$$

The standard deviation of both CDD and HDD of the synthetic data is generally similar to the actual data, with a few locations displaying more variability. In terms of CDD, Seattle (location 7) shows the greatest difference between the actual and synthetic data, with the synthetic data producing greater variation. In terms of HDD Phoenix (location 4) shows the worst comparison. In general, when the mean and standard deviation of the logistic distribution were optimized, comparison between the relative standard deviations of synthetic and actual data improved. The synthetic data using the original fit parameters for the logistic distribution result in a trend of over-predicting the range in CDD relative to the actual data, indicating greater variation across 20 years. The range in HDD both over and under-predicts the actual data. The optimal parameters for the logistic distribution result in a better match between the synthetic and actual range in CDD and the comparison in the range of HDD is essentially unchanged from the original fit parameters. Overall, the optimal parameters improve the comparison between synthetic and actual data.

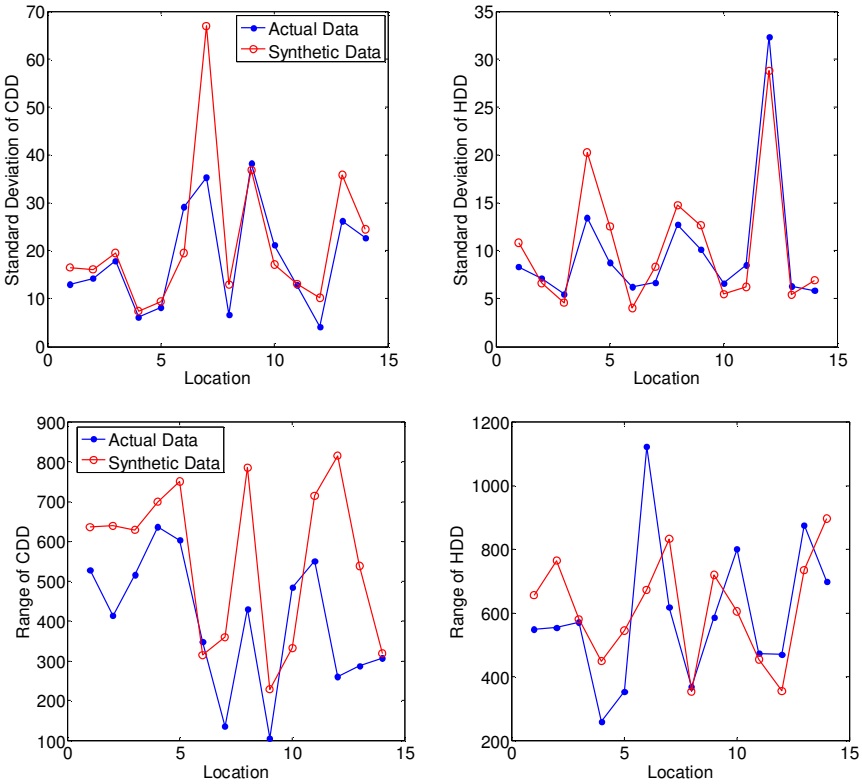

Figure 5-13 Standard deviation and range of cooling and heating degree days using a logistic distribution with mean 0.401 and standard deviation 1.303.

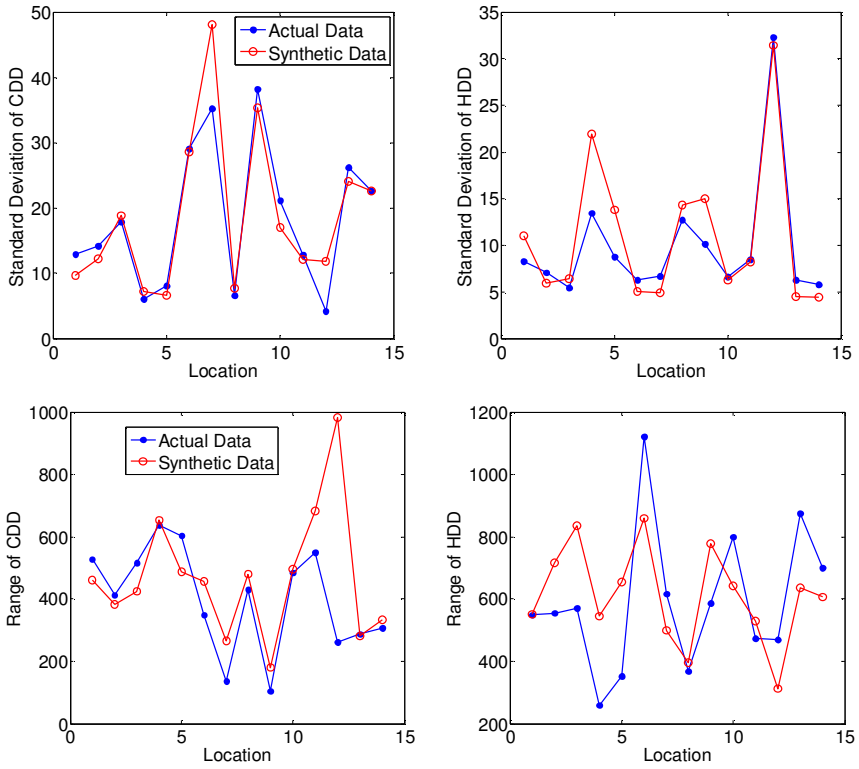

Figure 5-14 Standard deviation and range of cooling and heating degree days using a logistic distribution with mean 0.385 and standard deviation 1.186.

The FHyGSHP program has a logistic curve with mean 0.385 and standard deviation 1.186 hard-coded in so that the user is only required to supply a single year of weather and load data in the form of an input file. However, there may be situations in which the user knows or wishes to specify the details of how local weather varies, so FHyGSHP can take the mean and standard deviation of mean monthly temperature versus TMY3 temperature as inputs. For example, if the user has access to historical weather data, he/she could apply the same procedure used in this study to calculate a mean and standard deviation of temperature data as follows:

1) Calculate the mean monthly temperature of historical weather data
2) Calculate the mean monthly temperature of TMY3 data
3) Calculate the difference between (1) and (2) for all months and years
4) Combine all of the data into one set

5) Calculate the mean of this full data set
6) Calculate the standard deviation of this full data set.

In addition, they could use their own knowledge of local conditions to estimate the mean and standard deviation.

The mean and standard deviation of the logistic distribution fit to the data do not necessarily coincide with the mean and standard deviation of the actual data. The six step procedure described above was applied in all 14 locations examined in this study; in other words, the mean and standard deviation of a set of 240 data points (12*20) of ΔT_{month} data were calculated for each location. A logistic distribution was also fit to each of these data sets. Figure 5-15 shows the mean and standard deviation of the logistic fit versus the mean and standard deviation of the raw ΔT_{month} data (which is what the user is most likely to know), with each point representing a different location. The mean of the data and the fit are similar, but the standard deviation of the fit is approximately half that of the raw data. This indicates that the logistic fit generally lies inside of the data (i.e. it is narrower than the actual data). FHyGSHP uses Eq. (5.13) to transform from the mean of the actual data to the mean of the logistic fit and Eq. (5.14) to transform from the standard deviation of the data to the standard deviation of the fit.

$$\mu_{fit} = 0.9206\mu_{data} + 0.0555 \tag{5.13}$$

$$\sigma_{fit} = 0.5055\sigma + 0.1235 \tag{5.14}$$

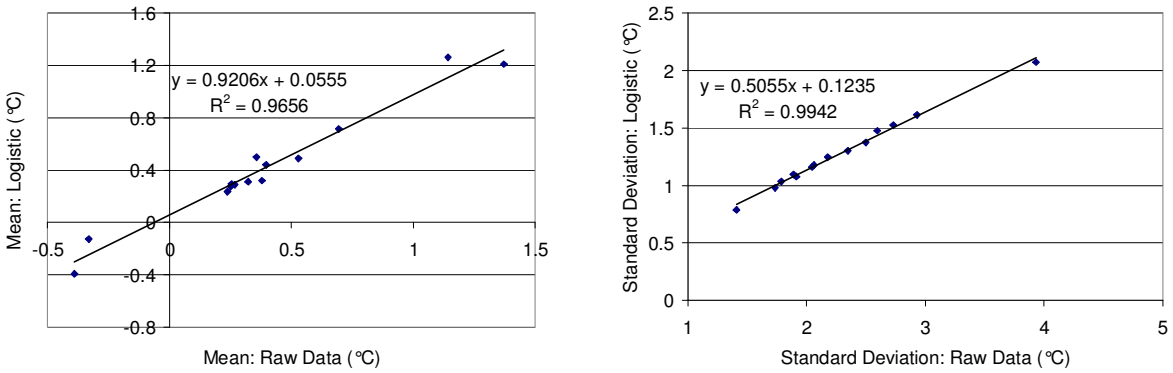

Figure 5-15 Relationship between the mean (left) and standard deviation (right) of the logistic fit and the raw ΔT_{month} data.

Figure 5-14 shows a significant disparity between the standard deviation of synthetic and actual data in Seattle and Phoenix, so 20 years of weather data were generated in these two locations using the general logistic fit with mean 0.385 and standard deviation 1.186 as well as the specific parameters fit to the data in just those locations. In Phoenix the specific logistic curve has mean 0.235 and standard deviation 0.98 while in Seattle the mean is -0.393 and the standard deviation is 1.246. The CDD and HDD in Seattle using the general (left) and specific (right) fits are shown in Figure 5-16. In the case of CDD, the general fit captures the behavior of the actual data well, but HDD is under-predicted. When the specific fit is used, the CDD in general are still similar, though the outliers are more significant, but HDD is much more similar.

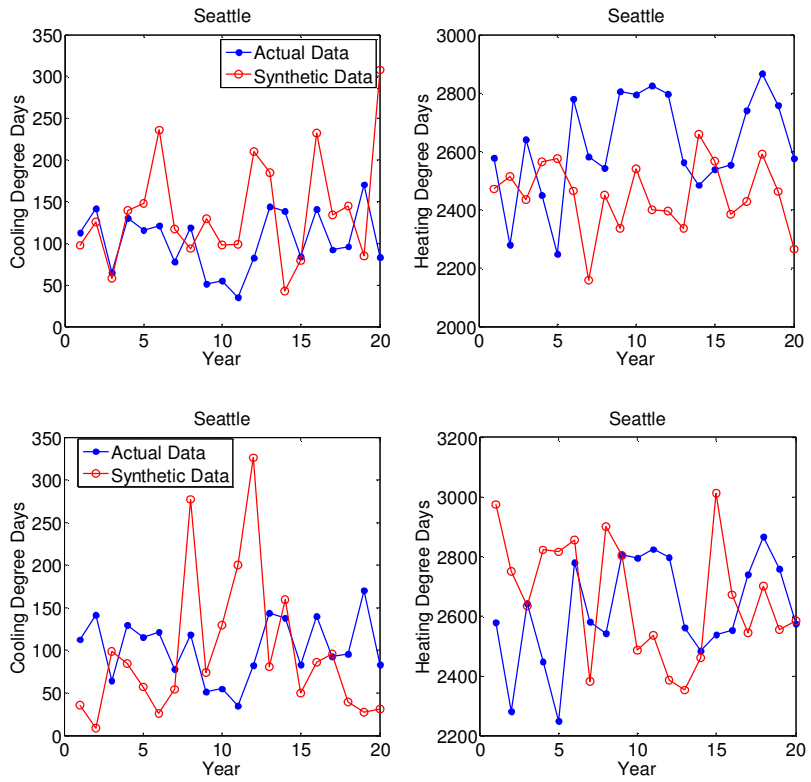

Figure 5-16 CDD and HDD in Seattle for 20 years generated using the general logistic fit (top) and a specific logistic fit (bottom).

Figure 5-17 shows how the standard deviation and range of the HDD and CDD of the two different logistic curves compare to the actual data. For the specific fit, the standard deviation of HDD and CDD over 20 years of synthetic data compare well to the actual data, but the range in values is much greater, greater even than when the general fit is used to generate synthetic data. This result indicates that the specific fit resulted in at least one significant outlier which greatly affected the range but did not lead to a dramatic increase in standard deviation.

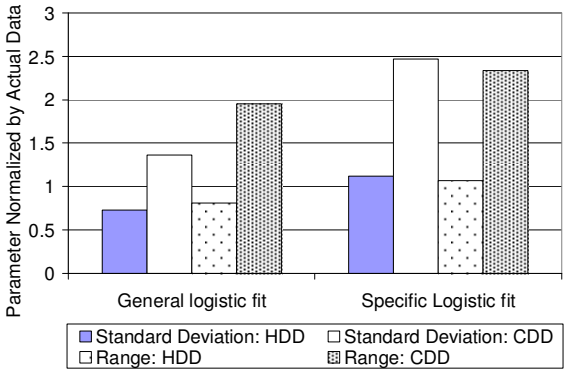

Figure 5-17 Comparison of standard deviation and range of HDD and CDD of the general and specific logistic fits to the actual values in Seattle.

Figure 5-18 shows CDD and HDD in Phoenix for both the general and specific fits. With the general fit, the CDD of the synthetic data tend to over-predict the actual CDD, and this over-prediction is reduced when the specific fit is used to generate the data. The specific fit also leads to a better reproduction of the range in HDD.

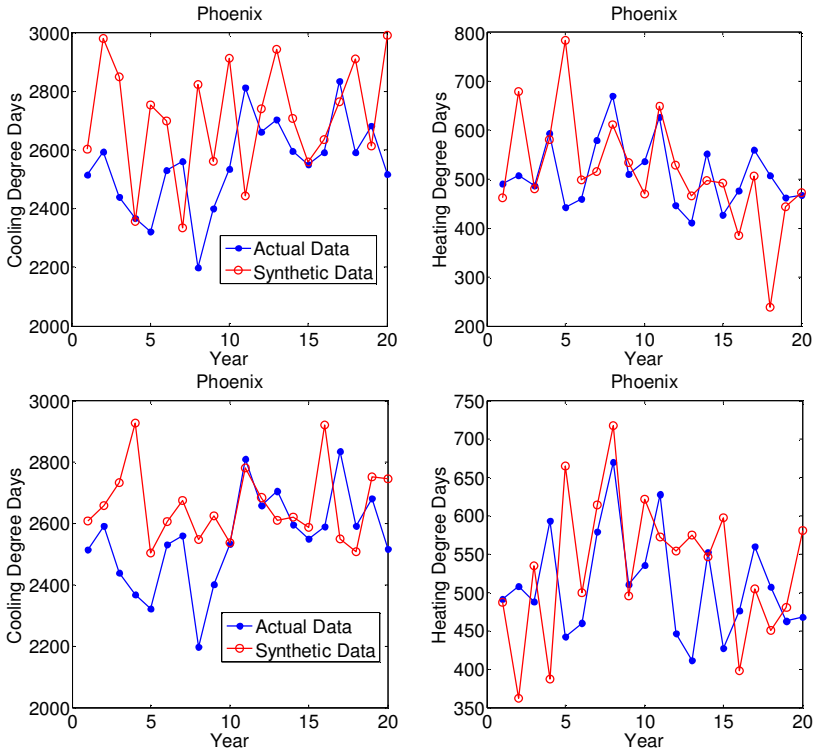

Figure 5-18 CDD and HDD in Phoenix for 20 years generated using the general logistic fit (top) and a specific logistic fit (bottom).

Figure 5-19 shows the comparison of standard deviation and range of CDD and HDD for the general and specific fits to the actual data. The standard deviation comparison is much improved when the specific fit is applied; both CDD and HDD are noisier than in the actual data, but the magnitude is reduced. As in the case of Seattle, the comparison of range is worse with the specific fit, again indicating that there is at least one significant outlier.

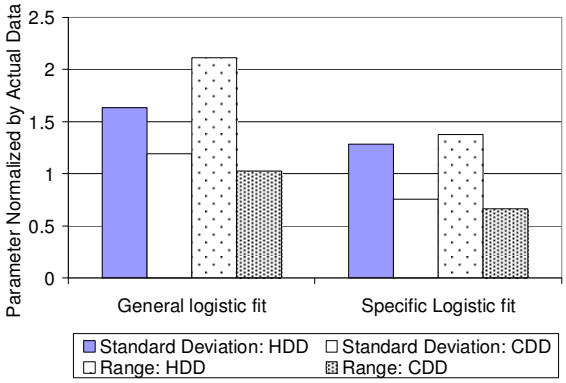

Figure 5-19 Comparison of standard deviation and range of HDD and CDD of the general and specific logistic fits to the actual values in Phoenix.

These results indicate that, in terms of CDD and HDD, the general fit produces acceptable results in a variety of locations, though there is a tendency for the standard deviation to be larger than it is in actual data. Using a fit that is more tailored to the location produces better results, but outliers still occur. These differences between the actual and synthetic data are not considered significant because the synthetic data tend towards greater weather variability and weather extremes, which coincides with generally accepted future climactic trends [77]. Ultimately, the synthetic data generation method has to be evaluated by comparing the design and performance of hybrid ground source heat pump systems designed using the synthetic and real data. This comparison is made in Section 5.2.4.

5.2.2 Generation of Synthetic Wet Bulb Temperature

The wet bulb temperature is related to the dry bulb temperature, so it is modified based on the perturbed dry bulb temperature. Figure 5-20 shows an example of the relationship between the mean daily wet bulb temperature and the mean daily dry bulb temperature. In FHyGSHP this relationship is developed from the input data file for the specific location considered.

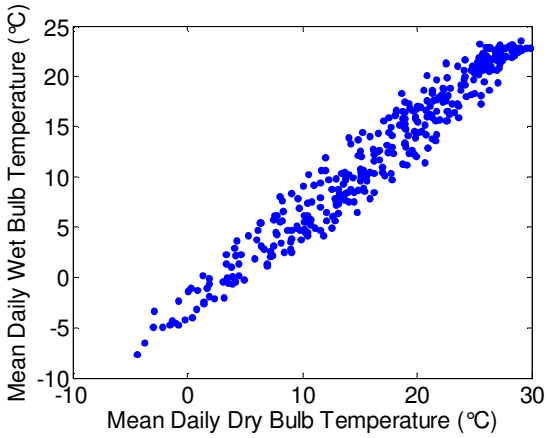

Figure 5-20 Mean daily wet bulb temperature as a function of the mean daily dry bulb temperature.

The relationship in Figure 5-20 is described by Eq. (5.16), where the mean daily dry bulb, $\overline{T}_{db,day}$, and wet bulb, $\overline{T}_{wb,day}$, temperatures are calculated from the input data using Eq. (5.15) and the parameters *m* and *b* are found using a least squares fit.

$$\overline{T}_{day} = \frac{T_{\max,day} + T_{\min,day}}{2} \tag{5.15}$$

$$\overline{T}_{wb,day} = m\overline{T}_{db,day} + b \tag{5.16}$$

The synthetic wet bulb temperature is then found from the synthetic dry bulb temperature as shown in Eq. (5.17).

$$\overline{T}_{wb,day,syn} = m\overline{T}_{db,day,syn} + b \tag{5.17}$$

The hourly wet bulb temperature is calculated by perturbing the input wet bulb temperature, T_{wb}, by the difference between the input and synthetic mean daily wet bulb temperatures as shown in Eq. (5.18). For example, each hour of January 31 is perturbed by the difference between the synthetic mean wet bulb temperature for January 31 and the input mean wet bulb temperature for January 31.

$$T_{wb,syn} = T_{wb} + \left(\overline{T}_{wb,day,syn} - \overline{T}_{wb,day}\right) \tag{5.18}$$

5.2.3 Generation of Synthetic Building Loads

The heating and cooling loads are also related to the dry bulb temperature. Figure 5-21 shows the total daily building load as a function of the mean daily dry bulb temperature.

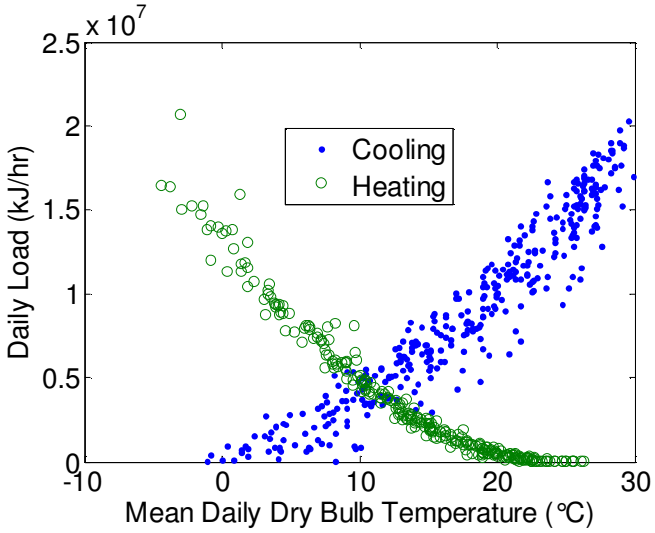

Figure 5-21 Total daily building load as a function of the mean daily dry bulb temperature.

A second order polynomial curve fit is applied to define the relationship between the load and the dry bulb temperature, as shown in Eq. (5.19). The daily load, Q_{day}, and mean dry bulb temperatures are calculated from the input data and the parameters a, b, and c are found using a least squares method.

$$Q_{day} = a\overline{T}_{db,day}^2 + b\overline{T}_{db,day} + c \tag{5.19}$$

The synthetic load, $Q_{day,syn}$, is calculated from the synthetic daily mean dry bulb temperature as shown in Eq. (5.20). In order to calculate the hourly load, the difference between the synthetic and input daily loads is divided by the number of hours in a given day in which a load occurs, n_Q, as shown in Eq. (5.21). For the hours in the input file for which a load occurs, the input load, Q_{hour}, is modified by ΔQ_{syn} to result in a synthetic hourly load, $Q_{hour,syn}$.

$$Q_{day,syn} = a\bar{T}_{db,day,syn}^2 + b\bar{T}_{db,day,syn} + c \tag{5.20}$$

$$\Delta Q_{syn} = \frac{Q_{day,syn} - Q_{day}}{n_Q} \tag{5.21}$$

$$Q_{hour,syn} = \Delta Q_{syn} + Q_{hour} \tag{5.22}$$

5.2.4 Comparison of System Design Found using Actual and Synthetic Data

The best method for determining how well the synthetic data model the behavior of real weather is to compare the optimal design of a hybrid ground source heat pump using 20 years of real weather data to the design using 20 years of synthetic weather data. In the baseline case, hourly building loads were estimated using EFLH [75] with real weather data from 1991 through 2010. An optimal design was found using these 20 years of data ordered sequentially from 1991 through 2010, but as shown in Section 5.1, the design can change depending on the order of the years. For example, in a cooling dominated building more heat is rejected to the ground than extracted, leading to an increase in ground temperature over time; a high heating load after several seasons of cooling can be met by a smaller GHX than if the high heating load occurs in the first year because the ground temperature is higher. In order to assess how the design changes due solely to the order of the years, the 20 years of real weather and estimated load data were randomly ordered to generate 20 different sequences of the 1991 through 2010 data. In other words, 20 different system designs are obtained by ordering the same 20 years of data in 20

different ways; no single year is repeated in determining the system design. The design using the data ordered sequentially is included for comparison. It should also be noted that based on the study detailed in Section 5.1, a furnace is included in the design for all cases examined in this section.

Table 5-5 presents a summary of the results of this study in Atlanta. The design parameters presented are:

- GHX – length of the ground heat exchanger in m
- CT – size of the cooling tower in kW
- Furnace – capacity of the furnace in kW
- LCC – Life Cycle Cost in $.

The first row is the design when the data are sequentially ordered from 1991 through 2010. The second row is the mean design of the 20 years of randomly ordered data. The third row is the standard deviation of the 20 designs relative to the mean. The fourth row is the range in the design parameter relative to the mean; for example, the range of the ground heat exchanger length is the maximum optimal length of the 20 designs minus the minimum optimal length of the 20 designs, divided by the mean of the 20 designs. The design parameters are also shown in Figure 5-22, where the horizontal line is the mean design.

Table 5-5 Variation in the design for 20 years of actual weather data randomly ordered (in Atlanta).

	GHX	CT	Furnace	LCC
Sequential	4528 m	609 kW	226 kW	$509,989
Mean	4680 m	643 kW	69 kW	$522,446
Relative standard deviation (%)	5.4	6.3	61.3	1.8
Relative range (%)	15.4	31.7	292.4	7.8

There is significant scatter in the size of the furnace, but this has minimal impact on the LCC; the furnace is inexpensive to operate and it influences LCC primarily in terms of reducing the size of the GHX required to meet heating loads. The scatter in the mean size of the GHX and CT are relatively small, although the range in values is more substantial, indicating the presence of outliers. However, the variability in these components still leads to a relatively small variability in LCC. These data provide a baseline for evaluating how well the synthetic weather data capture realistic behavior.

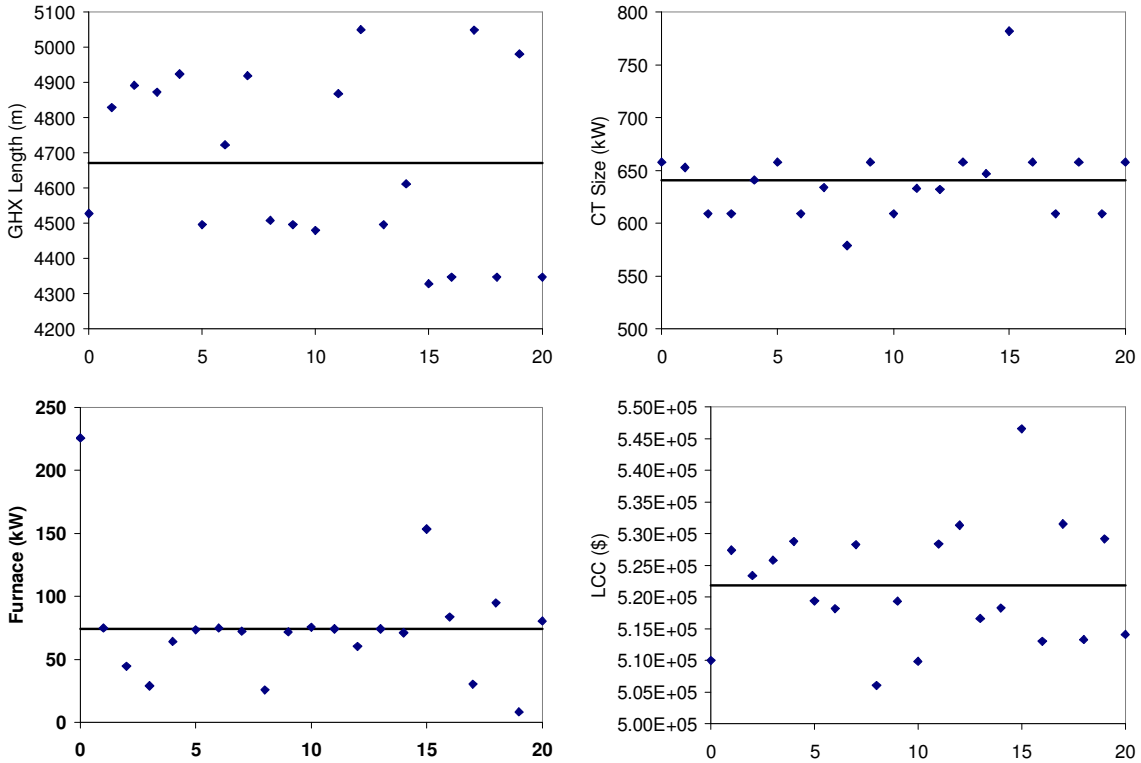

Figure 5-22 GHX length, CT size, Furnace size, and LCC for the sequentially (0) and 20 randomly (1 through 20) ordered sets of the actual weather data. The horizontal line is the mean of the data. (In Atlanta)

Three situations were examined using the real and synthetic weather data:

1) 20 years of randomly ordered weather data,
2) 20 years of data ordered from the greatest ratio of HDD to CDD to the least,
3) 20 years of data ordered from the greatest ratio of CDD to HDD to the least.

Five sets of synthetic data were used in this study in order to partially account for the randomness in the generation of the data. The results for all three of these cases are shown in Figure 5-23. Each bar chart shows four things:

- the magnitude of the parameter for the actual data,
- the magnitude of the mean of the parameter for the five sets of synthetic data,
- the standard deviation about the mean for the five sets of synthetic data in the form of error bars, and
- a straight line showing the design obtained using TMY3 weather data.

The length of the GHX is shown in the upper left, the size of the CT is shown in the upper right, the capacity of the furnace is shown in the lower left, and the LCC is shown in the lower right.

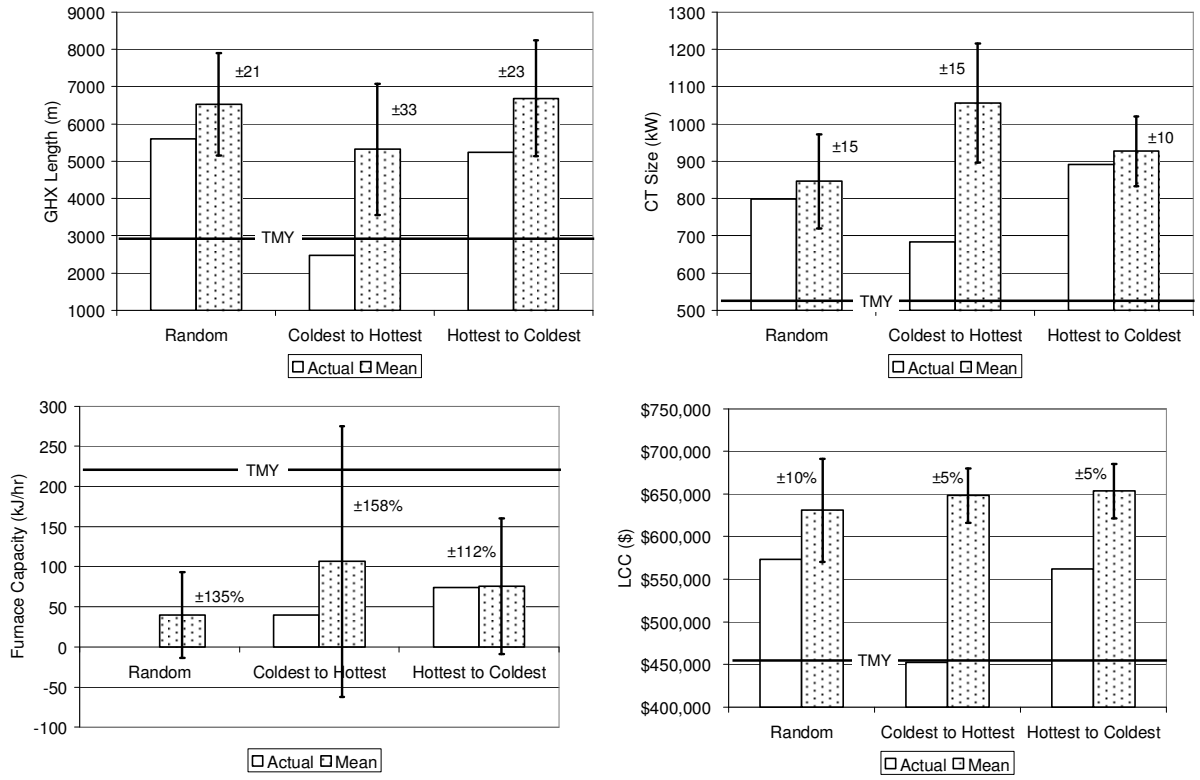

Figure 5-23 Design for actual data and mean design for five sets of synthetic data in Atlanta. In the first case the 20 years of data are randomly ordered; in the second case the 20 years are ordered so that the coldest year occurs first and the hottest year occurs last; in the third case the 20 years are ordered so that the hottest year occurs first and the coldest year occurs last. The line is the design using TMY3 weather data.

There is substantial variability in the size of the furnace, but this has only a slight impact on the variability of the GHX, CT, and LCC. The furnace capacity is selected based on a threshold; if the heating load exceeds a certain threshold, then the furnace is used to meet the additional heating load. In some of the designs, the furnace capacity is zero because it is more cost effective to use the GHX to meet the entire heating load (a larger GHX can also meet more of the cooling load). Even when a furnace is present, the GHX still meets the majority of the heating load, with the furnace only being used on extremely cold days, so variation in the size of the furnace does not necessarily lead to a dramatic change in the size of the GHX; it primarily stabilizes the size of the GHX, which is no longer sized to meet the peak load.

When the data are randomly ordered, the mean GHX size when using the synthetic data is greater than when using the actual data, but the standard deviation extends below the actual design. Similar behavior is seen for the CT and LCC for the randomly ordered data. When the data are ordered from the coldest to the hottest years, there is a more substantial difference between the actual and synthetic designs and even considering the standard deviation, there is no overlap between the actual and synthetic designs. When the years are ordered from hottest to coldest, the synthetic data also over-predict the actual data, but the standard deviation of the GHX and CT sizes overlap with the actual data. However, in this case the LCC does not overlap the LCC of the actual data; it is consistently larger due to the consistently larger LCC. In all cases the standard deviation exceeds that for randomly ordered actual data (refer to Table 5-5), indicating that the variability is due to the weather generation method.

Using TMY3 data, the GHX and CT sizes are smaller than when weather variability is taken into account. The peak heating and cooling loads are lower when using TMY3 data for each year of the simulation. The furnace capacity is significantly larger, indicating that more of the heating load is met by the GHX, which leads to the smaller GHX size. The lower cooling load led to a smaller CT. The lower loads and smaller equipment sizes also lead to the smaller LCC. In the prior work (see Section 5.1) it was found that when the weather was ordered with the coldest year first, the size of the GHX increased in order to meet the heating load in that first year, when the ground temperature has not increased due to heat being rejected to the ground during the cooling season. This work did not find the same behavior because of the presence of a furnace in all cases; the furnace capacity is much greater for the case when the coldest year is first, so the GHX size actually decreases some as compared to the randomly ordered data sets. In this work the most significant impact of the order of the weather is seen in the size of the cooling

tower and furnace, both of which can in practice be more easily re-sized if the weather is more severe than expected over the life of the system.

Figure 5-24 shows the same data for Phoenix. Phoenix is a much different environment from Atlanta. A typical undisturbed ground temperature in Phoenix is 21.7°C and the relative humidity is lower than in Atlanta, so it is efficient to meet heating loads using the ground, but cooling loads are often better met using a cooling tower since the wet bulb temperature results in a lower temperature heat sink. When the weather and load data are randomly ordered, there is significant variability in the length of the GHX, but the CT size is relatively stable and very similar to the size when actual data are used. When the different data sets are ordered in the same manner, either from the coldest to the hottest year or the hottest to the coldest year, the actual and synthetic designs are more similar, though the synthetic data tend to lead to an over-prediction of the GHX size relative to the actual data while the CT and furnace tend to be under-sized. The larger GHX can meet a larger percentage of heating and cooling loads, so the CT and furnace can be smaller. Although the GHX size increases in these cases, the LCC is lower than for the actual data. These observations indicate that for these situations, the increased first cost of the system due to the larger GHX is offset by the reduction in operational costs associated with a smaller CT.

The TMY3 design tends to agree more with the synthetic, ordered data, than with the randomly ordered, actual data. As in Atlanta, the heating and cooling loads associated with TMY3 data are lower than either the actual or synthetic conditions, which leads to lower LCC. The fact that the design using randomly ordered data is different from the design using ordered data may be due to the complexities involved in the optimization method.

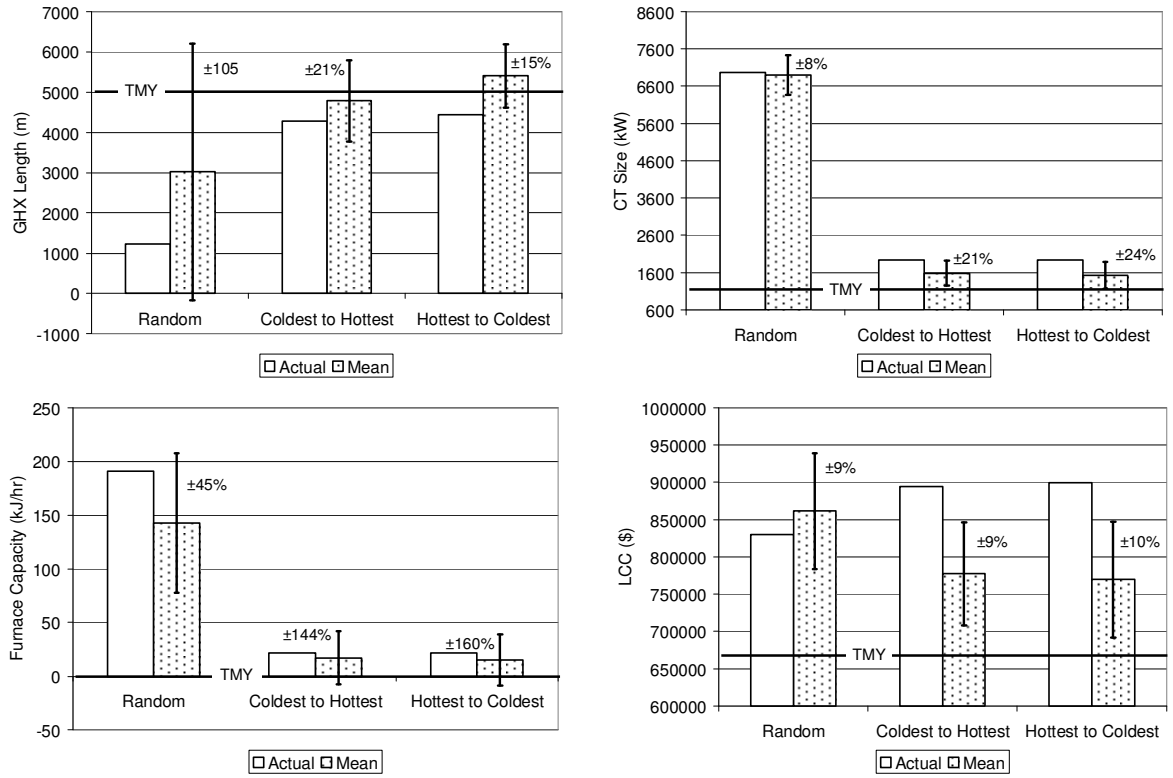

Figure 5-24 Design for actual data and mean design for five sets of synthetic data in Phoenix. In the first case the 20 years of data are randomly ordered; in the second case the 20 years are ordered so that the coldest year occurs first and the hottest year occurs last; in the third case the 20 years are ordered so that the hottest year occurs first and the coldest year occurs last. The line is the design using TMY3 weather data.

5.2.5 Conclusions

This study illustrates both the potential and the limitations of the method for deriving synthetic weather and load data. As stated in the introduction, the goal was to develop a procedure to derive synthetic weather and building load data that can be used in any climate in the lower 48 United States to realistically capture the actual variability of weather. The only user input required for this procedure is the standard information required for the FHyGSHP program: an input file containing a single year of hourly dry and wet bulb temperatures and cooling and heating loads. The synthetic data tend to display greater variability than the actual data in both the annual degree days and the major design features of the optimized system. Given the constraints of the design and the intended use of the synthetic data, these errors are considered acceptable, especially in view of expected greater variability in future weather patterns [77]. The

option for the user to input location specific fit parameters also gives the program wider usability.

In order to ensure that a CT Hybrid will be able to meet the building load at the end of system life, the most conservative design uses synthetic data ordered from the greatest to the least heating loads. However, this design will also lead to the largest GHX and may be the most expensive, and there is no guarantee that the worst case scenario will actually occur. In general, it is best to design the system using synthetic data that are randomly ordered.

Chapter 6 CT HyGSHP Control Strategies

This chapter contains a discussion of potential control strategies for a CT HyGSHP. Background on prior studies is provided, followed by a detailed discussion of one strategy, pre-cooling. After this introductory material, a study comparing the performance of several different control strategies in the context of a realistic CT HyGSHP system is discussed.

6.1 Background

Several prior studies have examined control strategies for CT HyGSHP systems. Three strategies that have been used are set point temperature control (T_{set}), differential temperature control (T_{diff}), and pre-cooling (PC). For the T_{set} strategy, the CT operates when the fluid temperature exceeds a specified set point temperature. For the T_{diff} strategy the CT operates when the fluid temperature exceeds the wet bulb temperature by a specified set point, ensuring that the CT does not operate if the environmental and fluid conditions are unfavorable for efficient and effective operation. Pre-cooling is designed to use the ground as a thermal storage device. The CT is used to cool the ground, which can then be used to cool the building at a later time more efficiently than if it were not pre-cooled. PC is an indirect method of meeting the building load by increasing the cooling capacity of the ground. These strategies can also be used in combination. This section reviews some of the research into HyGSHP control strategies.

Yavuzturk and Spitler [78] studied all three of these strategies, implementing them in a variety of ways. They evaluated the T_{set} strategy with the fluid temperature measured at either the inlet or outlet of the heat pump. The T_{diff} strategy was evaluated using the difference between the fluid temperature entering or exiting the heat pump and the wet bulb temperature; one differential temperature set point turned the CT on and another turned it off. The set point temperature (T_{set}) and differential temperature (T_{diff}) control values were constants selected by

the authors. *PC* was evaluated by activating it in three different ways: the CT operated (1) between 0:00 and 6:00 all year, (2) between 0:00 and 6:00 from January through March, or (3) between 0:00 and 6:00 from June through August. The second implementation is an example of seasonal *PC* while the last implementation is an example of diurnal *PC*. *PC* was combined with T_{set} in all three cases. The size of the GHX and CT were not optimized, nor was the implementation of any of the strategies optimized. The authors compared the performance of the hybrid system to a baseline GSHP system in Houston, TX and Tulsa, OK. In all cases, the addition of a CT led to a reduction in power consumption, but the cases using T_{diff} control produced the greatest reduction. The authors also performed an economic analysis of each system; the analysis did not include the cost of water or time of day electrical rates. The analysis indicates that all of the hybrid designs save money, with the T_{diff} strategy having the greatest cost reduction. Yi et al. [79] simulated a CT HyGSHP system in Hong Kong, using T_{set}, T_{diff}, and *PC* with T_{set} for a 10 year simulation period. This study also showed that T_{diff} produces the greatest decrease in operating costs and power consumption. The items included in the operating cost calculation are not individually presented and the cost of the water used in the CT may not be included.

Fan, et al. [80] analyzed a less traditional CT HyGSHP system. Their goal was to design a system and control strategy that would shift power consumption from periods of peak electrical rates to periods of off-peak electrical rates; their analysis used a peak rate that was three times the off-peak rate. The success of the system was based primarily on the success of the shift in load to off-peak time periods . The CT was used as a direct means of meeting cooling loads, but it was not used for *PC*. Instead, the heat pumps were used to cool the ground at specific times of the year. During these *PC* periods the heat pumps produce -5°C fluid to cool the ground. In some

cases this resulted in fluid that was sufficiently cooled by the ground to allow for direct cooling, bypassing the heat pump. Nearly 73% of the energy removed from the ground at night was replaced during the day in order to meet the cooling load; 27% of the cooling potential created by *PC* was lost. They also found that the power consumption was reduced during periods with cooling loads. The authors conclude that *PC* in this form is effective, but their analysis did not include all sources of power consumption (most significantly the circulating pump power) and did not include a cost analysis.

These studies provide a foundation for the study of the operation of HyGSHP systems, but the economic analyses are limited and the component sizes and control set points are not optimized. The remainder of this chapter will examine these various control strategies in detail, focusing in particular on the role of *PC*.

6.2 Pre-Cooling

In a Hybrid Ground Source Heat Pump (HyGSHP) there is the potential to use the GHX not only as a heat source or sink, but also for thermal storage. Thermal storage can be applied on either a seasonal or diurnal basis, or as a combination of the two. In the case of seasonal thermal storage, for example, energy from a solar collector could be stored in the ground during the summer and then removed from the ground during the winter to meet some of the winter heating demand [81–83]. An example of diurnal thermal storage is the operation of a cooling tower at night when energy rates are lower. Night time operation of a cooling tower is generally more efficient due to lower ambient temperature and cooling. The cooling provided by night time operation of the cooling tower is used to pre-cool the ground for the following day. The cooler ground leads to lower entering water temperature (EWT) to the heat pump, resulting in lower heat pump power consumption [80,84–86].

There are several potential benefits to using the GHX as thermal storage. First, the strategy more fully utilizes the expensive GHX, which would otherwise be present but unused during the thermal storage periods. Second, there is a potential to decrease the power consumption of the heat pump, saving both energy and money. Third, by using thermal storage during off-peak periods, there can be further cost savings.

The potential problem with the use of the GHX as a thermal storage is that more energy might be used and/or money spent operating the circulating pump and supplemental (e.g. cooling tower) equipment during the thermal storage period than is saved in heat pump operation. This study will focus on investigating the potential to use the GHX for thermal storage on a diurnal basis. The Duct Storage (DST) model [46] of the GHX is complex and results obtained with the DST model can be difficult to interpret. Therefore, the first step in evaluating pre-cooling is to develop a simple numerical model of the system. This model treats the ground as a 1-D hollow cylindrical volume with a specified time varying temperature at the inner boundary and a constant temperature at the outer boundary. The numerical model was validated against an analytical model. This model was used to develop a basic qualitative and quantitative understanding of the behavior of the ground and also to verify that the DST model is behaving as expected on a macroscopic scale.

6.2.1 Analytical and Numerical Models of the GHX

The simple analytical and numerical models are developed in order to understand the basic heat transfer behavior of the GHX as a thermal store. The performance metric that is examined is storage efficiency, defined as the ratio of the additional heat rejection to the ground that is achieved during day-time hours (relative to the case with no pre-cooling) to the heat

extraction from the ground during the night, as shown in Eq. (6.1). The models are described in detail below.

$$\eta_s = \left| \frac{q_{day,pre-cool} - q_{day}}{q_{night}} \right| \tag{6.1}$$

6.1.2.1 Analytical Model

In this section, a simple analytical model of a single borehole is developed. The analytical model is used to validate the numerical model (see Section 6.2.2.1), which is used for the majority of the calculations. The real borehole consists of two pipes coupled to the surrounding ground via a thermally conductive grout (Figure 6-1, left). In the analytical model, these details of the borehole are neglected (Figure 6-1, right); the outer diameter of the borehole is the inner boundary of the system. The heat transfer from this inner boundary into the surrounding ground will be evaluated using the model. The inner boundary condition is a time varying specified temperature while the outer boundary is a constant temperature that is equal to the un-disturbed ground temperature.

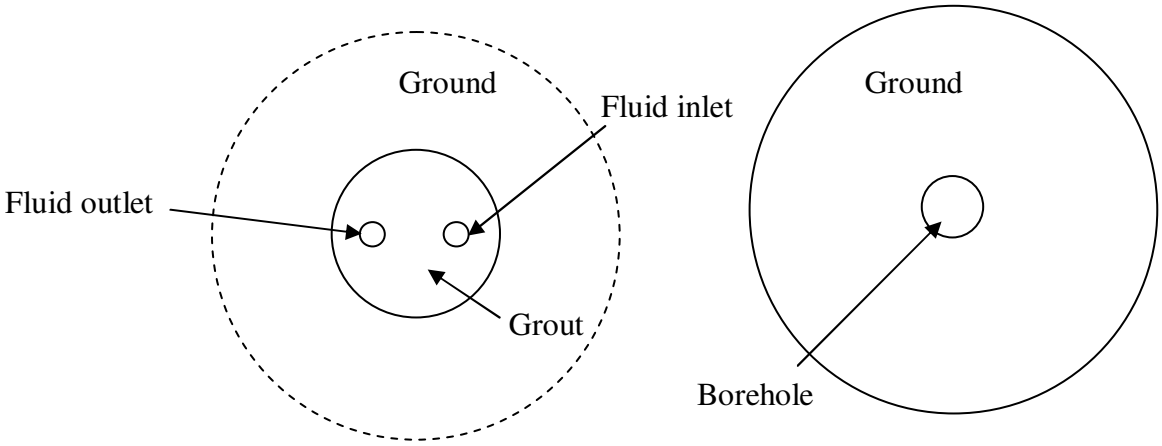

Figure 6-1 Left: Realistic borehole configuration. Right: Sketch of a single borehole and the surrounding ground used in the model.

The governing equation, boundary conditions (*BC1* and *BC2*), and initial condition (*IC*) are given in Eq. (6.2) with the variables defined in Table 6-1.

Table 6-1 Variable definition.

Symbol	Definition	Value
θ	Time	
t	Temperature at given radius and time	
r	Radius	
t_{in}	Inner boundary temperature, given as a function of time	
r_b	Borehole diameter	0.065 m (2.56 in)
r_o	Outer diameter for calculations	4.29 m (14.1 ft)
α	Thermal diffusivity	7.41e-7 m^2/s (0.69 ft^2/day)
C	Heat capacity	2619 kJ/m^3-K (39 Btu/ft^3-F)
k	Thermal conductivity	1.94 W/m-K (1.121 Btu/hr-ft-°F)
t_g	Undisturbed ground temperature	19.4 °C (67 °F)

$$\begin{aligned} &\frac{1}{\alpha}\frac{\partial t}{\partial \theta} = \frac{\partial^2 t}{\partial r^2} + \frac{1}{r}\frac{\partial t}{\partial r} \\ &BC1: \quad t\left(r_b, \theta\right) = t_{in}\left(\theta\right) - t_g \\ &BC2: \quad t\left(r_o, \theta\right) = 0 \\ &IC: \quad t\left(r, 0\right) = 0 \end{aligned} \tag{6.2}$$

The inner boundary condition, *BC1*, is non-homogeneous and time varying, so this problem can not be solved directly. Instead, the inner boundary condition will be dealt with by use of Duhamel's Theorem [87], which is presented in Eq. (6.3).

$$t(r,\theta) = \int_{\tau=0}^{\theta} U(r,\theta-\tau)F'(\tau)\,d\tau + \sum_{i=1}^{I} U(r,\theta-\tau_i)\,\Delta F_i \qquad (6.3)$$

The right side of *BC1* is rewritten as a time varying forcing function, $F(\theta)$, which may include I step changes of magnitude ΔF_i that occur at times τ_i. The forcing functions used in the analytical model are shown in Figure 6-2. These models are used in two ways, a "long day" model and a multiple day model. In the case of the long day model, night is any time less than 12 and day is any time greater than 12; therefore, τ_3 (see Figure 6-2) is simply a large number. In the multiple day model the same day is repeated; therefore, τ_3 is 24 hours and the forcing function pattern is repeated for a specified number of days. The derivative of the forcing function, $F'(\tau)$, is zero, so the first term of Eq. (6.3) can be neglected.

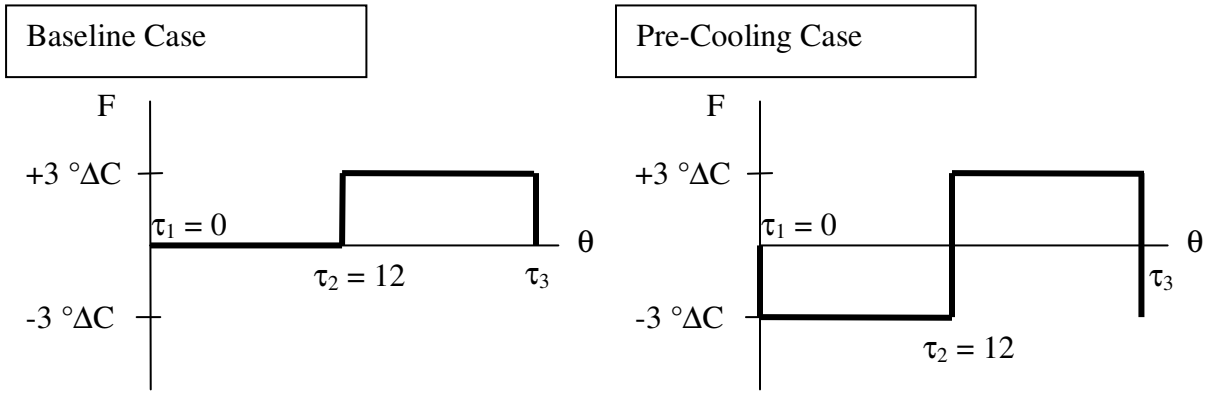

Figure 6-2 Forcing functions for BC1 for the baseline and pre-cooling cases.

The function U is found by substituting U into the governing equation and setting *BC1* to a value of 1, as shown in Eq. (6.4).

$$\begin{aligned}
&\frac{1}{\alpha}\frac{\partial U}{\partial \theta} = \frac{\partial^2 U}{\partial r^2} + \frac{1}{r}\frac{\partial U}{\partial r} \\
&BC1: \quad U\left(r_b, \theta\right) = 1 \\
&BC2: \quad U\left(r_o, \theta\right) = 0 \\
&IC: \quad U\left(r, 0\right) = 0
\end{aligned} \tag{6.4}$$

This problem can be re-written as a combination of three problems, as shown in Eq. (6.5).

$$U\left(r,\theta\right) = a\left(r\right) + b\left(\theta\right) + v\left(r,\theta\right) \tag{6.5}$$

This equation is substituted into the governing equation, boundary conditions, and initial condition as shown in Eq. (6.6). The solution of the *b* sub-problem results in zero, so that sub-problem is removed; the resulting two sub-problems are given in Table 6-2.

$$\begin{aligned}
&\frac{1}{\alpha}\left(\frac{\partial v}{\partial \theta} + \frac{db}{d\theta}\right) = \frac{\partial^2 v}{\partial r^2} + \frac{d^2 a}{dr^2} + \frac{1}{r}\left(\frac{\partial v}{\partial r} + \frac{da}{dr}\right) \\
&v\left(r_b,\theta\right) + a\left(r_b\right) = 1 \;\rightarrow\; v\left(r_b,\theta\right) = 0, \quad a\left(r_b\right) = 1 \\
&v\left(r_o,\theta\right) + a\left(r_o\right) = 0 \;\rightarrow\; v\left(r_o,\theta\right) = 0, \quad a\left(r_o\right) = 0 \\
&v\left(r,0\right) + b\left(0\right) + a\left(r\right) = 0 \;\rightarrow\; v\left(r,0\right) = -a\left(r\right), \quad b\left(0\right) = 0
\end{aligned} \tag{6.6}$$

Table 6-2 Sub-problem description.

$a(r)$	$v(r,\theta)$
$\frac{d^2a}{dr^2}+\frac{1}{r}\frac{da}{dr}=0$	$\frac{1}{\alpha}\frac{\partial v}{\partial \theta}=\frac{\partial^2 v}{\partial r^2}+\frac{1}{r}\frac{\partial v}{\partial r}$
$a(r_b)=1$	$v(r_b,\theta)=0$
$a(r_o)=0$	$v(r_o,\theta)=0$
	$v(r,0)=-a(r)$

The *a* sub-problem is solved first, as shown in the following equations.

$$\frac{d^2a}{dr^2}+\frac{1}{r}\frac{da}{dr}=\frac{1}{r}\frac{d}{dr}\left(r\frac{da}{dr}\right)=0 \tag{6.7}$$

$$r\frac{da}{dr}=c_1 \tag{6.8}$$

$$a=c_1\ln r+c_2 \tag{6.9}$$

The constants c_1 and c_2 are found by applying the boundary conditions.

$$1=c_1\ln r_b+c_2 \tag{6.10}$$

$$0=c_1\ln r_o+c_2 \tag{6.11}$$

$$c_2=-c_1\ln r_o \tag{6.12}$$

$$c_1=\frac{1}{\ln\left(\frac{r_b}{r_o}\right)},\quad c_2=-\frac{\ln r_o}{\ln\left(\frac{r_b}{r_o}\right)} \tag{6.13}$$

$$a=\frac{\ln\left(\frac{r}{r_o}\right)}{\ln\left(\frac{r_b}{r_o}\right)} \tag{6.14}$$

The *v* sub-problem is solved using separation of variables.

$$v(r,\theta)=R(r)\Theta(\theta) \tag{6.15}$$

$$v(r_b,\theta)=0\rightarrow R(r_b)=0 \tag{6.16}$$

$$v(r_o,\theta)=0\rightarrow R(r_o)=0 \tag{6.17}$$

$$R''\Theta+\frac{1}{r}R'\Theta=\frac{1}{\alpha}R\Theta' \tag{6.18}$$

$$\frac{R''}{R}+\frac{1}{r}\frac{R'}{R}=\frac{1}{\alpha}\frac{\Theta'}{\Theta} \tag{6.19}$$

R and Θ are functions of different variables, so the two sides of this equation can only be equal if they are equal to the same constant, $-\lambda^2$.

$$\frac{R''}{R}+\frac{1}{r}\frac{R'}{R}=-\lambda^2, \quad \frac{1}{\alpha}\frac{\Theta'}{\Theta}=-\lambda^2 \tag{6.20}$$

$$R''+\frac{1}{r}R'+\lambda^2 R=0 \tag{6.21}$$

$$\Theta'+\alpha\lambda^2\Theta=0 \tag{6.22}$$

Eq. (6.21) is in the form of a Bessel equation with a solution of the form of Eq. (6.23).

$$R(r)=AJ_0(\lambda r)+BY_0(\lambda r) \tag{6.23}$$

A suggested solution [26] is given in Eq. (6.24).

$$R_0(r)=Y_0(\lambda r_o)J_0(\lambda r)-J_0(\lambda r_o)Y_0(\lambda r) \tag{6.24}$$

The first boundary condition is applied to Eq. (6.24), resulting in the eigencondition as given in Eq. (6.25). Some of the initial zeros of this function are shown in Figure 6-3.

$$R_0(r_b)=0=Y_0(\lambda r_o)J_0(\lambda r_b)-J_0(\lambda r_o)Y_0(\lambda r_b)\rightarrow\lambda \tag{6.25}$$

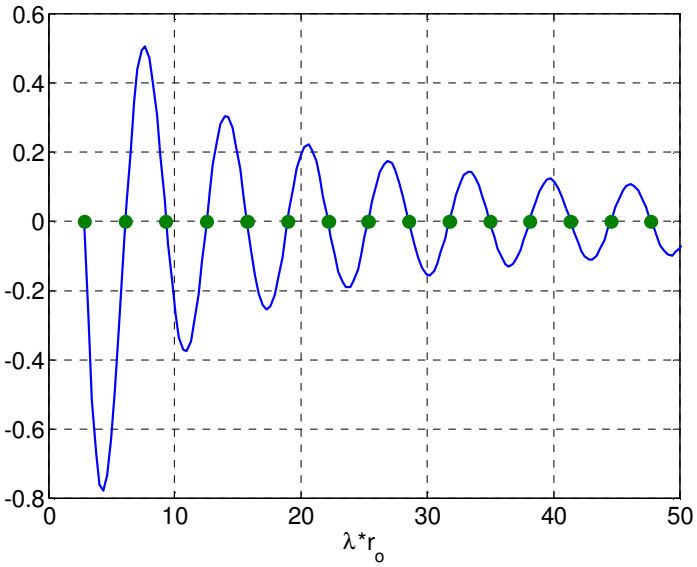

Figure 6-3 Zeros of the eigencondition.

The solution to Eq. (6.22) is shown in Eq. (6.26), where D is a constant.

$$\Theta(\theta) = De^{-\alpha\lambda^2\theta} \tag{6.26}$$

The total solution to the v sub-problem is given in Eq. (6.27).

$$v(r,\theta) = \sum_{n=1}^{\infty} A_n R_0 e^{-\alpha\lambda_n^2\theta} \tag{6.27}$$

The constants A_n are found by applying the initial condition to Eq. (6.27).

$$v(r,0) = -a(r) = \sum_{n=1}^{\infty} A_n R_0 \tag{6.28}$$

This equation can be solved by applying orthogonality and solving the resulting integrals as shown.

$$-\int_{r_b}^{r_o} a(r) r R_0 dr = \int_{r_b}^{r_o} A_n r R_0^2 dr \tag{6.29}$$

$$-\int_{r_b}^{r_o} a(r) r R_0 dr = A_n \frac{2\left[J_0^2(\lambda_n r_b) - J_0^2(\lambda_n r_o)\right]}{\pi^2 \lambda_n^2 J_0^2(\lambda_n r_b)} \tag{6.30}$$

$$A_n = -\frac{\pi^2 \lambda_n^2}{2} \frac{J_0^2(\lambda_n r_b)}{J_0^2(\lambda_n r_b) - J_0^2(\lambda_n r_o)} \int_{r_b}^{r_o} a(r) r R_0 dr \tag{6.31}$$

$$v = -\frac{\pi^2}{2} \sum_{n=1}^{\infty} \frac{\lambda_n^2 J_0^2(\lambda_n r_b)}{J_0^2(\lambda_n r_b) - J_0^2(\lambda_n r_o)} e^{-\alpha \lambda_n^2 \theta} R_0 \int_{r_b}^{r_o} a(r) r R_0 dr \tag{6.32}$$

$$v = -\frac{\pi^2}{2} \sum_{n=1}^{\infty} \frac{\lambda_n^2 J_0^2(\lambda_n r_b)}{J_0^2(\lambda_n r_b) - J_0^2(\lambda_n r_o)} e^{-\alpha \lambda_n^2 \theta} R_0 \frac{1}{\ln\left(\frac{r_b}{r_o}\right)} \int_{r_b}^{r_o} \ln\left(\frac{r}{r_o}\right) r R_0 dr \tag{6.33}$$

$$v = -\frac{\pi^2}{2} \sum_{n=1}^{\infty} \frac{\lambda_n^2 J_0^2(\lambda_n r_b)}{J_0^2(\lambda_n r_b) - J_0^2(\lambda_n r_o)} e^{-\alpha \lambda_n^2 \theta} R_0 \frac{1}{\ln\left(\frac{r_b}{r_o}\right)} \left[\int_{r_b}^{r_o} r R_0 \ln r \, dr - \int_{r_b}^{r_o} r R_0 \ln r_o \, dr \right] \tag{6.34}$$

$$v = -\frac{\pi^2}{2} \sum_{n=1}^{\infty} \frac{\lambda_n^2 J_0^2(\lambda_n r_b)}{J_0^2(\lambda_n r_b) - J_0^2(\lambda_n r_o)} e^{-\alpha \lambda_n^2 \theta} R_0 \frac{1}{\ln\left(\frac{r_b}{r_o}\right)} \left[\frac{2\{J_0(\lambda_n r_b)\ln(r_o) - J_0(\lambda_n r_o)\ln(r_b) - \ln r_o \, J_0(\lambda_n r_b) + \ln r_o \, J_0(\lambda_n r_o)\}}{\pi \lambda_n^2 J_0(\lambda_n r_b)} \right] \tag{6.35}$$

$$v = -\frac{\pi^2}{2} \sum_{n=1}^{\infty} \frac{\lambda_n^2 J_0^2(\lambda_n r_b)}{J_0^2(\lambda_n r_b) - J_0^2(\lambda_n r_o)} e^{-\alpha \lambda_n^2 \theta} R_0 \frac{1}{\ln(r_b) - \ln(r_o)} \left[\frac{2 J_0(\lambda_n r_o)\{\ln(r_o) - \ln(r_b)\}}{\pi \lambda_n^2 J_0(\lambda_n r_b)} \right] \tag{6.36}$$

$$v = \frac{\pi^2}{2} \sum_{n=1}^{\infty} \frac{\lambda_n^2 J_0^2(\lambda_n r_b)}{J_0^2(\lambda_n r_b) - J_0^2(\lambda_n r_o)} e^{-\alpha \lambda_n^2 \theta} R_0 \left[\frac{2 J_0(\lambda_n r_o)}{\pi \lambda_n^2 J_0(\lambda_n r_b)} \right] \tag{6.37}$$

$$v = \pi \sum_{n=1}^{\infty} \frac{J_0(\lambda_n r_o)}{J_0^2(\lambda_n r_b) - J_0^2(\lambda_n r_o)} e^{-\alpha \lambda_n^2 \theta} R_0 \tag{6.38}$$

$$v = \pi \sum_{n=1}^{\infty} \frac{J_0(\lambda_n r_o)}{J_0^2(\lambda_n r_b) - J_0^2(\lambda_n r_o)} e^{-\alpha \lambda_n^2 \theta} \left[Y_0(\lambda r_o) J_0(\lambda r) - J_0(\lambda r_o) Y_0(\lambda r) \right] \tag{6.39}$$

The total solution for *U* is the combination of Eqs. (6.39) and (6.14).

$$U(r,\theta) = \frac{\ln\left(\frac{r}{r_o}\right)}{\ln\left(\frac{r_b}{r_o}\right)} + \pi \sum_{n=1}^{\infty} \frac{J_0(\lambda_n r_o)}{J_0^2(\lambda_n r_b) - J_0^2(\lambda_n r_o)} e^{-\alpha \lambda_n^2 \theta} \left[Y_0(\lambda r_o) J_0(\lambda r) - J_0(\lambda r_o) Y_0(\lambda r) \right] \tag{6.40}$$

The final solution for the temperature is given in Eq. (6.41) with the forcing function information given in Table 6-3. For the long day model only ΔF_1 and ΔF_2 are needed; for a two day model ΔF_3 and ΔF_4 would also be used (and so on for additional days).

$$t(r,\theta) = U(r,\theta-\tau_1)\Delta F_1 + U(r,\theta-\tau_2)\Delta F_2 \tag{6.41}$$

Table 6-3 Forcing function details.

	ΔF_1	ΔF_2	ΔF_3	ΔF_4
τ (hr)	0	12	24	36
Baseline	0	+3	-3	+3
Pre-cooling	-3	+6	-6	+6

In order to quantify the energy transfer to and from the ground, the heat transfer needs to be calculated. The heat transfer is defined in Eq. (6.42). This equation involves the gradient of temperature, which ultimately requires calculation of the gradient of U with respect to r; this calculation is shown in Eq. (6.43).

$$q(\theta) = -2\pi r k \frac{\partial t}{\partial r} \tag{6.42}$$

$$\begin{aligned}\frac{\partial U}{\partial r} &= \frac{1}{r\ln\left(\frac{r_b}{r_o}\right)} + \pi\sum_{n=1}^{\infty}\frac{J_0(\lambda_n r_o)}{J_0^2(\lambda_n r_b) - J_0^2(\lambda_n r_o)} e^{-\alpha\lambda_n^2\theta}\lambda_n\left[-Y_0(\lambda_n r_o)J_1(\lambda_n r) + J_0(\lambda_n r_o)Y_1(\lambda_n r)\right] \\ &= \frac{1}{r\ln\left(\frac{r_b}{r_o}\right)} + \pi\sum_{n=1}^{\infty} A_n e^{-\alpha\lambda_n^2\theta}\end{aligned} \tag{6.43}$$

The heat transfer only needs to be found at the inner boundary, r_b, leading to Eq. (6.44).

$$\frac{\partial U(r_b,\theta-\tau_i)}{\partial r} = \frac{1}{r_b\ln\left(\frac{r_b}{r_o}\right)} + \pi\sum_{n=1}^{\infty} A_n e^{-\alpha\lambda_n^2(\theta-\tau_i)} = \frac{1}{r_b\ln\left(\frac{r_b}{r_o}\right)} + \pi\sum_{n=1}^{\infty} A_n e^{-\alpha\lambda_n^2\theta} e^{\alpha\lambda_n^2\tau_i} \tag{6.44}$$

The total heat transfer occurring during a given time period is then the integral of the product of this gradient and the magnitude of the forcing function during that time interval. As an example, the heat transfer during the night is given in Eq. (6.46) and the heat transfer during the day is given in Eq. (6.47). The model developed in this section is compared to the numerical model and the DST model in Section 6.3.2.1.

$$\int_{\theta_1}^{\theta_2} \frac{\partial U\left(r_b, \theta-\tau_i\right)}{\partial r} d\theta = \frac{\theta}{r_b \ln\left(\frac{r_b}{r_o}\right)} - \frac{\pi}{\alpha}\sum_{n=1}^{\infty} \frac{A_n}{\lambda_n^2} e^{-\alpha\lambda_n^2\theta} e^{\alpha\lambda_n^2\tau_i} \Bigg|_{\theta_1}^{\theta_2} \tag{6.45}$$

$$q_{night} = -2\pi r_b k \Delta F_1 \left[\frac{\tau_2-\tau_1}{r_b \ln\left(\frac{r_b}{r_o}\right)} + \frac{\pi}{\alpha}\sum_{n=1}^{\infty} \frac{A_n}{\lambda_n^2} e^{\alpha\lambda_n^2\tau_2} \left(e^{-\alpha\lambda_n^2\tau_1} - e^{-\alpha\lambda_n^2\tau_2}\right) \right] \tag{6.46}$$

$$q_{day} = -2\pi r_b k \Delta F_2 \left[\frac{\tau_3-\tau_2}{r_b \ln\left(\frac{r_b}{r_o}\right)} + \frac{\pi}{\alpha}\sum_{n=1}^{\infty} \frac{A_n}{\lambda_n^2} e^{\alpha\lambda_n^2\tau_3} \left(e^{-\alpha\lambda_n^2\tau_2} - e^{-\alpha\lambda_n^2\tau_3}\right) \right] \tag{6.47}$$

6.2.2.1 Numerical Model

This section outlines the development of the numerical model. Unlike the DST model, which has both numerical and analytical components, it is 1-D, does not account for the interaction between boreholes, does not include a calculation of the thermal resistance between the fluid in the u-tube and the ground (borehole thermal resistance), and is generally limited in the complexity that can be modeled. This model was developed because it allows more flexibility in defining boundary conditions than the analytical model. For example, if the pre-cooling time period was prior to 6 am, then between the hours of 6 am and 12 pm the inner boundary condition is a zero flux boundary. However, the analytical model does not offer a simple way to change from a specified temperature to a zero flux boundary condition. Unless otherwise noted, variable definitions are the same as in the analytical model.

The control volume used in the development of the numerical model is shown in Figure 6-4. ΔE_{st} is the stored thermal energy, Δr is the width of the element, and q is the heat transfer into/out of the element.

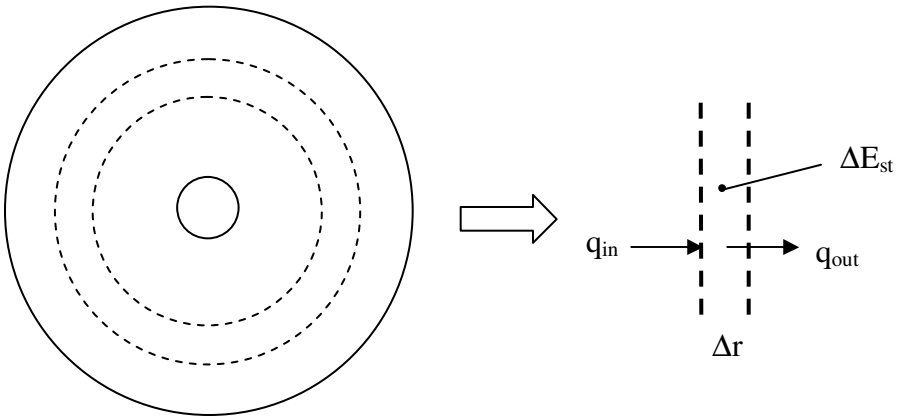

Figure 6-4 Sketch of the control volume used to develop the numerical method.

The energy balance on this element is given in Eq. (6.48).

$$q_{in} - q_{out} = \Delta E_{st} \tag{6.48}$$

The conductive thermal resistance, R_{cond}, is given in Eq. (6.49); it is used in the definition of the heat transfer (Fourier's Law) in Eq. (6.50).

$$R_{cond} = \frac{\ln\left(r_{out}/r_{in}\right)}{2\pi k} \tag{6.49}$$

$$q = \frac{\Delta t}{R_{cond}} = \frac{2\pi k \Delta t}{\ln\left(r_{out}/r_{in}\right)} \tag{6.50}$$

The energy storage term is defined in Eq. (6.51).

$$\Delta E_{st} = \rho c_p 2\pi r \Delta r \frac{\Delta t}{\Delta \theta} = \rho c_p 2\pi r \Delta r \frac{t^{+} - t}{\Delta \theta} \tag{6.51}$$

The nodal model is shown in Figure 6-5. Nodes 1 and N are determined by the boundary conditions.

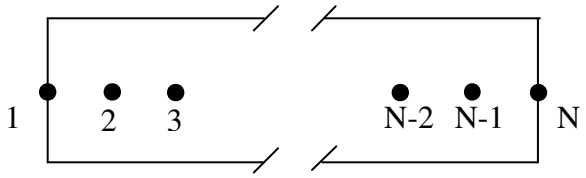

Figure 6-5 Nodal model.

A sketch of the nodal system used to develop the equations for the interior nodes is shown in Figure 6-6.

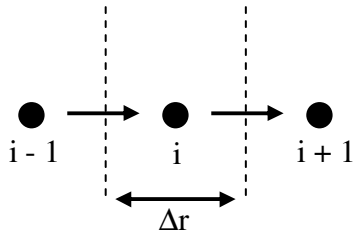

Figure 6-6 Nodal system for the interior nodes.

The energy balance on an internal node is given by Eq. (6.52).

$$\rho c_p r_i \left(r_{i+1} - r_i\right) \frac{t_i^+ - t_i}{\Delta\theta} = \frac{k\left(t_{i-1} - t_i\right)}{\ln\left(r_i / r_{i-1}\right)} - \frac{k\left(t_i - t_{i+1}\right)}{\ln\left(r_{i+1} / r_i\right)} \tag{6.52}$$

The Crank-Nicolson method is used, as shown in Eq. (6.53). The equation is rewritten as Eq. (6.55).

$$\rho c_p r_i \left(r_{i+1} - r_i\right) \frac{t_i^+ - t_i}{\Delta\theta} = \frac{k}{\ln\left(r_i / r_{i-1}\right)} \left[\frac{\left(t_{i-1} - t_i\right) + \left(t_{i-1} - t_i\right)^+}{2}\right] - \frac{k}{\ln\left(r_{i+1} / r_i\right)} \left[\frac{\left(t_i - t_{i+1}\right) + \left(t_i - t_{i+1}\right)^+}{2}\right] \tag{6.53}$$

$$\left[2\rho c_p r_i \left(r_{i+1} - r_i\right) t_i^+ - \frac{k\left(t_{i-1} - t_i\right)^+}{\ln\left(r_i / r_{i-1}\right)} \Delta\theta + \frac{k\left(t_i - t_{i+1}\right)^+}{\ln\left(r_{i+1} / r_i\right)} \Delta\theta\right] = \left[\rho c_p r_i \left(r_{i+1} - r_i\right) t_i + \frac{k\left(t_{i-1} - t_i\right)}{\ln\left(r_i / r_{i-1}\right)} \Delta\theta - \frac{k\left(t_i - t_{i+1}\right)}{\ln\left(r_{i+1} / r_i\right)} \Delta\theta\right] \tag{6.54}$$

$$t_{i-1}^+ \left[-\frac{k}{\ln\left(r_i / r_{i-1}\right)} \Delta\theta\right] + t_i^+ \left[2\rho c_p r_i \left(r_{i+1} - r_i\right) + \frac{k}{\ln\left(r_i / r_{i-1}\right)} \Delta\theta + \frac{k}{\ln\left(r_{i+1} / r_i\right)} \Delta\theta\right] + t_{i+1}^+ \left[-\frac{k}{\ln\left(r_{i+1} / r_i\right)} \Delta\theta\right] =$$
$$t_{i-1} \left[\frac{k}{\ln\left(r_i / r_{i-1}\right)} \Delta\theta\right] + t_i \left[2\rho c_p r_i \left(r_{i+1} - r_i\right) - \frac{k}{\ln\left(r_i / r_{i-1}\right)} \Delta\theta - \frac{k}{\ln\left(r_{i+1} / r_i\right)} \Delta\theta\right] + t_{i+1} \left[\frac{k}{\ln\left(r_{i+1} / r_i\right)} \Delta\theta\right] \tag{6.55}$$

This equation can be rewritten in terms of capacitance ($\underline{\underline{C}}$) and stiffness ($\underline{\underline{S}}$) matrices (Eq. (6.56)); the variable $\underline{t}$ is a vector of the temperature at all nodes.

$$\left(\underline{\underline{C}} + \underline{\underline{S}}\Delta\theta\right) \underline{t}^+ = \left(\underline{\underline{C}} - \underline{\underline{S}}\Delta\theta\right) \underline{t} \tag{6.56}$$

The capacitance and stiffness matrices are given in Eqs. (6.57) and (6.58), respectively.

$$\underline{\underline{C}} = 2\rho c_p \begin{bmatrix} 1 & & & \\ & r_2\left(r_3 - r_2\right) & & \\ & & \ddots & \\ & & & r_{N-1}\left(r_N - r_{N-1}\right) \\ & & & & 1 \end{bmatrix}_{NxN} \tag{6.57}$$

$$\underline{\underline{S}} = \begin{bmatrix} 0 & 0 & & & \\ -\dfrac{k}{\ln\left(r_i/r_{i-1}\right)} & \dfrac{k}{\ln\left(r_i/r_{i-1}\right)} + \dfrac{k}{\ln\left(r_{i+1}/r_i\right)} & -\dfrac{k}{\ln\left(r_{i+1}/r_i\right)} & & \\ & \ddots & \ddots & \ddots & \\ & & -\dfrac{k}{\ln\left(r_i/r_{i-1}\right)} & \dfrac{k}{\ln\left(r_i/r_{i-1}\right)} + \dfrac{k}{\ln\left(r_{i+1}/r_i\right)} & -\dfrac{k}{\ln\left(r_{i+1}/r_i\right)} \\ & & & 0 & 0 \end{bmatrix}_{NxN} \tag{6.58}$$

The value of 1 in the upper and lower corners of the capacitance matrix will force the temperatures at nodes 1 and N (inner and outer boundaries) to be equal to the temperatures specified for those nodes as part of the boundary conditions. These values are consistent with the specification in Figure 6-2.

The benefit of a numerical model is the ability to relatively easily change boundary conditions. Some calculations will change the inner boundary condition to a zero flux boundary, resulting in a change to the first row of the capacitance and stiffness matrices (but no change to the other rows or nodal energy balances). The energy balance on the inner node is developed as shown in the following equations.

$$\cancel{q_{in}} - q_{out} = \Delta E_{st} \tag{6.59}$$

$$\rho c_p r_1 \frac{\left(r_2 - r_1\right)}{2} \frac{t_1^+ - t_1}{\Delta\theta} = -\frac{k\left(t_1 - t_2\right)}{\ln\left(r_2/r_1\right)} \tag{6.60}$$

$$\rho c_p r_1 \frac{\left(r_2 - r_1\right)}{2} \frac{t_1^+ - t_1}{\Delta\theta} = -\frac{k}{\ln\left(r_2/r_1\right)} \frac{\left[\left(t_1 - t_2\right)^+ + \left(t_1 - t_2\right)\right]}{2} \tag{6.61}$$

$$\rho c_p r_1 (r_2 - r_1) t_1^+ + \frac{k (t_1 - t_2)^+}{\ln(r_2/r_1)} \Delta\theta = \rho c_p r_1 (r_2 - r_1) t_1 - \frac{k (t_1 - t_2)}{\ln(r_2/r_1)} \Delta\theta \qquad (6.62)$$

The modified capacitance and stiffness matrices are given in Eqs. (6.63) and (6.64).

$$\underline{\underline{C}} = 2\rho c_p \begin{bmatrix} \frac{1}{2} r_1 (r_2 - r_1) & & & \\ & r_2 (r_3 - r_2) & & \\ & & \ddots & \\ & & & r_{N-1} (r_N - r_{N-1}) \\ & & & 1 \end{bmatrix}_{NxN} \qquad (6.63)$$

$$\underline{\underline{S}} = \begin{bmatrix} \frac{k}{\ln(r_2/r_1)} & -\frac{k}{\ln(r_2/r_1)} & & & & \\ -\frac{k}{\ln(r_i/r_{i-1})} & \frac{k}{\ln(r_i/r_{i-1})} + \frac{k}{\ln(r_{i+1}/r_i)} & -\frac{k}{\ln(r_{i+1}/r_i)} & & & \\ & \ddots & \ddots & \ddots & & \\ & & -\frac{k}{\ln(r_i/r_{i-1})} & \frac{k}{\ln(r_i/r_{i-1})} + \frac{k}{\ln(r_{i+1}/r_i)} & -\frac{k}{\ln(r_{i+1}/r_i)} & \\ & & & 0 & 0 & \end{bmatrix}_{NxN} \qquad (6.64)$$

As in the analytical model the heat transfer across the inner boundary needs to be calculated, but in this case it will be calculated numerically as shown in Eq. (6.65).

$$q_b = -2\pi r_b k \sum_{\theta=\theta_1}^{\theta_2} \frac{t_2(\theta) - t_1(\theta)}{r_2 - r_1} \qquad (6.65)$$

6.3.2.1 Comparison of Analytical and Numerical Models

The numerical model was validated against the analytical model using the pre-cooling case shown in Figure 6-2 and the long day model. The time step in the numerical model is 900 s (15 min) and the spatial step is 0.02 m (0.79 in). The two models are compared at two points in time as shown in Figure 6-7. At the 6 hour time step the error based on the infinity norm is 0.0115°C and at the 24 hour time step the error is 0.025°C. The primary reason for the error is the inherent oscillations in the analytical model which occur at the step change in temperature. It

should also be noted that for the analytical solution with an outer boundary located at 4.29 m (14.1 ft) 52 terms were included in the summation in Eq. (6.40), but if the outer boundary is taken to lie at a larger radius then additional terms must be included to maintain accuracy. The number of terms required for calculation was determined by solving the problem with a given r_o with an increasing number of terms until the solution no longer changed. The approximate relationship between r_o and the number of terms, N, is given in Eq.(6.66).

$$N = 10\, r_o + 10 \tag{6.66}$$

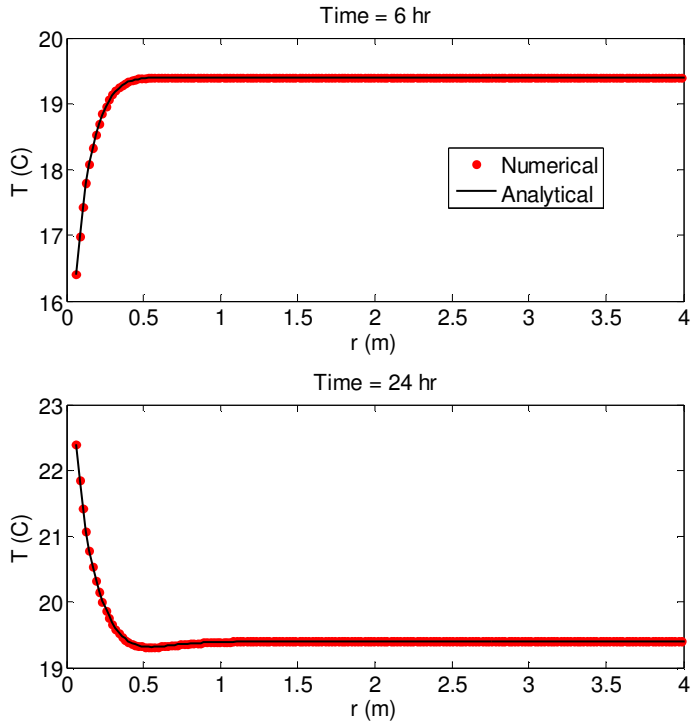

Figure 6-7 Comparison between the numerical and analytical models.

The storage efficiency of the analytical model is 0.6950 and for the numerical model it is 0.6827, less than a 2% difference. Therefore, the numerical model is accurately capturing the results. As a further check of both models, the efficiency was calculated for larger values of r_o; as expected, the efficiencies were unchanged. One other item of note is that this efficiency is similar to the value reported by Fan et al. [80].

Next, a comparison was made between the DST and numerical models. In the DST model, the borehole thermal resistance is calculated based on the thermal properties of the grout, the geometry of the u-tube and the borehole, and the thermal resistance between the fluid in the u-tube and the u-tube. The numerical model does not incorporate this calculation; instead, it specifies a temperature at the borehole wall rather than calculating one based on the fluid temperature and the borehole thermal resistance. In order to more closely match the numerical and DST models, the DST model was modified so that the borehole thermal resistance was essentially zero. In addition, the borehole length was set to 1 m, which matches the assumptions in the numerical model. The storage efficiency for each model is shown in Figure 6-8; the long term storage efficiency is 0.6827 and 0.6805 for the numerical and DST models, respectively. At a fundamental, simplistic level, the DST model behaves like the basic numerical model. The slight difference at the beginning can be accounted for by a difference in the definition of the boundary conditions.

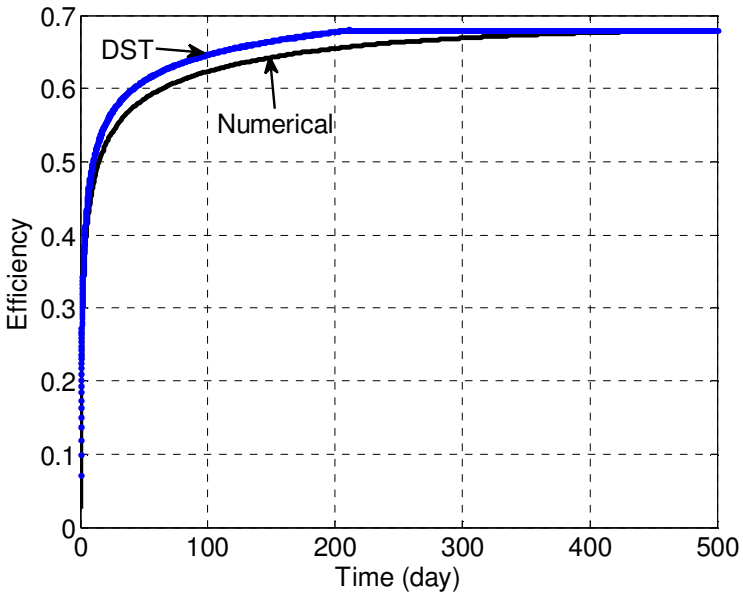

Figure 6-8 Comparison of the efficiency calculated from the DST and numerical models.

6.4.2.1 Numerical Model Results

The numerical model was used to calculate the temperature profile in the ground as a function of time for the pre-cooling cases shown in Figure 6-9. The baseline case has a 0°C specified inner boundary temperature during the night and a specified inner boundary temperature of 3°C above t_g during the day. Pre-cooling Case A has a specified inner boundary temperature during the night of 3°C below t_g and 3°C above t_g during the day. Pre-cooling Case B has a specified inner boundary temperature during the first six hours of the night of 3°C below t_g, 0°C for the remaining six hours of the night, and 3°C above t_g during the day. Pre-cooling Case C has a specified inner boundary temperature during the first six hours of the night of 0°C, 3°C below t_g for the remaining six hours of the night, and 3°C above t_g during the day.

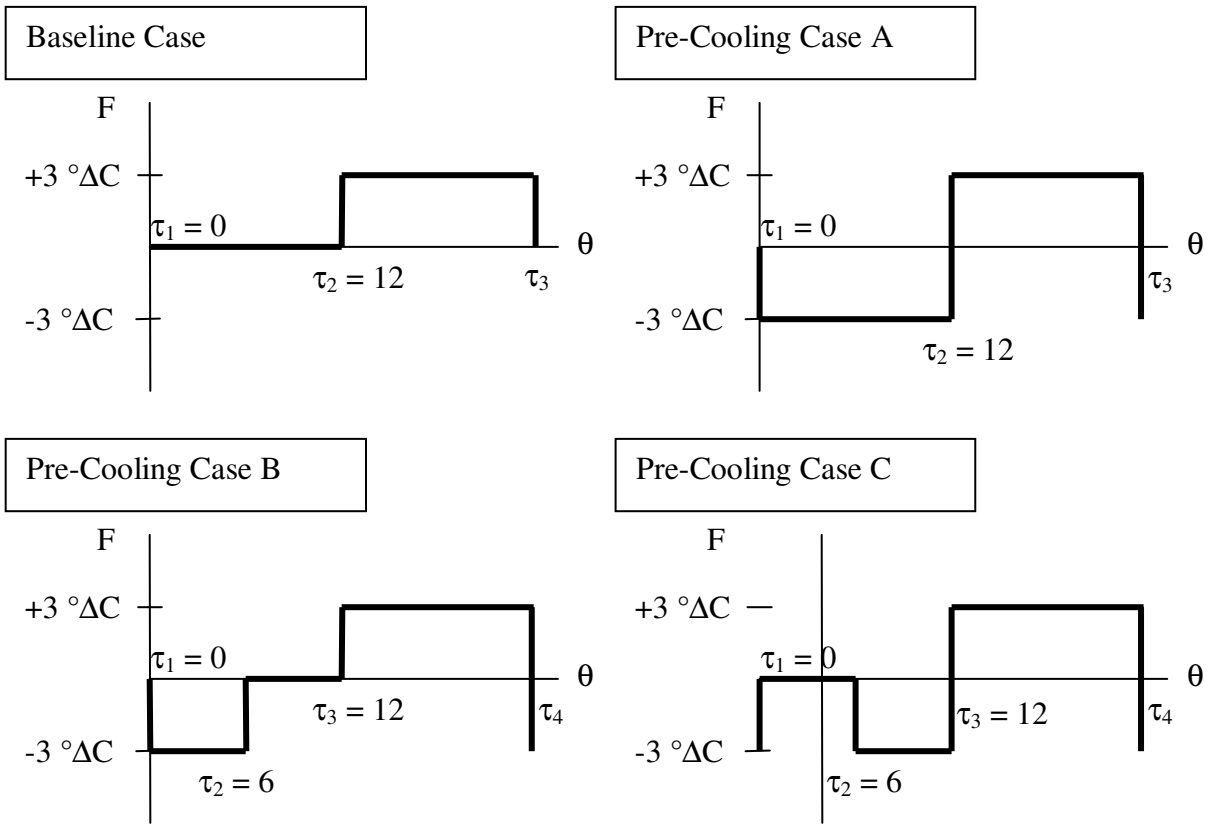

Figure 6-9 Profiles of the baseline and pre-cooling forcing functions.

Figure 6-10 shows the ground temperature (the initial temperature is 19.4°C) and heat flux profiles for the baseline and pre-cooling cases after one day of operation. After 1 day, the thermal waves for all cases have penetrated roughly the same distance into the ground, but the baseline case has only added heat to the ground, so the ground temperature has increased. For the pre-cooling cases there is actually a decrease in ground temperature from the initial condition between 0.4 and 0.75 m. These figures illustrate how pre-cooling operates.

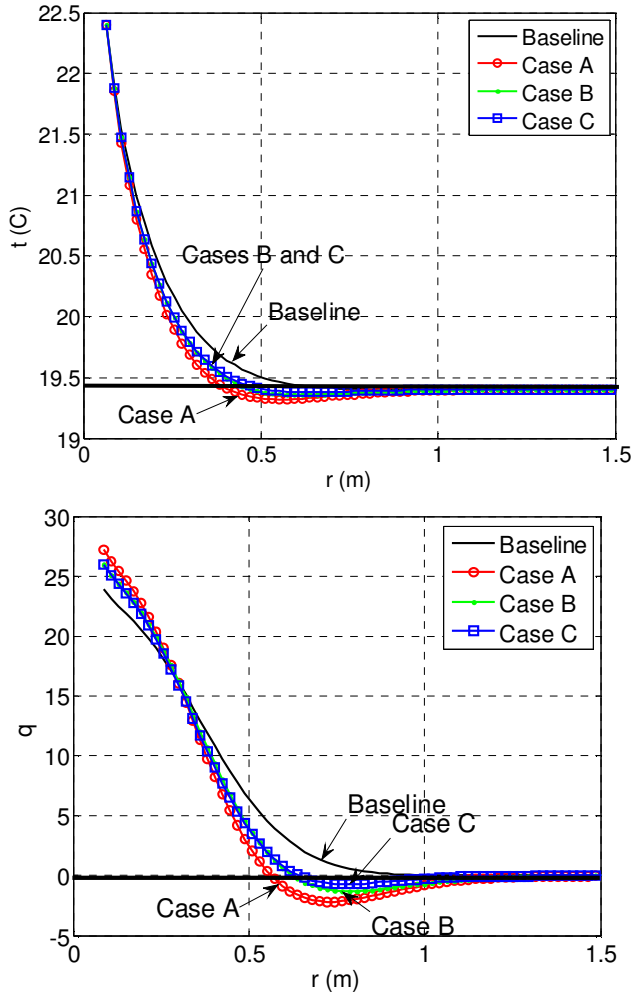

Figure 6-10 Left: Comparison of ground temperature for the different models at 24 hours. The initial ground temperature is 19.4°C. Right: Comparison of heat flux for the different models at 24 hours.

The storage efficiency was calculated for a long day model and for a model of a single day repeated over and over; in both cases, the model was run until the efficiency reached an

asymptote. For the long day model this required 200 days and for the repeated day model this required 1000 repeated days. The resulting efficiencies are given in Table 6-4. The long day model is intended to evaluate the maximum possible storage efficiency, which for the three pre-cooling models studied here is 73%. This means that at most 73% of the energy removed during the night can later be recovered in the form of additional thermal energy rejection. The remaining energy leaves the system through the outer boundary.

Table 6-4 Storage efficiency for different cases.

Pre-Cooling Case	Long Day	1000 Repeated Days
A	0.68	0.60
B	0.69	0.60
C	0.73	0.65

The storage efficiency is shown for the repeated day model in Figure 6-11. Initially the efficiency increases rapidly, but after approximately 100 days the increase slows down and eventually approaches an asymptote.

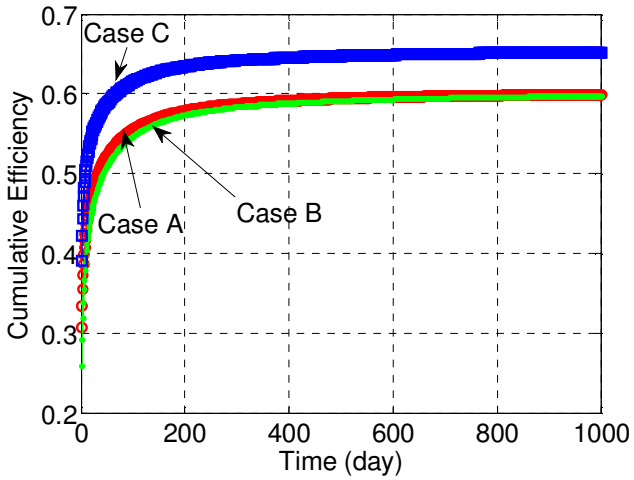

Figure 6-11 Cumulative storage efficiency for the three pre-cooling cases. Cases A and B are very similar.

In order to evaluate the conditions where pre-cooling is most effective, the storage efficiency was calculated as a function of the duration of pre-cooling, where pre-cooling is implemented immediately before the day began. For example, if the duration was 10 hours and

pre-cooling ended at 12, then pre-cooling started at 2. The results are shown in the left side of Figure 6-12; as the pre-cooling duration decreases, the storage efficiency increases. Pre-cooling can also occur at the beginning of the night with a break before day operation begins. For example, if the pre-cooling duration is 10 hours then pre-cooling ends at 10, there is no pre-cooling from 10 to 12, and day time operation starts at 12. The results of this case are shown in the right of the figure. Both sets of results indicate that pre-cooling is most effective when it is of shorter duration.

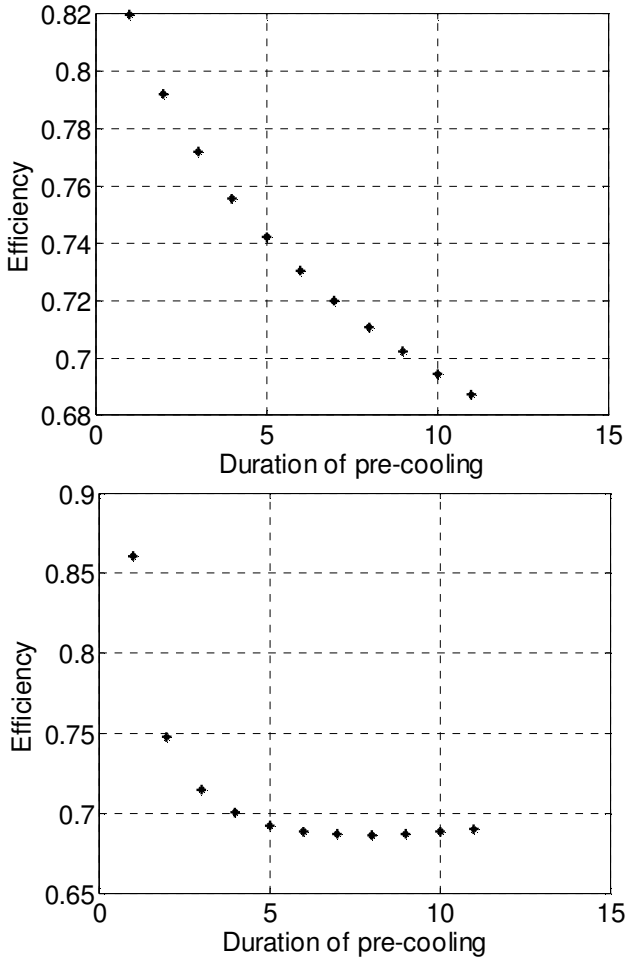

Figure 6-12 Storage efficiency as a function of the duration of pre-cooling. Left) Pre-cooling is prior to the start of the day. Right) Pre-cooling occurs, then there is a break, then the day starts.

A sensitivity study was conducted to evaluate the effect of the soil properties on the storage efficiency. There are two important parameters, the thermal conductivity, *k*, and the

volumetric heat capacity, *C*. If *k* is doubled and *C* remains the same, then the storage efficiency decreases by 10% because energy moves away from the borehole more quickly and less is stored. If *k* is halved and *C* remains the same, then the storage efficiency increases by 10% because energy moves away from the borehole more slowly. If *k* is held constant and *C* is doubled, the storage efficiency increases by 10% because more energy is stored in the ground and less leaves (or enters) through the outer boundary of the system. In this study, the baseline values for *k* and *C* are 1.94 W/m-K (1.121 Btu/hr-ft-°F) and 2619 kJ/m^3-K (39 Btu/ft^3-F), respectively.

The efficiency does not change when the specified inner boundary temperature changes from, for example, 3°C to 1°C as long as the night and day temperature offset is equal and opposite. If the night temperature offset is twice the day offset (e.g. -6°ΔC vs. +3°ΔC), there is a slight decrease in storage efficiency, but the change is so slight that it can be neglected. Storage efficiency, therefore, is not significantly impacted by the magnitude of the boundary conditions but can be impacted by the specific characteristics of the soil properties. The ideal soil for thermal storage has high heat capacity and low thermal conductivity. Note, however, that these characteristics are generally not ideal for standard HyGSHP systems. The next phase of this study is to evaluate *PC* in a realistic situation and compare it in practice to other control strategies.

6.3 Comparison of Control Strategies

6.3.1 Building Loads

Building loads are required in order to compare the performance of various control strategies, The building loads were synthesized using EFLH (Equivalent Full Load Hours) [75] with the building parameters shown in Table 6-5 and TMY weather files [73]. The loads were

calculated for four different climate zones as defined by the International Energy Conservation Code (IECC) [88,89] and shown in Table 6-6 and Figure 6-13. The comparison between cooling and heating loads in each location is shown in Table 6-7.

Table 6-5 Building design information.

Description	Value
Floor area	8856 m^2 (95,325 ft^2)
Number of floors	1
Floor height	3.05 m (10 ft)
Fraction of the floor area considered core	93.4%
Time constant for building mass	24 hrs
Overall loss coefficient for the building perimeter	12,662 kJ/hr-K
Overall loss coefficient for the building core	2,532 kJ/hr-K
Fraction of horizontal solar as gain to the building	1%
Hours of occupied period	9:00 to 21:00
Number of occupants during occupied period	953
Number of occupants during unoccupied period	5
Conditioned period	7:00 to 24:00
Lighting and equipment gain, weekdays	13.9 W/m^2
Lighting and equipment gain, Saturdays	13.6 W/m^2
Lighting and equipment gain, Sundays	7.5 W/m^2
Lighting and equipment gain, unoccupied periods	3.8 W/m^2
Infiltration rate	0.4 ACH
Infiltration rate during unconditioned periods	0.2 ACH
Fresh air during condition periods	1.6 CFM/ m^2
Minimum outdoor air temperature due to preheat system	-72.8 °C
Cooling set point temperature	24.4 °C
Set-up temperature difference	2.22 Δ°C
Heating set point temperature	21.1 °C
Set-back temperature difference	5.56 Δ°C

Table 6-6 Climate zone information for the four cities in the control strategy study.

City		Climate Zone		Ground temperature (°C)
St. Louis, MO	STL	4	Mixed-Humid	13.9
Atlanta, GA	ATL	3	Mixed-Humid	19.4
Phoenix, AZ	PHO	2	Hot-Dry	21.7
Salt Lake City, UT	SLC	5	Cold	13.3

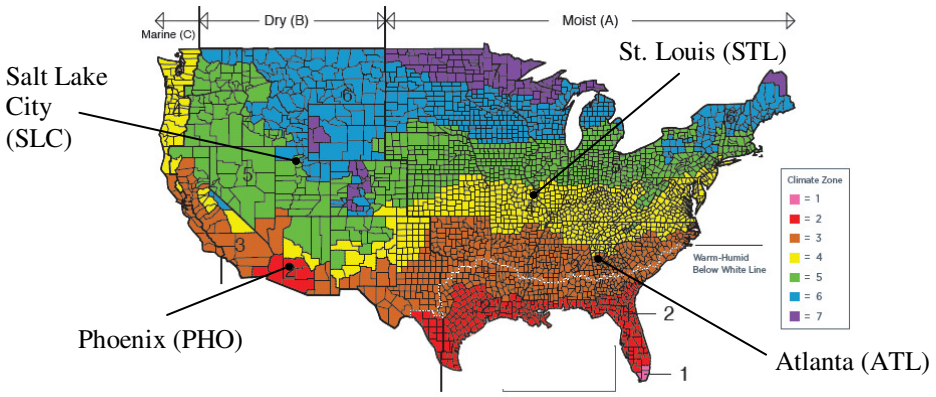

Figure 6-13 International Energy Conservation Code climate maps [89]**.**

Table 6-7 Comparison of cooling and heating loads.

City	Annual Cooling/Heating Load	Peak Cooling/Heating Load	Peak Cooling Load (kW)
STL	1.9	0.9	659
ATL	3.8	1.1	645
PHO	14.2	2.3	797
SLC	1.6	0.9	667

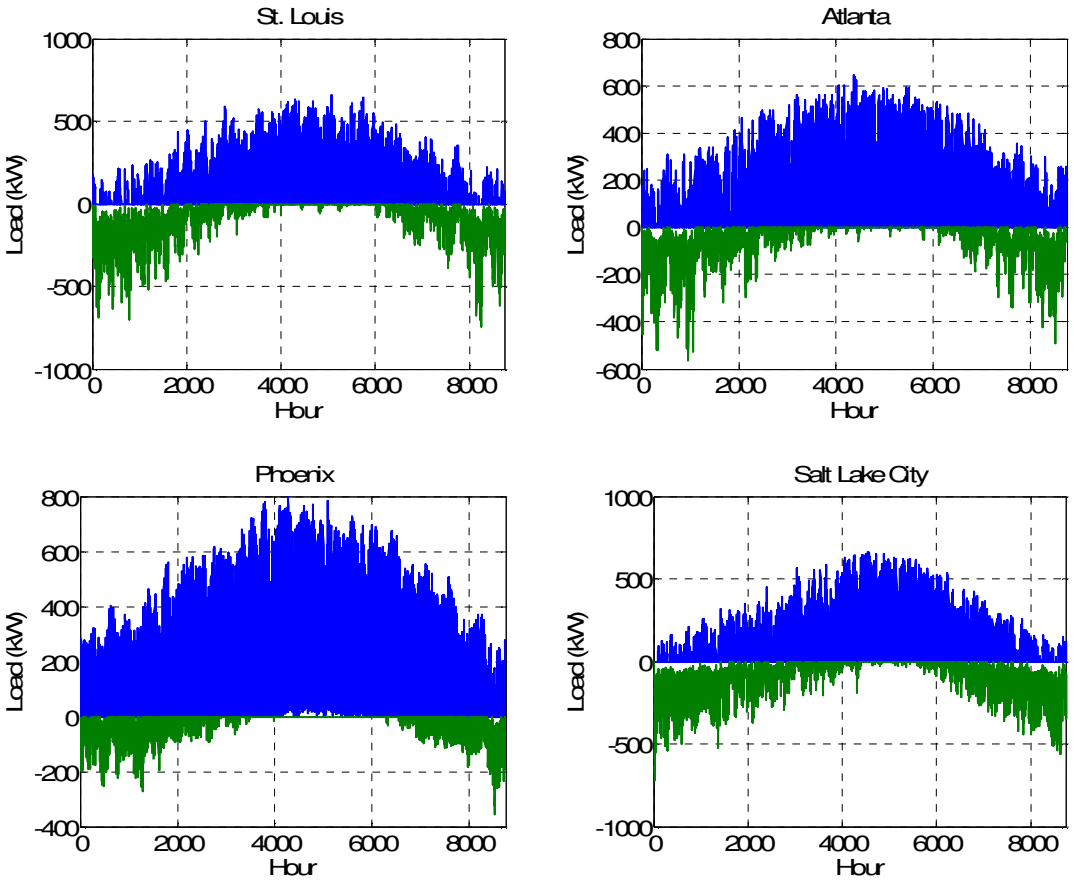

Figure 6-14 Building load profiles in each of the four climates.

Building loads at two locations in Las Vegas (zone 3) were estimated based on utility data and measurements of fluid temperatures and flow rates at a variety of points within the ground and building loops. These data were used to calibrate a building energy model. Load data generated using this model was then used to evaluate the control strategies in these two locations, referred to as L1 and L2. L1 is a mixed-use commercial facility and L2 is a school. The ground temperature is 25.6°C and the heating and cooling loads are compared in Table 6-8. Although these buildings are in Las Vegas, there are substantial heating loads because in the desert and at elevation, temperatures can decrease substantially at night resulting in significant heating loads early in the day.

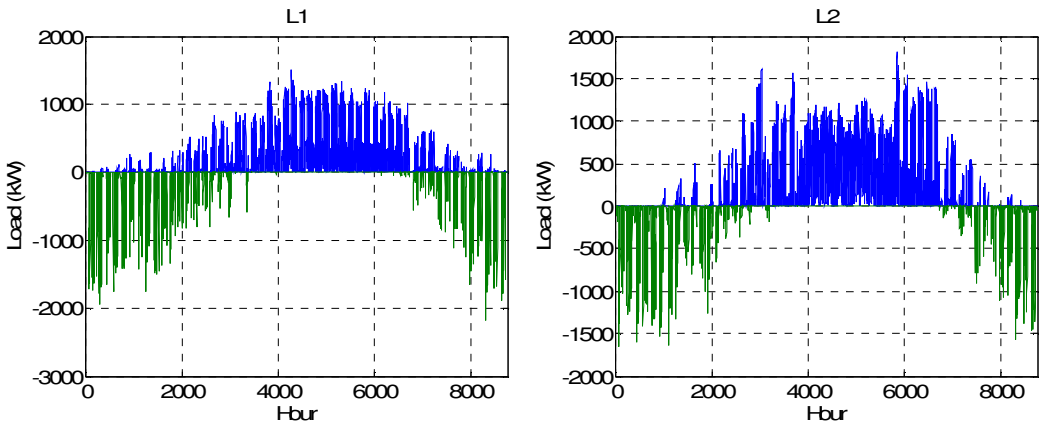

Figure 6-15 Building loads in Las Vegas.

Table 6-8 Comparison of heating and cooling loads.

City	Annual Cooling/Heating Load	Peak Cooling/Heating Load	Peak Cooling Load (kW)
L1	3.5	0.7	1503
L2	4.6	1.1	1814

6.3.2 Strategies Evaluated

Six methods of controlling a CT HyGSHP are examined in this part of the study; a GSHP system was also optimized to provide a baseline. Each control strategy (CS) is described below.

- CS0 – GSHP system design. When there is a building load, the GHX is used. The size of the GHX, L_{GHX}, is optimized.
- CS1 – Set point temperature control (T_{set}). When the temperature of the fluid upstream of the CT exceeds the set point CT1 the CT is activated at full speed. When the temperature of the fluid upstream of the GHX exceeds the set point GHX1 the GHX is activated. If there is a building load and neither the CT nor GHX has been activated based on the set point temperature, then the GHX will be activated. L_{GHX}, CT1, GHX1, and the CT size, CT_{size}, are optimized.
- CS2 – Differential set point temperature control ($T_{diff}\_T_{set}$). When the temperature of the fluid upstream of the CT exceeds the set point CT1 the CT is activated at full speed. When the temperature of the fluid upstream of the CT minus the wet bulb temperature

exceeds the set point CT2 the CT is activated at half speed. When the temperature of the fluid upstream of the GHX exceeds the set point GHX1 the GHX is activated. If there is a building load and neither the CT nor GHX has been activated based on the set point temperature, then the GHX will be activated. L_{GHX}, CT1, CT2, GHX1, and CT_{size}, are optimized.

- CS3 – Pre-cooling (PC). When the temperature of the fluid upstream of the CT exceeds the set point TPC during the day (defined as 7:00 to 21:00), if in addition the temperature of the fluid leaving the GHX exceeds the wet bulb temperature by DTPC, then the CT will be activated at full speed at night (defined as 21:00 to 7:00). The second set point, DTPC, is present to ensure that if the ground temperature is lower than the wet bulb temperature PC will not be used because it would lead to heating of the ground. L_{GHX}, GHX1, TPC, DTPC, and CT_{size}, are optimized.
- CS4 – Set point temperature control with PC (T_{set}_PC). The nominal control scheme is T_{set} (as described in CS1) but if the PC conditions are met as described in CS3, then the CT will operate at night (21:00 to 7:00) at full speed if the T_{set} strategy has not already determined that the CT will operate. L_{GHX}, CT1, GHX1, TPC, DTPC, and CT_{size}, are optimized.
- CS5 – Differential set point temperature control with PC (T_{diff}_T_{set}_PC). The nominal control scheme is T_{diff}_T_{set} (as described in CS2) but if the PC conditions are met as described in CS3, then the CT will operate at night (21:00 to 7:00) at full speed if the T_{diff}_T_{set} strategy has not already determined that the CT will operate. L_{GHX}, CT1, CT2, GHX1, TPC, DTPC, and CT_{size}, are optimized.

- CS6 – Differential set point temperature control with PC after 4 am ($T_{diff}_T_{set}$_PC_4am). This is the same as CS5 except PC, when required, only occurs from 4:00 to 7:00.

6.3.3 Results

The system design was optimized for each of the control strategies in each of the climate zones as shown in the following tables. The GSHP system design provides a baseline for evaluating the different strategies. Table 6-9 shows the design of the system and Table 6-10 shows the performance of the design in St. Louis for each control strategy. With no CT, the optimal GHX length is 18,440 m, but once a CT is added to the system this length decreases by more than a factor of two, leading to a substantial reduction in LCC. The case with the CT operating only in PC, CS3, is essentially the same as CS0, indicating that this strategy is non-optimal for a HyGSHP. The best of the designs assessed is CS2, differential temperature control. When PC is added to the nominal strategy as in CS4, CS5, and CS6, the design is essentially unchanged and, in fact, no or nominally little PC is used (see Table 6-10). The reasons for the minor differences between the designs for similar strategies (CS1 and CS4, CS2 and CS5 and CS6) are due to the limits of optimization as discussed in Chapter 4.

Table 6-9 System design in St. Louis.

	GHX Length (m)	CT size (kW)	CT2	CT1	GHX1	TPC	DTPC	LCC
CS0	18,440				-2			964,769
CS1	6897	404		26.7	10.5			680,422
CS2	7073	410	0.83	37.3	13.7			657,661
CS3	18,416	30			3.2	-1	20	980,659
CS4	7008	460		32	7.7	11.8	20	686,777
CS5	7071	420	1.1	37.2	12.3	3.1	20	658,183
CS6	7094	517	4.5	44.1	2.8	28.2	14.4	663,748

The performance data reveal some interesting behaviors in the operation of the system. The addition of a CT tends to lead to a slight increase in the heat pump power consumption because there is a greater increase in ground temperature over time relative to the nominal case

due to the reduction in volume of the ground used for heat rejection. The minimum EFT decreases from 10°C to 2°C, which means that during the heating season the EFT is lower in a hybrid system and the HP performance is slightly worse. This is reflected in the slight increase in the cost of electricity. The LCC cost does not decrease due to performance gains, but rather due to the ability to dramatically decrease the size of the GHX and thereby the first cost of the system.

Table 6-10 Performance results in St. Louis.

	CS0	CS1	CS2	CS3	CS4	CS5	CS6
LCC ($)	964,769	680,422	657,661	980,659	686,777	658,183	663,748
HP Power (kWh)	4,429,029	4,493,076	4,528,143	4,429,943	4,565,391	4,520,356	4,468,047
CT Power (kWh)	0	685,152	233,807	52	557,321	238,334	264,540
Pumping Power (kWh)	226,392	228,298	229,104	226,415	229,734	229,026	227,731
Min EFT (°C)	10	2	2	10	2	2	2
Max EFT (°C)	35	35	35	35	35	35	35
Qghx (kJ)	3.24E+10	9.63E+09	9.56E+09	3.24E+10	1.22E+10	9.39E+09	8.31E+09
Qct (kJ)	0	2.30E+10	2.32E+10	3.19E+06	2.06E+10	2.33E+10	2.42E+10
Electric Cost ($)	357,936	419,907	384,510	358,024	416,750	384,169	381,643
Hours of PC	0	0	0	32	740	0	0

A visual comparison of the control strategies is given in Figure 6-16. The y-axis is the LCC as compared to the LCC for the CS0 design; a negative value indicates that the LCC is lower than CS0. The x-axis is the total energy consumption as compared to the total energy consumption for CS0; a positive value indicates an increase in total energy consumption. All of the control strategies result in greater energy consumption because a hybrid system is less efficient than a GSHP system; the goal of a hybrid is to reduce the LCC without compromising the energy efficiency too much, so an ideal system will result in a point in the lower left corner of the plot (negative LCC, minimal increase in energy consumption). CS3 has the smallest increase in energy consumption, but the LCC increases. The set point temperature control and differential set point temperature control strategies all result in lower LCC, but the set point

temperature strategies (CS1 and CS4) lead to a greater increase in energy consumption than the differential temperature control strategies.

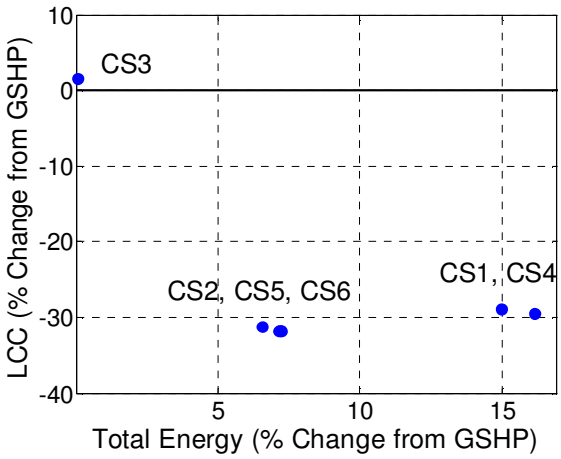

Figure 6-16 Percentage change in LCC versus the GHX only design as a function of the percentage change in total energy consumption versus the GHX only design.

The system design in Phoenix is given in Table 6-11. In this case, CS5 has a slightly lower LCC than CS2, but, in examining Table 6-12, it is revealed that PC is not used in CS5. Again, the slight difference between CS2 and CS5 is due to slight differences in the optimization, but, in essence, these two designs are the same. Unlike in St. Louis, in this climate CS3 is a more optimal design than CS0; a CT could be added and operated in PC only mode and lead to a smaller GHX and lower LCC. However, this type of operation is far from optimal as the LCC is still more than three times the cost of any of the other hybrid control strategies. Unlike in St. Louis, in Phoenix the HP performance improves with the addition of a CT (except in the case of CS3), although the overall cost of electricity increases due to the additional power required to operate the CT.

The optimal design for CS4 demonstrates that care is required in performing optimization. In this case, the starter method, which is designed to converge relatively quickly to a "good enough" design in order to provide a starting point for the main optimization converges

to a non-optimal point; in this case the length of the GHX is twice that of CS1. The main optimization searches the region near this point, so the actual optimum is never sampled. This, again, brings a focus on the need to carefully consider the balance between a faster, potentially less optimal optimization and a slower, potentially more optimal optimization. In the cases evaluated in this work, the greatest optimization errors occurred with the PC cases, in which there were two additional decision variables that had minimal impact on the LCC. For example, once TPC is larger than approximately 25°C, PC is very unlikely to occur, but the optimizer will continue to include TPC and the solution space will not be reduced in size such that less optimal points are excluded from consideration. There is a greater chance of converging to a local solution. (See Chapter 4 for a more complete discussion of optimization issues.)

Table 6-11 System design in Phoenix.

	GHX Length (m)	CT size (kW)	CT2	CT1	GHX1	TPC	DTPC	LCC
CS0	65,620	0	0	0	-2	0	0	2,623,340
CS1	2334	796	0	9.8	29	0	0	784,702
CS2	2148	1185	1.3	45.9	9.9	0	0	665,886
CS3	48,758	858	0	0	9.6	27.1	4.7	2,208,104
CS4	5252	1108	0	24.2	24.3	43.1	17.6	889,382
CS5	2050	1230	-5	42.8	29.4	41.4	-5	662,496
CS6	2294	1180	-5	47.8	20.9	44.3	10.7	669,294

Table 6-12 Performance results in Phoenix.

	CS0	CS1	CS2	CS3	CS4	CS5	CS6
LCC ($)	2,623,340	784,702	665,886	2,208,104	889,382	662,496	669,294
HP Power (kWh)	5,384,940	4,966,791	4,996,595	5,407,116	4,738,193	5,020,255	5,008,333
CT Power (kWh)	0	3,447,228	952,527	1,017,669	3,176,912	985,830	951,364
Pumping Power (kWh)	336,600	221,414	331,203	337,475	274,577	214,103	295,118
Min EWT (°C)	21	5	2	21	16	2	5
Max EWT (°C)	35	35	35	35	35	35	35
Qghx (kJ)	8.36E+10	2.97E+08	-3.08E+08	6.04E+10	2.41E+09	1.24E+08	7.01E+08
Qct (kJ)	0	8.18E+10	8.25E+10	2.32E+10	7.88E+10	8.21E+10	8.15E+10
Electric Cost ($)	460,827	675,492	503,778	525,219	656,859	499,812	502,453
Hours of PC	0	0	0	18,943	0	0	0

Figure 6-17 shows that all of the control strategies lead to a decrease in LCC, but the PC only strategy has the least reduction in LCC. As in St. Louis, the best strategies use differential temperature control.

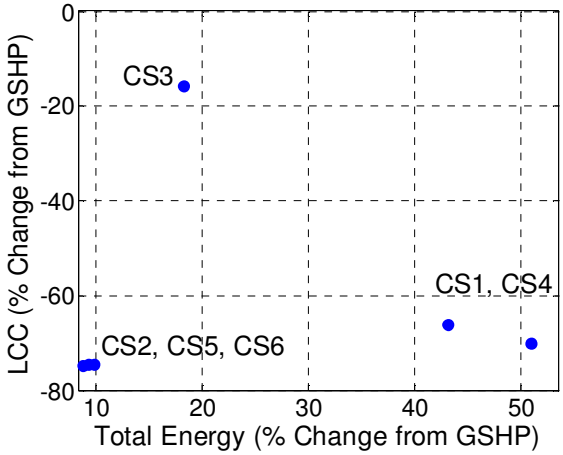

Figure 6-17 Percentage change in LCC versus the GHX only design as a function of the percentage change in total energy consumption versus the GHX only design.

The results in Atlanta and Salt Lake City show the same trends as those in St. Louis and Phoenix. The results for Las Vegas, location 1, are shown in Table 6-13 and. In this case CS3 is much better than CS0 in terms of LCC primarily because the length of the GHX is reduced by a factor of three. The temperature of the ground in Las Vegas is 25.6°C while the humidity is low, so it is often more effective to use the CT to reject heat than to use the ground. This is an unusual situation; in most other locations, the ground temperature is lower and the humidity is higher; Las Vegas is not a representative location for the behavior of a CT HyGSHP in the United States.

The addition of PC to set point temperature control (CS4 vs. CS1) led to a reduction in the LCC of 12.6% while the length of the GHX decreased by 12.5% and the CT size decreased by 66%. The decrease in LCC is due primarily to the decrease in the size of the GHX, though the smaller CT also uses less energy relative to CS1, so there are some operational savings as well. Although the CT is smaller for CS4 than CS1, it still rejects nearly the same amount of heat

because it operates for more hours. A total of approximately 36,500 hours of PC are possible, and in the case of CS4 PC is used for 25.6% of those hours. In this case, adding PC to the nominal set point temperature control scheme is more optimal than using just set point temperature control. However, of the control strategies examined, this is not the best strategy; CS2 is still the strategy which yields the lowest LCC.

Table 6-13 System design in Las Vegas, L1.

	GHX Length (m)	CT size (kW)	CT2	CT1	GHX1	TPC	DTPC	LCC
CS0	85,663	0	0	0	-2	0	0	3,558,618
CS1	12,963	2982	0	23.5	-2	0	0	1,353,090
CS2	11,159	1624	-0.2	48.5	23.6	0	0	1,135,525
CS3	28,585	3000*	0	0	18.7	18.2	9.1	1,921,032
CS4	11,342	1004	0	28.8	15.9	31.8	9.5	1,181,276
CS5	12,363	1798	7.1	49.8	2.5	45.6	3.6	1,177,358
CS6	12,363	1798	7.1	49.8	2.5	45.6	3.6	1,177,358

*Upper limit

Table 6-14 Performance results in Las Vegas, L1.

	CS0	CS1	CS2	CS3	CS4	CS5	CS6
LCC ($)	3,558,618	1,353,090	1,135,525	1,921,032	1,181,276	1,177,358	1,177,358
HP Power (kWh)	7,213,796	6,337,320	6,722,972	6,745,754	6,808,749	6,581,066	6,581,066
CT Power (kWh)	0	2,605,097	943,669	3,097,171	1,844,279	874,992	874,992
Pumping Power (kWh)	436,672	423,841	287,451	410,295	432,368	429,131	429,131
Min EWT (°C)	24	3	2	13	3	2	2
Max EWT (°C)	35	35	35	35	35	33	33
Qghx (kJ)	6.30E+10	-1.01E+10	-4.08E+09	-1.38E+10	-3.14E+09	-9.81E+09	-9.81E+09
Qct (kJ)	0	6.99E+10	6.53E+10	7.51E+10	6.46E+10	7.05E+10	7.05E+10
Electric Cost ($)	583,273	717,759	603,536	717,920	686,736	595,720	595,720
Hours of PC	0	0	0	29,089	9326	0	0

Consistent with the prior two cases, the differential temperature control strategies are the best. CS3 is viable in terms of significantly reducing LCC, but there is also a significant increase in energy consumption because of the large size of the CT. In practice, this energy consumption could be decreased some by using more than one CT, bringing them online as necessary to meet the load, but this type of design was outside the scope of the current work.

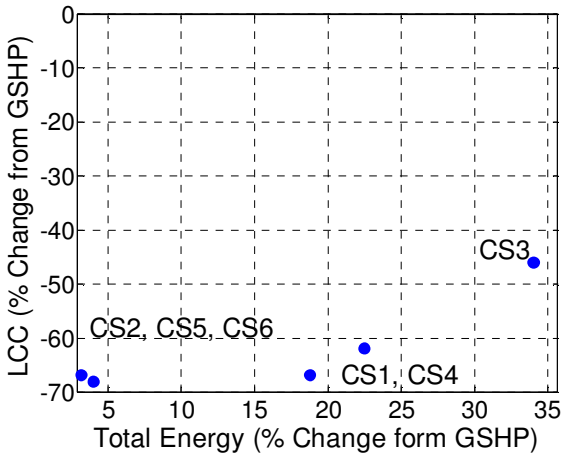

Figure 6-18 Percentage change in LCC versus the GHX only design as a function of the percentage change in total energy consumption versus the GHX only design.

The hybrid system design does not lead to a balanced ground load. In general, the cooling load on the ground exceeds the heating load even when a CT is added. A system optimized for LCC is not the same as a system optimized to balance the ground load. The LCC has the greatest sensitivity to the GHX size, which is one reason that there is less variation in the size of the GHX than in the size of the CT or the set points for a given strategy (see Chapter 8 for more information on sensitivity).

6.3.4 Control Strategies for an Existing System

A further evaluation of the control strategies is made by using the design method for HyGSHPs described in Ch. 34 of the 2011 ASHRAE Handbook – HVAC Applications [59]. This method was used to find a GHX length and CT size; each of the control strategies was then optimized for use with this design in each location. This analysis is designed to evaluate the performance of each control strategy as applied to a pre-existing design. The goal is to determine if the conclusions about the optimal strategy and the ineffectiveness of pre-cooling hold true if the size of the GHX and CT are the same for each design.

Based on a study by Hackel, et al, [11], the length of the GHX, L_{GHX}, can be estimated using a linear regression that is a function of the peak heating load, q_h, the ground temperature, t_g, and the temperature of the fluid exiting the heat pump, t_{wo} (see Eq.(6.67)). The only unknown value in this calculation is t_{wo}, which is calculated from Eq.(6.68) [53].

$$L_{GHX} = 254 \frac{ft \cdot h \cdot °F}{kBtu} \frac{q_h}{t_g - t_{wo}} \tag{6.67}$$

The parameter W is the power consumption at the design condition multiplied by the part load factor of the heat pump (PLF). The solution is insensitive to the value of PLF, so a constant value of 0.5 was used in the calculation. The inlet water temperature to the heat pump, t_{wi}, is 15°F below t_g [53]. The flow rate, Q_w, is 3 gpm/ton times the peak heating load in tons. The constant 500 is a conversion factor which also accounts for the density and specific heat of the fluid.

$$t_{wo} = t_{wi} - \frac{q_h - W}{500 \frac{Btu \cdot \min}{gal \cdot hr \cdot °F} Q_w} \tag{6.68}$$

The design for each location is shown in Table 6-15 using the ASHRAE method and the optimal design using the CS2 control method. The ASHRAE method generally over-sizes the GHX and under-sizes the CT, resulting in an increase in LCC over the optimal case. This is not surprising given the generality and simplicity of the ASHRAE method as opposed to the detailed optimizations conducted with FHyGSHP.

Table 6-15 GHX length and CT size using the ASHRAE method.

Site	ASHRAE Design		Optimal CS2 Design	
	GHX length (m)	CT Size (kW)	GHX length (m)	CT Size (kW)
St. Louis	9008	356	7073	410
Atlanta	6834	514	4069	764
Phoenix	4271	845	2148	1185
Salt Lake City	8686	373	6487	419
L1	26,456	878	11,159	1624
L2	20,025	1544	11,050	2843

The St. Louis and L1 results are presented here. CS2 is the optimal strategy when the GHX length and CT size are constant. Another item to note is that there is substantial agreement between the set points for the cases when PC is and is not used (e.g. CS1 vs. CS4); when PC is added it does not improve the performance.

Table 6-16 Control set points for a design with GHX and CT size based on ASHRAE recommendations in St. Louis.

	GHX Length (m)	CT size (kW)	CT2	CT1	GHX1	TPC	DTPC	LCC
CS1	9008	356	0	31.4	-0.7	0	0	736,116
CS2	9008	356	-5	38.1	-2	0	0	713,114
CS4	9008	356	0	32.9	-1	0.06	-3.9	749,331
CS5	9008	356	-5	40	-2	7.8	-5	725,774

Table 6-17 Performance of the designs in St. Louis.

	CS1	CS2	CS4	CS5
LCC ($)	736,116	713,114	749,331	725,774
HP Power (kWh)	4,537,837	4,464,716	4,546,028	4,423,817
CT Power (kWh)	405,472	199,134	754,647	579,084
Pumping Power (kWh)	229,293	227,687	229,399	226,552
Min EWT (°C)	5	5	5	5
Max EWT (°C)	35	35	34	34
Qghx (kJ)	1.61E+10	1.26E+10	1.46E+10	1.03E+10
Qct (kJ)	1.67E+10	1.99E+10	1.82E+10	2.21E+10
Electric Cost ($)	402,454	376,376	419,603	393,395
Hours of PC	0	0	0	0

In Las Vegas, for L1, when PC is added to either CS1 or CS2, the LCC decreases by a modest amount; in this case the reduction is due to the use of PC, as shown in Table 6-17. PC leads to a modest reduction in the power consumption of the HP. This is the only clear example in all of the cases tested where PC makes a difference, and in this case the reduction in LCC is

small. Las Vegas is also an outlier in terms of climate because the undisturbed ground temperature is often greater than the wet bulb temperature and therefore a CT is often the better heat rejection option.

Table 6-18 Control set points for a design with GHX and CT size based on ASHRAE recommendations in Las Vegas, building L1.

	GHX Length (m)	CT size (kW)	CT2	CT1	GHX1	TPC	DTPC	LCC
CS1	26,456	877	0	32.5	26.1	0	0	1,709,144
CS2	26,456	877	4.7	41.3	6.6	0	0	1,654,096
CS4	26,456	877	0	31.7	6.6	14.3	19.8	1,707,814
CS5	26,456	877	-0.8	41.3	6.6	24	15.8	1,651,931

Table 6-19 Performance of the designs in Las Vegas, building L1.

	CS1	CS2	CS4	CS5
LCC ($)	1,709,144	1,654,096	1,707,814	1,651,931
HP Power (kWh)	6,962,616	6,751,352	6,853,962	6,731,188
CT Power (kWh)	961,169	565,870	1,350,616	630,916
Pumping Power (kWh)	431,103	431,079	431,778	430,770
Min EWT (°C)	19	16	15	15
Max EWT (°C)	33	33	32	32
Qghx (kJ)	1.27E+10	-1.64E+09	3.22E+09	-2.59E+09
Qct (kJ)	4.94E+10	6.29E+10	5.85E+10	6.38E+10
Electric Cost ($)	640,535	587,639	648,172	589,243
Hours of PC	0	0	9084	1182

6.4 Conclusions

Pre-cooling is an ineffective control strategy for operating a hybrid ground source heat pump. Pre-cooling is effective in decreasing loop temperatures, but the performance gain in the heat pumps is insufficient to offset the increased power consumption associated with operating the cooling tower and circulating pump. The only case where pre-cooling was beneficial was Las Vegas and the reduction in life cycle cost was small relative to the added complexity of the system. Set point and differential set point temperature control schemes for cooling tower hybrid ground source heat pump operation are optimal on the basis of minimizing life cycle cost. In general, the differential temperature control strategy will result in a more optimal design and it is recommended. For a control scheme of minimal complexity, set point or differential temperature

control are recommended because the addition of pre-cooling to these strategies does not lead to performance gains.

There are several limitations to this study. The cooling tower was not operated at variable speeds, and this may make some difference in the conclusions of the study. However, when set point control was used with 50% instead of 100% fan speed, the design was comparable to differential temperature control. Incorporating variable fan speed with set point control may be preferable to using differential temperature control due to the simplicity of set point control. The thermal conductivity and heat capacity of the ground heat exchanger were held constant for all of the simulations. A ground source heat pump works best when heat quickly diffuses from the region around the borehole, whereas *PC* works best when the diffusion is slow, so if pre-cooling works well the ground source heat pump may perform poorly during normal operation. Finally, the economic parameters were not varied from location to location; the same electric and water rates were used in all climates. None of these assumptions are expected to change the conclusions of the study, but they would change the magnitude of the results.

Chapter 7 FHyGSHP (Fast Hybrid Ground Source Heat Pump)

The FHyGSHP program has been developed in order to fill some of the gaps in the existing design tools for hybrid ground source heat pump (HyGSHP) systems. The goal is to create a program that provides a method for optimizing the size of the components in a HyGSHP design and the control set points for operating the system. The program includes a wide array of user selectable options and inputs such that the program can be used by practitioners or researchers. Some of the key features incorporated in FHyGSHP are:

- optimization of component sizes and control set points,
- multiple system configurations,
- weather variability,
- extensive economic analysis including time of day rates and fluid costs,
- specification of an upper limit on the total change in ground temperature,
- specification of a lower limit on energy savings relative to a conventional system,
- and multiple controls strategies, including pre-cooling.

These features are described in more detail in the latter portion of this chapter, while the first part discusses some of the existing design tools.

7.1 Existing Design Tools

There are a number of tools that can be used for ground source heat pump (GSHP) design and a few that also include HyGSHP design; a few of these models are discussed here. Kavanaugh [1,90] developed methods for designing a GSHP and HyGSHP system that do not require hourly load data; GshpCalc implements the method for GSHP design [91]. Based on user inputs such as peak heating and cooling loads and some specifications regarding the ground properties, heat pump properties, etc., the program outputs a design in a few seconds. The user

can optimize the design by repeating the calculation with different inputs. Unlike GshpCalc, FHyGSHP optimizes the design, including control set points, and models a hybrid system. In addition, FHyGSHP uses more detailed component models and inputs. The trade off is that FHyGSHP requires additional calculation time, especially for optimization.

GLHEPRO is another commercially available design program; it was developed at Oklahoma State University [92]. This tool uses the g-function model for the ground heat exchanger (GHX). The user inputs include monthly building loads, bore-field configuration, borehole radius and depth, and heat pump performance data. The program can run a simulation using the input data or it can size the system to meet the specified loads. There is also an option to size the GHX and supplemental device in a HyGSHP using optimization. The optimization requires initial guess values for the ratio between the GHX length in the HyGSHP and the GHX length in a GSHP system, the ratio of the load met by the supplemental device to the load met by the GHX, and the initial step size for these parameters (used by the optimization algorithm). FHyGSHP also optimizes the GHX length and size of the supplemental device (cooling tower); in addition, the control set points are optimized.

Two additional design tools have been referenced in the literature [51], but details of how the packages calculate a design, such as whether or not they include a hybrid option or use optimization, were not available. However, the details of the GHX models incorporated into these packages are available and are detailed here. Geostar [93] models the GHX in two parts: inside the borehole and outside the borehole. The region outside the borehole is modeled using an analytical finite line source model [23] and the region inside the borehole is modeled by a quasi-three-dimensional solution that accounts for the temperature variation with depth [94] with the solutions coupled at the borehole wall. The interaction between boreholes is accounted for by

superposition. GEOEASE II also combines different methods. The borehole thermal resistance is calculated using the method developed by Zeng [94] and the cylinder source model is used to calculate the difference between the temperature at the borehole wall and the ground [34]. The g-function model is used to determine the response of the ground to the heat input and load aggregation [34] is used to reduce computation time.

TRNSYS [15] is a program in which a system can be created from a library of stock component models or user-generated component models written in FORTRAN. TRNSYS can be used to simulate system operation at sub-hourly time steps and includes the DST model of the ground heat exchanger in the component library. HyGCHP is a TRNSYS-based distributable software program developed for and funded by ASHRAE Research Project RP 1384 [4,11]. HyGCHP allows the user to optimize the design of a conventional (cooling tower and boiler), GSHP, or hybrid GSHP system in order to minimize LCC (Life Cycle Cost). The HyGCHP program was modified and partially validated as part of a subsequent DOE study [7,57] and is freely available [95].

FHyGSHP is an extension of HyGCHP. It is a standalone FORTRAN executable that can optimize a hybrid design more quickly than HyGCHP. Preliminary tests show that a 5 year simulation in FHyGSHP takes 21% as long as the same case in HyGCHP, a factor of 5 reduction in computational time. It includes and improves upon some of the same features in existing programs, but also includes new features. Some of the key features incorporated in FHyGSHP are:

- optimization of component sizes and control set points,
- multiple system configurations,
- weather variability,

- extensive economic analysis including time of day rates and fluid costs,
- specification of an upper limit on the total change in ground temperature,
- specification of a lower limit on energy savings relative to a conventional system,
- and multiple controls strategies, including pre-cooling.

7.2 Program Structure

An executable FORTRAN program is called by a Graphical User Interface (GUI) built in EES (Engineering Equation Solver) [96]. The user is required to supply an input file containing a single year of hourly data: the first column of the file is the time of year in hours (1 to 8760 hours), the second column is the cooling load in kJ/hr, the third column is the heating load in kJ/hr, the fourth column is the dry bulb temperature in °C, and the fifth column is the wet bulb temperature in °C. This information can be obtained from any of a number of building simulation programs. If desired, the user can supply a file containing multiple years of hourly data. The GUI contains several windows, each containing a different set of inputs that the user can modify or leave as defaults. This section describes each of these windows and briefly discusses the inputs that can be set within each window. When the user chooses to run the program, a series of files are generated containing the inputs in a format that can be read by the executable program; this is the manner in which the user inputs are passed to the program. These files can be accessed directly if the user prefers to bypass the GUI and operate the program directly (see Appendix C for more details). The help documentation is included in the Appendix and contains more extensive information about the inputs to the program.

7.2.1 Main Diagram Window

The *Main Diagram Window* is the home base for the program, consisting of buttons that link to the other input windows; this screen can be returned to from any of the other windows by

selecting the home button. A screen shot of the *Main Diagram Window* is shown in Figure 7-1. At the upper left, the system to be simulated is selected from a list of radio buttons. *Conventional* refers to a system with a furnace and cooling tower, *Ground Source Heat Pump* is a system with only a ground heat exchanger and *Cooling Tower Hybrid* is a system with a cooling tower and ground heat exchanger. When either the *Ground Source Heat Pump* or the *Cooling Tower Hybrid* system is selected, the user has the option of including a furnace in the design (the inclusion of a furnace is the default option) and comparing that design to the conventional system design. If this latter option is selected then the program will calculate both the conventional and otherwise selected system designs and performance.

The *Detailed Schematic* is accessed by clicking anywhere in the box surrounding those words in the *Main Diagram Window*. The windows for the heat pump and furnace, circulating pump, ground heat exchanger, and cooling tower are accessed by clicking on the image of the object. The list at the right of the window provides access to each of the windows listed by clicking on the name of that window. At the lower right, the default input file can be loaded by selecting *Load Inputs* and then selecting the defaults file. New input files can be saved by selecting the *Save Inputs* button. The *Run* button will run the executable FORTRAN program; if optimization is being performed and the user needs to stop the calculation, perhaps to change the program settings, the *Stop* button can be selected. If this button is selected, the optimization will restart from the beginning. The user also has the option of closing the command window that opens when the program is run.

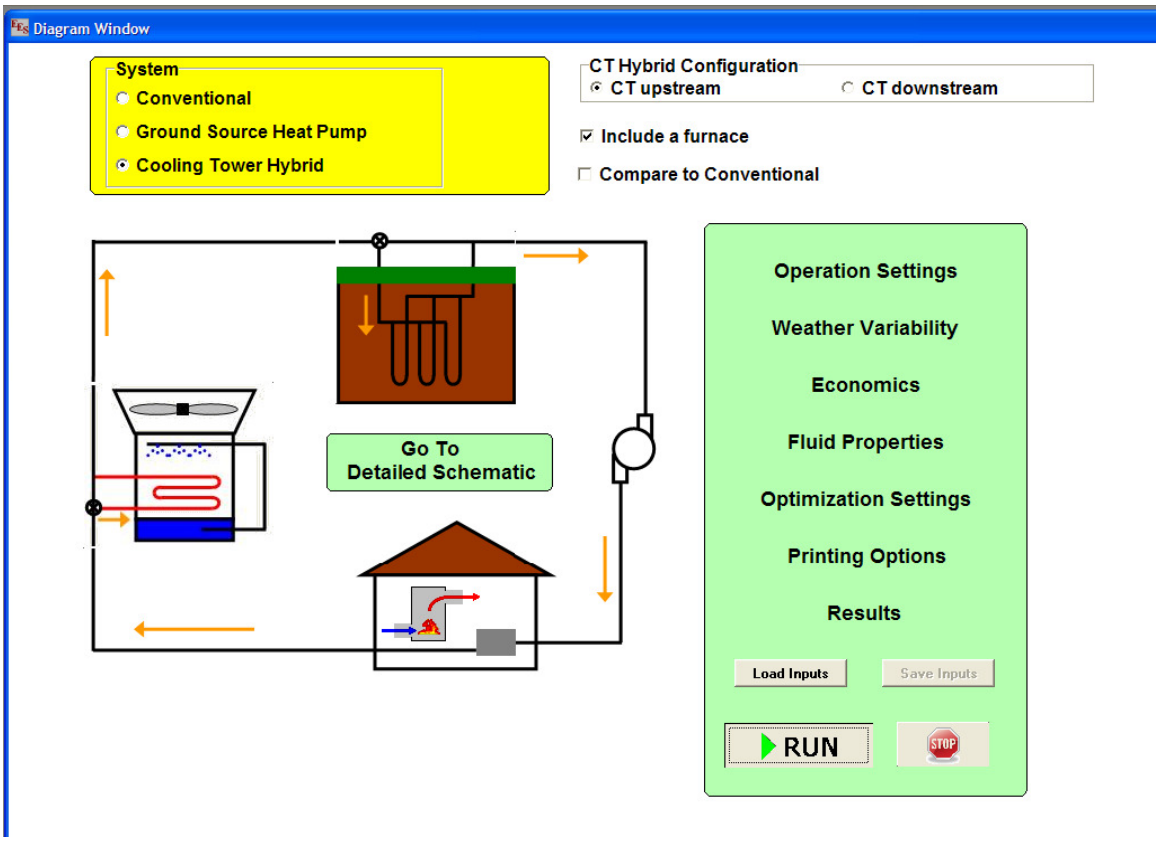

Figure 7-1 Screen shot of the main diagram window.

7.2.2 Operation Settings

The *Operation Settings* window contains the most important settings for the program operation; a screen shot is shown in Figure 7-2. In this window the user selects the file containing the building heating and cooling loads and enters the directory in which output files should be saved. The simulation time step is selected from a drop down menu and can take one of four values: 0.25 hr, 0.5 hr, 0.75 hr, or 1 hr; 0.5 hr is the default. The *Unit System* can be selected as either SI or English units; the user may input information in the specified unit system, but output data are all printed in SI units. The number of years to be simulated is set in the *Duration of the simulation.*

The *Control Strategy* is selected from the dropdown menu; each strategy is briefly mentioned here, but Chapter 6 contains more details. *Hybrid control* is the default option for controlling the cooling tower hybrid ground source heat pump (CT HyGSHP) design with or

without a furnace. *Pre-cooling (PC)* operates the CT in a CT HyGSHP only during the overnight hours; the GHX meets the entire cooling loads during the daytime hours. *Hybrid control with PC* is a combination of the prior two options. *Hybrid control with PC after 4 am* is a combination of hybrid control and PC, but PC only operates during the night after 4 am. *Hybrid control, set points only* uses the hybrid control scheme, but when optimization is used only the control set points are optimized. *Hybrid control with PC, set points only* uses the combination of hybrid control and PC, but only control set points are optimized.

If the user would like to optimize the system design, the check box next to *Optimization* is selected. When this box is checked, the user has the additional option of creating a sensitivity map. This is a plot that shows how much the LCC changes for a given change in one of the design parameters (e.g. GHX size, CT size, or set point). The program is hard coded to first find an optimal design and then find the optimal design when the selected design parameter is perturbed from its optimal value by (-20%), (-10%), (10%), and (20%) for the GHX and CT size or (-2°C), (-1°C), (1°C), and (2°C) for the set point temperatures.

If the user has decided to compare the system being designed to the conventional system (selected in the *Main Diagram* window) and already knows the design of the conventional system, then the *Conventional system design known* check box can be selected. The design is then entered in the lower right box labeled *System Design* under the *Conventional* heading. When optimization has been selected, an initial guess for the system design can be entered in this region as well for the *GSHP*, *CT Hybrid*, or *Conventional* designs. However, the user also has the option of using a simple sizing method based on ASHRAE guidelines [59] by checking the *ASHRAE Sizing* box; this method is detailed in Appendix A. When optimization is not being used, the known design is entered in this region.

At the upper right are two options for the individual who wishes to explore the behavior of these systems. The first option examines ground load imbalance. When this box is checked, the user can input an allowable temperature change over the life of the system; during optimization, if the design of the system results in a ground temperature change that exceeds the allowable change, a penalty is added to the life cycle cost so that the design will be rejected by the optimizer. The second option allows the user to specify the required reduction in energy consumption of the system relative to a conventional system. If the conventional system design is not known, then when this box is checked the program will first optimize a conventional system in order to calculate the energy consumption and then optimize the specified ground source heat pump or hybrid ground source heat pump design. If the energy consumption of the new system is not reduced from the conventional system by the specified amount, a penalty function is added to the life cycle cost and the system design is rejected. These options may be used in combination or individually. A word of caution, however it is possible for the user to enter a value for the energy consumption that the system can not meet. For example, the user may specify that the energy consumption must be reduced by 75%, but there may not be any system design that is capable of meeting this goal. In this situation, the best result will be returned.

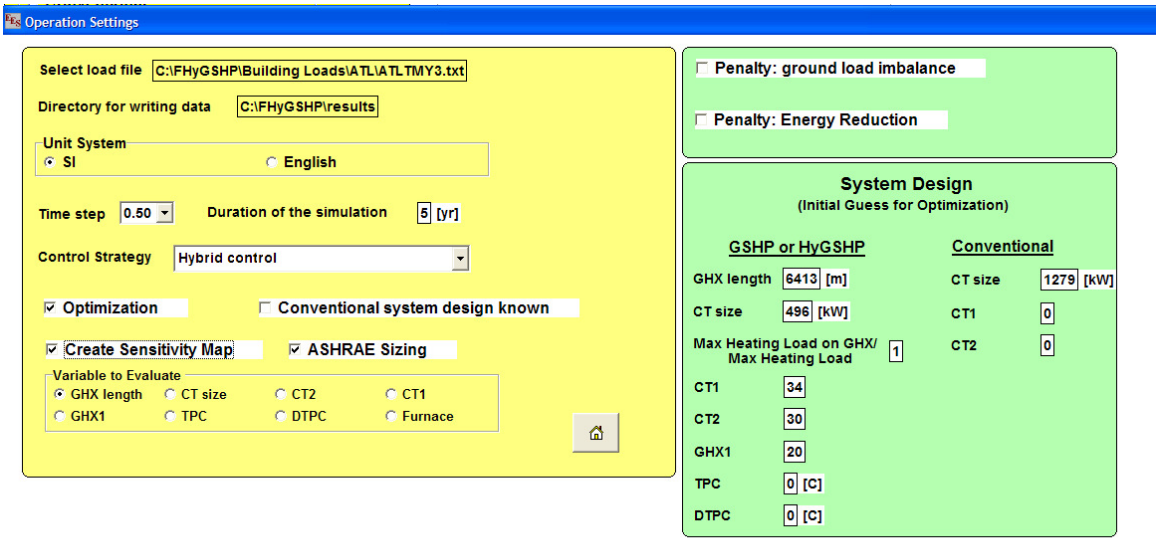

Figure 7-2 Screen shot of the operation settings window.

7.2.3 Detailed Schematic

The *Detailed Schematic* window is accessed by clicking within the green box containing the words *Go To Detailed Schematic* shown in Figure 7-1. Figure 7-3 shows a screen shot of the *Detailed Schematic* window overlaid on the *Main Diagram* window. The detailed schematic shows the location of each component with respect to the others and provides an indication of where the control set point temperatures are measured.

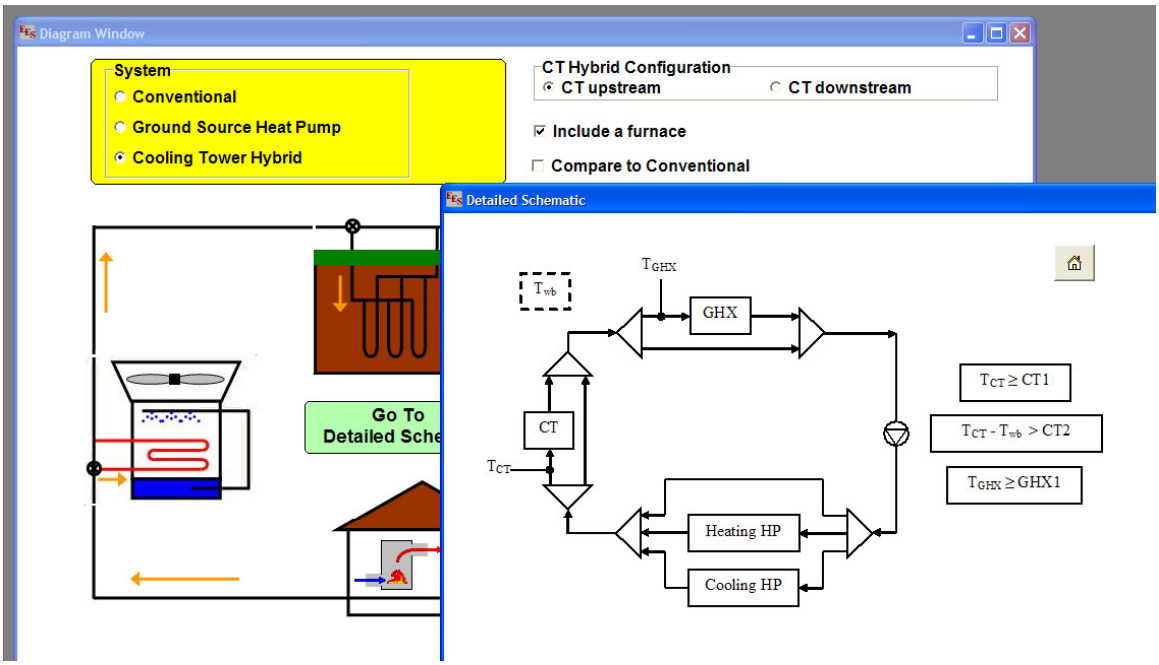

Figure 7-3 Screen shot of the detailed schematic window.

7.2.4 Heat Pump Inputs

The *Heat Pump Inputs* diagram window is accessed by clicking on the picture of the house in the Main diagram window; a screen shot of this window is shown in Figure 7-4. The yellow box in the upper left contains the most important input, the temperature constraints. If the temperature of the fluid entering the heat pump is less than *Minimum EFT* or greater than *Maximum EFT* a penalty function is added to the life cycle cost in order to indicate that the system design does not operate within the physical limitations of the equipment. The *Performance* box contains information relating to the default performance of the heat pump as well as the conditions of the room air. The fan operation can be either continuous (the heat pump fan runs whenever the building is occupied) or intermittent (the heat pump fan operates only when there is a building load). The values in this region generally do not need to be changed. The *Furnace* box allows the furnace efficiency to be set. The *Performance Curves* box allows the user to enter information for their specific heat pump, if desired. The curve fits are described in detail in Chapter 2.

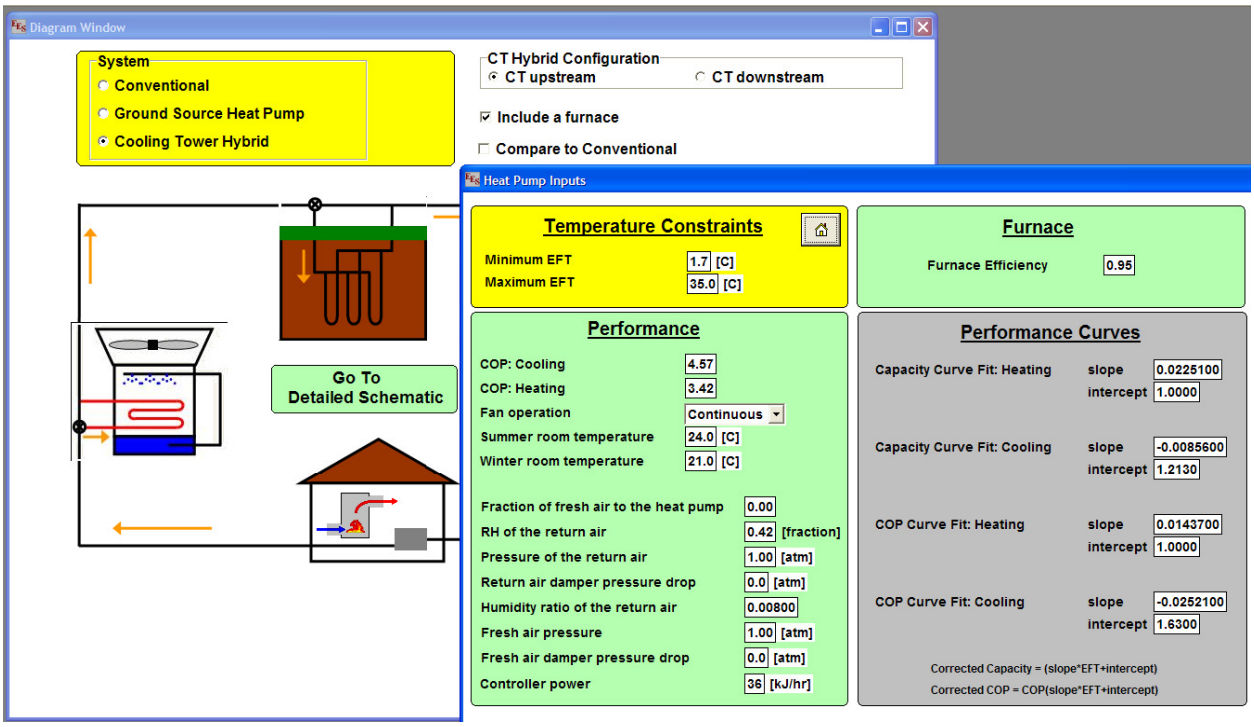

Figure 7-4 Screen shot of the heat pump inputs screen.

7.2.5 Circulating Pump

There are four settings for the circulating pump that are combined to calculate the circulating pump power consumption as shown in the screen shot in Figure 7-5; see Chapter 2 for details of the calculation. The rated pump power consumption is calculated by multiplying the *Pump power per peak block load* input by the peak cooling load. The *Fraction of the pressure drop in the GHX* is an estimate of the portion of the total pressure drop in the system (GHX, heat pumps, header pipes, etc.) that occurs in the GHX. The larger this number, the greater the difference between the pumping power when the GHX is used versus when it is bypassed. The *Total pump efficiency* and the *Efficiency of the motor* are the final two inputs; they can be based on actual manufacturer data or according to the best judgment of the user.

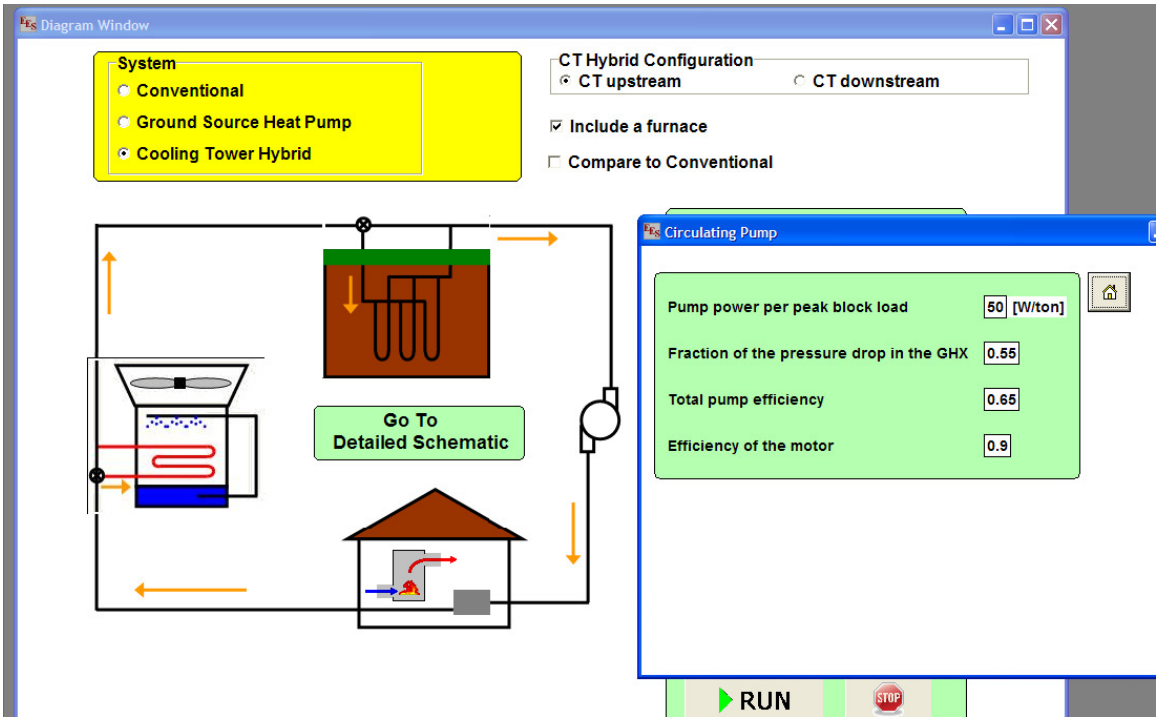

Figure 7-5 Screen shot of the circulating pump window.

7.2.6 Ground Heat Exchanger Inputs

The ground heat exchanger model requires a relatively large number of inputs, as can be seen in Figure 7-6. The size of the U-tube piping used in the borehole is selected at the top of the window; one of four commonly used sizes can be selected using radio buttons. The remaining inputs are related to the thermal characteristics of the ground and the geometry of the borehole. The *Ground thermal conductivity*, *Ground heat capacity*, and *Ground temperature* can be obtained from a thermal response test [65], ASHRAE guidelines [59], or another source of information available to the user. The geometric parameters are based on standard design specifications for a ground source heat pump system. The *Grout thermal conductivity* and *Pipe thermal conductivity* are material properties of the grout and pipe.

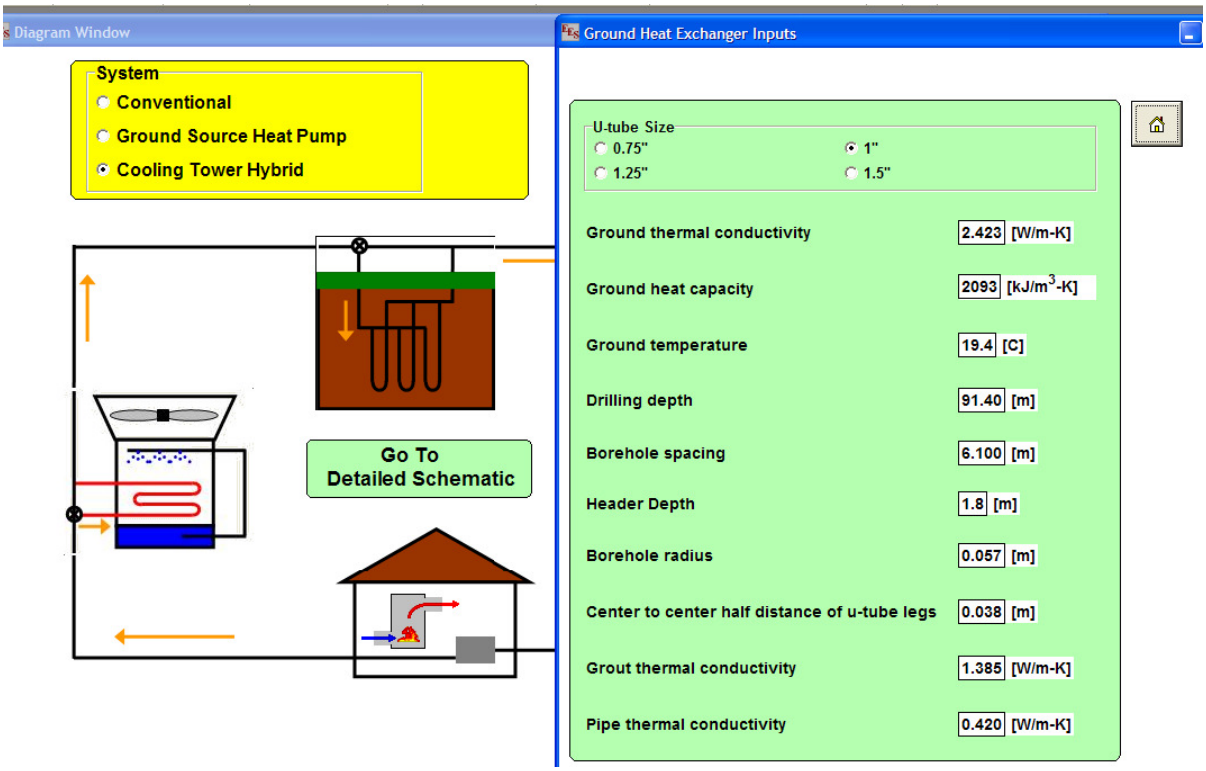

Figure 7-6 Screen shot of the ground heat exchanger inputs window.

7.2.7 Cooling Tower Inputs

Figure 7-7 is a screen shot of the inputs for the cooling tower. For a more extensive discussion of how these parameters are used, see Chapter 2. The yellow box labeled *Fan Speed* contains the most important settings; the default fan operation is the button labeled *Continuous*, but if the user does not have a cooling tower that accommodates continuous operation, it is possible to select a single- or two-speed fan. If *1 speed* is selected, the *Highest speed* box appears and the user can determine what the single speed is; a value of 1 corresponds to 100%. If *2 speed* is selected, then the *Lowest speed* option also appears and the user can set the two possible operation speeds. When *Continuous* is selected, the fan speed will vary between 10% and 100% (0.1 and 1) as described in Chapter 2. If the control strategy selected includes pre-cooling (PC), the *Cooling tower speed in PC* can be set in this screen.

The two boxes at the right contain information related to the manufacturer specifications. The *Design Conditions* are used to calculate the power consumption and fluid flow rate through

the cooling tower. The *Scale Factors* are used to scale some of the hard-coded cooling tower calculations to fit a specific manufacturer's values; see Chapter 2 for the details.

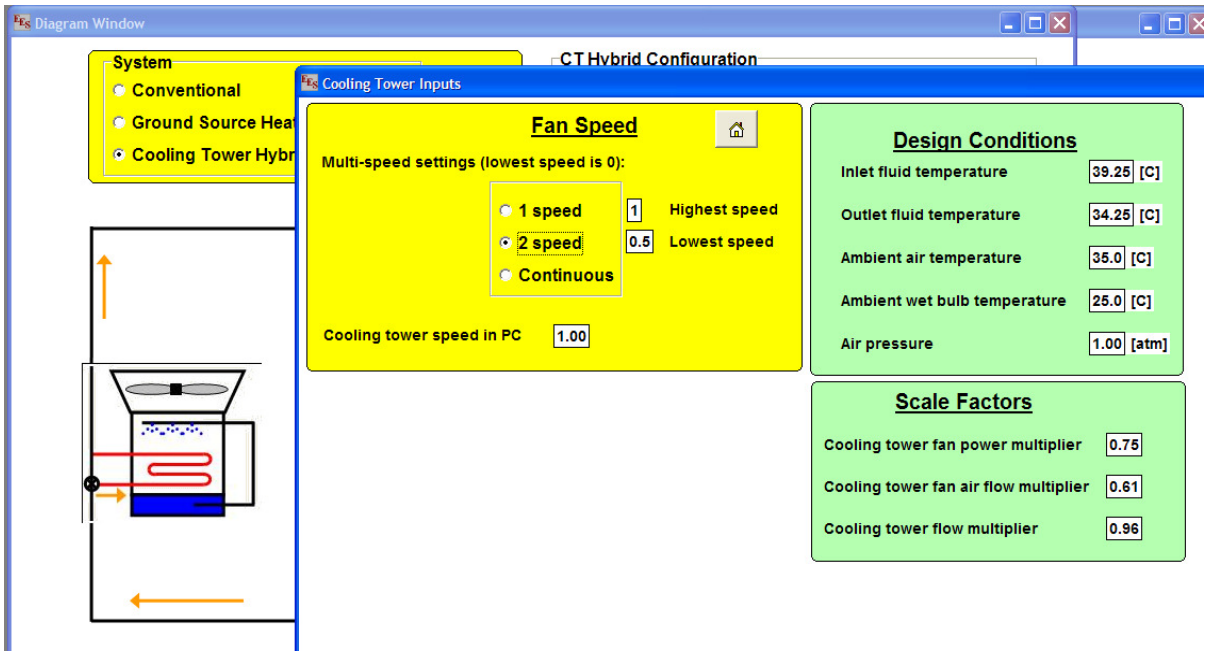

Figure 7-7 Screen shot of the cooling tower inputs window.

7.2.8 Weather Variability

As noted in Chapter 5, FHyGSHP includes the option of generating synthetic weather based on the input load file. The option for generating weather is selected in the *Weather Variability* window as shown in Figure 7-8. When the *Calculate synthetic weather and building loads* box is checked, the program will generate synthetic weather and load data. The user also has the option of providing the program with a multi-year weather and load file. In either situation, the data can be ordered (1) randomly, (2) as-supplied (if the user provides a multi-year data file), (3) from the greatest to least cooling loads based on the ratio of cooling to heating degree days, or (4) from the greatest to least heating loads, based on the ratio of heating to cooling degree days. If synthetic weather is generated, the user has the option of generating the

weather from a custom temperature distribution by inputting a mean and standard deviation of the monthly mean temperature or using the default distribution described in Chapter 5.

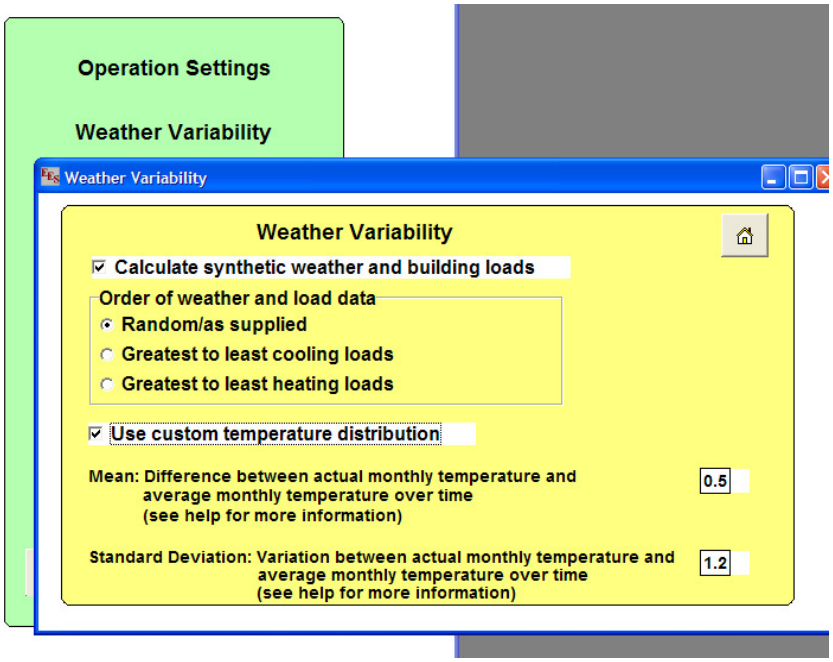

Figure 7-8 Screen shot of the weather variability window.

7.2.9 Fluid Properties

The *Fluid type* for the loop can be selected from the drop down menu in the fluid properties window as shown in Figure 7-9; the fluid can be either *Water*, as shown in the figure, or *Propylene Glycol*, which is actually a mixture of water and propylene glycol. If propylene glycol is selected, the *Minimum loop temperature* is set by the user in order to determine the percentage of propylene glycol that is required in the loop. The relationship between the propylene glycol concentration and temperature is shown in Figure 7-10. The fluid density, specific heat, and propylene glycol percentage are calculated by the program and displayed in the fluid properties window; these calculations are discussed in Chapter 2.

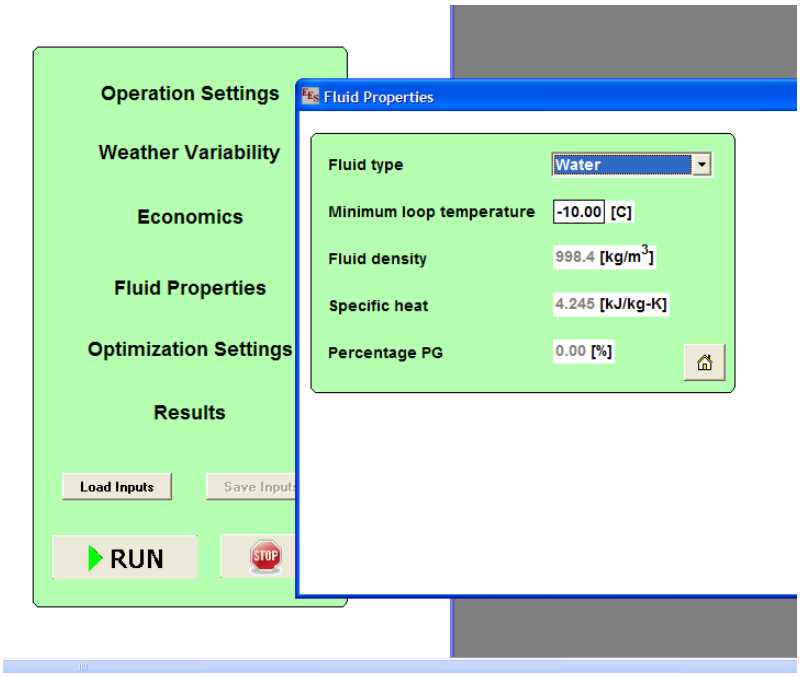

Figure 7-9 Screen shot of the fluid properties window.

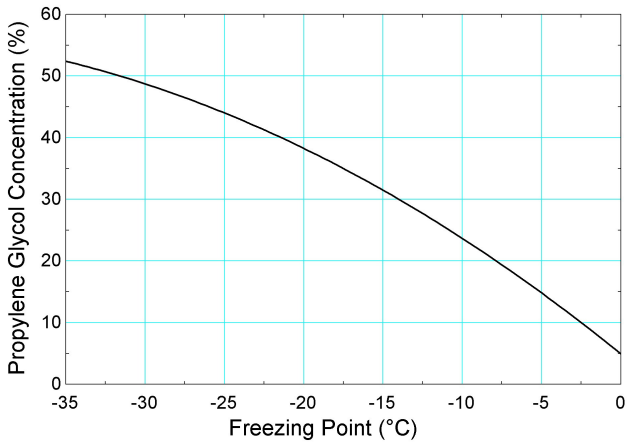

Figure 7-10 Concentration of propylene glycol as a function of the freezing point of the mixture.

7.2.10 Economic Values

The inputs for the economic calculations are entered in the *Economic Values* window as shown in Figure 7-11. The *Economic Parameters* section includes the general information that is required by the P1-P2 method (see Chapter 2). The *Fuel Rates* region allows the time of day and time of year electrical rates to be entered as well as demand and ratchet charges and the cost of gas. These values are most easily found by examining an existing utility bill or looking at the website of the local utility. The *Other Costs* included in the economic analysis are the installation

cost of the GHX and the cost of water for the cooling tower operation. The *CT first cost multiplier* is used to scale the baseline cost of a 10 ton cooling tower from $4500 to a value that may be more appropriate based on information that the user may have (note, however, that the cost should still be based on a 10 ton cooling tower); details of the CT cost calculation are given in Chapter 2. A cost for the interior HVAC components, such as the heat pumps, can be included in the economic analysis if the user enters values in the two spaces shown. The annual HVAC cost is an estimate of the maintenance costs. The default analysis does not consider HVAC cost because in general systems are being compared to one another and it can be assumed that the HVAC costs are the same for different systems (i.e. the major differences between systems are in the ground heat exchanger or cooling tower).

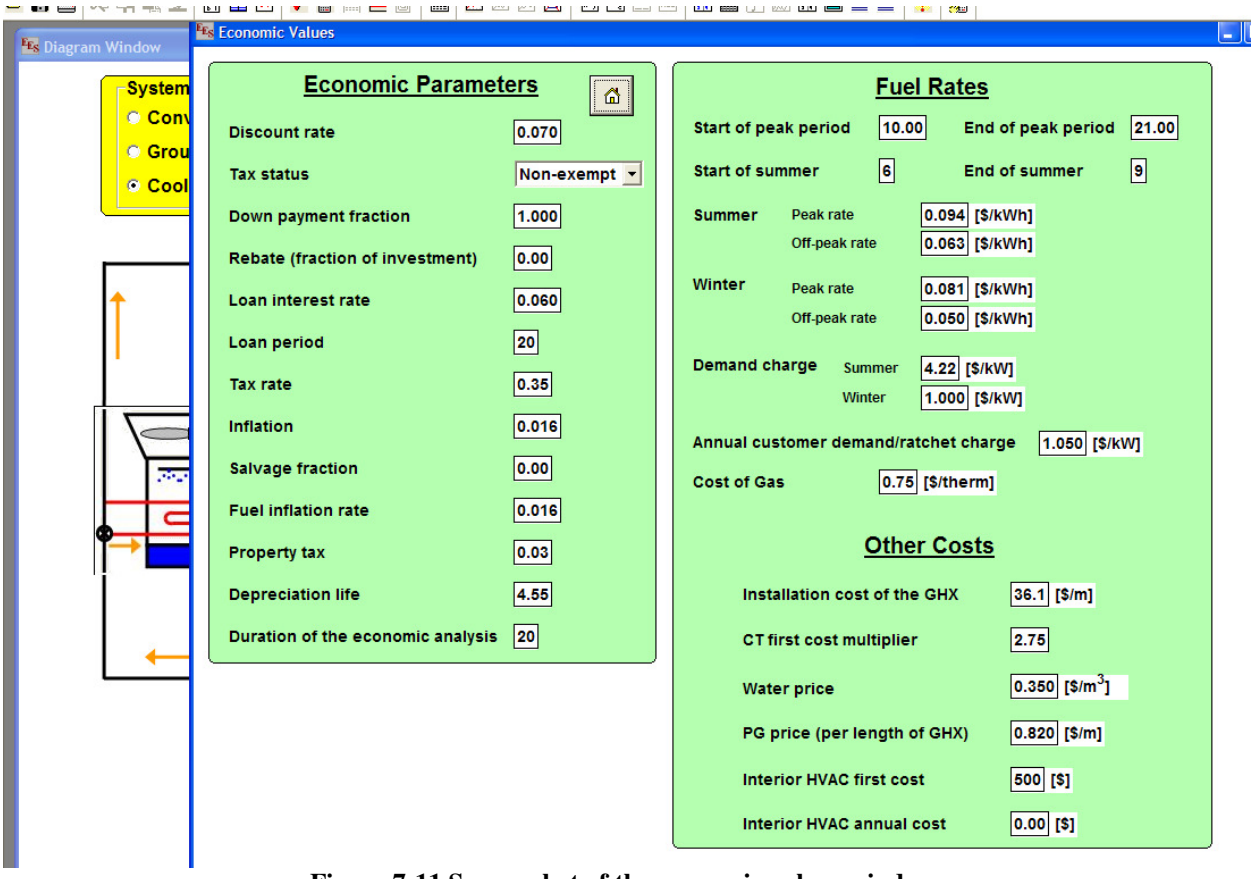

Figure 7-11 Screen shot of the economic values window.

7.2.11 Optimization Settings

A screen shot of the *Optimization Settings* window is shown in Figure 7-12. Two optimization algorithms are built into the program, DIRECT and SUBPLEX (see Chapter 4 for details). There are three possible optimization methods called *Starter*, *Nominal*, and *Mix*. In the *Starter* method, an initial coarse optimization is performed followed by a finer optimization; the algorithm to be used in each optimization is selected from the *Main Method* and *Starter Method* regions. The *Nominal* method uses just one of the algorithms. The *Mix* method is similar to the *Starter* method, but instead of performing a coarse initial optimization, both optimizations are carried out in depth. This method can be the most accurate in terms of finding the global minimum but also generally requires the greatest computation time.

If the ASHRAE Sizing method is not selected in the *Operation Settings* window, then the limits on the optimization space can be set in the upper right of the *Optimization Settings* window. The *Termination Criteria* are set in the lower right of the window; there are three primary means to terminate the optimization: maximum number of iterations, maximum number of function evaluations, and number of iterations for which the optimal value is unchanged. This last option is simply a means of stopping the optimization if the program is not finding a better optimum after the specified number of iterations; this prevents the program from bogging down in one region of the optimization space.

The DIRECT and SUBPLEX methods each have specific settings that can be accessed from the *Advanced Options: DIRECT* window or the *Advanced Options: SUBPLEX* window. These parameters are discussed in detail in Chapter 4.

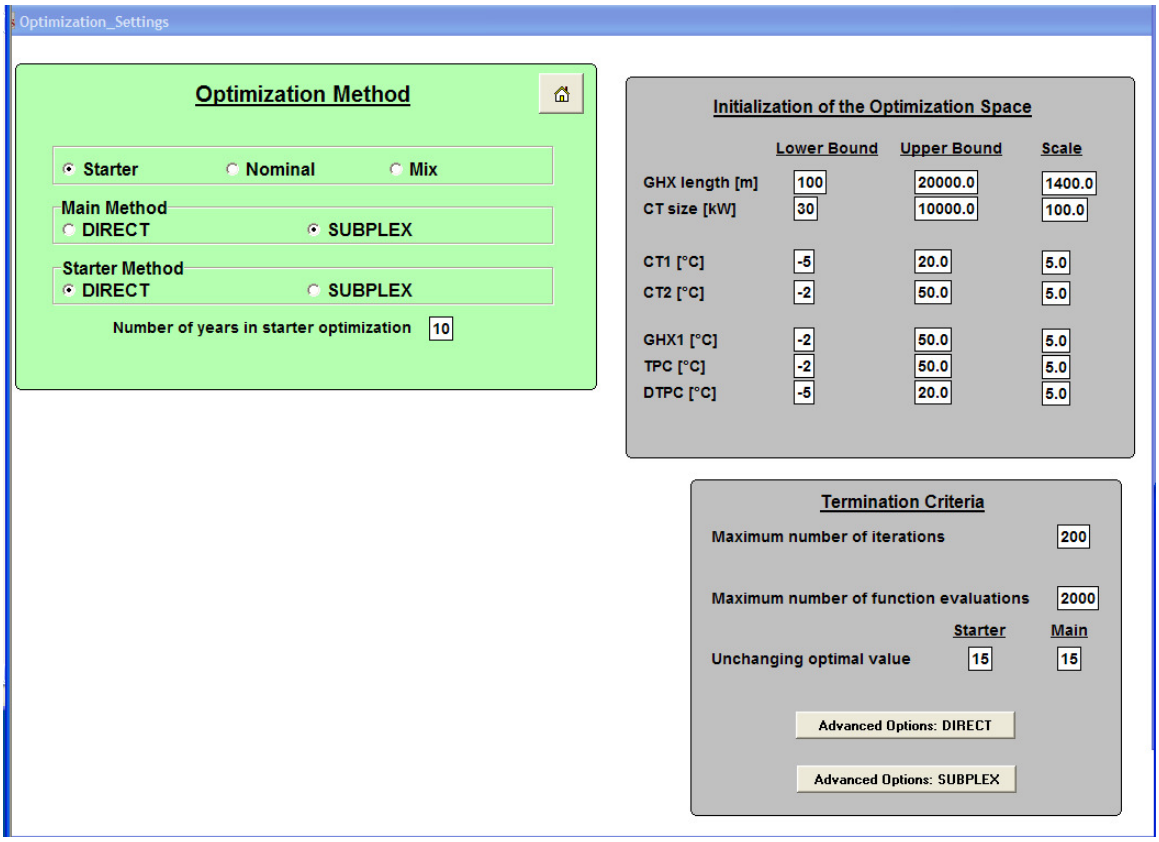

Figure 7-12 Screen shot of the optimization settings window.

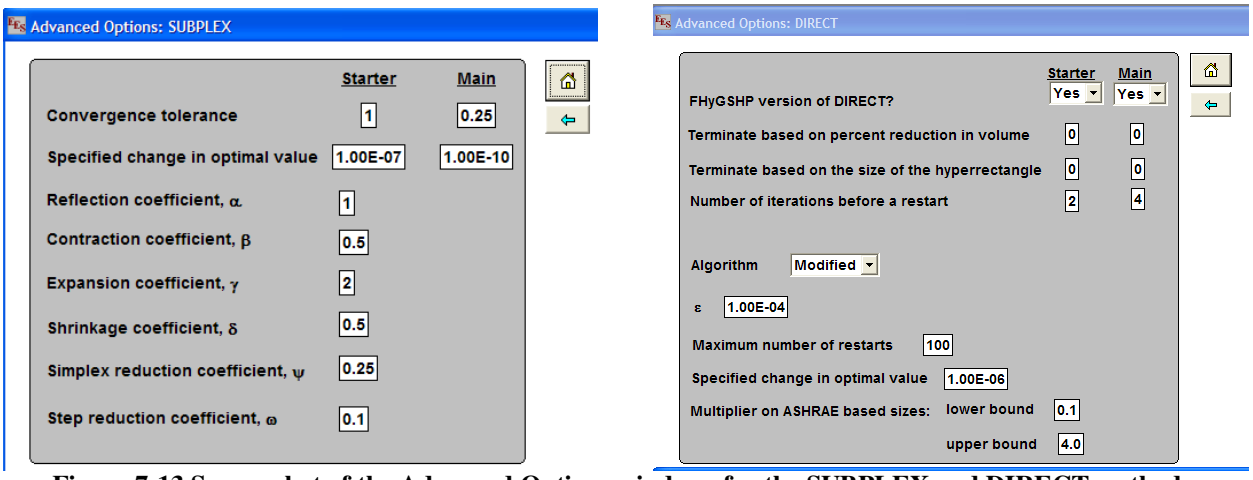

Figure 7-13 Screen shot of the Advanced Options windows for the SUBPLEX and DIRECT methods.

7.2.12 Key Results

The *Key Results* window, shown in Figure 7-14, contains some of the outputs from the simulation. More extensive results can be printed out as described in Section 7.2.13. This window appears at the completion of a single simulation or optimization run.

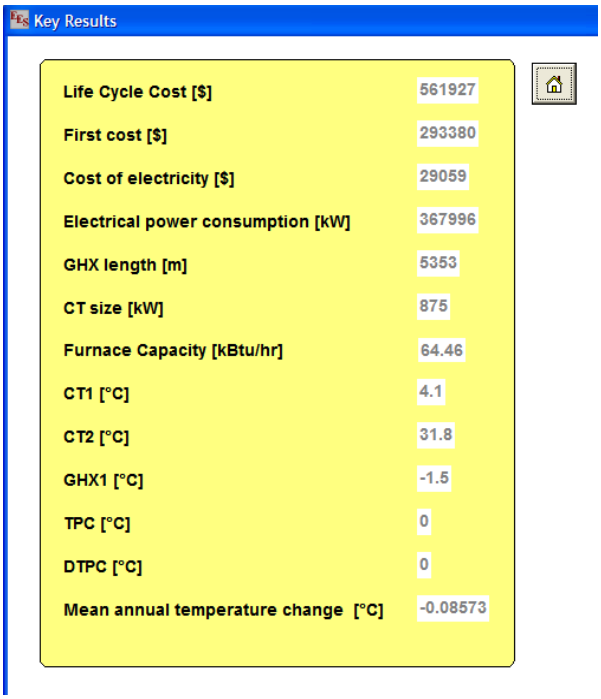

Figure 7-14 Screen shot of the key results window.

7.2.13 Printing Options

Once a design has been selected and a single simulation is being run, the user can print data at each time step in order to analyze the design in more depth; these data are not printed during the optimization. The information that can be printed is shown in Figure 7-15. The *Power Consumption* and *Heat Transfer Data* are printed in units of kJ/hr; in order to calculate an integrated value, the user can multiply the data by the time step. The *Temperature Data* are printed in °C and the *Flow Rate Data* are printed in kg/hr. The *Cooling Tower Fan Speed* is unit-less; multiplying the fan speed by 100 converts the fan speed to a percentage of full speed.

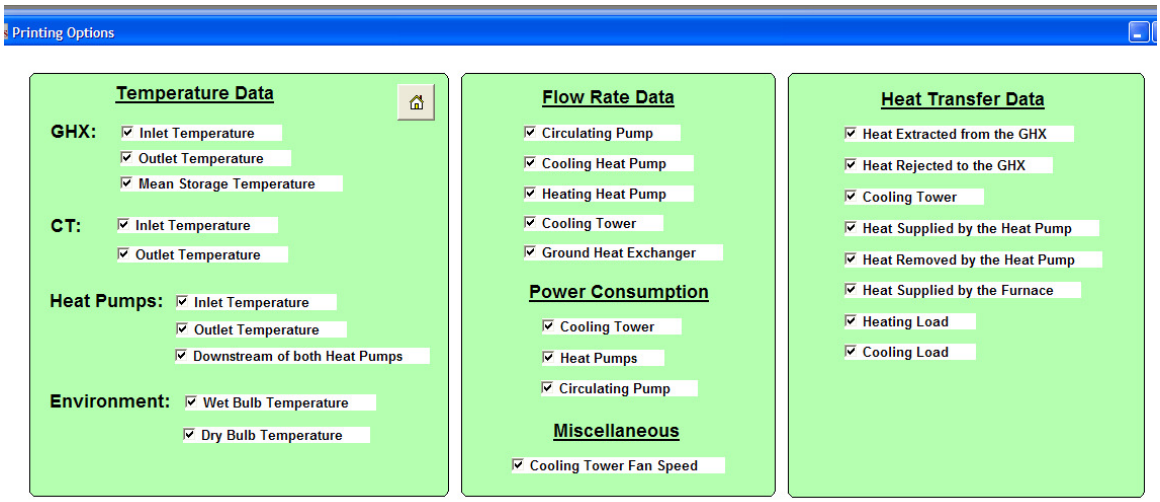

Figure 7-15 Screen shot of the printing options diagram window.

7.2.14 File Locations

FHyGSHP contains seven directories. The *Building Loads* directory contains several building load files that can be used as examples to help the user build their own file or can be used by the user as test cases. The *image* folder contains the pictures used in the GUI. The *include files* and *interp files* folders contain information used by the program and should not be modified. The *namelist_files* folder contains the files written by the GUI and used by the executable program. Upon completion of either a single simulation or an optimization, these files are copied to the directory specified by the user in the *Operation Settings* window because they contain all of the important inputs to the program and will be overwritten when a new simulation is run. The *results* folder is the default location for output from the program; when the user specifies a directory in the *Operation Settings* window, the output is written to that location instead of the *results* folder. The *main_program* folder contains the executable program and associated files.

7.3 An Example of the Program Operation

In general, the user will not have to enter inputs on all of the screens; the default settings will often be acceptable. The key screens are the *Main Diagram* window, *Operation Settings*,

and the *Ground Heat Exchanger Inputs* window for cases where a GHX is part of the design. The following screen shots show the window that appears once the user selects the *Run* button in the *Main Diagram* window. If FHyGSHP is being used to perform a single simulation, then the screen shown in Figure 7-16 is displayed. A progress bar is shown during the simulation; in Figure 7-16 the simulation is 12% complete. Figure 7-17 shows the display when the single simulation is complete. The system design and life cycle cost are shown. If the user has chosen to print any of the results, then these results are printed immediately after the simulation is complete and a progress bar lets the user know how much of the printing process has been completed.

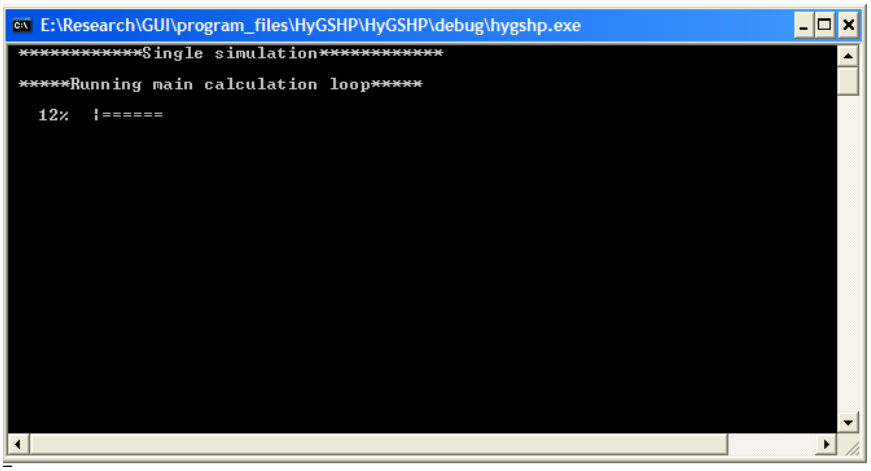

Figure 7-16 Screen shot of the command window that is displayed when a single simulation is running.

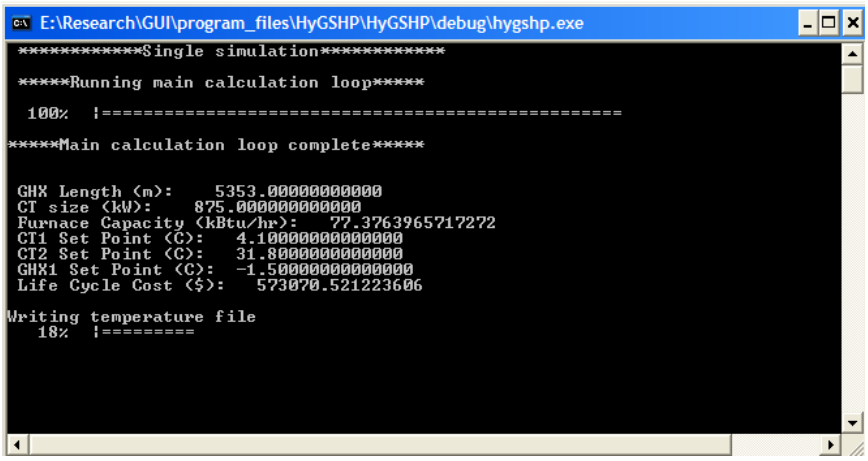

Figure 7-17 Screen shot of the command window that is displayed after the single simulation has completed and data is being written to a file.

Figure 7-18 is the screen that appears when the DIRECT method is used for optimization. The first portion of the text provides information about the settings of the optimization, including the values over which each optimization variable can range. Instead of optimizing the furnace capacity, the ratio of a load set point to the peak heating load is optimized which is why the *Bounds on Furnace* is presented as a ratio rather than as the furnace capacity. The first three runs of the optimization are shown below the main header information; in this case the GHX length is the only variable that is changing in these first three runs.

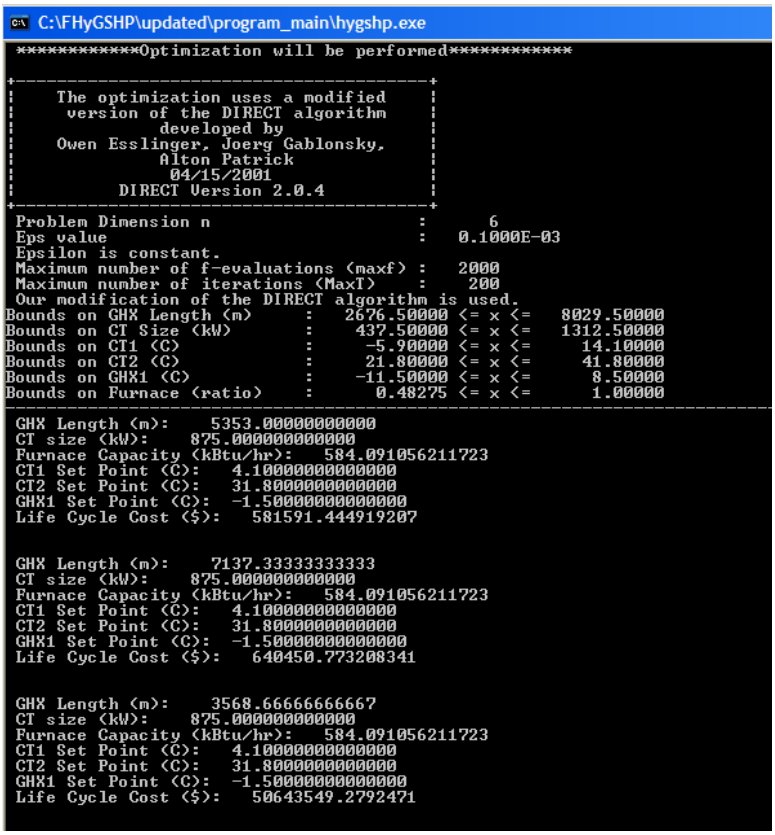

Figure 7-18 Screen shot of the command window when optimization is being performed using the DIRECT method.

Figure 7-19 shows the display when the SUBPLEX optimization method is being used. The information presented is similar to the DIRECT method as discussed above.

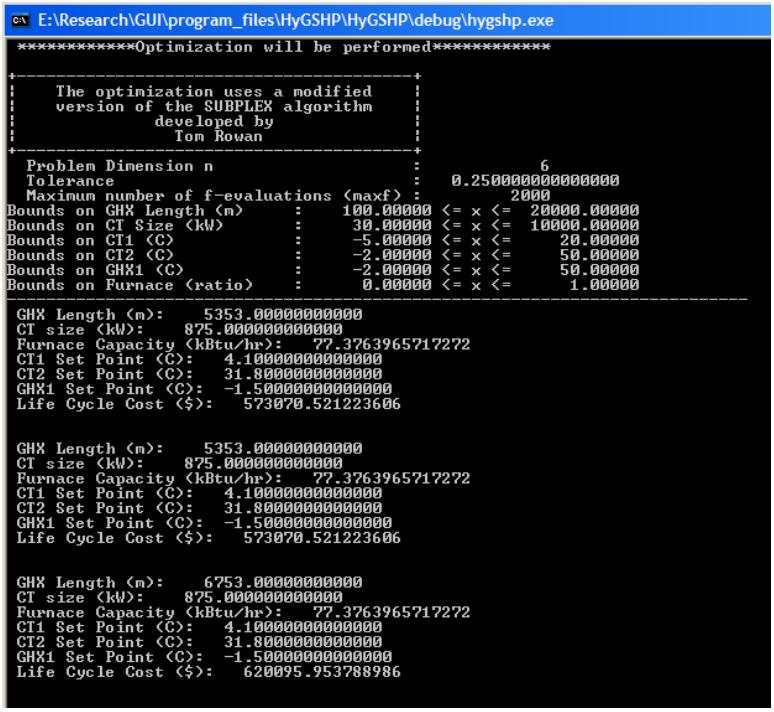

Figure 7-19 Screen shot of the command window when optimization is being performed using the SUBPLEX method.

Additional information on FHyGSHP, including default input values, installation instructions, the help documentation, and a discussion of running the program in batch mode, can be found in the appendices.

7.4 Comparison to HyGCHP

FHyGSHP was built using the basic framework of HyGCHP, but unlike HyGCHP it was not built on a TRNSYS framework. FHyGSHP was programmed in FORTRAN in order to increase flexibility and improve computational speed. FHyGSHP still uses some of the components from the TRNSYS library (such as Types 557 [97] and 510 [16]), but the TRNSYS-specific commands have been removed and the FORTRAN code is used directly. Removing the computational overhead associated with TRNSYS provides an immediate improvement in computational speed.

FHyGSHP also more intelligently implements the optimization, which results in significant computational savings. For example in HyGCHP, if a constraint is violated during the first month of the simulation, the entire simulation must be completed before the optimizer can select a new design. If the design selected by the optimizer in FHyGSHP is incapable of meeting the building loads within the constraints of the problem (see Chapter 4), the simulation exits early and the optimizer selects a new design, which leads to substantial time savings. The LCC returned to the optimizer when the simulation exits early grows in a manner that is proportional to how far under-capacity the design is (as evidenced by how early the simulation is terminated due to temperature limit violations). The LCC that is returned is a multiple of a baseline LCC; this baseline is initially set to 1e8, but once a simulation has successfully completed, that LCC becomes the baseline for the duration of the optimization. The baseline LCC is multiplied by the ratio of the total simulation time (e.g. 10 years) divided by the time at which the violation occurred (e.g. hour 760) causing the simulation run to end early. In this manner, the LCC returned to the optimizer is larger if the violation occurs early in the simulation, indicating that the design is far from optimum.

A pseudo-code for this method is given in Eq.(7.1), where F is the value of the LCC for the first valid design. The factor of two is used to ensure that the value of LCC for a case when the entering fluid temperature (EFT) temperature has been violated can not be lower than the optimal value when there are no temperature violations. The example shows how both designs are rejected, but one design is recognized to be much worse than the other, so the optimizer will not necessarily remove the region containing the poor design from further consideration.

$$if\ (\text{EFT limit violated})$$

$$LCC = 2 \bullet F \bullet \frac{total\ time}{time\ of\ violation}$$

exit calcuation loop

Example: (7.1)

$$F = 100,000 \qquad total\ time = 8760$$

$$Bad\ design:\ time\ of\ violation = 50$$

$$LCC = 3.5e7$$

$$Poor\ design:\ time\ of\ violation = 8720$$

$$LCC = 2e5$$

Table 7-1 shows the results of an optimization of a building in St. Louis for a10 year simulation duration with ½ hour time steps using both HyGCHP and the recommended general optimization method (see Chapter 4) in FHyGSHP. FHyGSHP has a slightly larger GHX and smaller CT, but the designs are similar. Care was taken to use the same inputs, such as the cost of the GHX and the GHX geometry, for both programs, there are some minor differences in the calculations in FHyGSHP and HyGCHP (such as the calculation of heat pump power consumption). FHyGSHP converged to an optimal design in 1/6 of the time required by HyGCHP even though there were more function evaluations. Part of the reason that there were more function evaluations in less time is that roughly half of these function evaluations resulted in an early exit from the calculation loop.

Table 7-1 Comparison between HyGCHP and FHyGSHP optimizations.

Method	Function evaluations	Time (hr)	GHX (m)	CT (kW)	LCC ($)	First Cost ($)		
						GHX	CT	Total
HyGCHP	249	3.9	6413	479	682,350	236,750	63,991	300,740
FHyGSHP	816	0.61	6825	383	709,697	251,979	54,227	306,206

The LCC of the optimal design from HyGCHP was calculated using FHyGSHP and the LCC of the optimal design from FHyGSHP was calculated using HyGCHP, as shown in Table

7-2 under the heading “Swapped”. There are two things to note about these results. First, FHyGSHP calculates a larger value for LCC due to slight differences in the power consumption calculation. Second, the HyGCHP optimal design has a lower LCC in FHyGSHP than the FHyGSHP design, which illustrates the difficulty of optimization discussed in Chapter 4. In this case, the FHyGSHP optimizer found a design very near the optimal design, but in order to reduce calculation time the program does not make significant effort to find a slightly better result. Changing the optimization settings would lead to a more optimal result.

Table 7-2 LCC for each design as calculated from the other program.

Method	Swapped			Original		
	GHX (m)	CT (kW)	LCC ($)	GHX (m)	CT (kW)	LCC ($)
HyGCHP	6825	383	700,442	6825	383	709,697
FHyGSHP	6413	479	696,273	6413	479	682,350

In addition to reducing computational speed, programming directly in FORTRAN allows FHyGSHP to be designed specifically for the problem at hand. For example, TRNSYS determines convergence in a given time step by evaluating the change in the value of the output from every component in the system between iterations; if the change is sufficiently small, the time step has converged. This level of check is unnecessary for this problem. Instead of looking at all outputs from all components, FHyGSHP looks at the change in the temperature across the GHX (if present), heat pumps, and CT (if present) to determine convergence. In addition (unlike in TRNSYS) in FHyGSHP those calculations that do not change during the simulation or during a time step can be removed from the iterative loop. For example, the control decision is made using the system temperatures from the prior time step, so rather than placing the controller within the iteration loop, where the decision can change with each iteration, it is placed outside of the loop and the decision is constant for all iterations that occur in a given time step.

Chapter 8 Case Studies Using FHyGSHP

This chapter presents the results of a series of studies on the operation and design of hybrid ground source heat pump (HyGSHP) systems using the FHyGSHP program. These studies illustrate some of the ways in which FHyGSHP can be used to explore how HyGSHP systems behave. The ratio of annual and peak cooling to heating loads as well as the magnitude of the peak cooling and heating loads for the files used in this study are listed in Table 8-1; the ground temperature at the start of the simulation is also provided. All simulations use actual annual weather data and building loads calculated from that data so that each year of the simulation has different weather and load data. The summary load data in Table 8-1 are calculated using 20 years of data (i.e. the total cooling loads for 20 years are divided by the total heating loads for 20 years to find the annual cooling to heating ratio). Many of the simulations use less than the full 20 years of data, so there is some discrepancy between the summary load data and the load data for the specific simulation; the data in Table 8-1 are only meant to provide a rough idea of how cooling and heating loads compare in each location.

Table 8-1 Annual and peak cooling and heating load ratios.

	Annual Cooling/Heating	Peak Cooling/Heating	Peak Cooling (kW)	Peak Heating (kW)	Ground Temperature (°C)
Atlanta	3.13	0.79	494	629	19.4
St. Louis	1.48	0.56	504	900	13.9
Salt Lake City	1.09	0.64	529	825	13.3
Phoenix	14.29	2.59	646	249	21.7

8.1 Time Related Studies

When the cooling and heating loads on the GHX are imbalanced, the ground temperature changes over time. If the system is a GSHP then the longer the life of the system, the larger the GHX must be in order to be able to meet the ground load at the end of life. This section presents

a study of the change in optimal system design as a function of simulation duration and also examines the effect of time step size on the design.

8.1.1 Simulation Duration

When the only source/sink for meeting building loads is the GHX, the design and LCC are highly dependent on the simulation duration because the optimization parameter is LCC. A GSHP is often designed such that the ground load is balanced [59] and therefore the ground temperature does not change significantly during the life of the system. However, when the focus is on minimizing LCC, the ground temperature can change over time. In fact, the optimal design is generally one in which the GHX can just meet the building load while keeping the heat pumps within their operating temperature limits during the last year of operation. In a cooling dominated system, this means that the ground temperature may increase by 5 – 10°C after 20 years of operation. If the time frame is only 5 years, the ground temperature increase may be only 2°C. If a GHX system that is designed using a 5 year time frame is operated for longer, the system will not be able to meet the cooling load beyond the 5 year period.

Figure 8-1 shows the GHX length and Figure 8-2 shows the LCC of an optimized GSHP system as a function of simulation length in Atlanta, St. Louis, Salt Lake City, and Phoenix. The figure on the left does not include a furnace and the figure on the right does include a furnace. As expected, the longer the system life (i.e. simulation duration), the larger the GHX and the larger the LCC. When a furnace is added to the system, there is essentially no change in LCC, which is consistent with the finding in the prior section. The GHX length is a bit more variable with the addition of a furnace, but the overall trend is the same as when there is no furnace. The take away message is that a GSHP system needs to be designed with the system life in mind in order

to ensure that it is not under-sized at end-of-life. Also, the time frame used to analyze a system has a profound impact on the system design for these types of systems.

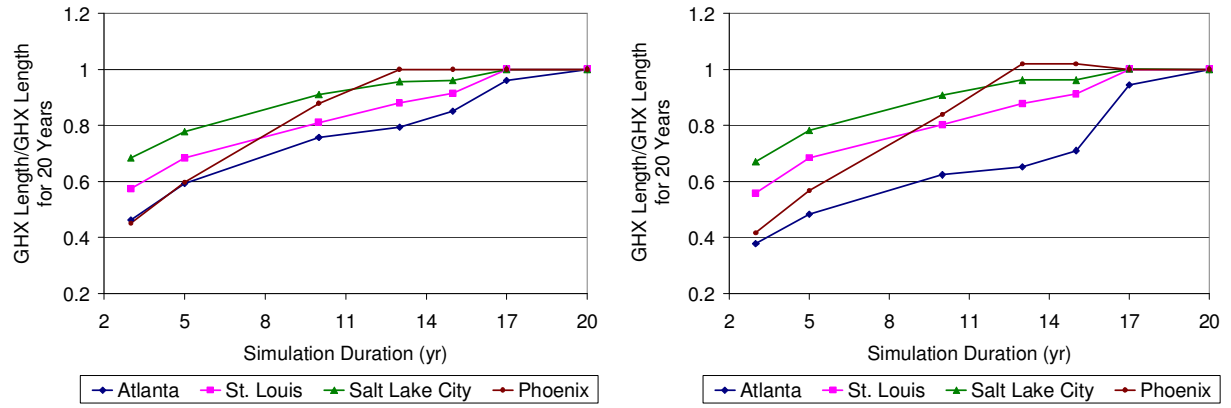

Figure 8-1 Change in GHX length as a function of the duration of the simulation. The values are normalized by the result for a 20 year simulation. Left: GSHP without a furnace. Right: GSHP with a furnace.

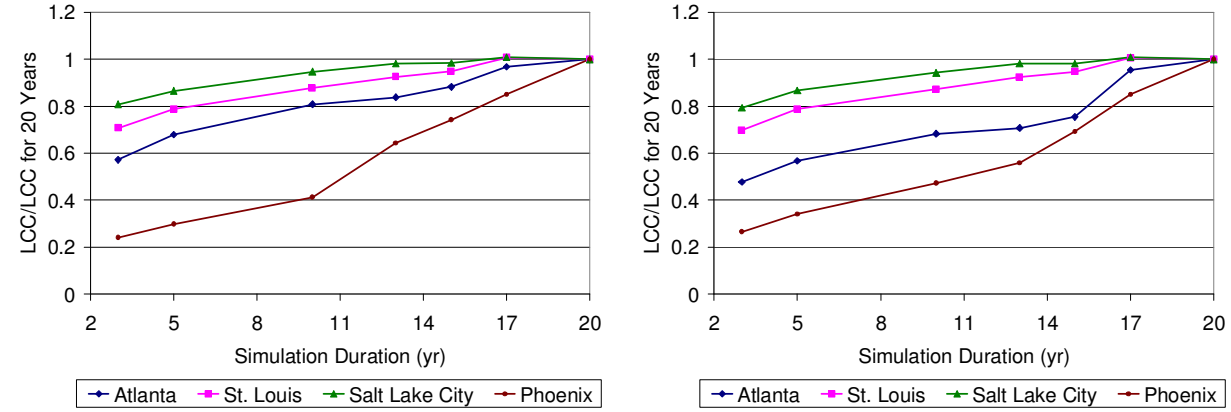

Figure 8-2 Change in LCC as a function of the duration of the simulation. The values are normalized by the result for a 20 year simulation. Left: GSHP without a furnace. Right: GSHP with a furnace.

Figure 8-3 shows the change in LCC, GHX length, CT size, and furnace capacity for a CT Hybrid with and without a furnace as a function of the simulation duration in Atlanta. The figure at the left is the case without a furnace and the figure at the right is the case with a furnace. When the system is a CT Hybrid, there is less variation in the design and LCC as a function of the time frame of the optimization as compared to the case when the system is a GHX. Adding a furnace to the system adds more "noise" to the result since the addition of even a small furnace

can have a major impact on how large the GHX must be. The behavior in Phoenix, shown in Figure 8-4, follows this same pattern.

In these two locations, the cooling loads far exceed the heating loads. Therefore the addition of a CT tends to stabilize the system design. The addition of a CT leads to a more balanced ground load, which reduces the increase in ground temperature over time and mitigates the need for a large GHX. When the ground load is balanced within each year of the simulation, adding additional years to the life of the system has little impact on the design.

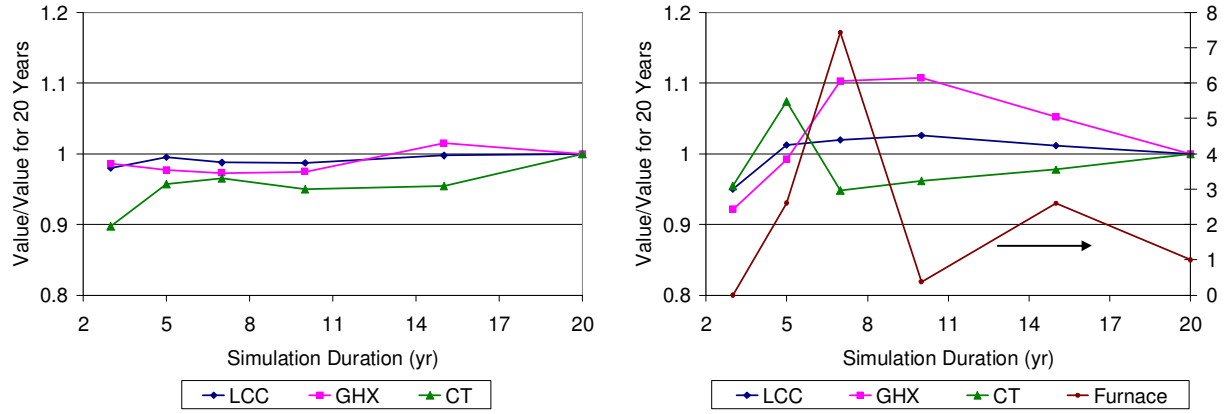

Figure 8-3 Change in LCC, GHX length, CT size, and Furnace capacity (when present) as a function of the duration of the simulation in Atlanta. The values are normalized by the result for a 20 year simulation. Left: CT Hybrid without a furnace. Right: CT Hybrid with a furnace.

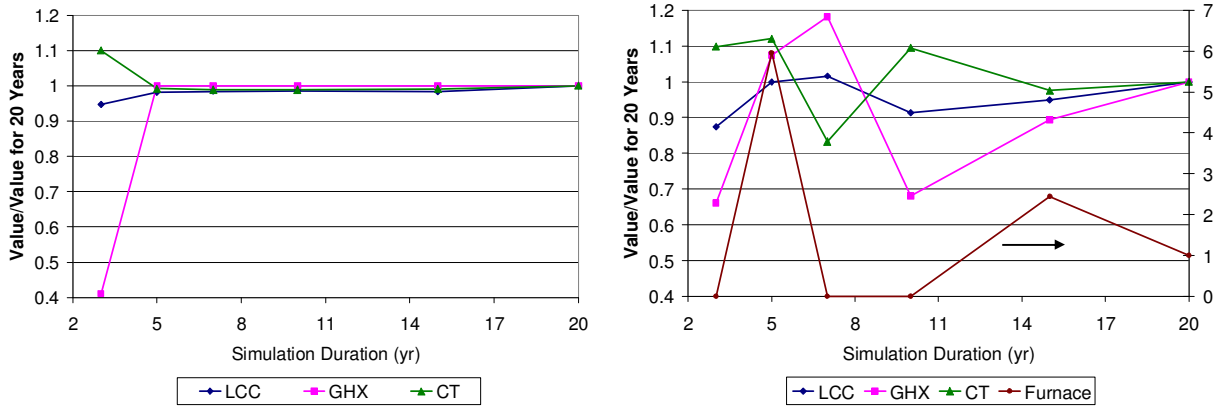

Figure 8-4 Change in LCC, GHX length, CT size, and Furnace capacity (when present) as a function of the duration of the simulation in Phoenix. The values are normalized by the result for a 20 year simulation. Left: CT Hybrid without a furnace. Right: CT Hybrid with a furnace.

The situation in St. Louis, shown in Figure 8-5, and Salt Lake City, shown in Figure 8-6, is different. When there is no furnace, the designs tend to vary with simulation duration up to approximately 15 years, after which the change in the design is not as dramatic. When a furnace is added, the LCC tends to show less variation with simulation duration. In these two locations, cooling loads exceed heating loads, but the difference is not as large as in Phoenix or Atlanta. In these two locations, the addition of a furnace has a much more significant impact because it removes some of the heating load from the ground. In neither case, however, does the system design stabilize as quickly as in Phoenix or Atlanta when there is no furnace.

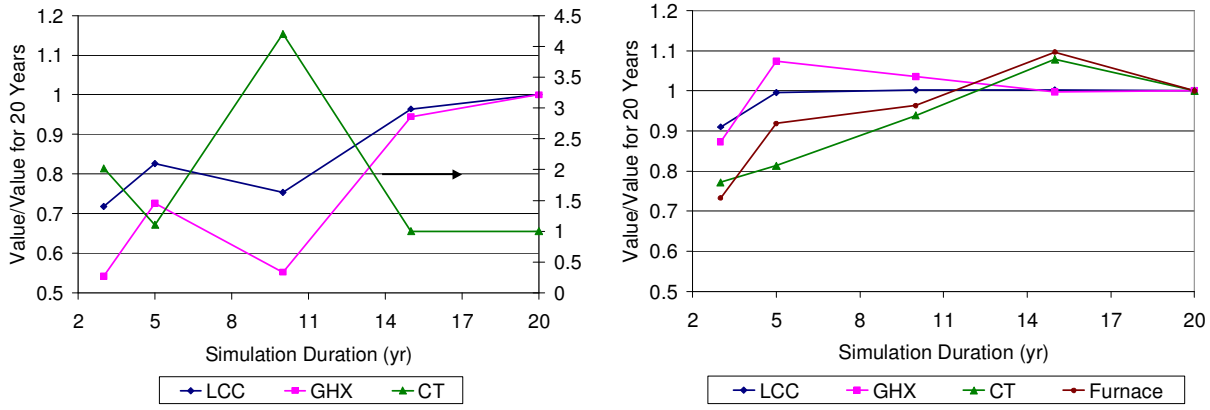

Figure 8-5 Change in LCC, GHX length, CT size, and Furnace capacity (when present) as a function of the duration of the simulation in St. Louis. The values are normalized by the result for a 20 year simulation. Left: CT Hybrid without a furnace. Right: CT Hybrid with a furnace.

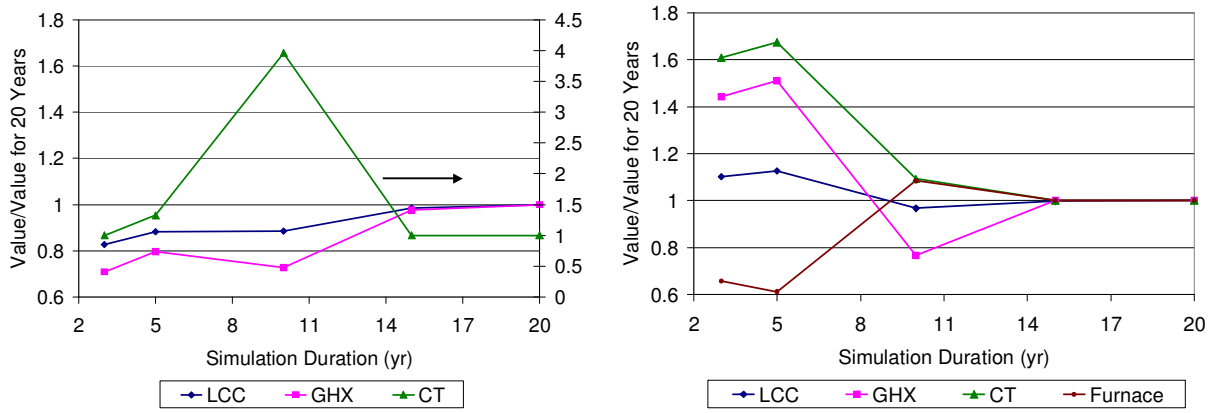

Figure 8-6 Change in LCC, GHX length, CT size, and Furnace capacity (when present) as a function of the duration of the simulation in Salt Lake City. The values are normalized by the result for a 20 year simulation. Left: CT Hybrid without a furnace. Right: CT Hybrid with a furnace.

This study demonstrates how much the design and cost of a system can vary as a function of the life of the system. For scoping or comparative studies, it is often sufficient to use a five year simulation, but this should only be performed with the knowledge that a more accurate design will require a longer simulation duration that is more in line with the actual anticipated life of the system.

8.1.2 Time Step

The time step size can be set to 0.25, 0.5, 0.75, or 1 hour. The input file contains load and weather data for each hour of the year, with the load being defined as the rate of the energy demand. The rate of the energy demand is treated as constant for the entire hour. Eq. (8.1) is a simple example of a load calculation; the rate of the energy demand is the same for a 1 hour and a ¼ hour time step, but the energy demand is a function of the time step length (e.g., 1000 kJ for 1 hour or 250 kJ for ¼ hour), so the integrated energy for the hour is preserved when the time step size is changed. In this situation, the importance of time step size is related to the control decision. In a hybrid system, a shorter time step allows for the CT fan speed to change or for the CT or GHX to be bypassed for a portion of the hour rather than operating the system in the same way for the entire hour. In reality, the magnitude of the load is unlikely to be constant over the

course of the hour; a future version of FHyGSHP could include a method for accounting for the hourly variability of the load.

$$\dot{Q}_{input,hr} = 1000\frac{kJ}{hr} \Rightarrow Q_{input,hr} = 1000\frac{kJ}{hr} \bullet 1hr = 1000\,kJ$$
$$\dot{Q}_{1/4\ hr} = 1000\frac{kJ}{hr} \Rightarrow Q_{1/4\,hr} = 1000\frac{kJ}{hr} \bullet 0.25\,hr = 250\,kJ \Rightarrow 250\,kJ \bullet 4 = 1000\,kJ \quad (8.1)$$

Figure 8-7 shows the LCC of a GSHP in Phoenix for time step sizes of ¼, ½, and 1 hour as a function of simulation duration. The LCC at each point has been normalized by the LCC of a 20 year simulation with ¼ hour time steps. There is very little change in the LCC as a function of time step size; there are no control decisions to be made in this system because if there is a load, the GHX can not be bypassed.

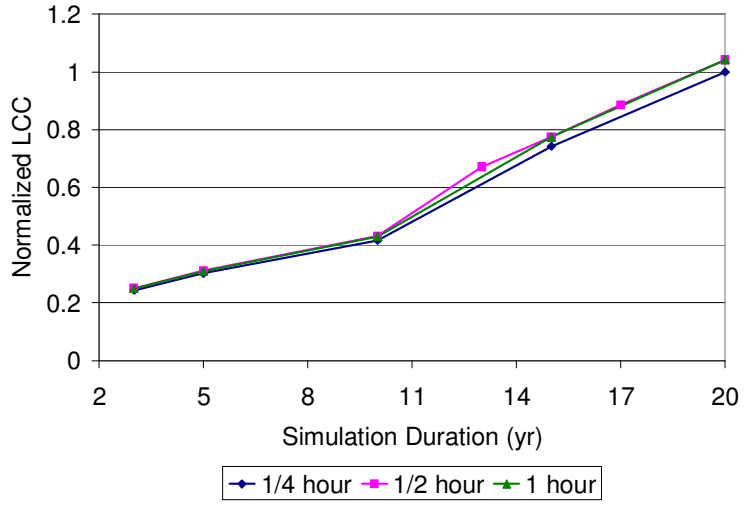

Figure 8-7 LCC for a GSHP system in Phoenix as a function of simulation duration and time step size.

Figure 8-8 shows the variation in LCC with time step size for a CT Hybrid system; the LCC is normalized by the LCC for a 20 year simulation duration and ¼ hour time step size. There is more variation in the LCC for different time step sizes. There are multiple control decisions for a CT Hybrid, including whether or not to bypass the CT or GHX and, if the CT is not bypassed, what the fan speed should be. Allowing these control decisions to vary during the

course of an hour leads to design and operational differences that impact the LCC. A time step size of ½ hour is generally recommended in order to capture sub-hourly control decisions without requiring the additional run time associated with a ¼ hour time step, but ¼ hour time steps may produce a result that better mirrors real world operational decision making and should be used when refining a design.

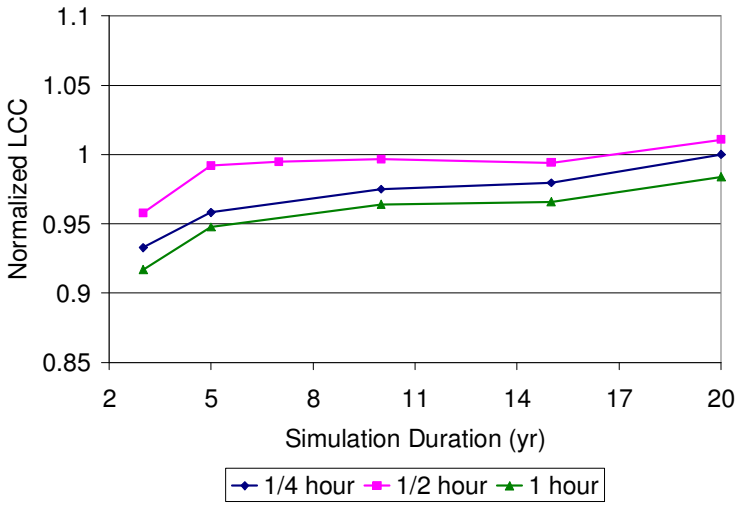

Figure 8-8 LCC for a CT Hybrid system in Phoenix as a function of simulation duration and time step size.

8.2 System Configuration

The seven unique configurations that can be analyzed in FHyGSHP are listed in Table 8-2, where CT is cooling tower and GHX is ground heat exchanger. The seven configurations can be divided into three main categories: Conventional, Ground Source Heat Pump (GSHP), and Cooling Tower (CT) Hybrid. The design of each of these systems was optimized for a five year simulation in Atlanta, GA, St. Louis, MO, Phoenix, AZ, and Salt Lake City, UT. The different system designs and performance will be discussed and compared in this section.

Table 8-2 System configurations that can be modeled in FHyGSHP.

Configuration			GHX	CT	Furnace
Conventional	Conv	CT for cooling, furnace for heating	No	Yes	Yes
GSHP	GSHP	GHX for heating and cooling	Yes	No	No
	GSHP_f	GHX for heating and cooling with a furnace to help meet peak heating loads	Yes	No	Yes
CT Hybrid	CT_up	GHX for heating and cooling with a CT upstream of the GHX to help meet cooling loads	Yes	Upstream	No
	CT_down	GHX for heating and cooling with a CT downstream of the GHX to help meet cooling loads	Yes	Downstream	No
	CT_up_f	GHX for heating and cooling with a CT upstream of the GHX to help meet cooling loads and a furnace to help meet heating loads	Yes	Upstream	Yes
	CT_down_f	GHX for heating and cooling with a CT downstream of the GHX to help meet cooling loads and a furnace to help meet heating loads	Yes	Downstream	Yes

8.2.1 The Effect of a Furnace

The GSHP and CT Hybrid configurations may or may not include a furnace as part of the system design; this section examines how the design and performance change when a furnace is included in the configuration. For a cooling dominated situation, the addition of a furnace to a GSHP design has a small impact, as can be seen in Figure 8-9. This figure shows the GHX length, life cycle cost (LCC), first cost (i.e., cost of installing the GHX), and the operating cost (i.e., the cost of electricity, gas, and water over the life of the system) of the system with a furnace normalized by the same values for a system without a furnace. The difference between the designs in all four locations is less than 5% for all of the variables examined. This is the expected result; the length of the GHX in a GSHP for a cooling dominated system is based primarily on the cooling loads, so adding a furnace has essentially no impact on the design.

One reason for the difference between the two systems is the imperfection of the optimization. The certainty of a solution being the global optimum is compromised by requiring

the optimization to converge to a solution within a reasonable time frame. This is the primary cause of the difference between a design with and without a furnace in Phoenix; if adding a furnace is more costly, then the furnace should simply have been sized to zero and the design should have been the same as the design without a furnace. This behavior is also demonstrated to a lesser extent in Salt Lake City and Atlanta, where the LCC increases by approximately 0.1% when a furnace is added to the system, and in St. Louis, where the LCC decreases by approximately 0.1%. In each of these cases, once the optimization was in the neighborhood of an optimum it did not spend more time trying to refine the design in order to obtain a modestly better result.

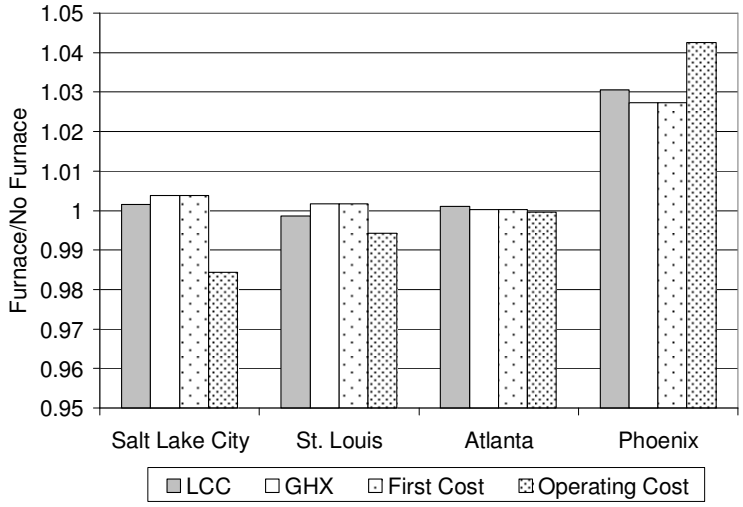

Figure 8-9 Design and cost of a GSHP system with a furnace versus one without a furnace.

The addition of a furnace to a CT Hybrid has a more interesting effect. Figure 8-10 shows how the design of CT Hybrid with the CT placed upstream of the GHX changes when a furnace is added. In Salt Lake City and St. Louis, both of which have significant heating loads relative to cooling loads, the addition of a furnace allows the GHX length to decrease by 50% and 24%, respectively. In order to compensate for the reduction in the amount of the cooling load that can be met by the GHX, the CT size increases by 330% in Salt Lake City and 205% in St. Louis. In

St. Louis the net effect is that the LCC increases by less than 0.1% when a furnace is added to the system because the decrease in the first cost of the GHX is offset by the increase in the first and operating cost of the CT. In Salt Lake City, the decrease in the size of the GHX is more significant and the reduction in first cost is sufficient to offset the increase in operating cost such that the net effect of adding a furnace is to decrease LCC by 10%.

In Atlanta and Phoenix the system becomes more expensive when a furnace is added (see the note about optimization above). In Atlanta the addition of a furnace leads to a reduction in GHX length of 31% and an increase in CT size of 15%. The first cost decreases but operating costs increase and the overall effect is that the LCC is essentially unchanged. In Phoenix the addition of a furnace leads to a significant increase in the GHX length. When a furnace is added, less heat is removed from the ground for heating, so the ground temperature increases more over time, requiring an increase in the size of the GHX in order to compensate for the reduction in cooling performance of the GHX. The increase in the first cost of the system is much greater than the decrease in operating costs associated with a smaller CT, so the overall system is more expensive. Again, the optimizer ideally would have removed the furnace from the system. This is an example that illustrates the importance of the user in interpreting the results of any software tool.

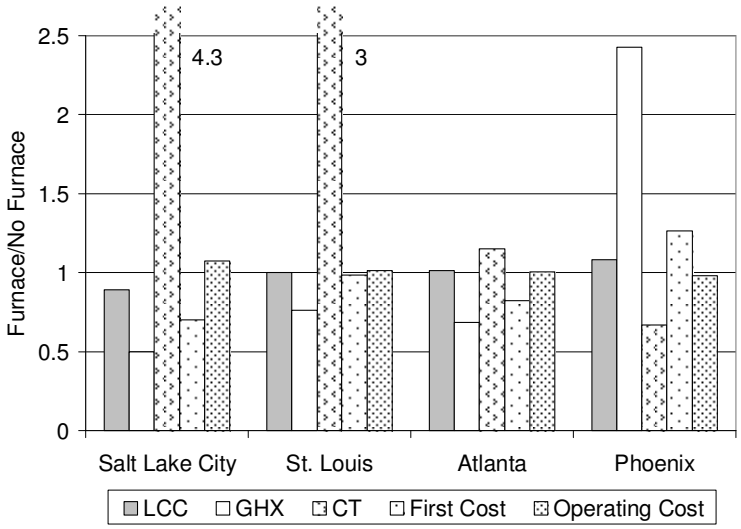

Figure 8-10 Design and cost of a CT Hybrid system with the CT upstream of the GHX; comparison between a system with and without a furnace.

8.2.2 The Effect of a Cooling Tower

Adding a CT to a GSHP system has a pronounced impact on the performance of the system. Figure 8-11 is a comparison between a (1) CT Hybrid without a furnace and the CT placed upstream of the GHX and (2) a GSHP system without a furnace; the other CT Hybrid configurations show the same general trends. *DT Ground* is a measure of the total change in the mean ground temperature over the life of the simulation, with a positive value indicating an increase and a negative value indicating a decrease, and *Imbalance* is a measure of the load imbalance on the ground and is always taken as positive. In general, the ground temperature increases over time because more heat is rejected to the ground than is removed (this is the imbalance). For all locations, the addition of a CT leads to a reduction in the increase in the ground temperature over time associated with a reduction in the load imbalance; i.e., a portion of the cooling load is met by the CT so the ground load between heating and cooling is more balanced. In Phoenix, the increase in ground temperature is completely counter-acted, becoming a decrease as the ground is used almost exclusively for heating (for this particular case, the GHX meets only 6% of the cooling load).

The LCC is lower with the CT. In Atlanta and Phoenix the reduction is significant and this is due to the substantial decrease in first cost due to the reduction in the size of the GHX. The magnitude of the heating load relative to the cooling load in these locations is smaller than in St. Louis and Salt Lake City, so the addition of a CT means that the size of the GHX can be reduced more than it is in St. Louis or Salt Lake City. The operating costs increase in all locations because the CT is more expensive to operate than the GHX; it requires more electricity and there is additional water consumption.

This result illustrates the advantage and disadvantage of a CT Hybrid. The first and overall cost of the system can be reduced, but this comes at the cost of increasing energy consumption. FHyGSHP is a tool which can be used to assess the advantages and disadvantages of various system configurations for a specific building and location, allowing the user to take into account the relative importance of the often competing factors of reducing cost or reducing energy consumption.

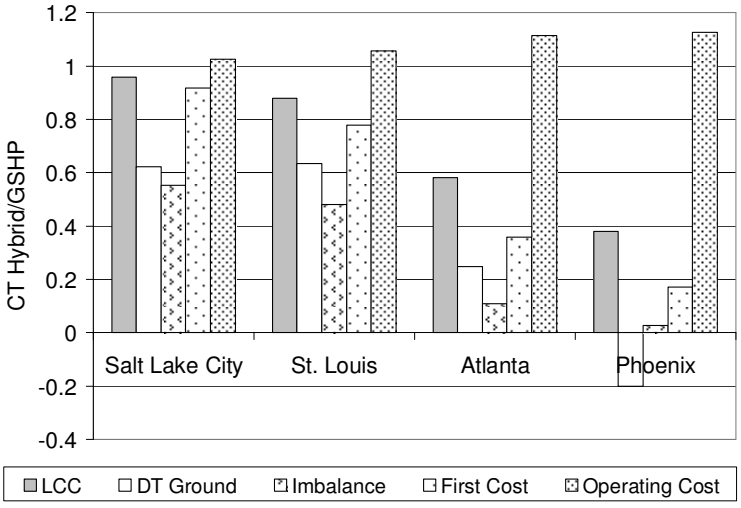

Figure 8-11 Comparison between a system with a CT Hybrid and a GSHP system. The CT Hybrid has no furnace and the CT is upstream of the GHX, but the trends are the same for the other CT Hybrid configurations.

8.2.3 The Effect of the Location of the Cooling Tower

The location of the CT relative to the GHX could impact the performance of the system. In a location such as St. Louis, the undisturbed ground temperature is a relatively low 13.9°C, which is less than the wet bulb temperature during the summer. Therefore, it makes sense to place the CT upstream of the ground so that the CT does an initial portion of the cooling and the ground does additional cooling. In a location such as Phoenix, the ground temperature is high and the wet bulb temperature is low, so it may make more sense for the CT to be located downstream of the GHX. In this configuration, the GHX does the initial cooling and the CT performs additional cooling. This portion of the study was focused on determining if there is a preferred location for the CT in each of the four locations.

Figure 8-12 compares some of the economic factors for a CT Hybrid system with the CT downstream of the GHX versus a system with the CT upstream of the GHX. The figure on the left is for a system without a furnace and the figure on the right is for a system with a furnace. When there is no furnace in the system, the LCC and first cost are larger for the downstream configuration in all locations, though in Salt Lake City and Phoenix there is barely any difference between the two configurations. The increase in LCC is due to the increase in GHX length, which is discussed below. When a furnace is included in the system the LCC decreases in St. Louis and decreases in Phoenix, Atlanta, and Salt Lake City for the downstream configuration. The upstream configuration generally has lower LCC, first cost, and operating cost.

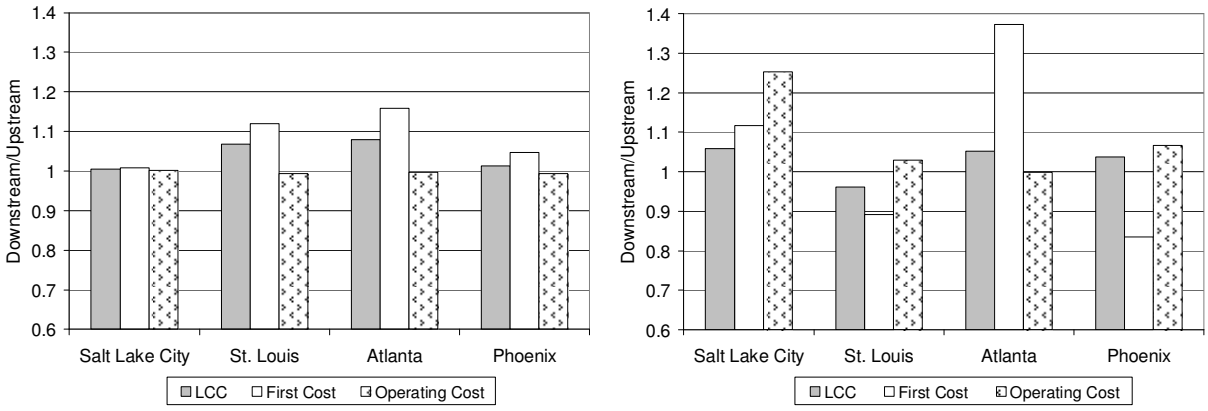

Figure 8-12 Comparison of costs for a CT Hybrid with the CT downstream versus a CT Hybrid with a CT upstream. Left: System with no furnace; Right: System with a furnace.

Figure 8-13 shows a comparison of the design and ground load imbalance between the CT Hybrid with the cooling tower downstream of the GHX and the system with the CT upstream of the GHX. The figure on the left does not include a furnace. In Salt Lake City the downstream configuration is only slightly different from the upstream configuration when there is no furnace in the system. When the CT is downstream of the GHX, the GHX is the first option for cooling, and in Salt Lake City the portion of the cooling load met by the GHX increases from 80% to 83%. The ground temperature increases more rapidly than when the CT is upstream of the GHX, therefore the GHX is less capable of meeting the full cooling load as time progresses and the size of the CT must increase relative to the upstream configuration.

This behavior also occurs in St. Louis and Atlanta. The difference for those two locations is that the increase in the size of the CT is accompanied by an increase in the size of the GHX. In Atlanta the portion of the cooling load met by the GHX increases from 29% for the upstream configuration to 46% for the downstream configuration; in St. Louis the portion increases from 68% to 80%. This increase in cooling performed by the ground is much greater than occurred in Salt Lake City, so the GHX must increase in size. However, in the downstream configuration it is still more economical to allow the GHX to become hotter and increase the size of the CT than

to simply increase the size of the GHX enough to minimize the increase in ground temperature. The net effect of placing the CT downstream of the GHX in Salt Lake City, Atlanta, and St. Louis is to use the GHX to meet a greater portion of the cooling load, which increases the ground temperature more than in the upstream configuration, thereby requiring a larger CT to compensate for reduced GHX cooling in the later years of the simulation.

Phoenix is a little different. The size of the GHX does increase for the same reasons as the other locations, but the CT size does not and the magnitude of the ground load imbalance decreases when the CT is downstream; however, the direction of that imbalance changes. When the CT is upstream of the GHX, the GHX meets a mere 6% of the cooling load. The GHX is present almost solely to meet the heating load and the ground load imbalance is due to more heat being removed from the ground than being rejected to it. In fact, at the end of the simulation the ground temperature has decreased by 1.9°C. When the CT is placed downstream of the GHX, the GHX meets 12% of the cooling load. This doubling of the cooling load on the ground leads to an increase in ground temperature of 1.5°C over time; the ground load imbalance is now such that more heat is rejected to the ground than removed in heating. The size of the GHX increases to minimize the effect on the system performance, but the size of the CT decreases because the GHX is sufficiently meeting the cooling load.

When a furnace is included in the system the results change. In Salt Lake City, the furnace meets approximately 19% of the heating load when the CT is upstream of the GHX and approximately 12% of the heating load when the CT is downstream of the GHX, while the portion of the cooling load met by the GHX increases from 42% to 54% when the CT is placed downstream. In this case, the fact that the GHX temperature increases more in the downstream configuration is a benefit for heating, so the furnace is used less in that configuration. It is also

interesting that when the furnace is added to the system, the GHX meets a lesser portion of the cooling load (42% vs. 80% for the upstream configuration), because the overall size of the GHX decreases relative to the system with no furnace. The CT size decreases in the downstream configuration because the GHX meets more of the cooling load. Note that the initial ground temperature in Salt Lake City, 13.3°C, is sufficiently low that it is a good option for cooling and it takes more time to increase the temperature to a point at which the GHX is no longer efficient in cooling; this is not the case in Atlanta or Phoenix.

In St. Louis, the inclusion of a furnace leads to a reduction in GHX length relative to the system without a furnace. When the CT is placed downstream of the GHX, the portion of the heating load met by the furnace increases slightly from 2.3% to 3.9%, which is a sufficient shift of heating load to lead to a reduction in the size of the GHX. This reduction in GHX length, plus the reduction in CT size, leads to a higher ground temperature over time. However, this system is still able to meet the loads at the end of the simulation. In Atlanta the GHX length increases substantially for the downstream configuration relative to the upstream configuration. The difference between Atlanta and St. Louis is 1) Atlanta has a higher undisturbed ground temperature and 2) Atlanta has greater cooling loads. In St. Louis, where the ground temperature is approximately 13.9°C, there is more margin for the ground temperature to increase before cooling loads can no longer be met efficiently than there is in Atlanta, where the initial ground temperature is already 19.4°C. This requires an increase in GHX size in Atlanta when the GHX is first in line for cooling and an increase in CT size to compensate for the rapid increase in GHX ground temperature.

In Phoenix, the addition of a furnace results in a larger GHX and smaller CT for the downstream configuration, which is similar to the case without the furnace. As in the case

without a furnace, the ground load imbalance switches form a heating dominated imbalance for the upstream configuration to a cooling dominated imbalance for the downstream configuration. However, because of the presence of a furnace, some of the heating load is shifted from the ground to the furnace, so the cooling load imbalance is larger than in the case without a furnace.

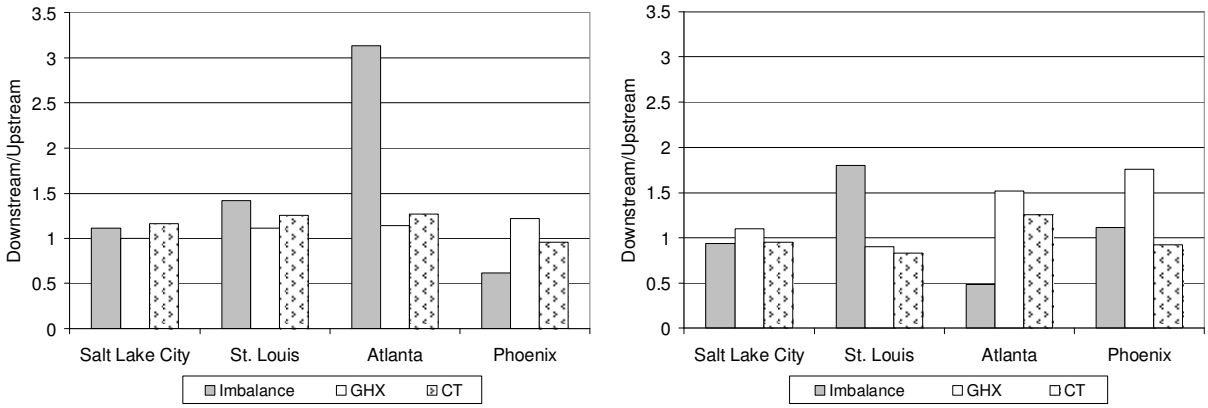

Figure 8-13 Comparison of system design and ground temperature change for a CT Hybrid with the CT downstream versus a CT Hybrid with a CT upstream. Left: System with no furnace; Right: System with a furnace.

The general trend is for the downstream configuration to have a larger GHX and CT than the upstream configuration and a greater load imbalance on the ground. The GHX tends to meet a greater portion of the cooling load when the CT is downstream of the GHX. These effects are reflected in the economic results shown in Figure 8-12. The downstream configuration generally has a greater LCC, but this is due primarily to the first cost of the system. The operating costs of the two configurations are similar.

This study illustrates the complexity of these systems. It is difficult to predict what the optimal design will be because of the feedback between the components in the system; a larger GHX may mean the CT can be smaller, but a furnace may mean the GHX can be smaller, and as the system operates the ground temperature changes such that the CT may be a more efficient

source of cooling, and so on. The best option is to use a tool such as FHyGSHP to conduct scoping studies to determine the configuration and design for a specific building and location.

8.2.4 Comparison of the Configurations

The cost and energy consumption of each configuration with a GHX for a five year period (see Section 8.1 for justification of why this is a reasonable time frame) as compared to the conventional system is shown in Figure 8-14 for St. Louis; the results are similar in the other three locations. In all cases, adding a GHX leads to an increase in the LCC of the design due to the large first cost associated with the GHX, but the energy consumption generally decreases; when a furnace is added to a CT Hybrid, the energy consumption increases relative to the system without a furnace, but the LCC decreases.

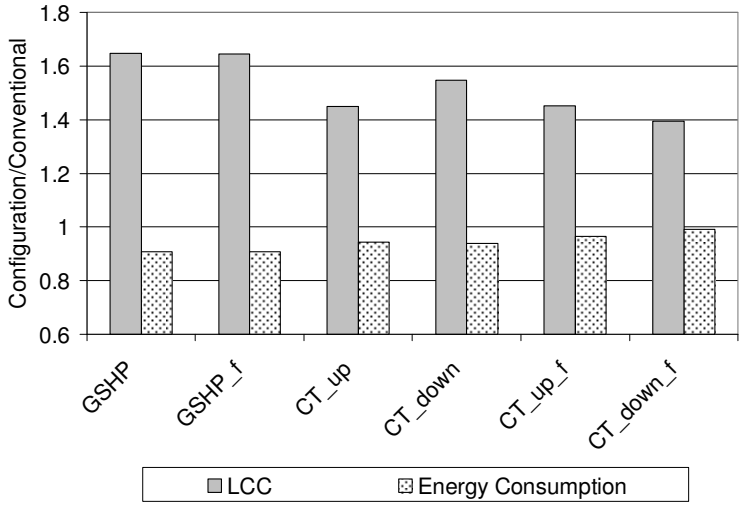

Figure 8-14 Comparison of each design containing a GHX to the conventional system in St. Louis. See Table 8-2 for the meaning of the configuration labels on the x-axis.

8.3 Sensitivity Map

FHyGSHP includes an option to examine the sensitivity of a design to the optimized parameters. For example, if the user selects "GHX length" under the "Sensitivity Map" option then five optimizations are run: 1) nominal, 2-5) optimization of all parameters except the GHX length, which is set to 80%, 90%, 110%, and 120% of the nominal size. This section shows an

example of a sensitivity study of a CT Hybrid without a furnace in Atlanta, St. Louis, Salt Lake City, and Phoenix.

Figure 8-15 shows how the LCC changes when the GHX length changes. When the GHX is under-sized, the optimizer was only able to find a valid design in one case, St. Louis. When the GHX is over-sized, the LCC generally increases, though this again led to some cases when the optimizer was unable to find a valid design. This result indicates that the design is very sensitive to GHX length.

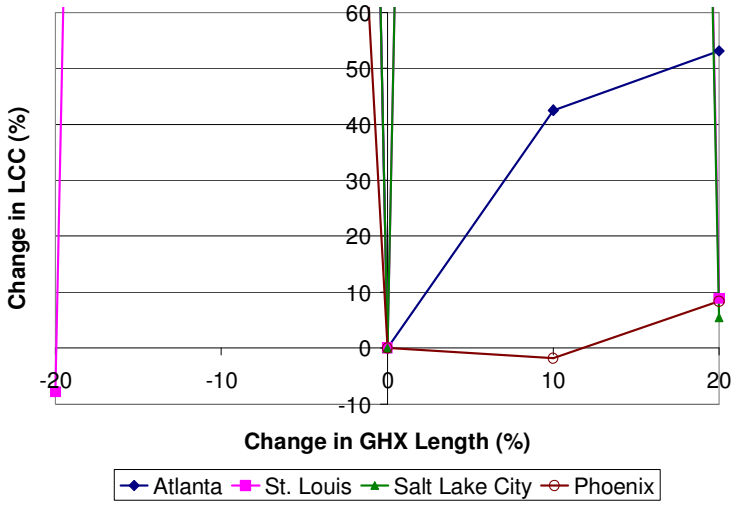

Figure 8-15 Change in LCC as a function of the change in the size of the GHX.

Figure 8-16 shows the change in LCC as a function of the change in size of the CT. Unlike in the case where the GHX length was fixed, the optimizer did not have problems finding an optimal design when the CT size was fixed, indicating that the system is less sensitive to changes in CT size. A second item of note is that the perceived optimal design is not the design with the minimum LCC. The sensitivity map option functions by first finding an optimal design by varying all of the design parameters, including CT size; this is the design represented by the point (0, 0) in Figure 8-16 and should be the optimal design. Four additional optimizations are then run with four different fixed CT sizes to find the best design for each of those cases. In

theory, these four optimizations should not result in a LCC that is less than that found by the initial optimization. However, as can be seen in Figure 8-16, several of the optimizations with fixed CT size found lower values of LCC than the initial optimization. This illustrates the effect of choosing to allow the optimizer to stop at a "near optimal" design rather than continuing the optimization to improve LCC by a relatively small amount.

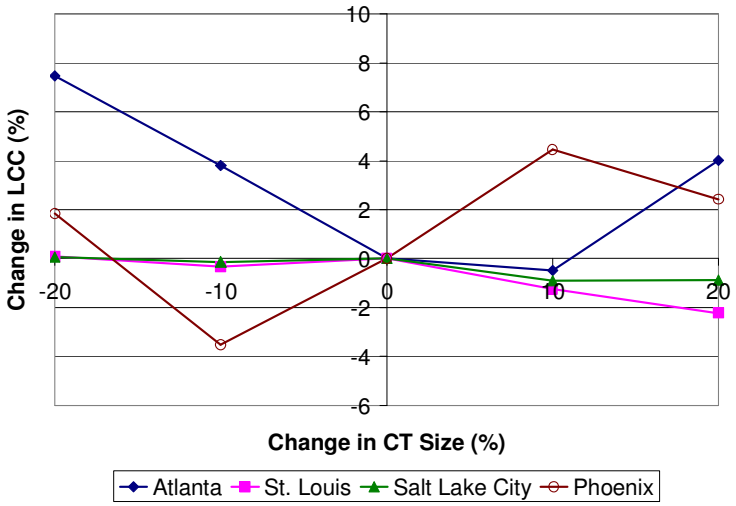

Figure 8-16 Change in LCC as a function of the change in the size of the CT.

Finally, the change in LCC as a function of the change in each of the control set points is shown in Figure 8-17. The limitations of optimization are apparent in this situation as well. In Atlanta and St. Louis LCC is insensitive to CT1 and CT2 over the range considered, while LCC in Phoenix and Salt Lake City is more sensitive to these set points. All locations display a degree of sensitivity to change in GHX1. Overall, the LCC is most sensitive to GHX length, but changing the CT size within a range of ±20% or the control set points within a range of ±2°C can lead to a 10% change in LCC. This study demonstrates the use of FHyGSHP to understand how a design parameter impacts the LCC of a system.

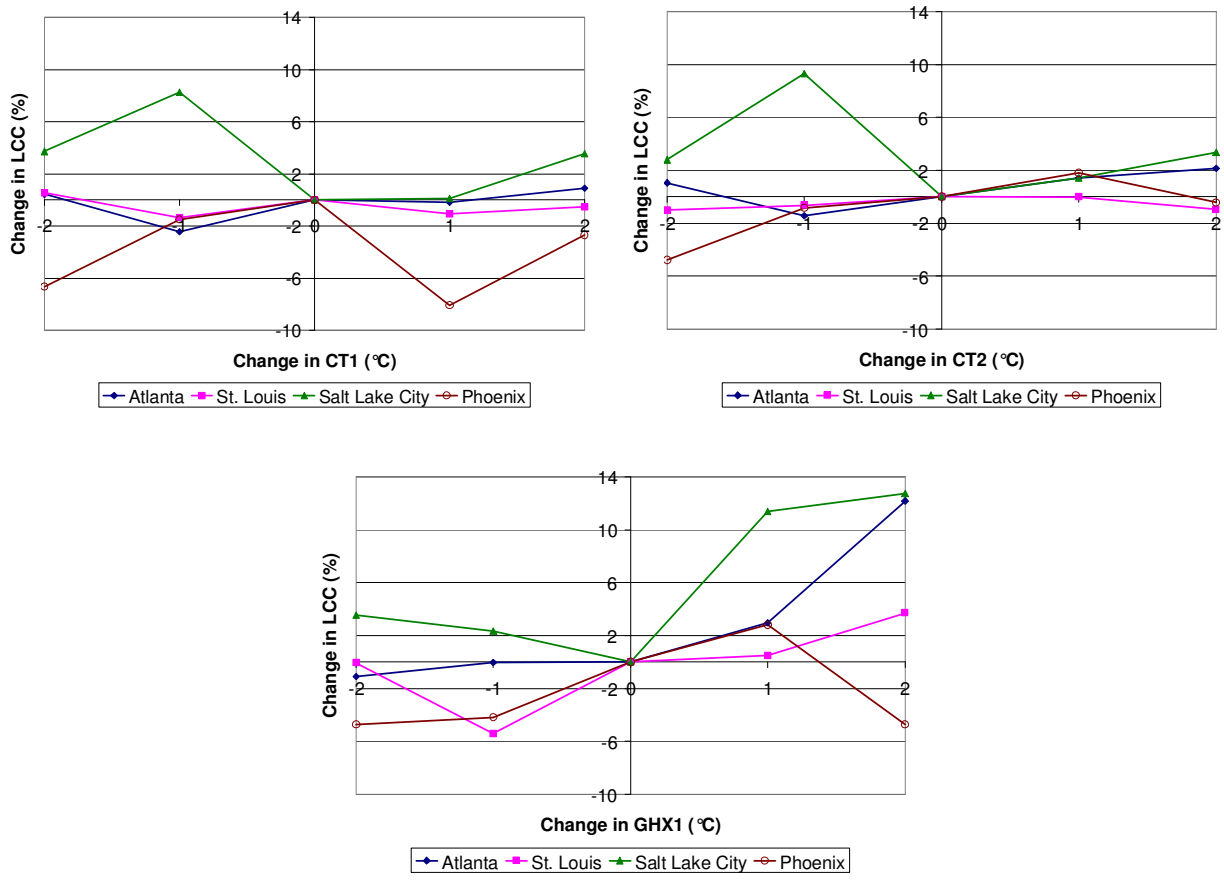

Figure 8-17 Change in LCC as a function of the change in (top left) CT1, (top right) CT2, and (bottom) GHX1.

8.4 Multi-speed CT

The CT power consumption is proportional to the cube of the fan speed and the square of the CT size, therefore, a larger CT operating at a lower fan speed is less expensive to operate and more energy efficient than a smaller tower operating at full speed. The effect of fan speed on the system design was investigated by optimizing the design of a system using a single fan speed, two fan speeds, or continuous fan operation. The list of the specific cases studied is shown in Table 8-3. Details on the implementation of continuous fan speed operation are in Section 2.3.2; single and two speed fan operation are detailed in Section 6.3.2.

Table 8-3 List of cooling tower fan speed studies.

# of Speeds	High speed	Low speed
1	100%	n/a
1	50%	n/a
2	100%	50%
2	75%	25%
Continuous	100%	10%

For single speed operation, the user of FHyGSHP enters the high speed (where 1 = 100%); for two speed operation the user enters both the high speed and the low speed. Continuous operation is hard-coded into the program.

Figure 8-18 shows the LCC for each of the cases listed in Table 8-3 normalized by the LCC of the system using continuous control of the CT in Atlanta, St. Louis, Salt Lake City, and Phoenix. Continuous operation yields the lowest LCC in all but Salt Lake City. However, even in Salt Lake City the LCC for continuous operation is only 2% greater than the best case. This is the expected result; continuous operation allows for a better match between fan speed and the current condition of the system. There is no general trend to indicate whether single or two speed operation is better, though in general a strategy that includes a low fan speed (i.e., single speed operation at 50% or two speed operation at 75% and 25%) results in lower LCC.

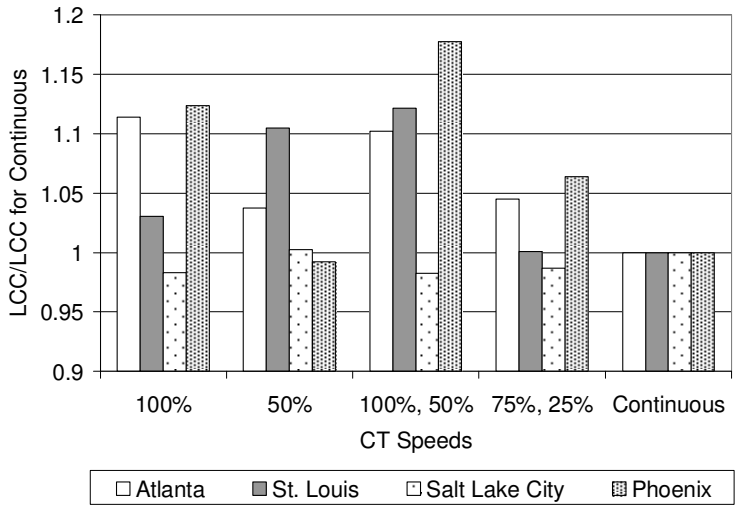

Figure 8-18 LCC of the case studied divided by the LCC for the continuous control scheme.

Figure 8-19 shows the first cost of each control scheme on the left and the operating cost of each control scheme on the right; in both cases the cost has been normalized by the cost of the continuous scheme. The first cost associated with continuous operation is on the higher end of the range of costs, but it is consistent with the other schemes. The operating cost associated with continuous operation is at the low end of the range of costs. Again, this is expected. A significant portion of the operating cost is related to the CT fan speed; by allowing for continuous operation, the fan speed is less likely to be higher than necessary to meet the cooling load. It is expected that if the relationship used to calculate continuous CT fan operation was optimized to the specific location and building under consideration, the monetary and energy savings would be even greater.

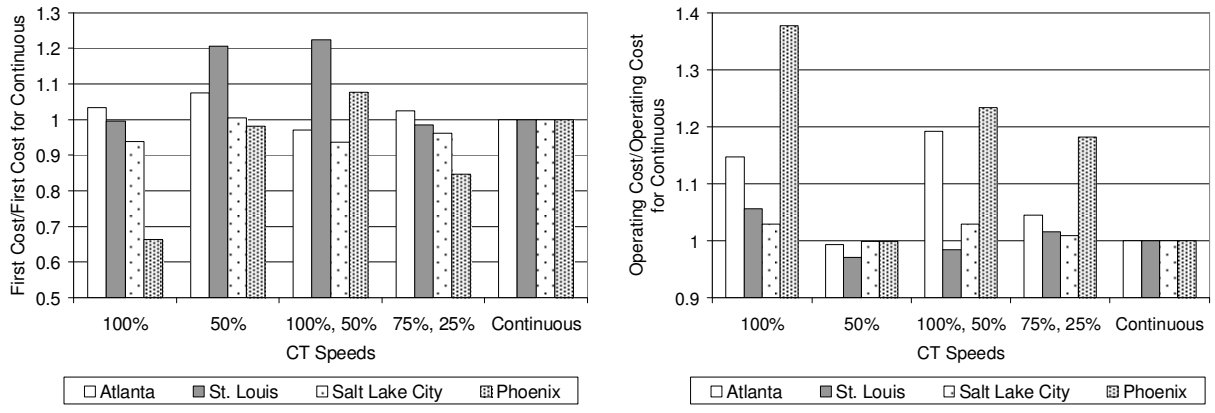

Figure 8-19 First cost and operating cost of the systems using different cooling tower control schemes. Left: First cost. Right: Operating cost.

8.5 Economic Parameters

The studies documented in this thesis were conducted using the same nominal economic parameters, but the design of a system is affected by these parameters. This study examined two factors that impact a CT Hybrid: the ratio of peak electrical rates to off-peak rates and the cost of water. The results presented here are for St. Louis, but similar studies can be carried out using

FHyGSHP for any location and using information provided by the user that is specific to that location.

The left side of Figure 8-20 shows how the GHX length, CT size, and LCC change as the ratio of peak to off-peak electrical rates increases; the values are normalized by the results at the baseline value of 1.5. The right side of Figure 8-20 shows the percent of the total cooling load met by the GHX as a function of peak to off-peak electrical rates. The LCC increases linearly with the peak electrical rate. The GHX length increases initially and then levels off, while the size of the CT decreases and then levels off; the percentage of the cooling load met by the GHX increases with the peak electrical rate and then levels off. This is the expected trend. As the cost of electricity increases, more of the load should shift to the more efficient method of cooling, but after a certain threshold the system stabilizes on a design.

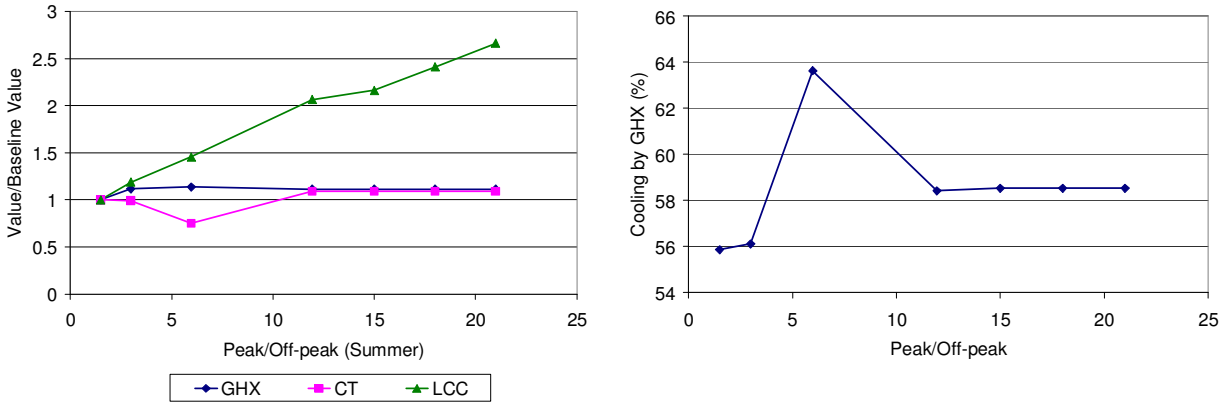

Figure 8-20 Left: Variation in GHX length, CT size, and LCC as a function of the ratio of the peak to off-peak electrical rates during the summer in St. Louis. Right: Percentage of the total cooling load met by the GHX as a function of the peak to off-peak ratio.

Figure 8-21 shows the variation in GHX length, CT size, and LCC as the cost of water increases and the percentage of the cooling load met by the GHX as the cost of water increases. As expected, as the cost of water increases less of the cooling load is met by the CT because

operating costs are lower with the GHX. This study illustrates the importance of using the best economic information available in order to ensure the most accurate design.

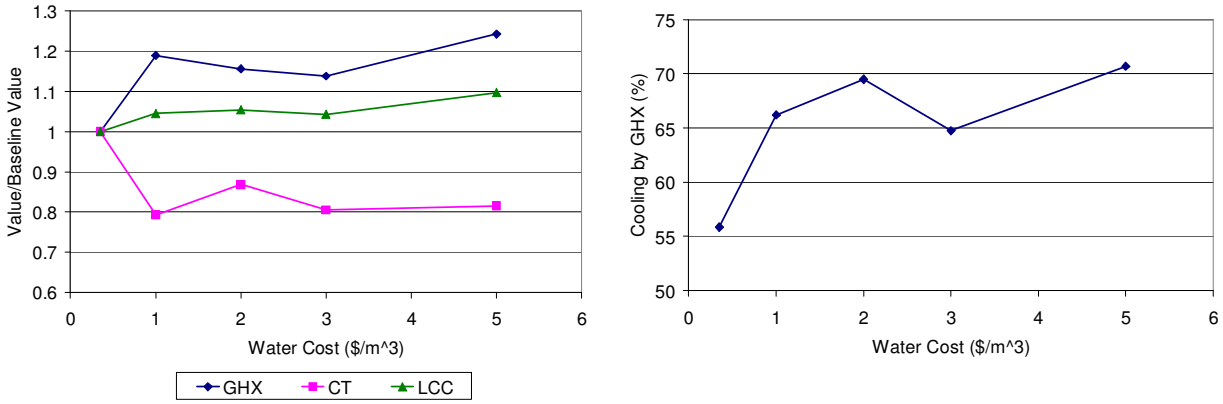

Figure 8-21 Left: Variation in GHX length, CT size, and LCC as a function of the cost of water in St. Louis. Right: Percentage of the total cooling load met by the GHX as a function of the water cost.

8.6 GHX Parameters

As with the economic parameters, the bore-field geometry and thermal characteristics were the same for all of the studies in this thesis, but the optimal design is a strong function of the GHX parameters. The sensitivity of GHX length and LCC of a GSHP system to thermal conductivity, heat capacity, and borehole spacing is shown in Figure 8-22. The length and LCC are normalized by the value associated with the baseline case, which was used in the other studies. As expected, as thermal conductivity increases the size of the GHX decreases because heat diffuses away from the borehole more quickly and it is a more efficient sink for cooling. As heat capacity increases, more energy is required to increase the temperature of the bore-field, so a smaller GHX can meet the cooling load. The GHX length decreases as the borehole spacing increases because there is less interference between adjacent boreholes. The design is particularly sensitive to the borehole spacing; once it is below a certain value the GHX length increases rapidly.

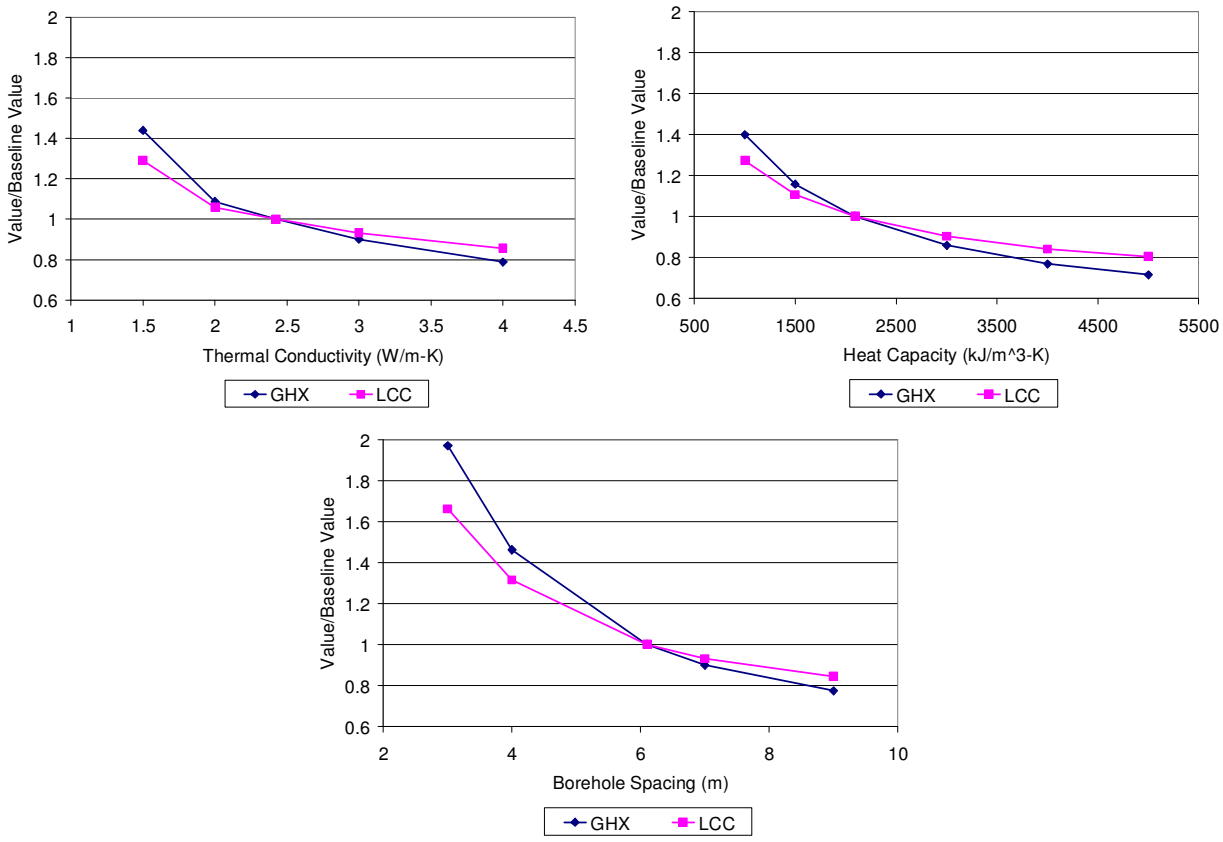

Figure 8-22 GHX Length and LCC of a GSHP system as a function of thermal conductivity (top left), heat capacity (top right), and borehole spacing (bottom) in Atlanta.

The behavior is different for a CT Hybrid, as shown in Figure 8-23. Although there is some variation in the design of the system as each of the parameters change, the overall trend in LCC is flat relative to the variation when the system is a GSHP. This effect is related to the presence of the CT. The CT size and operation can be varied to compensate for changes in the performance of the GHX due to changes in the characteristics of the ground. In addition, it is simpler to install a larger CT in an existing CT Hybrid to compensate for an under-performing GHX than it is to increase the size of the GHX (this latter case could occur if the ground characteristics used in the design process differ from the actual characteristics of the installed system). The first cost of the GHX is the primary driver of the LCC, so decreasing the variation in the GHX decreases the variation in the LCC. Table 8-4 shows the range of variation of LCC

for the GSHP and CT Hybrid systems; these values demonstrate the greater stability in terms of LCC and GHX length associated with a hybrid system as the ground properties vary. This type of study could be used by a designer to find a design that accounts for the uncertainty in relevant design parameters such as thermal conductivity.

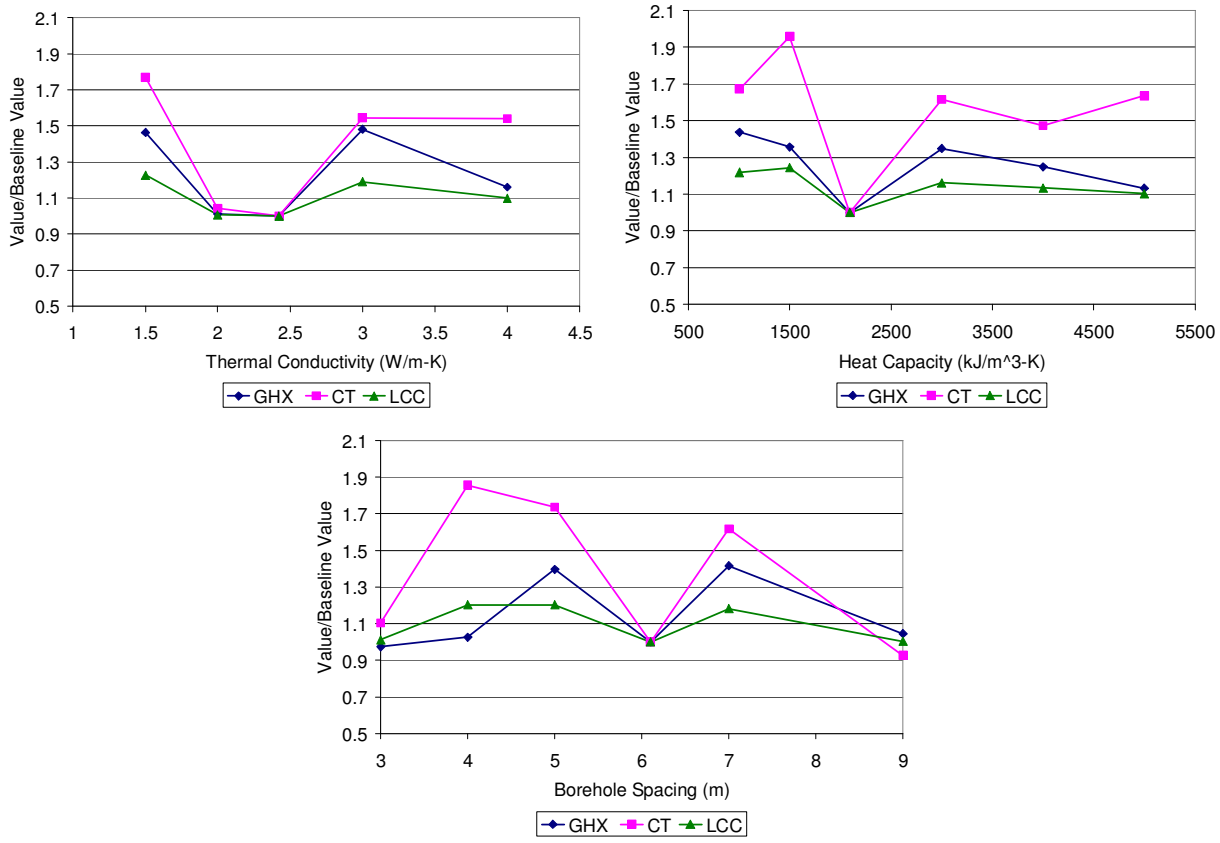

Figure 8-23 GHX Length and LCC of a CT Hybrid system as a function of thermal conductivity (top left), heat capacity (top right), and borehole spacing (bottom) in Atlanta.

Table 8-4 Range of variation in LCC for GSHP and CT Hybrid systems.

Parameter	GSHP Range in LCC	CT Hybrid Range in LCC
Thermal Conductivity	-20% to +30%	0% to +23%
Heat Capacity	-15% to +30%	0% to +25%
Spacing	-15% to +66%	0% to +20%

Chapter 9 Conclusions and Future Work

9.1 Conclusions

This thesis has documented a variety of work related to the design and operation of cooling tower hybrid ground source heat pumps (CT HyGSHP) in a cooling dominated environment. A software tool, FHyGSHP, was developed to allow users to simulate and design a CT HyGSHP.

The Duct STorage (DST) model [46] was used in the FHyGSHP tool in order to simulate the performance of a ground heat exchanger (GHX). Temperatures and flow rates from two existing, operational systems with a GHX were measured in order to validate the accuracy of the DST model on a short term basis. This validation found that the DST model captures the measured behavior of the GHX, but inputs to the model (such as the thermal conductivity of the ground) have a significant impact on the fidelity of the model. Calibration of the model to the actual performance of the GHX that is being simulated will always yield the best agreement between simulation and reality.

The key inputs to the model are hourly building heating and cooling loads and the dry and wet bulb temperatures. These parameters are usually obtained using Typical Meteorological Year (TMY) data. TMY data is an average weather year calculated from historical data; building loads are calculated using these data. GSHP and CT HyGSHP systems are typically designed considering the total life of the system, which is generally on the order of 20 years. When TMY based weather and loads are used for a multi-year simulation, the same load and weather data are repeated for every year of the simulation. This means that the design is determined without considering the year-to-year weather variation that actually occurs. A method was developed to generate synthetic weather and load data from a single year of weather and load data that

incorporates random variation. In this way a system design can be based on a multi-year simulation that incorporates realistic year-to-year weather variation. This method has been incorporated into FHyGSHP.

Appropriate optimization methods have been evaluated and incorporated into FHyGSHP to enable optimization of the GHX length, CT size, furnace size, and control set points to minimize life cycle cost (LCC). The basic methods were modified to improve the speed of the optimization for the given problem and increase the chance that the optimization will converge. An optimal design can also be found based on a requirement for energy reduction versus a conventional system (i.e., a furnace and cooling tower) or for a limit on the change in the ground temperature over time.

Standard CT HyGSHP control strategies were evaluated and included in FHyGSHP. The pre-cooling strategy was examined in detail. This strategy can operate independently or in conjunction with other control strategies to cool the GHX during the night in order to improve heat transfer efficiency during the following day. In general, operating the system in pre-cooling was determined to be less favorable than operating the system based on the instantaneous load and temperature conditions.

FHyGSHP was developed to improve upon existing design tools. Some of the items included in FHyGSHP that are not found in other design tools are:

- the option to include a furnace in a GSHP or CT HyGSHP system,
- continuously variable CT fan speed operation,
- the inclusion of pre-cooling as a control strategy,
- the ability to include year-to-year weather variation in the design,
- sensitivity study,

- the ability to specify an upper limit on the total change in ground temperature, and
- the ability to specify a lower limit on energy savings relative to a conventional system.

A study of system configuration was conducted using FHyGSHP. This study revealed the importance of modeling the system using sub-hourly time steps and the value of being able to compare conventional, GSHP, and CT HyGSHP systems in order to determine the best design for a system given a specific location and building load profile. Additional studies include:

- evaluation of the control of cooling tower fan speed,
- the sensitivity of the design to the simulation duration and time step size, and
- the sensitivity of the design to time of day rates and water cost.

FHyGSHP is now available for use by other researchers and designers for evaluating CT HyGSHP designs.

9.2 Future Work

There are areas where additional work will provide a more complete picture of HyGSHP performance and improve the usefulness of FHyGSHP. This section outlines some of the future areas for research, but is by no means an exhaustive list.

9.2.1 Control Strategies

Although extensive research into control strategies was conducted, there are additional strategies which should be evaluated. In particular, Xu [13] developed the following control strategies:

- Load control – if the cooling load is high, run the CT more; in practice, the temperature drop across the heat pumps can be monitored to determine if the CT should operate.

- Forecast control – operate the components based on the forecast heat pump loads, where the forecast period could be anywhere from 12 hours to weeks. A related alternative is to base the "forecast" on the historical loads (i.e. base the control for tomorrow on the loads from today).
- Varied loop temperature control – monitor the variation in loop temperature over a prior time period (48 hours, for example); an increase indicates an increase in cooling loads, so the cooling tower should run more often. If the temperature decreases, the cooling loads have decreased and the cooling tower should be operated less often.

Xu found that the load control strategy, with a set point of -6Δ°C (-10.8Δ°F) was applicable to a wide range of buildings and climates; the forecast control strategy resulted in the largest savings and was valid for a variety of buildings and climates; the varied loop temperature control strategy also performed well, but the set point was not as generally applicable. More extensive comparison of these methods to the methods included in FHyGSHP would provide more information regarding the optimal operation of a CT HyGSHP.

Currently, the furnace in FHyGSHP is controlled and sized based on a load set point, but in reality it would be controlled by a temperature set point. The control scheme in FHyGSHP should be modified for this type of control. This would require two values to be optimized for the furnace, the capacity and the set point temperature. Another improvement to the control strategies would be the ability to vary the set point temperatures over time. As the temperature of the ground changes over time or if the building load profiles change, the optimal control of the system is likely to change as well. Using a single set of control set points for the entire life of the system is unlikely to lead to optimal performance.

9.2.2 GHX Models

A multitude of GHX models exist, but there is very little quantitative information in the literature discussing their relative computational efficiency and accuracy. One study that evaluated the accuracy of several models was conducted by Shonder et al. [47]. Five different commercially available programs (they do not specify which ones they used) were used to calculate the design length of the GHX; the variation between the programs was ±7% and ±16% for cooling and heating dominated sites, respectively. The authors used the DST model, which they had validated in a prior study, as the baseline for comparison. More recently, Spitler et al. [51] performed a comparison of the GHX implementation in six commercially available programs: Geostar, TRNSYS, HVACSIM+, GEOEASE II, EnergyPlus, and eQuest. In this study, each model was evaluated by comparing the average heat flow rate to the bore field and the exiting fluid temperature from the bore field to experimentally measured results. The authors found that the prediction of the fluid temperature exiting the GHX varied significantly between the models and suggested additional investigations to determine the cause. The DST model performed as well or better than other models when compared to experimental data. In both cases the papers looked at commercial design packages so the GHX models were not examined in a stand-alone condition.

It would be useful to understand the differences between some of the GHX models, in particular the DST and g-function models [29,30,98], both of which are commonly used in design tools. This knowledge could be used to determine if there are situations in which one model is preferred over another.

9.2.3 Some General Improvements to FHyGSHP

There are several areas for improvement in FHyGSHP that will ultimately make it a more useful and reliable tool for researchers and designers alike. As stated throughout this work, the

optimization methods are imperfect; there is a compromise between the time required to complete the optimization and accuracy. More study into the selection of an algorithm that more consistently locates an optimal or near optimal value (defined as within 10% of the optimum) would be useful. Alternatively, it would be useful to refine the values of the optimization parameters in order to provide more consistency. This latter effort would reduce the amount of user interaction required to determine if the result is sufficiently accurate. Improving the optimization can also be accomplished by improving the method for determining the initial guess for the optimization. The current version of FHyGSHP adapts the ASHRAE sizing method [59], but this method does not provide estimates of control set points nor does it account for the specific system configuration (e.g. CT downstream or upstream of the GHX, the inclusion of a furnace). More extensive use of FHyGSHP to design systems for a variety of locations and building types would provide a set of data that could be used to develop a new method of providing a complete set of guess values that are more specific to the problem.

The equation for calculating the CT fan speed in continuous operation needs to be further refined, perhaps using optimization studies, in order to determine the relationship that yields the optimal performance. In addition, the drive losses associated with a variable speed drive need to be incorporated into the model. There should also be an option for the user to enter the relationship between fan speed and fluid and wet bulb temperature for the CT fan speed. Increased flexibility in the system configurations that can be simulated would also be beneficial. The conventional system is currently defined as a CT and furnace on the air side of the building, but different buildings and regions of the country have different definitions of a conventional system; therefore, additional options would improve the applicability of the program. At this point, if the conventional system is different from the one defined in this program, the user could

use a different building energy program (e.g. EnergyPlus [99], eQuest [100], TRNSYS [101], etc.) to model the conventional system and then compare to the GSHP and CT HyGSHP designs from FHyGSHP. The disadvantage is that the assumptions in the calculations of cost and power consumption may differ between different programs. Along a similar vein, in some regions of the country a closed circuit cooling tower may not be the most appropriate supplemental heat rejection device, so the addition of alternative options would be an improvement.

Finally, perhaps the most important improvement would be an extensive validation of the program. Ideally, the load and weather information for several years of operation in an existing system would be input to FHyGSHP, using the existing system design, and the cost and power consumption of the system calculated by FHyGSHP would be compared to the actual data. The initial conditions of the GHX would need to be well known (thermal conductivity, diffusivity, temperature, etc.) and the control scheme would have to be approximated as nearly as possible. This is a difficult task, but FHyGSHP could be used as a primary design tool for these systems with confidence if such a task were accomplished.

Appendix A ASHRAE Sizing Method

One method for designing a ground source heat pump is detailed in Chapter 34 of the ASHRAE Handbook – HVAC Applications [59]. The implementation of this method in FHyGSHP is described in this section; some modifications are made to the method in applying it to the specific problem in this research and some variable definitions are different from the ASHRAE method. Readers interested in using the ASHRAE method should review [1] as some of the modifications and assumptions detailed here may not be appropriate for other systems. There are a significant number of variables used in this calculation that are listed at the end of this appendix. This appendix presents a summary of the method. Although not included, the required unit conversions are performed in FHyGSHP.

A.1 Furnace Sizing

The number of hours in which heating, h_h, or cooling, h_c, occur, the mean hourly heat load, $q_{h,mean}$, and the maximum heating, $q_{h,max}$, and cooling, $q_{c,max}$, loads are calculated from the input file containing the weather and load information. The ratio of the thermal conductivity, k_g, to the heat capacity, c_g, is the thermal diffusivity, α_g. The calculations also require the undisturbed ground temperature, t_g, thermal conductivity of the grout, k_{grout}, and diameter of the borehole, d_b.

When a furnace is included in the system design, the size of the furnace is determined by optimizing the value of $Q_{set,ratio}$. The ground heat exchanger meets the heating load up to Q_{set} and the furnace meets the difference between the heating load and Q_{set} if the load exceeds Q_{set}. $Q_{set,ratio}$ is the ratio of Q_{set} to the maximum heating load. The initial guess value for $Q_{set,ratio}$ is determined as shown in Eq.(A.1). The maximum heating load is scaled based on this guess value, as indicated in Eq.(A.2), for use in the subsequent calculations.

$$Q_{set,ratio,guess} = \frac{Q_{set,guess}}{q_{h,\max}} = \frac{\max\left[q_{h,mean}, 0.75\left(q_{h,\max} - q_{h,mean}\right)\right]}{q_{h,\max}} \quad \text{(A.1)}$$

$$q_{h,\max} = q_{h,\max}\, Q_{set,ratio,guess} \quad \text{(A.2)}$$

The length of the ground heat exchanger is determined for both heating and cooling and the larger length is used as the ground heat exchanger length. The calculation of the length is described next.

A.2 Ground Heat Exchanger Length

The line source model consists of an infinitely long line source or sink in an infinite medium of initial temperature T_0; the temperature is then calculated at any radial location, assuming only radial heat transfer from the line and a constant heat transfer rate during the period of interest [21,22]. A superposition method is applied to calculate the temperature over different time periods. The cylindrical source model is similar to the line source model, but the function for calculating the temperature at a point in the medium is more complex and is more accurate for a wider range of time scales and geometries [22,26]. The ASHRAE method estimates the size of the ground heat exchanger by applying the cylindrical source model.

One assumption of the model is steady state heat transfer, but as in the case of the line source model, superposition can be applied to account for transient behavior. The ASHRAE method includes heat transfer at three different time scales: hourly, monthly, and annually. Variables that refer to one of these time periods have subscripts of *h* (hourly), *m* (monthly), and *a* (annually). The length of the ground heat exchanger required to meet the maximum cooling load is calculated from Eq.(A.3) and the length of the ground heat exchanger required to meet the maximum heating load is calculated from Eq.(A.4). If the system is a ground source heat pump

only system, the ground heat exchanger length is the maximum of L_c and L_h. The variables in these equations are defined in the subsequent discussion.

$$L_c = \frac{q_a R_{ga} + \left(q_{c,\max} - W_c\right)\left(R_b + PLF_c\, R_{gm} + R_{gd}\, f_{sc}\right)}{t_g - 0.5\left(t_{wi,c} + t_{wo,c}\right) + t_p} \tag{A.3}$$

$$L_h = \frac{q_a R_{ga} + \left(q_{h,\max} - W_h\right)\left(R_b + PLF_h\, R_{gm} + R_{gd}\, f_{sc}\right)}{t_g - 0.5\left(t_{wi,h} + t_{wo,h}\right) + t_p} \tag{A.4}$$

The net heat transfer to the ground on an annual basis, q_a, is estimated as shown in Eq. (A.5). If q_a is negative, then the cooling load is greater than the heating load. The equations for length include three time dependent thermal resistance terms, R_{ga}, R_{gm}, and R_{gd} (Eqs.(A.6), (A.7), and (A.8) respectively). The time span over which a thermal pulse interacts with the ground is a year for R_{ga}, a month for R_{gm}, and a few hours for R_{gd}. The borehole resistance, R_b, is a measure of the thermal resistance associated with the grout, pipe, fluid, and interfaces between the materials within the borehole. For this thesis, R_b is estimated as 0.163 h-ft-°F/BTU based on the calculation performed in the DST model.

$$q_a = q_{c,\max} + q_{h,\max} \tag{A.5}$$

$$R_{ga} = \frac{G_f - G_1}{k_g} \tag{A.6}$$

$$R_{gm} = \frac{G_1 - G_2}{k_g} \tag{A.7}$$

$$R_{gd} = \frac{G_2}{k_g} \tag{A.8}$$

Each thermal resistance term contains a G factor, defined in Eq.(A.9). Fo is the Fourier number, which is a dimensionless time, defined in Eq.(A.10) for the relevant time spans, τ,

which are defined in Eq.(A.11). The annual time span is represented by τ_1, the monthly time span is represented by τ_2 (τ_1 + 30 days), and the hourly time span is represented by τ_f (1/4 of a day).

$$G_f = \frac{\log\left(Fo_f\right)+1.3165}{13.166}$$
$$G_1 = \frac{\log\left(Fo_1\right)+1.3165}{13.166} \qquad \text{(A.9)}$$
$$G_2 = \frac{\log\left(Fo_2\right)+1.3165}{13.166}$$

$$Fo_1 = \frac{4\alpha_g\left(\tau_f - \tau_1\right)}{d_b^2}$$
$$Fo_2 = \frac{4\alpha_g\left(\tau_f - \tau_2\right)}{d_b^2} \qquad \text{(A.10)}$$
$$Fo_f = \frac{4\alpha_g\,\tau_f}{d_b^2}$$

$$\tau_1 = 3650\ days$$
$$\tau_2 = 3680\ days \qquad \text{(A.11)}$$
$$\tau_f = 3680.25\ days$$

The term f_{sc} is the short circuit factor; this factor accounts for the fact that some heat transfer occurs within the borehole between the u-tube legs. The flow rate through the ground heat exchanger is often set in the range of 2.5 to 3 gpm per ton of cooling [2]; for several of the parameters in this calculation a value of 3 gpm per ton (either cooling or heating, depending on the use of the parameter) is used. The value of f_{sc} associated with a flow rate of 3 gpm per ton is 1.04 [59].

When the capacity of the heat pump exceeds the building load the heat pump operates at part load and the performance is degraded. Part load factor (PLF) is a means of quantifying this degradation; it is defined as the ratio of the heat pump efficiency when operating at part load and

the heat pump efficiency when operating at steady state [102]. Based on the information in the references [102,103] and data from test runs of the simulation, PLF_c and PLF_h are set to a value of 0.85. The calculation also requires an estimate of the power consumption of the heat pumps at design load; for this program the work required is estimated from the part load factor, the maximum load (either cooling or heating) and the *COP* (coefficient of performance) as shown in Eq.(A.12).

$$W = PLF\,\frac{q_{\max}}{COP} \tag{A.12}$$

The temperature of the fluid entering the heat pump in cooling is estimated as 25°F above the ground temperature and the temperature of the fluid entering the heat pump in heating is estimated as 15°F below the ground temperature based on recommendations in the ASHRAE method [59] (see Eq.(A.13)).

$$\begin{aligned} t_{wi,c} &= t_g + 25 \\ t_{wi,h} &= t_g - 15 \end{aligned} \tag{A.13}$$

The fluid flow rate, Q_w, is estimated as shown in Eq.(A.14) based on Kavanaugh and Rafferty [53]. An estimate of the outlet temperature from the heat pump in cooling is obtained from Eq.(A.15) and the estimate of the outlet temperature from the heat pump in heating is obtained from Eq.(A.16).

$$Q_w = 3\left[\frac{gpm}{ton}\right] q_{h,\max} \tag{A.14}$$

$$t_{wo,c} = t_{wi,c} - \frac{\left(q_{c,\max} - W_c\right)}{500\,Q_w} \tag{A.15}$$

$$t_{wo,h} = t_{wi,h} - \frac{\left(q_{h,\max} - W_h\right)}{500\,Q_w} \tag{A.16}$$

The final component required for the calculation of the length of the ground heat exchanger is the temperature penalty, t_p. When a bore-field consists of a single borehole, the heat transfer can be calculated based solely on how that borehole interacts with the ground. When there is more than one borehole, the calculation of heat transfer between any single borehole and the ground has to account for the fact that neighboring boreholes are also transferring heat to or from the ground. The presence of nearby boreholes leads to a degradation of heat transfer. This degradation is accounted for by including a temperature penalty in the calculation. The ASHRAE method [59] includes information for estimating the temperature penalty, t_p in Eqs.(A.3) and (A.4); for this work a value of 3.8°F is used. For a ground source heat pump only system, the length of the ground heat exchanger is estimated as the maximum of L_c and L_h. The method for sizing a cooling tower ground source heat pump is discussed next.

A.3 Cooling Tower Hybrid

When the system is a cooling tower hybrid the sizing of the ground heat exchanger and cooling tower are based on correlations from Hackel, et al. [11] which are included in the ASHRAE method. The estimate of the ground heat exchanger length for the hybrid system is given in Eq.(A.17), where the constant 254 has units of ft-hr-°F/kBTU. This correlation is for a thermal conductivity of 1.4 BTU/ft-hr-°F, but as this is only an estimate for the optimization program, no adjustments are made to correct for the user defined thermal conductivity.

$$L_{hyb} = 254\frac{q_{h,\max}}{t_g - t_{wo,h}} \tag{A.17}$$

The size of the cooling tower is estimated from Eq.(A.18), where the constant 4.72 has units of ft/ton-°F.

$$CT = 1.3\left[q_{c,\max} - \frac{L_{hyb}}{4.72\left(t_g - 0°F\right)} \right] \tag{A.18}$$

α_g = Thermal diffusivity of the ground [ft^2/day]

τ_1 = Time of operation, 3650 days

τ_2 = Time of operation, 3680 days

τ_f = Time of operation, 3680.25 days

c_g = Heat capacity of the ground [BTU/ft^3-°F]

CT = Cooling tower size [BTU/hr]

d_b = Borehole diameter [ft]

Fo_1 = Fourier number associated with τ_1

Fo_2 = Fourier number associated with τ_2

Fo_f = Fourier number associated with τ_f

f_{sc} = Short-circuit heat loss factor

G_1 = g-factor associated with Fo_1

G_2 = g-factor associated with Fo_2

G_f = g-factor associated with Fo_f

h_c = Hours of cooling in a year [hr]

h_h = Hours of heating in a year [hr]

k_g = Thermal conducitivy of the ground [BTU/hr-ft-°F]

k_{grout} = Thermal conducitivy of the grout [BTU/hr-ft-°F]

L_c = Ground heat exchanger length for cooling [ft]

L_h = Ground heat exchanger length for heating [ft]

L_{hyb} = Ground heat exchanger length [ft]

PLF_c = Part load factor in the design month for cooling [-]

PLF_h = Part load factor in the design month for heating [-]

q_a = Net annual average ground load [Btu/h]

$q_{c,\max}$ = Peak annual cooling load [Btu/h]

$q_{h,\max}$ = Peak annual heating load [Btu/h]

$q_{h,mean}$ = Mean annual heating load [Btu/h]

$Q_{set,guess}$ = Guess for the furnace heating setpoint [-]

Q_w = Flow rate assuming 3 gpm/ton of heating [gpm]

R_b = Borehole thermal resistance [ft-hr-°F/BTU]

R_{ga} = Thermal resistance of the ground associated with an annual pulse [ft-hr-°F/BTU]

R_{gd} = Thermal resistance of the ground associated with a peak daily pulse of energy of 4 to 6 hours [ft-hr-°F/BTU]

R_{gm} = Thermal resistance of the ground associated with a monthly pulse [ft-hr-°F/BTU]

t_g = Undisturbed ground temperature [°F]

t_p = Temperature penalty to account for borehole thermal interference [°F]

$t_{wi,c}$ = Temperature of the fluid at the inlet of the cooling heat pump [°F]

$t_{wi,h}$ = Temperature of the fluid at the inlet of the heating heat pump [°F]

$t_{wo,c}$ = Temperature of the fluid at the outlet of the cooling heat pump [°F]

$t_{wo,h}$ = Temperature of the fluid at the outlet of the heating heat pump [°F]

W_c = Power consumption at the design cooling load [W]

W_h = Power consumption at the design heating load [W]

Appendix B Optimization

This appendix provides details relating to the SUBPLEX and DIRECT optimization techniques; the use of optimization in FHyGSHP is discussed in Chapter 4.

B.1 SUBPLEX

The Nelder-Mead simplex algorithm (NMS) is a direct search optimization method. Each step of the method contains a simplex of points that approximate the optimal solution. A triangle is an example of a simplex in two dimensions; a tetrahedron is an example in three dimensions. The objective function is evaluated at each vertex of the simplex (e.g. vertices of a triangle) and the vertices are ranked based on the value of the objective function at each vertex, x, from 1 to $N+1$, where N is the number of decision variables. The goal is to replace the worst vertex, x_{N+1}, with a new point defined by Eq. (B.1):

$$x(\mu) = (1+\mu)\bar{x} - \mu x_{N+1} \tag{B.1}$$

where $\bar{x}$ is the centroid of the convex hull as defined by Eq. (B.2) (e.g., the centroid of the simplex once the worst vertex is removed) and μ is a constant defined below.

$$\bar{x} = \frac{1}{N}\sum_{i=1}^{N} x_i \tag{B.2}$$

The NMS algorithm consists of 5 basic moves, reflection (r), expansion (e), outside contraction (oc), inside contraction (ic), and, rarely, shrink. Each iteration uses one or more of these moves. The value of μ is based on which move is used according to Eq. (B.3) [104].

$$-1 < \mu_{ic} < 0 < \mu_{oc} < \mu_r < \mu_e \tag{B.3}$$

Typical values are $\{\mu_r, \mu_e, \mu_{oc}, \mu_{ic}\} = \{1,2,1/2,-1/2\}$[67]. The exit criteria is that either $f(x_{N+1}) - f(x_1) < \tau$ (the difference between the worst and best function evaluation in the simplex is less than a tolerance), where τ is a user defined convergence criterion, or the maximum number of iterations has been reached.

Once the initial simplex is generated, the objective function is evaluated at each vertex, x, and the worst vertex, x_{N+1}, is reflected through the centroid, to a new point, x_r. Figure B-1 shows an example in two dimensions [104].

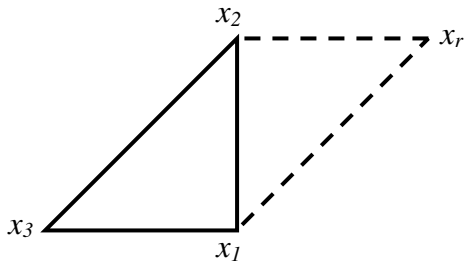

$$x_1 = \{1,0\}' \quad x_2 = \{1,1\}' \quad x_3 = \{0,0\}'$$

$$\bar{x} = \frac{1}{2}\left[\begin{Bmatrix}1\\0\end{Bmatrix} + \begin{Bmatrix}1\\1\end{Bmatrix}\right] = \left\{1, \frac{1}{2}\right\}'$$

$$x_r = (1+\mu_r)\bar{x} - \mu_r x_3, \; \mu_r = 1$$

$$x_r = 2\left\{1, \frac{1}{2}\right\}' - 1\{0,0\}' = \{2,1\}'$$

Figure B-1 Example of the reflection move in NMS.

If the best value of the function in the new simplex occurs at x_r, then an expansion move is made in the same direction to obtain the point x_e, as shown in Figure B-2. If $f(x_e)$ is less than $f(x_r)$, then the point x_{N+1} is replaced by x_e such that the worst point has been removed from the simplex. If $f(x_e)$ is greater than or equal to $f(x_r)$, then x_{N+1} is replaced by x_r. In either case, the vertices of the new simplex are sorted such that the vertex yielding the lowest function value is x_1 and the vertex yielding the highest function value is x_{N+1}. Assuming the exit criteria are not met, the next iteration begins with this new simplex.

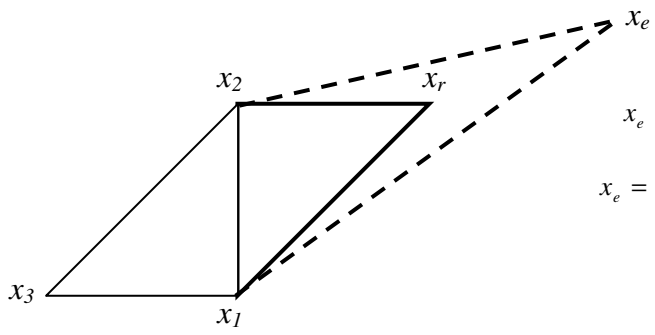

$$x_e = (1+\mu_e)\bar{x} - \mu_e x_3,\ \mu_e = 2$$

$$x_e = 3\left\{1, \frac{1}{2}\right\}' - 3\{0,0\}' = \left\{3, \frac{3}{2}\right\}'$$

Figure B-2 Example of the expansion move in NMS.

If x_r is neither the best nor worst point such that $f(x_1) \le f(x_r) < f(x_N)$, then x_{N+1} is replaced by x_r, the vertices of the simplex are sorted and the next iteration begins with this new simplex. If x_r is between the worst and second worst points such that $f(x_N) \le f(x_r) < f(x_{N+1})$ then the outside contraction (*oc*) move is made. If $f(x_{oc}) \le f(x_r)$ then x_{N+1} is replaced by x_{oc}, the vertices are re-ordered, and the next iteration begins with the new simplex.

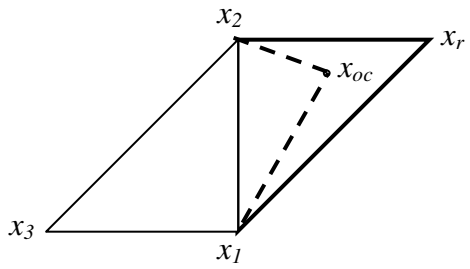

$$x_{oc} = (1+\mu_{oc})\bar{x} - \mu_{oc} x_3,\ \mu_{oc} = \frac{1}{2}$$

$$x_{oc} = \frac{3}{2}\left\{1, \frac{1}{2}\right\}' - \frac{1}{2}\{0,0\}' = \left\{\frac{3}{2}, \frac{3}{4}\right\}'$$

Figure B-3 Example of the outside contraction move in NMS.

If $f(x_r) \ge f(x_{N+1})$, meaning that x_r is the worst point, the inside contraction move is used. If $f(x_{ic}) < f(x_{N+1})$ x_{N+1} is replaced by x_{ic}, the vertices are sorted, and the next iteration begins with the new simplex.

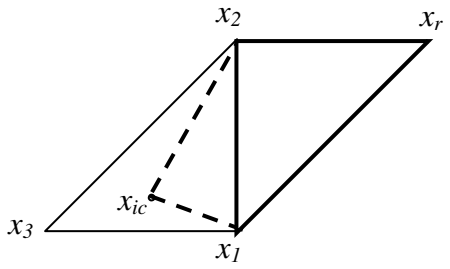

$$x_{ic} = (1+\mu_{ic})\,\bar{x} - \mu_{ic} x_3,\ \mu_{ic} = -\frac{1}{2}$$

$$x_{ic} = \frac{1}{2}\left\{1, \frac{1}{2}\right\}' + \frac{1}{2}\{0,0\}' = \left\{\frac{1}{2}, \frac{1}{4}\right\}'$$

Figure B-4 Example of the inside contraction move in NMS.

If $f(x_{oc}) > f(x_r)$ or $f(x_{ic}) \geq f(x_{N+1})$ the shrink move is used. In essence, all but the best vertex of the simplex from the beginning of the iteration is changed to form a new simplex. The variable μ_s determines how the variable changes.

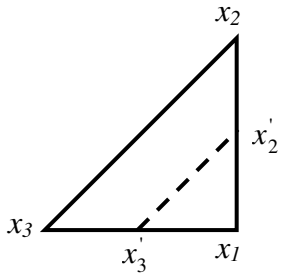

$$x_i = x_1 - \mu_s(x_i - x_1) \quad i = 2..N+1, \mu_s = \frac{1}{2}$$

$$x_2' = x_1 - \frac{x_2 - x_1}{2} = \left\{1, \frac{1}{2}\right\}'$$

$$x_3' = x_1 - \frac{x_3 - x_1}{2} = \left\{\frac{1}{2}, 0\right\}'$$

Figure B-5 Example of the shrink move in NMS.

A flowchart outlining these steps is given in Figure B-6. NMS has reached convergence when the maximum number of iterations has been reached or the difference between the best and worst function evaluations in the simplex is less than the specified tolerance, τ. NMS is not guaranteed to find a global minimum. If the values of the various μ are too large, the method can step over an optimal value. If the values are too small, the method can become bogged down, or stagnate, around a local or non-optimal solution [69].

According to Rowan [67], NMS has the following characteristics:

- Can be used on noisy functions
- Inefficient for $N > 5$

- Works poorly if infeasible points are rejected rather than using a penalty function
- $O(N^2)$ storage ($N+1$ vertices each of size N)

Rowan designed the SUBPLEX method to improve upon the NMS method. Several optimization techniques determine the optimum by defining an improved search direction for each iteration; the SUBPLEX method expands this concept by defining improved subspaces for each iteration and using NMS to search those subspaces. SUBPLEX adds four parameters to the five of NMS; all are listed in Table B-1.

Table B-1 List of SUBPLEX parameters and their values (Rowan).

Parameter	Description	Value	Recommended Value
μ_r	Reflection coefficient	$(0,\infty)$	1
μ_e	Expansion coefficient	$(1,\infty)$	2
μ_{oc}	Outside contraction coefficient	(0,1)	0.5
μ_{ic}	Inside contraction coefficient	(-1,0)	-0.5
μ_s	Shrinkage coefficient	(0,1)	0.5
ψ	Simplex reduction coefficient	(0,1)	0.25
ω	Step reduction coefficient	(0,1)	0.1
nsmin	Minimum number of subspace dimensions	[1,*nsmax*]	min(2,N)
nsmax	Maximum number of subspace dimensions	[*nsmin*,*N*]	min(5,N)

The simplex reduction coefficient, ψ, affects the accuracy of the subspace search and the step reduction coefficient, ω, determines how the step-size is scaled; *nsmin* and *nsmax* set the bounds on the subspace dimensions. The algorithm is composed of two loops, the outer loop in which the step size and subspaces are set, and the inner loop in which the NMS algorithm is used on each subspace. Rowan refers to an iteration of the outer loop as a cycle.

After the completion of each cycle and before proceeding to the inner loop, the SUBPLEX program must set the step size and orientation, the number of subspaces, the dimensions of each subspace, and the orientation of each subspace. The step is scaled based on

the progress in the prior cycle; this is shown in Eq. (B.4), where Δx is the separation between the vertices in successive iterates of the algorithm. If $\|\Delta x\|_1$ is large then significant progress has been made (e.g. a large region of the subspace has been searched) and the step size can be increased for computational efficiency. If little progress was made, such as when the contraction or shrink moves are used, the step size is reduced. A small value of ω will lead to rapid convergence, likely to a local minimum. A large value requires more computation time, but is more likely to find a global minimum. If there is only one subspace, then NMS has reduced the simplex by ψ and the step size is also reduced by ψ so that the next cycle will start with the same simplex that the prior cycle ended with.

$$\begin{aligned} &SCALE: \\ &step = \begin{cases} \min\left(\max\left(\frac{\|\Delta x\|_1}{\|step\|_1}, \omega \right), \frac{1}{\omega} \right) \bullet step & \#\ of\ subspaces > 1 \\ \psi \bullet step & \#\ of\ subspaces = 1 \end{cases} \\ &ORIENTATION: \\ &step_i = \begin{cases} sign(\Delta x_i) \bullet |step_i| & \Delta x_i \neq 0 \\ -step_i & \Delta x_i = 0 \end{cases} \end{aligned} \tag{B.4}$$

One of the disadvantages of NMS is that it is inefficient for problems with a large number of decision variables ($N > 5$). The SUBPLEX method combats this problem by creating several mutually orthogonal subspaces of small dimension that, when combined, consider all of the decision variables. For example, there may be a problem with five decision variables. The SUBPLEX method could divide this problem into a two dimensional subspace and a three dimensional subspace. In the 2D subspace, two of the five variables are optimized using NMS while the other three variables are held constant. Once the 2D subspace has reached the NMS

termination criterion, the "optimal" values of the first two variables are held constant and the 3D subspace is analyzed using NMS by varying the remaining three variables. Once this analysis meets the NMS termination criterion the solver exits the inner loop and, assuming the termination criterion for the outer loop has not been met, the step and subspaces are re-calculated and the NMS loop is executed as before.

The termination criterion for the inner (NMS) loop is based on the spacing of the vertices of the simplex. Once the simplex has been sufficiently reduced in size, as defined by the value of ψ, the inner loop terminates. Therefore, the smaller the value of ψ, the more accurate the optimization becomes. The termination criterion for the outer loop is based on Δx and the step size as shown in Eq. (B.5). The step size is included in this test because Δx can be small when the step size is large. This situation can occur, for example, if the step size is so large that it has stepped over the optimum and the contraction or shrink moves are used.

$$\frac{\max\left(\left\|\Delta x\right\|_{\infty}, \left\|step\right\|_{\infty} \bullet \psi\right)}{\max\left(\left\|\Delta x\right\|_{\infty}, 1\right)} \leq tol \tag{B.5}$$

Although the SUBPLEX method overcomes some of the limitations of NMS, it still has the limitation that global convergence is not guaranteed. In practice, the SUBPLEX method has been found to converge to different optima based on the value of the initial guess. Another limitation is that it is designed for unconstrained decision variables; therefore, bounds on the variables are not taken into account when the sample points are selected (they are enforced after the fact) and the search may be inefficient for constrained problems.

The original SUBPLEX method terminates when the simplex becomes small or when the maximum number of function evaluations has occurred. Two additional termination criteria were added to the method for FHyGSHP. In the one case, if the current best value of the function does

not change for a specified number of function evaluations, then the optimization process is terminated. In the other case, if the current best value of the function changes by a specified small amount, then the optimization process is terminated. These criteria are meant to prevent the program from spending significant time trying to find a modestly better solution.

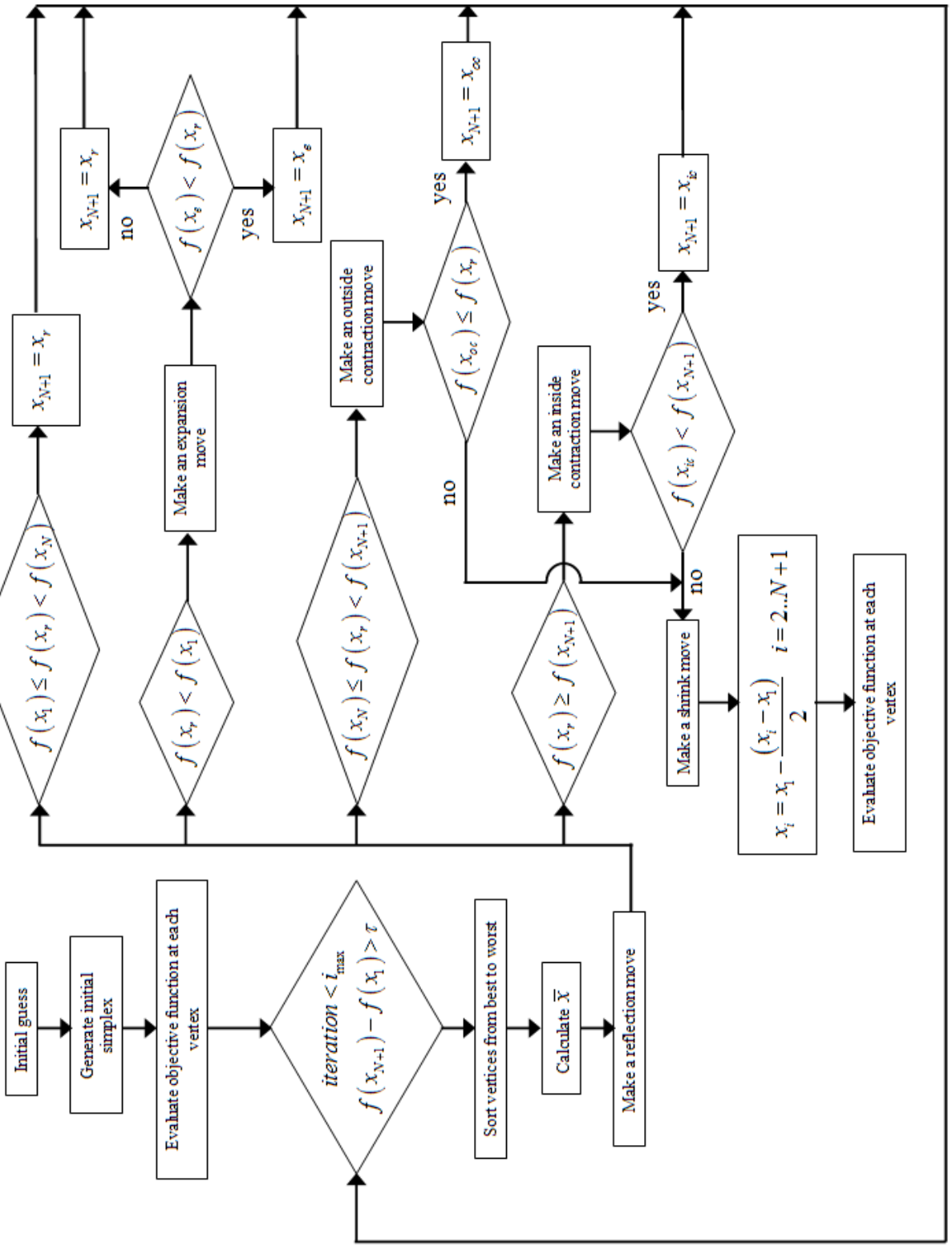

Figure B-6 Flowchart of the NMS method.

B.2 DIRECT Optimization Method

The SUBPLEX method is a practical direct search method, but there is no proof of convergence to a global solution and, in practice, SUBPLEX does not always find a global optimum, so an alternative optimization scheme was sought. The DIRECT scheme (DIviding RECTangles) is also a direct sampling method; the solution space, defined by the boundaries on the decision variables, is sampled in order to locate a global optimum. Finkel and Kelley [70] show that "certain subsequences of the sample points converge to points that satisfy the necessary conditions for optimality… DIRECT is, in the limit, an exhaustive search and will, if [the function] is continuous, find an arbitrarily accurate approximation to the global minimum." Global convergence is guaranteed in the limit, but in practice the optimization is stopped after a finite number of function evaluations, so care is still required to ensure that the optimal returned is satisfactorily close to the global optimum. The original and modified versions of the method are described in this section.

B.1.1 Original Formulation

The DIRECT method was first proposed by Jones, et al. [68] as an improvement on Lipschitzian approaches to global optimization, which require knowledge of the Lipschitz constant, *L*. *L* is the maximum rate of change of the objective function as defined in Eq. (B.6).

$$L = \max_{(u,t)\in D} \left| f_u(u,t) \right| \tag{B.6}$$

The value of *L* is frequently unknown and would have to be estimated for the optimization process. The *estimated* value, $\tilde{K}$, becomes a trade off between finding a local and global optimum; if the constant is large, encompassing the unknown value of *L*, then global convergence is guaranteed but it will require significant computation time. If the constant is smaller an optimal value may be found more quickly, but it may also be a local optimum. The

DIRECT method removes the necessity to know or estimate *L* by defining a value in situ. The search begins by looking at the entire hypercube defined by the bounds on the decision variables and eventually focusing down to the region containing the global optimum.

The easiest way to understand the DIRECT method is to first present the concept in 1D and then expand to a more detailed 2D example. Consider an objective function with one decision variable that has an upper and lower bound. These bounds form an interval over which the minimum value of the objective function is to be found. The DIRECT method divides this initial interval into three intervals and determines the value of the objective function at the center of each interval. This is the first or initial iteration of the algorithm (see Figure B-7).

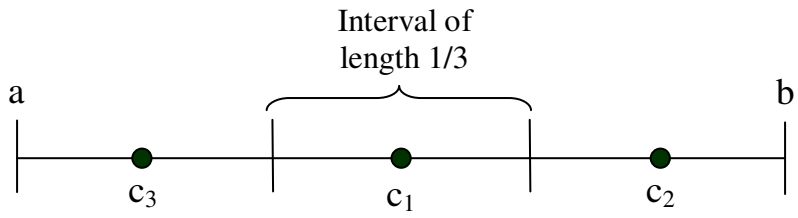

Figure B-7 Initial division into equal intervals.

The next step is to decide how to further divide the intervals in order to efficiently approach the minimum value. This is where the idea of *L* is used. If *L* were known, then the interval containing the minimum value of Eq. (B.7) would be selected for division. But *L* is unknown for this problem.

$$\begin{matrix} f(c) - Ll \\ l = \text{interval length} = \dfrac{b-a}{2} \end{matrix} \qquad \text{(B.7)}$$

Figure B-8 represents a plot of the value of the objective function, *f(c),* at the center of each of 10 intervals plotted against the size of the interval; note that some intervals have the same length. The convex hull of a function is the smallest convex set that encloses all points in

the function; in this figure, the two line segments are the convex hull. All of the function values are above this line (convex) and three of the points are on the line (smallest convex set). The reason this is significant is that the slope of each line segment is an estimate of *L*. The points on the line are potentially optimal since they are minima of Eq. (B.7) for a given interval length. Those intervals will be further subdivided in the next iteration.

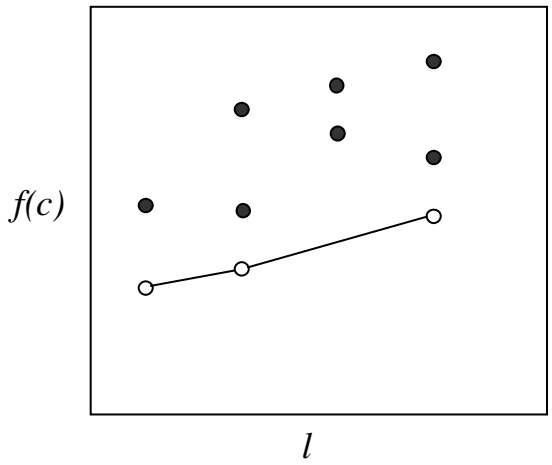

Figure B-8 Value of the function at the center point of each of 9 intervals.

The following example steps through the initial iterations of the DIRECT method as applied to the quadratic function in Eq. (B.8) [71], thereby extending the 1D concept to a more typical 2D problem.

$$f(x) = 10 + (x_1 - 5.3)^2 + (x_2 - 5.3)^2, \quad \Omega = [0,10]^N \tag{B.8}$$

The optimal point is $x^* = (5.3, 5.3)^T$ and the optimal function value is $f^* = 10$. The initial solution space includes all potential values of x_1 and x_2 and so extends from 0 to 10 in both directions as shown in Figure B-9. For this 2D problem the solution space is a square, but in general it is an n-dimensional hypercube. The initial interval contains just the center point of the hypercube, point 1, and is the entire square rather than just a line as in the 1D example. As in the

1D case, the interval is split into thirds in each direction; in this case, points 2 and 3 are sampled in the x_1 direction and points 4 and 5 are sampled in the x_2 direction. If there were more dimensions, two additional points would be sampled in each additional dimension.

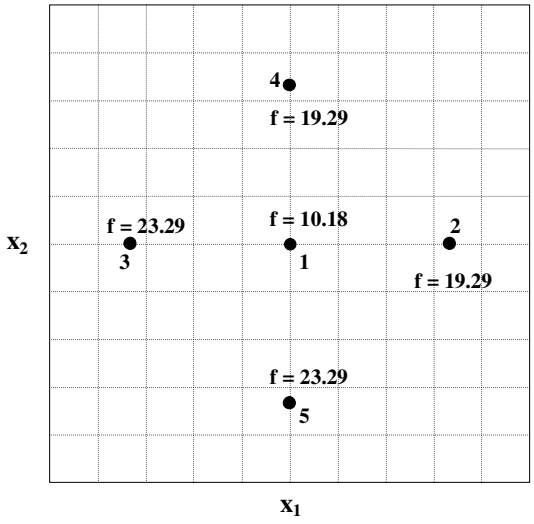

Figure B-9 Initial grid for the solution to the quadratic problem.

The first iteration contains the five function evaluations shown in Figure B-9, but the question remains as to what the intervals look like. The hypercube needs to be divided into hyper-rectangles that represent the five intervals of the first iteration. The division rules are fairly simple: the division is always in thirds along the longest side of the hyper-rectangle in order to ensure that the longest dimension will decrease; the order of the division in each dimension is determined from Eq. (B.9), where i is the dimension, c is the center point of the hypercube, δ is 1/3 of the side length of the cube and e_i is a unit vector defining the direction.

$$w_i = \min\left\{ f\left(c + \delta e_i\right), f\left(c - \delta e_i\right)\right\} \tag{B.9}$$

Eq. (B.10) shows the analysis for the current example.

$$w_1 = \min\{f(2), f(3)\} = 19.29$$
$$w_2 = \min\{f(4), f(5)\} = 19.29 \quad \text{(B.10)}$$

The first division occurs in the direction perpendicular to the minimum value of *w* and then division is perpendicular to the direction of the next smallest value of *w* until division has occurred in all dimensions. In this case, the values are equal, so division is first perpendicular to x_1 and then perpendicular to x_2. The division is shown in Figure B-10.

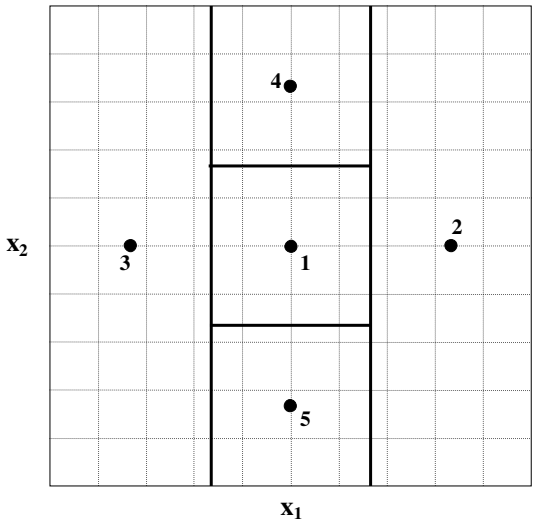

Figure B-10 Initial sub-division of the hyper-cube into hyper-rectangles.

The next step is to determine which of these hyper-rectangles to divide in the next iteration. Potentially optimal hyper-rectangles are defined by Eq. (B.11), where $\tilde{K} > 0$ (estimate of *L*), *d* is the dimension of the hyper-rectangle, *c* is the center of the hyper-rectangle, f_{min} is the current best function value, and ε is a constant. The algorithm is relatively insensitive to the value of ε in the range of 10^{-3} to 10^{-7}, so a value of 10^{-4} is used [68].

$$f(c_j) - \tilde{K}d_j \le f(c_i) - \tilde{K}d_i, \forall i, \text{and}$$
$$f(c_j) - \tilde{K}d_j \le f_{\min} - \varepsilon|f_{\min}| \quad \text{(B.11)}$$

The first of these two conditions is tested in two loops, where hyper-rectangle *j* is compared to each hyper-rectangle *i* to determine if the first condition in Eq. (B.11) is satisfied. The minimum found in Eq. (B.12) and the maximum found in Eq. (B.13) generate bounds on the value of $\tilde{K}$. If $\tilde{K}_{\min}$ is greater than or equal to $\tilde{K}_{\max}$ the first condition is satisfied.

$$\tilde{K}_{\min} = \min_{i \in I_2} \frac{f(c_i) - f(c_j)}{d_i - d_j}, \quad I_1 = \{ i \in I : d_i > d_j \} \tag{B.12}$$

$$\tilde{K}_{\max} = \max_{i \in I_1} \frac{f(c_j) - f(c_i)}{d_j - d_i}, \quad I_1 = \{ i \in I : d_i < d_j \} \tag{B.13}$$

If the first condition is satisfied, then the second condition is checked by setting $\tilde{K}$ equal to $\tilde{K}_{\min}$. If this condition is also met, then the hyper-rectangle *j* is potentially optimal. For the example here, hyper-rectangles 1 and 2 are potentially optimal and are subdivided using the division rules already discussed, resulting in Figure B-11.

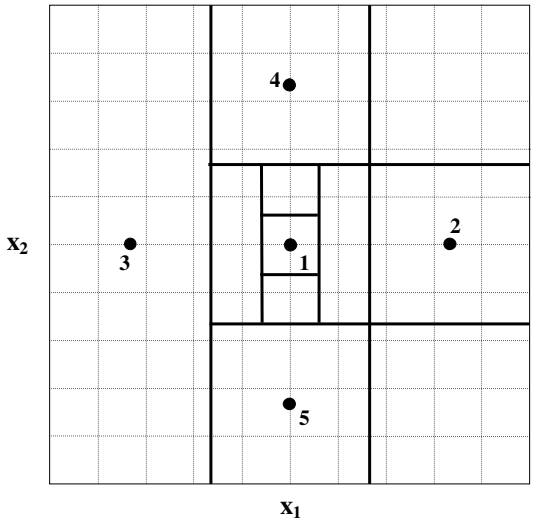

Figure B-11 Subdivision of potentially optimal hyper-rectangles.

The function evaluations of the second iteration are shown in Figure B-12. As in the first iteration, division occurs first perpendicular to x_1 and then perpendicular to x_2. The potentially optimal hyper-rectangles after this iteration are 1, 3, and 8.

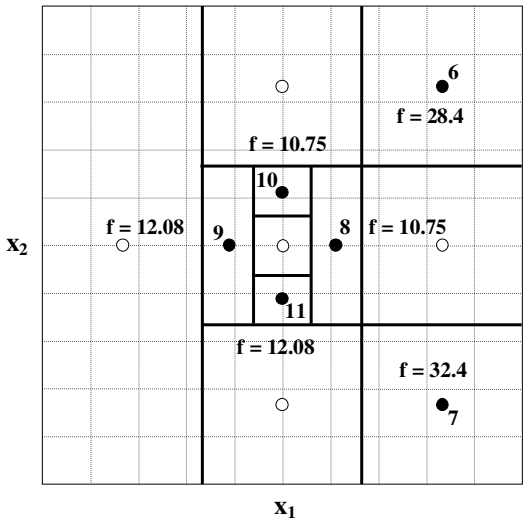

Figure B-12 Results of the second iteration.

The hyper-rectangles in the third iteration are shown in Figure B-13; function values and point labels have been removed for clarity. It is clear that the optimization is starting to narrow in on the optimal point of $x^* = (5.3, 5.3)^T$, but additional iterations are required in order to meet the termination criterion.

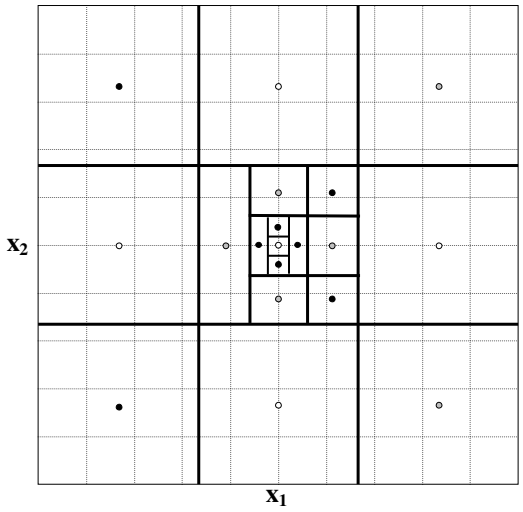

Figure B-13 Results of the third iteration.

B.1.2 Modified DIRECT method

Gablonsky, et al. [71], made two modifications to the original DIRECT algorithm. In the original version, the dimension of the hyper-rectangle, *d*, is the distance from the center of the hyper-rectangle to a vertex, but the modified version uses the longest side of the hyper-rectangle. Thinking back to the 1D concept, the hyper-rectangles are grouped by *d* (instead of *l*); the modified version will lead to fewer groupings and save some computational effort. In the original version of the code, if more than one hyper-rectangle has dimension *d* (recall Figure B-8), multiple hyper-rectangles could be divided, but in the modified version only one of the hyper-rectangles in a group can be divided for the next iteration. Both of these modifications lead to a more locally biased search because fewer hyper-rectangles are analyzed, but the algorithm is more efficient and generally still finds the global optimum.

Several additional modifications have been made to the DIRECT program based on observation of how the method behaves when used with this specific problem. The greatest limitation of the DIRECT method is speed; because the method considers the entire solution space, there can be a significant number of function evaluations. If the maximum number of function evaluations is set low so that the program will terminate early, the run time can be

reduced but the global optimum may not be found. Based on observation of how the program behaves with this function, a restart option has been added. If the best function value improves for a specified number of iterations, then the program restarts with different boundaries on the GHX length and CT size variables. The new boundaries are defined by a multiplier on the current best point which defines a lower and upper boundary (which must still be contained within the original boundaries). In this way the solution space is reduced and the optimal value can be found more quickly. This method, however, is not foolproof; it is possible to reduce the size of the solution space too quickly and thereby miss the global optimum.

Another modification is the addition of a limit on the number of iterations that the current best function value can be repeated before the program exits. This is the same as the first modification to the SUBPLEX method and is used to prevent the program from spending an inordinate amount of time finding a slightly better optimum.

Appendix C Running FHyGSHP in Batch Mode

There may be times when the user of FHyGSHP wishes to run several simulations with different settings without having to manually press run for each new simulation; for example, a batch run could be set up to run several different simulations over night or over the weekend. This chapter presents a script written in Python (http://python.org/) that can be used to operate in batch mode. Other scripting languages could be used, but this script provides the basic methodology. More information about FHyGSHP is found in Chapter 7.

In the standard operation of FHyGSHP, the graphical user interface (GUI) is used to enter the system parameters and simulation settings for the current simulation. For example, the user can select a configuration, weather/load file, ground heat exchanger design information, etc. When *run* is selected, most of the values entered into the GUI are written to namelist files located in the *namelist_files* directory; the *load file* and the *directory for writing data* are written to the *loadfilename.txt* file in the *Building Loads* directory. These files are read by the executable program.

When running multiple simulations in batch mode, the first step is to determine which inputs to vary; the full list of inputs to the program is in Appendix D. As an example, consider a study of different system configurations in a single location. For this study, the *directory for writing data* is different for each run. The configuration is controlled by several variables: *conv*, *strat*, and *downstream*. For a conventional system configuration, *conv* has a value of 1; for all other systems it has a value of 0. The control strategy is determined by *strat* and can have the following values:

- 3 – hybrid control
- 5 – pre-cooling (PC)

- 7 – hybrid control with PC
- 8 – hybrid control with PC after 4 am
- 10 – hybrid control, set points only
- 13 – hybrid control with PC, set points only
- 0 – ground source heat pump

For a cooling tower (CT) hybrid the placement of the CT relative to the ground heat exchanger (GHX) is determined by the value of *downstream*; the CT is downstream of the GHX if the value is 1 and upstream of the GHX if the value is 0.

The variable for the *directory for writing data* is *dirname*, so the variables that need to be changed are *dirname*, *conv*, *strat*, and *downstream*. *Dirname* is found in *loadfilename.txt* in the *Building Loads* directory and the remaining variables are in *op_set.txt* in the *namelist_files* directory. The GUI is used to generate these files and then template files are created and saved in the same directory (the program is hard-coded to look in the *namelist_files* and *Building Loads* directories). Figure C-1 shows *loadfilename.txt* as written by the GUI and Figure C-2 shows a portion of *op_set.txt* as written by the GUI. Figure C-3 and Figure C-4 show the template version of each of these files, respectively. The difference between the nominal and template files is that the numerical value of the variables that are going to be changed by the Python script are replaced by the variable name:

- E:\Research\GUI\program_files\results → $dirname$
- strat = 3 → strat = $strat$
- downstream = 0 → downstream = $downstream$
- conv = 0 → conv = $conv$

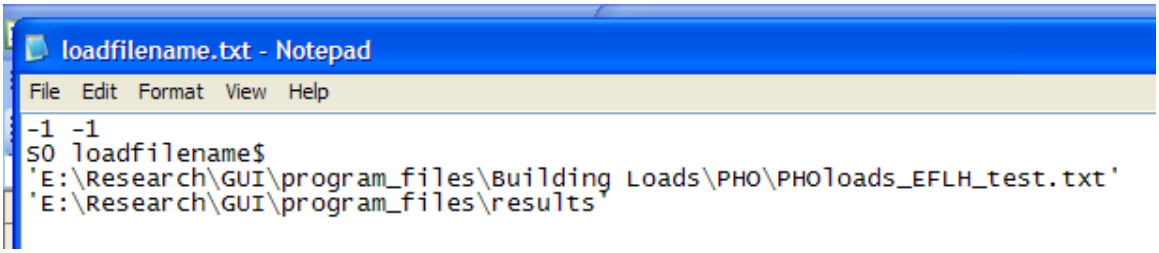

Figure C-1 Contents of *loadfilename.txt*.

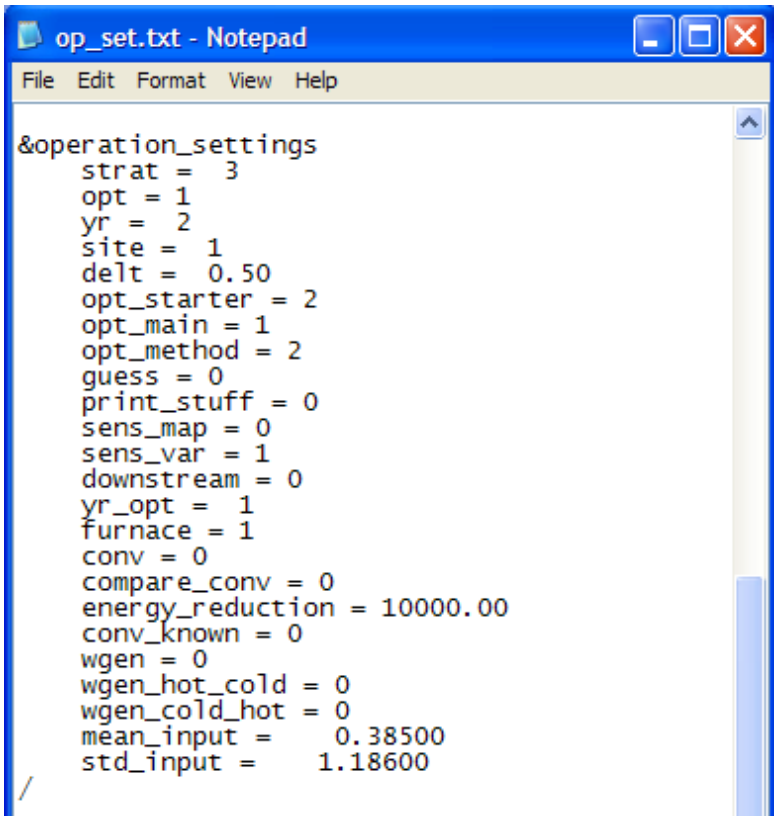

Figure C-2 The *operation_settings* section of *op_set.txt*.

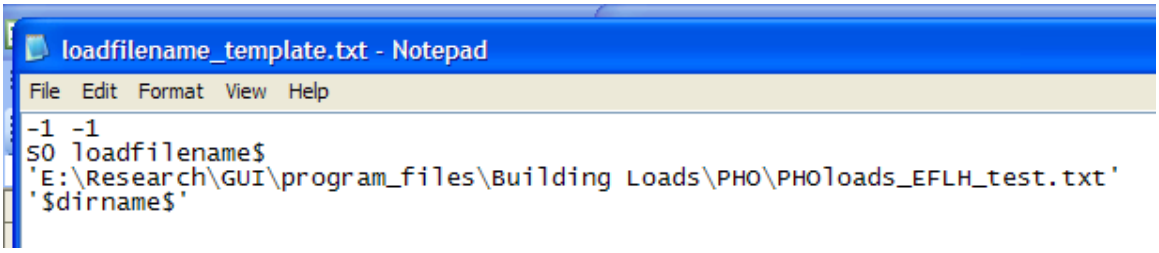

Figure C-3 Contents of *loadfilename_template.txt*.

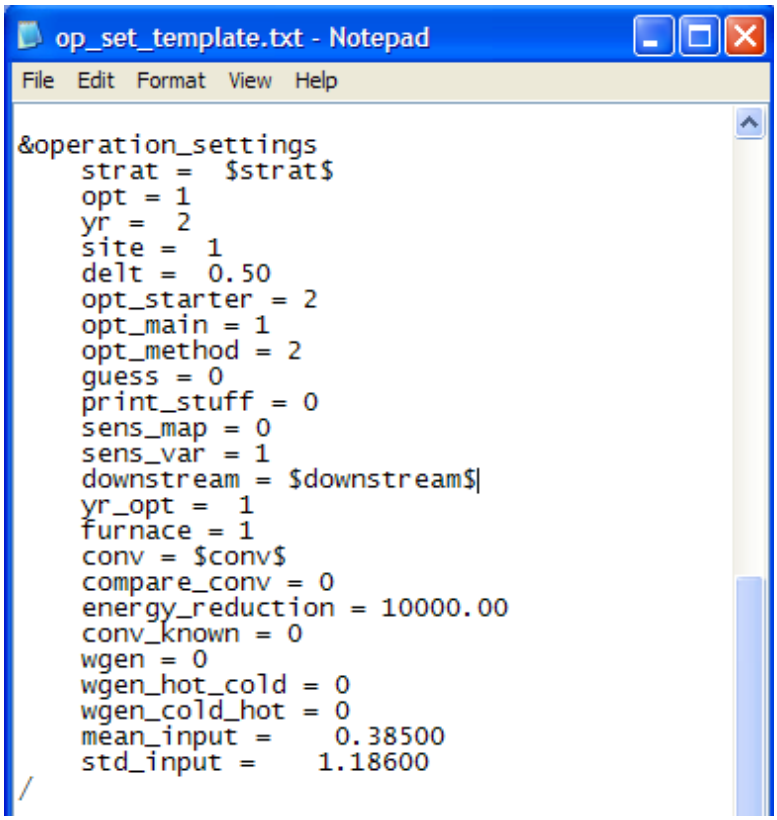

Figure C-4 The *operation_settings* section of *op_set_template.txt*.

The Python code for completing this configuration study is below. Program comments are preceded by #.

```
################################################################################
#Import various standard libraries that are required for the code#
################################################################################
from __future__ import division        # remove this line if using Python 3
from __future__ import print_function  # remove this line if using Python 3

# Import necessary modules.
import sys
import subprocess
import itertools
import os
import shutil
from collections import OrderedDict

# Initialize a few variables.
var_values  = OrderedDict({})
var_count   = {}  # not used yet...

############################
##### BEGIN USER INPUT ####
############################
```

```
##########################################################################
#Define the template files and the name of the file that will be generated from the template file#
##########################################################################

# Specify the template file to read and the name of the new file to write.
# If 'save_new_files' is False, new_file is overwritten each time.
# If 'save_new_files' is True, the set of inputs are appended to the file name for each run
# (this results in a lot of files being generated).
maindir ='C:\FHyGSHP'
template_file  =  ' '.join([maindir, '\Building Loads\loadfilename_template.txt'])
new_file       = ' '.join([maindir, '\Building Loads\loadfilename.txt'])
template_file2  = ' '.join([maindir, '\\namelist_files\op_set_template.txt'])
new_file2       = ' '.join([maindir, '\\namelist_files\op_set.txt'])
save_new_files = False

# Specify the command to run after generating the new file.
command = [' '.join([maindir, '\program_main\program_main\hygshp.exe'])]  # use a list rather than spaces

##########################################################################
#List the value of the variable that is to be changed for each simulation
#The values are stored in the matrix var_values in the order dirname, strat, downstream, #and conv
#var_values['set1'] contains the four values for the first simulation run
##########################################################################

# Define the tokens to replace and their values (the first token that is set varies the slowest,
#the last token varies the fastest).
#These are dictionary pairs: the key is on the left hand side (i.e. $filename$) while
#the value associated with that key is on the right hand side (i.e. name of the file)
#order: $dirname$,$strat$,$downstream$,$conv$
var_values['set1'] = ['C:\FHyGSHP\\results\PHO\conventional',3,0,1]
var_values['set2'] = ['C:\FHyGSHP\\results\PHO\GSHP',0,0,0]
var_values['set3'] = ['C:\FHyGSHP\\results\PHO\CT_hybrid_upstream', 3,0,0]
var_values['set4'] = ['C:\FHyGSHP\\results\PHO\CT_hybrid_upstream', 3,1,0]

#########################
##### END USER INPUT ####
#########################

##########################################################################
#The src files will be copied to the directory specified by dirname after the simulation is #complete
##########################################################################

src1 = ' '.join([maindir, '\\namelist_files\component_inputs.txt'])
src2 = ' '.join([maindir, '\\namelist_files\direct_optim.txt'])
src3 = ' '.join([maindir, '\\namelist_files\op_set.txt'])
src4 = ' '.join([maindir, '\\namelist_files\optim_settings.txt'])

##########################################################################
```

#This is the main body of the code; this loop will iterate over the size of var_values (i.e. #set1, set2, set3, set4.
#The template file is read and a new file (such as op_set.txt) is written. Then, the variable #names (such as $strat$) are replaced by the values in var_values. Finally, the executable #program is called. Once the run is complete, the next simulation is started.
#filename is the name and location of the building load file
##

```
for entry in var_values:
    dirname = var_values[entry][0]
    strat = var_values[entry][1]
    downstream = var_values[entry][2]
    conv = var_values[entry][3]

# Open the template file for reading.
    with open(template_file, 'r') as f_template:

        # Generate a new new_file name if required.
        if save_new_files:
            inputs_as_string = '_'.join([str(val).replace('.','p') for val in inputs])  # join the input values with '_' and
                                                                                          replace '.' with 'p'
            split_name = new_file.split('.')                                  # split the new_file name at all '.'s
            split_name[0] = split_name[0] + '_' + inputs_as_string            # combine the first part of the new_file name with
                                                                                the inputs
            new_file_name = '.'.join(split_name)                              # put the new_file name back together
        else:
            new_file_name = new_file                          # new_file will be overwritten with each new set of inputs
            new_file_name2 = new_file2                         # new_file will be overwritten with each new set of inputs

        with open(new_file_name, 'w') as f_new:

            # Loop over the lines in the template file and write each to the new file.
            for line in f_template:
                new_line = line
                new_line = new_line.replace('$dirname$',dirname)          # replace token in line with value
                f_new.write(new_line)
            f_new.close()

    with open(template_file2, 'r') as f_template2:
        with open(new_file_name2, 'w') as f_new:

            for line in f_template2:
                new_line = line
                new_line = new_line.replace('$strat$',str(strat))         # replace token in line with value
                new_line = new_line.replace('$downstream$',str(downstream))           # replace token in line with value
                new_line = new_line.replace('$conv$',str(conv))       # replace token in line with value
                f_new.write(new_line)
            f_new.close()

            # Run a program from the command line.
            print("Running '{0}'...".format(' '.join(command)), end=' ')         # display the program being run
            sys.stdout.flush()                                  # this is sometimes necessary to see output from the line above
            fortran_prog = subprocess.Popen(command)                          # start the command line program
            fortran_prog.wait()
```

```
        print(' finished.')

        # Copy the src files to the specified directory
        shutil.copy(src1, dirname)
        shutil.copy(src2, dirname)
        shutil.copy(src3, dirname)
        shutil.copy(src4, dirname)
        shutil.copy(filename, dirname)

print('\n\nBatch Run Complete\n')
```

Appendix D Definition of FHyGSHP Inputs and Outputs

D.1 Inputs: Namelist Files

The following tables list the inputs to the program that are written to files that are read by the executable program using the FORTRAN *namelist* command. The inputs are written by the GUI into one of four files located in the *namelist_files* directory: *op_set.txt*, *component_inputs.txt*, *optim_settings.txt*, and *direct_optim.txt*. Each table lists the inputs contained in one of these four files; the headings within each table indicate the section within the file that contains the inputs, which are usually related to the heading in some way (for example, "COP" is located under the heading "heat pumps"). When an input is obsolete it is marked as unused.

Table D-1 Inputs contained in *op_set.txt*.

Label	Default Value	Units	Definition
heat pumps			
slopeh	0.02251	1/°C	Slope of the line used to adjust the heating heat pump capacity to the entering fluid temperature
inth	1		Intercept of the line used to adjust the heating heat pump capacity to the entering fluid temperature
slopec	-0.00856	1/°C	Slope of the line used to adjust the cooling heat pump capacity to the entering fluid temperature
intc	1.213		Intercept of the line used to adjust the cooling heat pump capacity to the entering fluid temperature
slopeh_cop	0.01437	1/°C	Slope of the line used to adjust the heating heat pump COP to the entering fluid temperature
inth_cop	1		Intercept of the line used to adjust the heating heat pump COP to the entering fluid temperature
slopec_cop	-0.02521	1/°C	Slope of the line used to adjust the cooling heat pump COP to the entering fluid temperature
intc_cop	1.63		Intercept of the line used to adjust the cooling heat pump COP to the entering fluid temperature
Frac_OA	0		Fraction of the heat pump air that is drawn from the outdoors
P_AIR_OA	1	atm	Air pressure
FRAC_POW_C	1		Multiplier to adjust the catalog value of the power consumption of the cooling heat pump
FRAC_CAP_C	1		Multiplier to adjust the catalog value of the capacity of the cooling heat pump
FRAC_CAP_H	1		Multiplier to adjust the catalog value of the power consumption of the heating heat pump
FRAC_POW_H	1		Multiplier to adjust the catalog value of the capacity of the heating heat pump

Label	Default Value	Units	Definition
Per_PG	25.3065	%	Percent of the working fluid that is propylene glycol
mode	2		unused
DP_AIR_OAi	0	atm	Pressure drop of the outdoor air across the damper
cop_c	4.57		Nominal COP of the cooling heat pump
cop_h	3.42		Nominal COP of the heating heat pump
RH_AIR_RET	0.42		Relative humidity of the air in the building
P_AIR_RET	1	atm	Pressure of the air in the building
DP_AIR_RET	0	atm	Pressure drop of the air in the building across the damper
w_AIR_RET	0.008	kg water vapor/kg dry air	Humidity ratio of the air in the building
T_DHW_IN	40		unused
P_AIR_IN	1		unused
DP_AIR_OA	0		unused
Flow_fluid	1000		unused
CONTPOW	36	kJ/hr	Power consumption of the heat pump controller
LOAD_MODE	1		unused
FlowMode	0		unused
operation settings			
strat	3		Control strategy: 3 - hybrid control 5 - PC control of the CT 7 - hybrid control with PC 8 - hybrid control with PC after 4 am 10 - hybrid control, set points only 13 - hybrid control with PC, set points only
opt	1		0 - single simulation, 1 - optimization
yr	5	years	Simulation duration
site	1		unused
delt	0.5	hour	time step size (0.25, 0.5, 0.75, or 1 hour)
opt_starter	2		Optimization algorithm for the starter (first stage) optimization if necessary: 1 - SUBPLEX 2 - DIRECT
opt_main	1		Optimization algorithm for the main (second stage) optimization if necessary: 1 - SUBPLEX 2 - DIRECT
opt_method	2		Optimization method: 1 - Nominal (use one of the algorithms) 2 - Starter (use coarse first stage optimization and a finer second stage optimization) 3 - Mix (first stage optimization using DIRECT and second stage optimization using SUBPLEX)
guess	0		0 - Use ASHRAE sizing method, 1 - Use user input guess values
print_stuff	0		unused
sens_map	0		0 - Do not create a sensitivity map, 1 - Create a sensitivity map
sens_var	1		Select the variable whose sensitivity will be evaluated:

Label	Default Value	Units	Definition
			1 - GHX length
			2 - CT size
			3 - CT2
			4 - CT1
			5 - GHX1
			6 - TPC
			7 - DTPC
			8 - Furnace
downstream	0		0 - CT upstream of the GHX, 1 - CT downstream of the GHX
yr_opt	1	years	Number of years of the first stage (or starter) optimization
furnace	1		0 - no furnace in the system, 1 - include a furnace
conv	0		0 - do not simulate a conventional system, 1 - simulate a conventional system
compare_conv	0		0 - do not compare to a conventional system, 1 - compare to a conventional system
energy_reduction	10000		Ratio of the energy of the system relative to a conventional system; values less than 1 require the non-conventional system to be more energy efficient.
conv_known	0		0 - conventional system design unknown, 1 - conventional system design known
wgen	0		0 - use just the input load/weather data, 1 - generate synthetic load/weather data
wgen_hot_cold	0		0 - use default load/weather data (whether input or synthetic), 1 - order the default data from hottest to coldest year
wgen_cold_hot	0		0 - use default load/weather data (whether input or synthetic), 1 - order the default data from coldest to hottest year
mean_input	0.385		Mean of the logistic fit for generating synthetic data
std_input	1.186		Standard deviation of the logistic fit for generating synthetic data
opt_zero_design_conv			
totallength	0		unused
size_tower	826	kW	Guess or known CT size for a conventional system
CT1	7.7	°C	Guess or known CT1 set point for a conventional system
CT2	0	°C	Guess or known CT2 set point for a conventional system
GHX1	0		unused
tpc	0		unused
dtpc	0		unused
Qset_ratio	1		unused
opt_zero_design_hybrid			
totallength	5353	m	Guess or known GHX length for a GSHP or CT Hybrid system
size_tower	875	kW	Guess or known CT size for a CT Hybrid system
CT1	4.1	°C	Guess or known CT1 set point for a CT Hybrid system
CT2	31.8	°C	Guess or known CT2 set point for a CT Hybrid system

Label	Default Value	Units	Definition
GHX1	-1.5	°C	Guess or known GHX1 set point for a GSHP or CT Hybrid system
tpc	0	°C	Guess or known TPC set point for a CT Hybrid system
dtpc	0	°C	Guess or known DTPC set point for a CT Hybrid system
Qset_ratio	0.9655		Guess or know ratio of furnace capacity to peak heating load for a GSHP or CT Hybrid system with a furnace
CT (cooling tower)			
MODE_AIR	2		unused
EWT_IN_DESIGN	39.25	°C	Design inlet fluid temperature
EWT_OUT_DESIGN	34.25	°C	Design outlet fluid temperature
T_AIR_DESIGN	35	°C	Design dry bulb air temperature
T_WB_DESIGN	25	°C	Design wet bulb air temperature
P_air_design	1	atm	Design air pressure
N_COEFFS	4		Number of coefficients for calculating the CT fan speed power consumption using the relationship: $\dot{P}_{fan} = \dot{P}_{fan,rated}\left[a_0 + a_1\gamma + a_2\gamma^2 + a_3\gamma^3 + \ldots\right]$
Y(1)	0		a_0
Y(2)	0		a_1
Y(3)	0		a_2
Y(4)	1		a_3
dst_params (ground heat exchanger model)			
DEPTH	1.8	m	Borehole header depth
R0	0.057	m	Borehole radius
DPIPES	0.038	m	Center to center half distance between u-tube legs
Rpo	0.0167	m	Outside radius of the u-tube pipe
Rpi	0.01372	m	Inside radius of the u-tube pipe
Lb	1.385	W/m-K	Grout thermal conductivity
Lpipe	0.42	W/m-K	Thermal conductivity of the u-tube pipe
Lgap	0.52	W/m-K	Thermal conductivity of the air gap between the u-tube pipe and grout
NPIPES	-1		Negative of u-tubes per borehole, do not change
Gap	0	m	Size of the gap between the u-tube and the grout
Tref	30	°C	Reference temperature
Par21	-1		unused
ISO	2		Insulation indicator: 1 - insulation on the top of the storage volume that covers a fraction of the storage height defined by FRISO 2 - insulation on the top of the storage volume that extends beyond the boundary of the storage volume by the fraction FRISO
FRISO	0		Insulation height fraction
THISO	0	m	Insulation thickness
RISLAM	0.029	W/m-K	Thermal conductivity of the insulation
TIMO3	25	years	Number of simulation years
TSTMAX	100	°C	Maximum storage temperature
TGRAD	0		Initial thermal gradient

Label	Default Value	Units	Definition
IPRE	0	years	Number of pre-heating years
TCMAX	13.333	°C	Maximum pre-heating temperature
TCMIN	13.333	°C	Minimum pre-heating temperature
TCPH	0	day	Pre-heat phase delay
TAIRM	13.333	°C	Average air temperature
ATAIR	9	°C	Amplitude of the air temperature
TAPH	2764800	day	Air temperature phase delay
ILAY	1		Number of layers in the ground, do not change
LFPRT	0		unused
LPRT	0		unused

Table D-2 Inputs contained in *component_inputs.txt*.

Label	Default Value	Units	Definition
CT (cooling tower)			
MULT_CTFANP	0.75		Cooling tower fan power multiplier
MULT_CTFANFL	0.61		Cooling tower fan air flow multiplier
MULT_CTFLUIDFL	0.96		Cooling tower flow multiplier
Lo_SPD_PC	1		Fan speed for pre-cooling
spd1	1		High fan speed (used with single and two speed control)
spd2	1		Low fan speed (used with two speed control)
nspeeds	10		1 - singe speed operation, 2 - two speed operation, 10 - continuous fan speed operation
HP (heat pumps)			
Continuous	1		0 - the heat pump fan only operates when there is a load, 1 - the heat pump fan operates whenever the building is occupied
t_air_ret_c	24	°C	Temperature of the air in the room during the cooling season (May through Sept.)
t_air_ret_h	21	°C	Temperature of the air in the room during the heating season (Oct. through April)
TMIN_GHP	1.7	°C	Minimum allowable temperature of the fluid entering the heat pump
TMAX_GHP	35	°C	Maximum allowable temperature of the fluid entering the heat pump
LPS_TOT	1500		unused
blowpow	671.1	kJ/hr	Power consumption of the blower in the heat pump
DST (ground heat exchanger model)			
MaxDrillDepth	91.4	m	Maximum depth of the borehole
SpacingBores	6.1	m	Center to center borehole spacing
K_g_W	2.423	W/m-K	Ground thermal conducivity
c_g_kJm3K(1)	2093	kJ/m^3-K	Volumetric heat capacity
tground	19.4	°C	Undisturbed ground temperature
Fluid_props (working fluid properties)			
RHO_FLUID	1019.033	kg/m^3	Density of the working fluid, calculated
cp_fluid	3.916416	kJ/kg-K	Specific heat of the working fluid, calculated
FLUID_TYPE	2		1 - water, 2 - propylene glycol

Label	Default Value	Units	Definition
Iso_Loop	0		unused
Furnace_n			
eff_furnace	0.95		Efficiency of the furnace
Boiler_n			
htr_eff	0.65		unused
htr_UA	0.8		unused
Circulating pump			
PumpKWPer	5	W/10 ton	Pumping power per ton of peak cooling divided by 10
PdropPctGHX	0.55		Percentage of the pressure drop assumed to occur in the GHX
PD_TOT_MAX	1	atm	Maximum pressure drop
eff_pump	0.65		Total pump efficiency
eff_motor	0.8		unused
eff_motor2	0.9		Efficiency of the pump motor
Economics			
DISC_RATE	0.07		Discount rate
COMM	1		0 - not a commercial building, 1 - commercial building
LOAN_INT_RATE	0.06		Interest rate on the loan
DOWN_PAYMT	1		Amount of the down payment (1 = 100%)
REBATE	0		Rebate as a fraction of the intitial cost
years_loan	20	years	Number of years of the loan
TAX_RATE	0.35		Effective income tax rate
INFLATION	0.016		General inflation rate
SALVAGE_FRAC	0		Salvage value as a fraction of the initial cost
FUEL_INFL	0.016		Fuel inflation rate
PROP_TAX	0.03		Property tax rate
DEPR_LIFE	4.55	years	Depreciation life
YEARS_ANALYSIS	20	years	Years to consider in the economic analysis
peak_last	21	hour	End of the daily peak rate period (21 = 9 pm)
peak_first	10	hour	Start of the daily peak rate period
Summer_First	6	month	First month of summer
Summer_Last	9	month	Last month of summer
COST_PKkwh	0.094	$/kWh	Summer: peak electrical cost
COST_OFFPKkwh	0.063	$/kWh	Summer: off-peak electrical cost
Cost_kWh_OnW	0.081	$/kWh	Winter: peak electrical cost
Cost_kWh_OffW	0.05	$/kWh	Winter: off-peak electrical cost
COST_kW	4.22	$/kW	Summer: demand charge
Cost_kW_W	1	$/kW	Winter: demand charge
COST_KWR	1.05	$/kW	Ratchet charge
COST_GHXperM	36.1	$/m	Cost of GHX
COST_PGperM	0.82	$/m	Cost of propylene glycol
COST_WATperM3	0.35	$/m^3	Cost of water
MULT_FSTCLOSED	2.75		Multiplier on the first cost of the CT
FIRST_INCR_HP_PERTON	500	$/ton	First cost of the heat pump per ton of capacity
COST_IN_ANN	0	$	Annual cost of the heat pump equipment (accounts for maintenance, etc)
mode_lcc	2		unused
nalternatives	1		unused

Label	Default Value	Units	Definition
MAINT_PG	50	$	Maintenance cost associated with using propylene glycol
MAINT_CLOSED10I	290.5	$/10 tons	Maintenance cost of the cooling tower, scaled based on the CT size
MULT_MNTCLOSED	1.2		Multiplier on the maintenance cost for the cooling tower to adjust for other manufacturer
FIRST_CLOSED10I	4500	$/10 tons	First cost of the cooling tower, scaled based on the cooling tower size
load_pen_fact	100000	°C	Specifies how much the ground temperature can change over the life of the system; a large value indicates that this constraint is not applied to the problem
temp_pen_fact	1		unused
COST_gas	7.11E-06	$/kJ	Cost of natural gas

Table D-3 Inputs contained in *optim_settings.txt*.

Label	Default Value	Units	Definition
optimization_settings			
tol1_main	0.25		Tolerance on the main (aka second stage) optimization for the SUBPLEX method
tol1_starter	1		Tolerance on the starter (aka first stage) optimization for the SUBPLEX method
tol2	0.25		Tolerance on the main (aka second stage) optimization for the SUBPLEX method
tolfac	0.25		Tolerance on the main (aka second stage) optimization for the SUBPLEX method
nf1	2000		Maximum number or function evaluations in the optimization
nf2	2000		Maximum number or function evaluations in the optimization
nfinc	2000		Maximum number or function evaluations in the optimization
count_lim_main	15		Limit on the number of times the optimizer can return the same minimum function evaluation before quitting in the main (aka second stage optimization
count_lim_starter	15		Limit on the number of times the optimizer can return the same minimum function evaluation before quitting in the starter (aka first stage) optimization
dfmin_lim_main	1E-10		Limit on the difference between the minimum function evaluation before the optimizer quits in the main (aka second stage) optimization
dfmin_lim_starter	1E-07		Limit on the difference between the minimum function evaluation before the optimizer quits in the starter (aka first stage) optimization
optim_params			
alpha	1		Reflection coefficient for SUBPLEX optimization
beta	0.5		Contraction coefficient for SUBPLEX optimization
gamma	2		Expansion coefficient for SUBPLEX optimization
delta	0.5		Shrinkage coefficient for SUBPLEX optimization

Label	Default Value	Units	Definition
psi	0.25		Simplex reduction coefficient for SUBPLEX optimization
omega	0.1		Step reduction coefficient for SUBPLEX optimization
optimization_settings_1			
scales_in(1)	1400	m	Scale for the optimization of the GHX length
scales_in(2)	100	kW	Scale for the optimization of the CT size
scales_in(3)	5	°C	Scale for the optimization of CT1
scales_in(4)	5	°C	Scale for the optimization of CT2
scales_in(5)	5	°C	Scale for the optimization of GHX1
scales_in(6)	5	°C	Scale for the optimization of TPC
scales_in(7)	5	°C	Scale for theoptimization of DTPC
x_in_conv(1)	0	m	unused
x_in_conv(2)	1560	kW	Initial guess for the optimization of the CT size in a conventional system
x_in_conv(3)	0	°C	Initial guess for the optimization of CT1 in a conventional system
x_in_conv(4)	0	°C	Initial guess for the optimization of CT2 in a conventional system
x_in_conv(5)	0	°C	unused
x_in_conv(6)	0	°C	unused
x_in_conv(7)	0	°C	unused
lower_in(1)	100	m	Lower bound for the optimization of GHX length
lower_in(2)	30	kW	Lower bound for the optimization of CT size
lower_in(3)	-5	°C	Lower bound for the optimization of CT1
lower_in(4)	-2	°C	Lower bound for the optimization of CT2
lower_in(5)	-2	°C	Lower bound for the optimization of GHX1
lower_in(6)	-2	°C	Lower bound for the optimization of TPC
lower_in(7)	-5	°C	Lower bound for the optimization of DTPC
upper_in(1)	40000	m	Upper bound for the optimization of GHX length
upper_in(2)	10000	kW	Upper bound for the optimization of CT size
upper_in(3)	20	°C	Upper bound for the optimization of CT1
upper_in(4)	50	°C	Upper bound for the optimization of CT2
upper_in(5)	50	°C	Upper bound for the optimization of GHX1
upper_in(6)	50	°C	Upper bound for the optimization of TPC
upper_in(7)	20	°C	Upper bound for the optimization of DTPC
x_in_hybrid(1)	3926	m	Initial guess for the optimization of the GHX length in a CT Hybrid
x_in_hybrid(2)	1336	kW	Initial guess for the optimization of the CT size in a CT Hybrid
x_in_hybrid(3)	-0.8	°C	Initial guess for the optimization of CT1 in a CT Hybrid
x_in_hybrid(4)	44.2	°C	Initial guess for the optimization of CT2 in a CT Hybrid
x_in_hybrid(5)	16.5	°C	Initial guess for the optimization of GHX1 in a CT Hybrid
x_in_hybrid(6)	0	°C	Initial guess for the optimization of TPC in a CT Hybrid
x_in_hybrid(7)	0	°C	Initial guess for the optimization of DTPC in a CT Hybrid
x_in_hybrid(8)	1		Initial guess for the optimization of the furnace in a CT Hybrid

Table D-4 Inputs contained in *direct_optim.txt*.

Label	Default Value	Units	Definition
direct_optim			
DIReps	0.0001		Tolerance for the DIRECT method when selecting potentially optimal intervals; this value can be reduced if the optimization results are unsatisfactory.

Label	Default Value	Units	Definition
DIRmaxf	2000		Maximum number of function evaluations in the DIRECT method
DIRmaxT	200		Maximum number of iterations in the DIRECT method
DIRalg	1		0 - Use the original version of the DIRECT algorithm, 2 - Use the Gablonsky modification of the DIRECT algorithm
logfile	2		The unit number assigned to the logfile
fglobal	-1.00E+101		unused
fglper	0		unused
volper_main	0		Used in the DIRECT optimization to terminate the optimization if the volume of the hyperrectangle is reduced by the specified amount in the main (aka second stage) optimization
sigmaper_main	0		Used in the DIRECT optimization to terminate the optimization if the relevant dimension of the hyperrectangle is reduced by the specified amount in the main (aka second stage) optimization
term_fmin	0.000001		Limit on the difference between the minimum function evalaution before the optimizer quits
restart_lim	100		Maximum number of times the DIRECT optimization can restart
cont_starter	15		Limit on the number of times the optimizer can return the same minimum function evaluation before quitting in the main (aka second stage optimization
cont_main	15		Limit on the number of times the optimizer can return the same minimum function evaluation before quitting in the starter (aka first stage) optimization
nom_main	0		0 - Use the FHyGSHP modifications to the DIRECT method, 1 - Do not use the FHyGSHP modifications to the DIRECT method in the main (aka second stage) optimization
multiplier_l	0.1		Multiplier to set the lower bound on the GHX and CT size when the ASHRAE sizing method is used
multiplier_u	4		Multiplier to set the upper bound on the GHX and CT size when the ASHRAE sizing method is used
shrink_starter	2		Number of times the function evaluation can increase before the optimization boundaries are reset in the starter (aka first stage) optimization
volper_starter	0		Used in the DIRECT optimization to terminate the optimization if the volume of the hyperrectangle is reduced by the specified amount in the starter (aka first stage) optimization
sigmaper_starter	0		Used in the DIRECT optimization to terminate the optimization if the relevant dimension of the hyperrectangle is reduced by the specified amount in the starter (aka first stage) optimization
nom_starter	0		0 - Use the FHyGSHP modifications to the DIRECT method, 1 - Do not use the FHyGSHP modifications to the DIRECT method in the starter (aka first stage) optimization
shrink_main	4		Number of times the function evaluation can increase before the optimization boundaries are reset in the main (aka second stage) optimization

D.2 Inputs: Heat Pump and Building Load Files

In cooling, the total heat pump capacity and power consumption are corrected for the dry and wet bulb temperature using the data in *interp stuff\cool.txt*. The default file contains data based on the gang-of-heat-pumps model mentioned in Chapter 2, but the user can modify this file if desired. The first row of data is the dry bulb temperature in °C and the second row is the wet bulb temperature in °C. Three columns of data start below the second row. The first column is the correction factor for the total cooling capacity, the second column is a correction factor for the sensible cooling capacity (unused by FHyGSHP), and the third column is a correction factor for the power consumption. In the default file, there are six values for the dry bulb temperature and five for the wet bulb temperature. The first five rows below the row of wet bulb temperatures are the correction factors for each of the five values of the wet bulb temperature and the first value of the dry bulb temperature. There are five additional sections below this first section. In FHyGSHP this data file is interpolated to obtain the correction factor for the actual dry and wet bulb temperature.

In heating, the heat pump capacity and power consumption are corrected for the dry bulb temperature by interpolating the data in *interp stuff\heat.txt*. In this file the first column is the dry bulb temperature, the second column is the correction factor for the heating capacity, and the third column is the correction factor for the power consumption in heating.

The building load file, examples of which are found in Building Loads, contains the cooling and heating load as well as the dry and wet bulb temperature for each hour of the year. The first column is the time of year in hours (TIME), ranging from 1 to 8760; the second column is the cooling load at each of those hours in kJ/hr (QCOOL); the third column is the heating load at each of those hours in kJ/hr (QHEAT); the fourth column is the dry bulb temperature at each hour in °C (TAMB); the fifth column is the wet bulb temperature at each hour in °C (TWB).

D.3 Results

When a single simulation is run the *results_day.txt* file, placed by default in the *results* folder, contains some of the summary results. The label associated with each result and the meaning of that label are listed in Table D-5.

Table D-5 Definition of the contents of the results_dat.txt file.

Label	Description
FUEL_COST	Integrated total fuel cost ($)
ANNUAL_FUEL	Annual fuel cost ($)
LCC2	Life cycle cost ($)
MIN_GCHX	Minimum temperature of the fluid entering the heat pump (°C)
MAX_GCHX	Maximum temperature of the fluid entering the heat pump (°C)
PUMP_POWER	Total circulating pump power (kW)
Pfan	Total cooling tower fan power consumption (kJ/hr)
Qct	Total cooling tower heat rejection (kJ/hr)
POW_SPRAY_KJHR	Total power consumption of the cooling tower spray pump (kJ/hr)
Qghx	Total heat rejection to the ground heat exchanger (kJ/hr); this value is negative if more heat is extracted from the ground than rejected to the ground
p_hp_int	Total heat pump power consumption (kW)
Q_REJ	Magnitude of the heat removed from the fluid loop at the heat pump to meet the heating load (kJ/hr). Calculated using mdot*cp*(Tout - Tin)
Q_ABS	Magnitude of the heat rejected to the fluid loop at the heat pump to meet the cooling load (kJ/hr)
GALLONS_WATER	Total water consumption of the cooling tower (gallons)
DRIFT_GPH_C	Total water consumption of the cooling tower associated with drift (gallons)
EVAP_GPH_C	Total water consumption of the cooling tower associated with evaporation (gallons)
BLOW_GPH_C	Total water consumption of the cooling tower associated with blow down (gallons)
ELEC_KW	total electrical power consumption (kW)
FIRST_GCHX	First cost of the GHX ($)
FIRST_CLOSED	First cost of the CT ($)
FIRST_COST	Total first cost ($)
MAINT_GCHX	Maintenance cost associated with the GHX (associated with maintaining the propylene glycol) ($)
MAINT_CLOSED	Maintenance cost associated with the CT ($)
COST_ELEC	Total cost of electricity ($)
EWT_PENALTY	A non-zero value indicates that the heat pump temperature constraint(s) has been violated ($)
COST_WATER	Total cost of water used by the CT ($)
COST_DEMAND	Total demand cost ($)
COST_MAINT	Total maintenance cost ($)
PD_TOT	Estimate of the pressure drop in the system
TOTAL_ENERGY_kJ	Total electrical energy consumption (kJ)
TOTAL_LENGTH_m	GHX length (m)
Size_Tower_kW	Cooling tower size (kW)
CT1	CT set point CT1 (°C)
CT2	CT set point CT2 (°C)
GHX1	GHX set point GHX1 (°C)
TPC	Pre-cooling set point TPC (°C)
DTPC	Pre-cooling set point DTPC (°C)

Label	Description
Temp_AnnChange	Annual ground temperature change, calculated as the overall ground temperature change divided by the length of the simulation (°C)
Storagevolume	Volume of the ground heat exchanger, calculated as (0.525*borehole spacing)^2*pi*depth*#
num	Number of boreholes
Total_PC	Total number of hours of PC operation (hours)
Imbalance_pen	Value of the penalty applied if the ground temperature change is outside a specified range; only used if Penalty: ground load imbalance is selected ($)
Cost_Gas	Total cost of natural gas ($)
Qf_cap	Furnace capacity (kBTU/hr)
GHX_temp_change	Total change in the average GHX temperature over the total simulation length (°C)
qghx_ratio	Ratio of the total cooling load on the ground to the total heating load on the ground
Source_elec	Total source natural gas energy consumption (using a site to source factor of 1.047) (kJ)
Source_gas	Total source electrical energy consumption (using a site to source factor of 3.34) (kJ)
Source_total	Total source energy (kJ)
energy_pen	Value of the penalty applied if the energy consumption is not reduced relative to the conventional system by the specified amount ($)
furnace_tot(kJ/hr)	Total heating load met by the furnace (kJ/hr)
ghx_tot(kJ/hr)	Total heating load met by the GHX (kJ/hr)

Appendix E Getting Started with FHyGSHP

FHyGSHP can be used to determine the optimal design and operation of a cooling tower hybrid ground source heat pump (CT HyGSHP) for large, cooling dominated buildings (e.g., office buildings). This document provides instructions for FHyGSHP; more detail on the models used in the program can be found in the accompanying documentation located in the *help_documentation* directory.

E.1 Installation

The program, FHyGSHP.exe, and associated directories should be placed in C:\FHyGSHP in order to ensure that all files will be found by the program.

E.2 Basic Program Structure

Running the file FHyGSHP.exe opens the graphical user interface (GUI) for the program. All of the user inputs are entered into this program; when the program is run, these inputs are printed to five input files located in the *namelist_files* directory. These files are read by the program *C:\FHyGSHP\main_program\program_main\hygshp.exe*. Upon completion of a single simulation, the file *results_day.txt* is written, by default, to the directory *results* and contains a summary of the key results. During an optimization the file *optimization_summary.txt* is written to the *results* directory and contains information for each simulation run during the course of optimization. Additional optional files are written as described below.

E.3 Enter Simulation Parameters

Run the file FHyGSHP.exe. The Main Diagram Window (see Figure E-1) appears when the program is opened. Specify the system configuration being modeled in the upper portion of the screen. The Conventional system includes a cooling tower (CT) and furnace; the Ground Source Heat Pump (GSHP) system can include a ground heat exchanger and, if the box next to

Include a furnace is checked, a furnace. The inclusion of a furnace may be useful when the building heating loads exceed the cooling loads. The Cooling Tower Hybrid (CT HyGSHP) system includes a ground heat exchanger, a cooling tower, and, if the box next to *Include a furnace* is checked, a furnace. When a CT HyGSHP is modeled, the CT can be located either upstream or downstream of the ground heat exchanger. When a GSHP or CT HyGSHP is modeled, if the box next to *Compare to Conventional* is checked, then the selected system will be compared to a conventional system. If you wish to run the program in batch mode (see Appendix C for more information), check the box next to *Just print input files* in order to generate the input files read by the executable program.

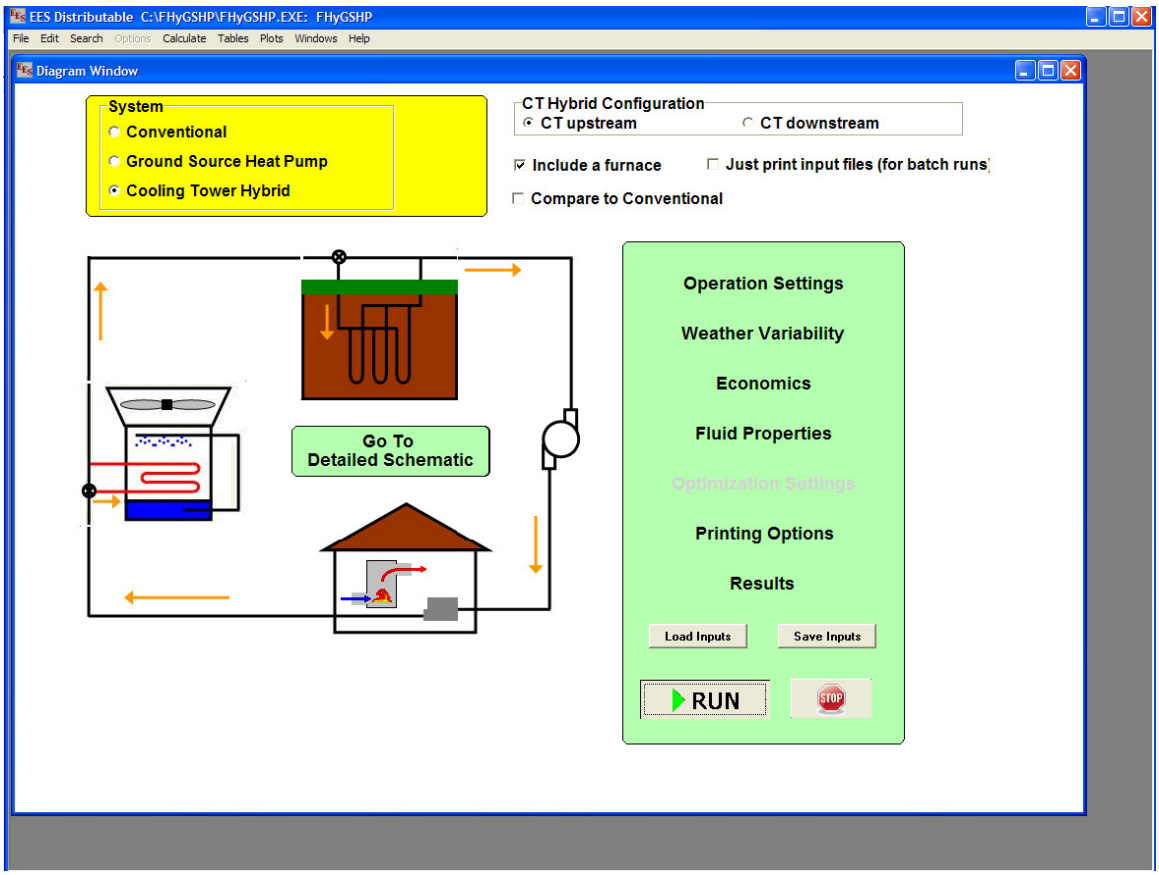

Figure E-1 Main Diagram Window.

Once the system to be modeled has been specified, click on the components in the cartoon to enter information about each component that is specific to your design. For example, if you click on the cartoon of the ground heat exchanger, the Ground Heat Exchanger Inputs screen (see Figure E-2) will appear and you can enter design information such as the drilling depth and borehole spacing as well as site specific information such as the thermal conductivity of the ground. Note that you can also access these windows by selecting Windows from the menu bar.

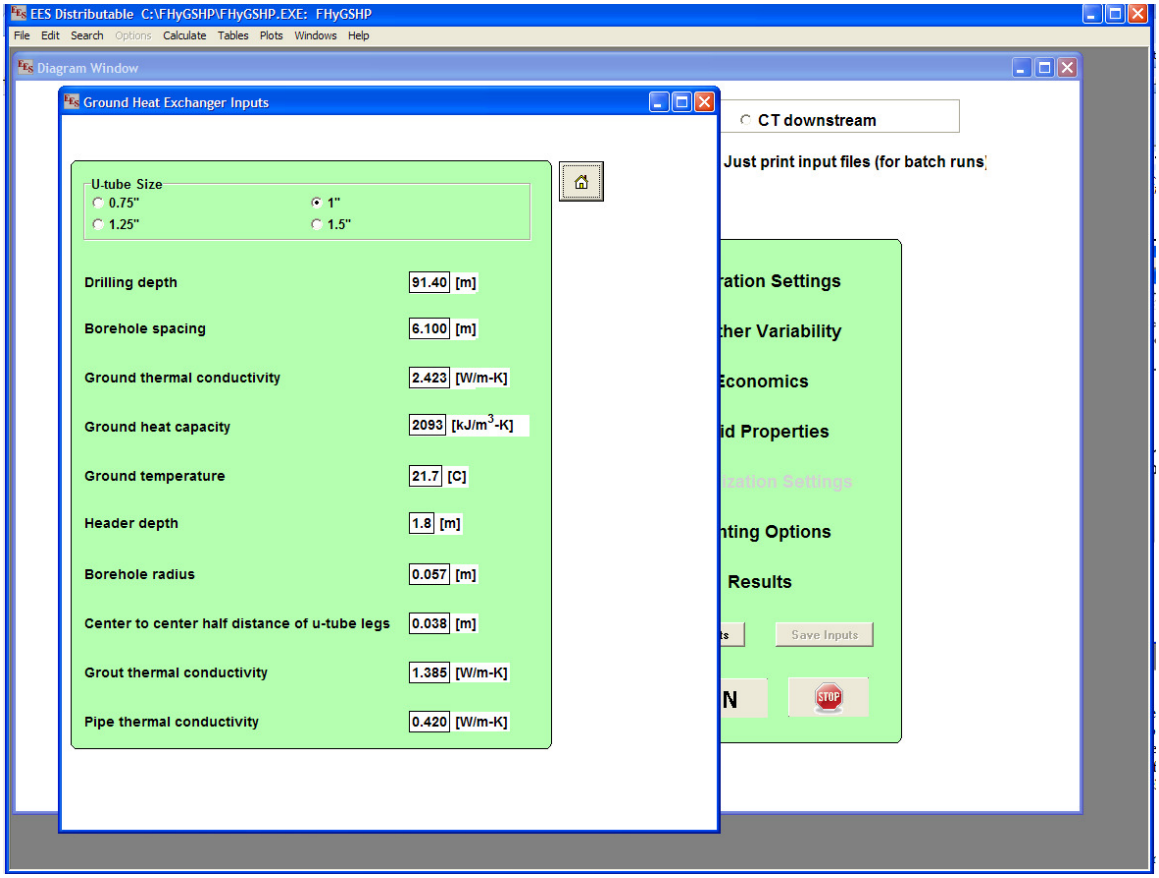

Figure E-2 Ground Heat Exchanger Inputs.

Click on Operation Settings to open Operation Settings (see Figure E-3). Click in the box next to *Select load file* to open a browser window and select the building load file. This file must have the same format as the example files provided in the *Building Loads* directory; each line of

the file contains the cooling and heating loads and dry and wet bulb temperatures for a single hour. By default, the file must contain 8760 hours, or a single year, of data, but multiple full years of data can be entered.

By default, output files are written to *C:\FHyGSHP\results*, but you can enter a different location. Most files written by the GUI or the executable program will be overwritten each time the program is run, so either move the files to a new location yourself or select a different directory to ensure that the data are saved. If the box next to *Optimization* is not checked, then a single simulation will be calculated for the duration specified. The known system design is entered in the box at the lower right.

If optimization is selected, then you can enter an initial guess for the design in this same space if the box next to *ASHRAE Sizing* is unchecked. If *Compare to Conventional* is checked in the *Main Diagram Window* and the conventional system design is know, it is entered in this space. When optimization is performed, a sensitivity map can be calculated and penalties can be added for the ground load imbalance and/or required reduction in energy consumption relative to a conventional system.

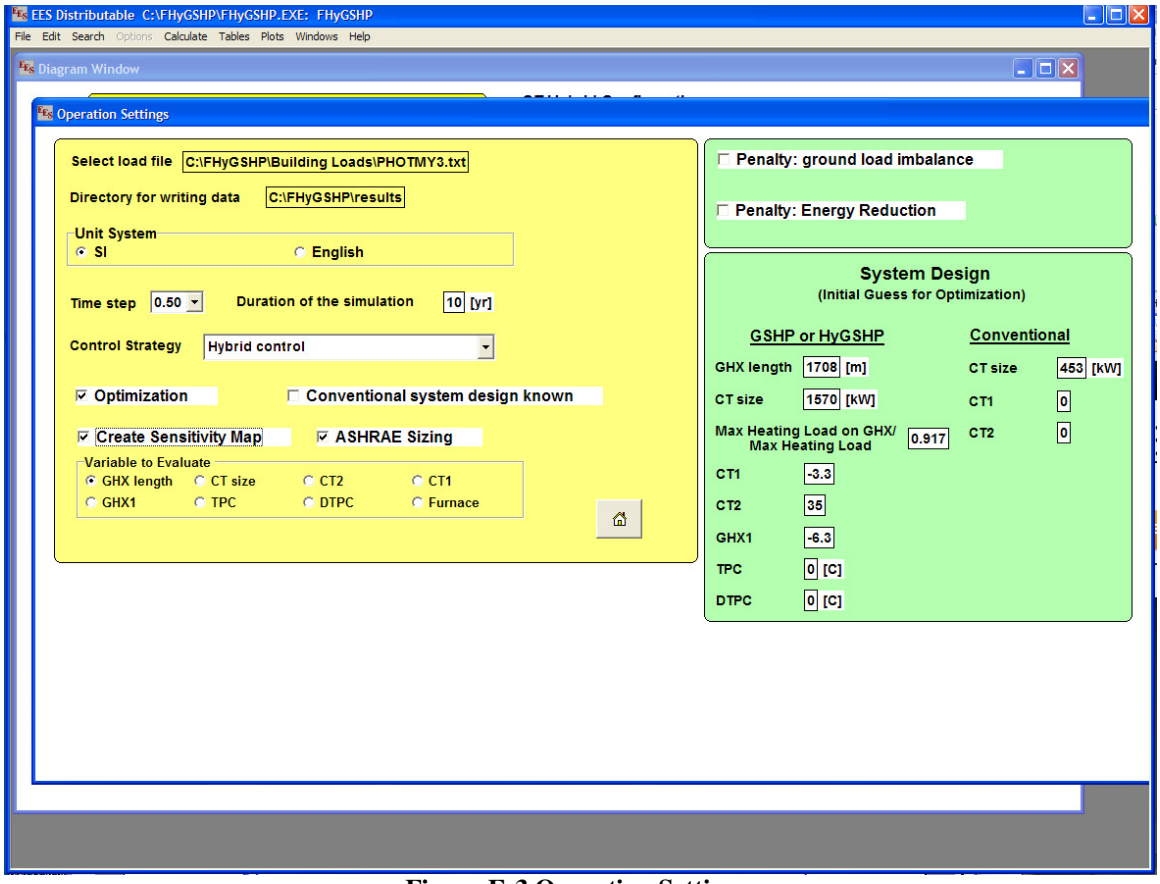

Figure E-3 Operation Settings.

By default, if the building load file contains a single year of data but you want to model multiple years, then the single year of data is repeated for each year of the simulation. If you want to generate synthetic data that mimic year-to-year weather variation, click on Weather Variability in the Main Diagram Window. The method for generating the synthetic data is described in detail in Chapter 5. The key to the method is a logistic probability distribution of the variation in the annual mean monthly dry bulb temperature. The mean and standard deviation of the distribution are 0.385 and 1.186, respectively, by default, but if you know statistical information about your local conditions, you can enter it in this window. You can also specify that the data be ordered randomly, from the year of greatest to least cooling load, or from the year of greatest to least heating load. This ordering can be performed on a multi-year input building load file as well as on the synthetic data.

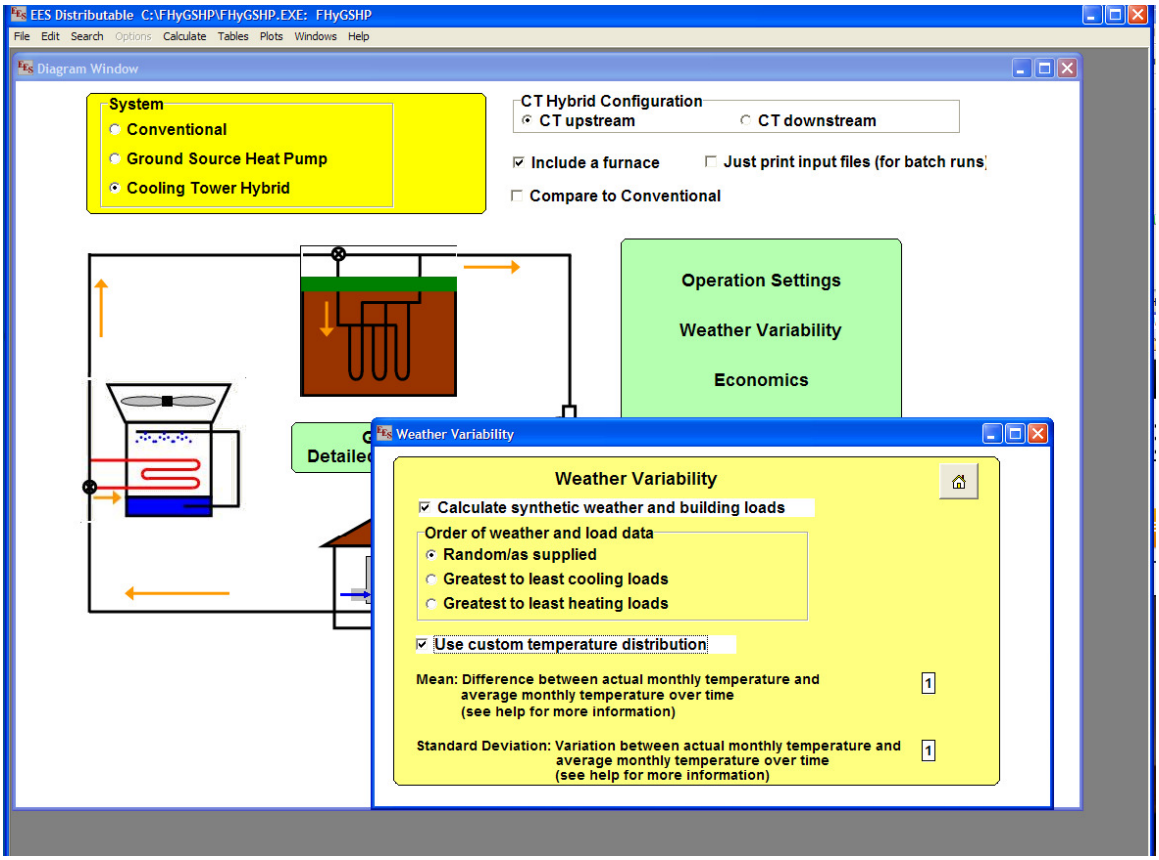

Figure E-4 Weather Variability.

Click on Economics in the Main Diagram Window to open Economic Values (see Figure E-5) and enter your local economic information.

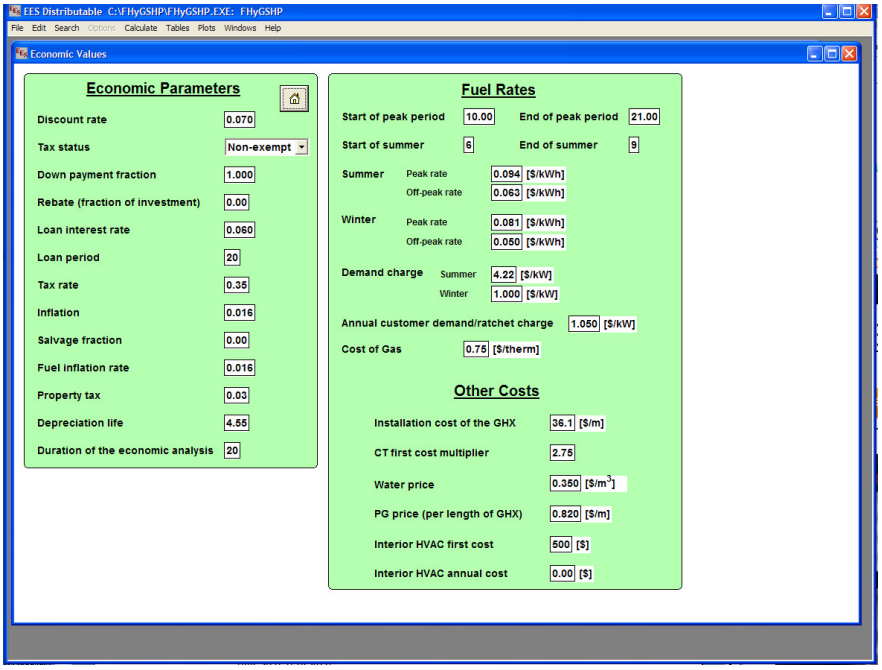

Figure E-5 Economic Values.

In some locations, the temperature of the fluid in the ground loop can drop below the freezing point of water, requiring the addition of propylene glycol to ensure that the fluid will not freeze. Click on Fluid Properties in the Main Diagram Window to open Fluid Properties (see Figure E-6). The fluid type is selected from the drop down menu next to *Fluid type* and can be either water or propylene glycol. If propylene glycol is selected, then the minimum loop temperature is required to calculate the amount of propylene glycol in the fluid.

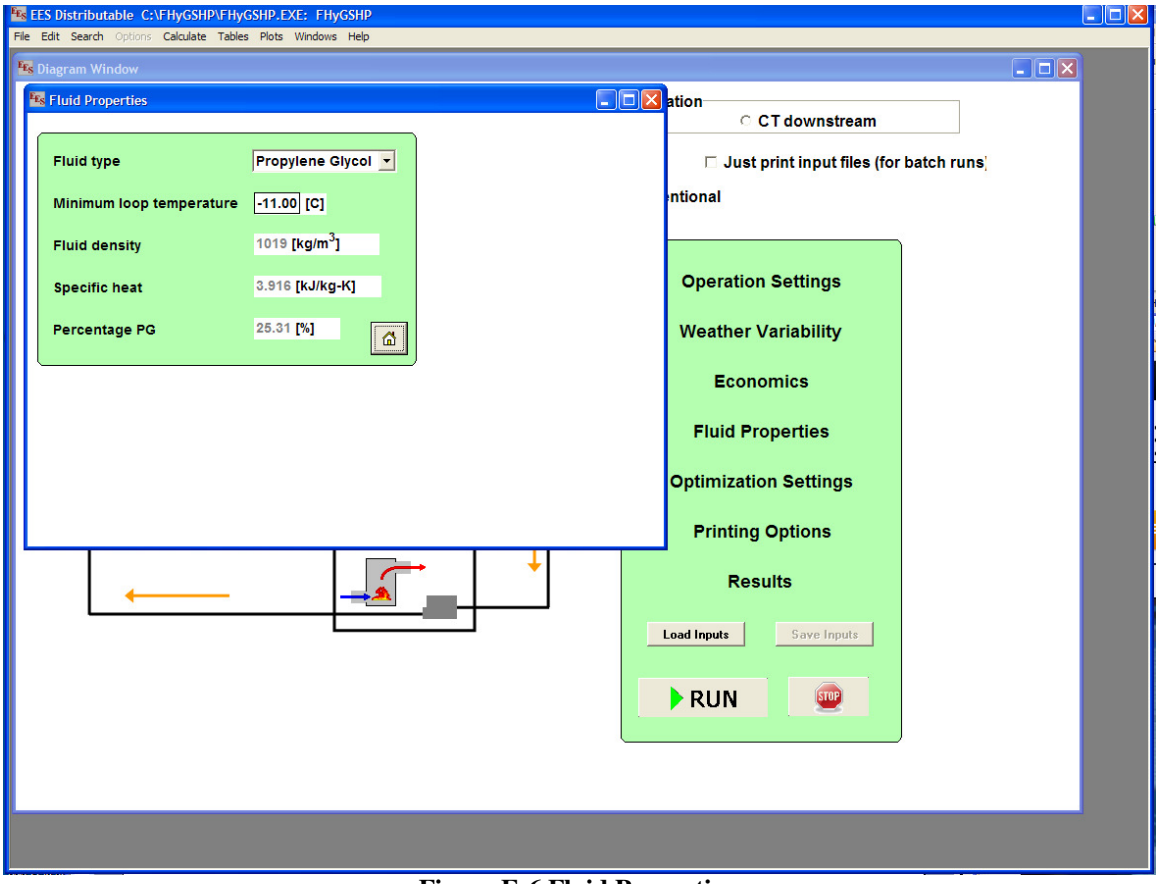

Figure E-6 Fluid Properties.

When performing an optimization, click on Optimization Settings in the Main Diagram Window to open Optimization Settings (see Figure E-7). More information about these settings can be found in the accompanying documentation; they should not be modified unless you are familiar with optimization concepts.

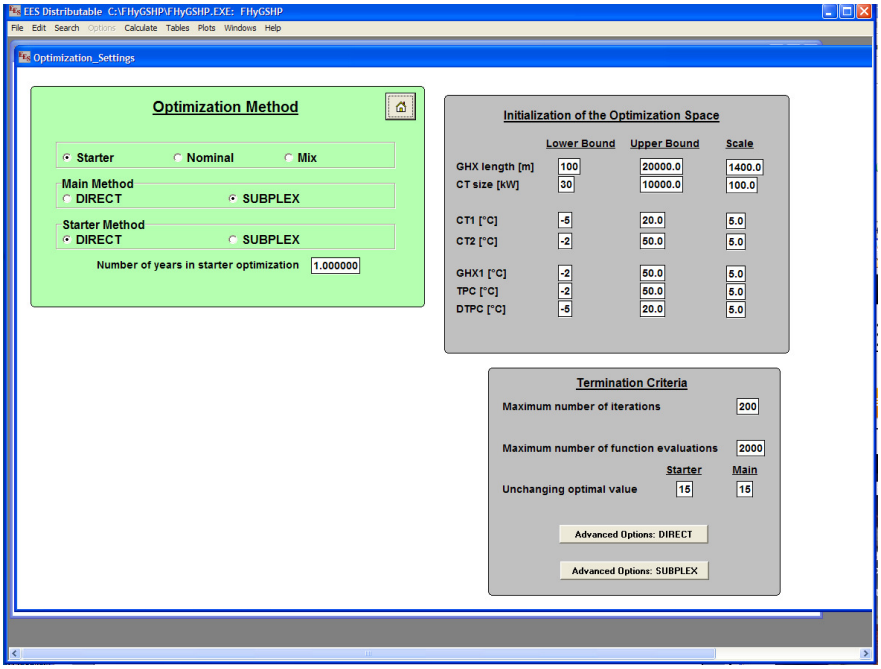

Figure E-7 Optimization Settings.

When a single simulation is run, some data can be printed at each time step of the simulation; these data can be selected by accessing Printing Options (see Figure E-8). All of the files are written by default to the *results* directory, but can also be written to the directory you specify in Operation Settings. *Temperature Data* are written to *temperature_summary.txt*; *Flow Rate Data* are written to *flow_rate_summary.txt*; *Power Consumption* are written to *power_summary.txt*; *Miscellaneous* are written to *misc_summary.txt*; and *Heat Transfer Data* are written to *heat_transfer_summary.txt*.

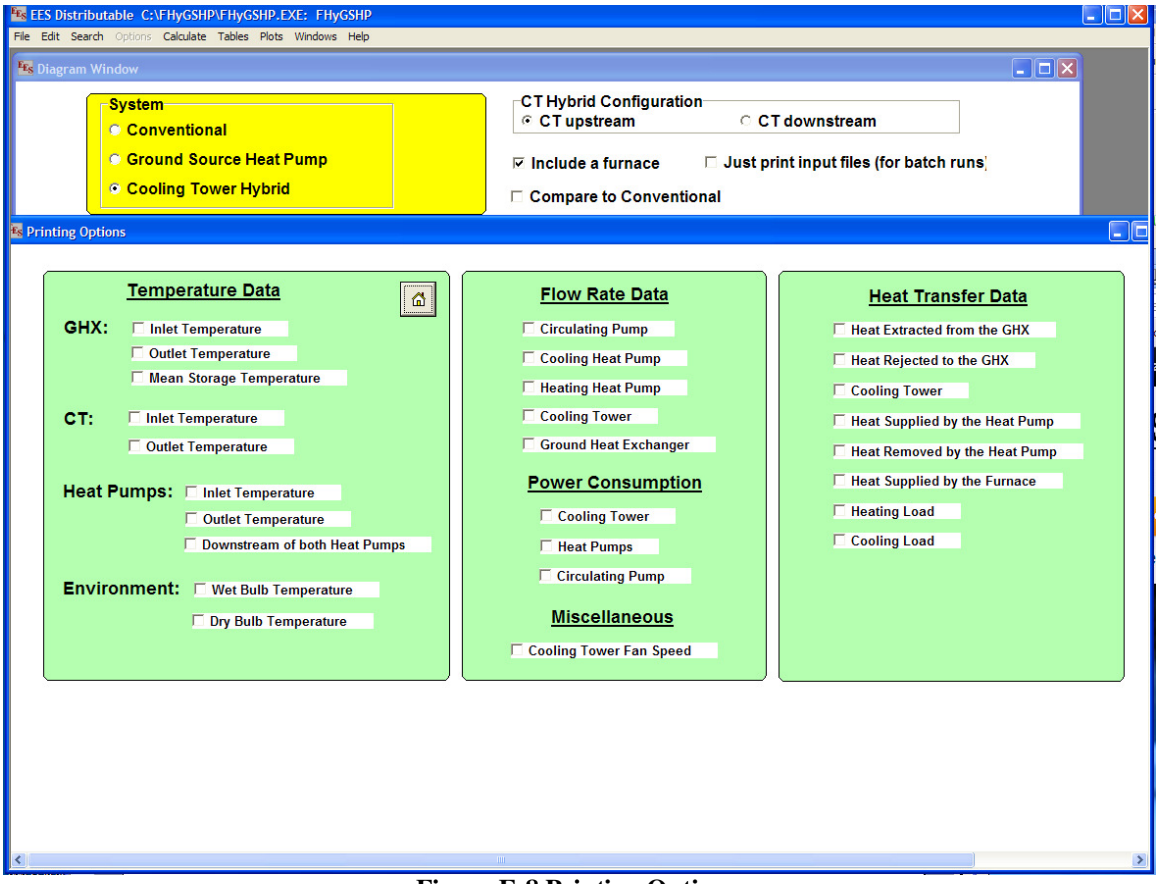

Figure E-8 Printing Options.

E.4 Run the Program

At the bottom right of the Main Diagram Window, there are buttons labeled *Load Inputs* and *Save Inputs*. The program comes with a file named *defaults.var* that contains default values for all of the inputs to the program; this file can be loaded using the *Load Inputs* button. You can save your own *.var* files using the *Save Inputs* button. This button is grayed out initially. Once you have successfully run the program, this button will be available. Another option to enable *Save Inputs* is to select *Calculate* in the menu bar and then *Solve*.

When you are ready to run the program, simply press the *Run* button. A command window will open so that you can view the progress of a single simulation or optimization. If you want to stop an optimization, press the *Stop* button. The program will stop once the current simulation run is complete. A pop up window will display the text *Invalid pointer operation.*;

you can dismiss this window. When an optimization is stopped early the *Save Inputs* button will be grayed out.

E.5 Post Processing

In the case of a single simulation, the following files are written to the *results* directory or the directory you specified in Operation Settings:

- Input files
    - *component_inputs.txt*
    - *direct_optim.txt*
    - *op_set.txt*
    - *optim_settings.txt*
    - *print_options.txt*
- Output files
    - *results_day.txt*
        - Summary results for the entire simulation duration
    - *temperature_summary.txt (optional)*
        - Temperature data printed at each time step
    - *flow_rate_summary.txt (optional)*
        - Flow rate data printed at each time step
    - *power_summary.txt (optional)*
        - Power consumption data printed at each time step
    - *misc_summary.txt (optional)*
        - Miscellaneous data printed at each time step
    - *heat_transfer_summary.txt (optional)*

        - Heat transfer data printed at each time step

In the case of optimization, the following files are written to the *results* directory or the directory you specified in Operation Settings:

- Input files
    - *component_inputs.txt*
    - *direct_optim.txt*
    - *op_set.txt*
    - *optim_settings.txt*
    - *print_options.txt*
- Output files
    - *results_day.txt*
        - Summary results for the entire simulation duration; for optimization this is generally not for the optimal design
    - *optimization_summary.txt*
        - System design and performance for each simulation run during optimization
    - *summary.txt*
        - Overall optimization summary
    - *subplex_main.txt* or *direct_main.txt*
        - Summary of the main or second stage optimization; subplex if the SUBPLEX algorithm is used, direct if the DIRECT algorithm is used.
    - *subplex_starter.txt* or *direct_starter.txt*

- Summary of the starter or first stage optimization; subplex if the SUBPLEX algorithm is used, direct if the DIRECT algorithm is used.

References

[1] Kavanaugh S., 1998, "A Design Method for Hybrid Ground-Source Heat Pumps," ASHRAE Transactions, **104**(2), pp. 691–698.

[2] Kavanaugh S., and Rafferty K., 1997, Design of Geothermal Systems for Commercial and Institutional Buildings, ASHRAE.

[3] ASHRAE, 1995, Commercial/Institutional Ground Source Heat Pumps Engineering Manual, Caneta Research, Inc., American Society of Heating, Refrigerating and Air-Conditioning Engineers, Inc.

[4] Hackel S., 2008, "Development of Design Guidelines for Hybrid Ground-Coupled Heat Pump Systems," University of Wisconsin - Madison.

[5] Phetteplace G., and Sullivan W., 1998, "Performance of a Hybrid Ground-Coupled Heat Pump system," ASHRAE Transactions, **104**(1B), pp. 763–770.

[6] Singh J. B., and Foster G., 1998, "Advantages of using the hybrid geothermal option," The Second Stockton International Geothermal Conference, The Richard Stockton College of New Jersey.

[7] Hackel S., and Pertzborn A., 2011, "Effective Design and Operation of Hybrid Ground-Source Heat Pumps; Three Case Studies," Energy and Buildings, **43**(12), pp. 3497–3504.

[8] Ramamoorthy M., Chiasson A. D., Spitler J. D., and D P., 2001, "Optimal Sizing of Hybrid Ground-Source Heat Pump Systems That Use a Cooling Pond as a Supplemental Heat Rejecter —," ASHRAE Transactions, **107**(2000), pp. 26–38.

[9] Li S., Yang W., and Zhang X., 2009, "Soil temperature distribution around a U-tube heat exchanger in a multi-function ground source heat pump system," Applied Thermal Engineering, **29**(17-18), pp. 3679–3686.

[10] Pertzborn A., Nellis G., and Klein S., 2011, "Impact of weather variation on ground-source heat pump design," HVAC&R Research, **17**(2), pp. 174–185.

[11] Hackel S., Nellis G. F., and Klein S. A., 2009, "Optimization of Cooling Dominated Hybrid Ground Coupled Heat Pump Systems RP#1384," ASHRAE Transactions, paper TRNS-00116-2008.

[12] F-Chart Software, 2012, "Engineering Equation Solver."

[13] Xu X., 2007, "Simulation and Optimal Control of Hybrid Ground Source Heat Pump Systems," Oklahoma State University.

[14] Trane, 2007, “High Efficiency Horizontal & Vertical Water Source Comfort System Axiom ™ 1 / 2 - 5 Tons — 60 Hz Model GEH / GEV,” (June).

[15] Klein S. A., Beckman W. A., Mitchell J. W., Duffie J. A., Thornton J. W., Mitchell J. C., Braun J. E., Evans B. L., Urban R. E., Williams P. M., Bradley D. E., and McDowell T. P., 2004, “TRNSYS, A Transient System Simulation Program, User’s Manual, Version 16.”

[16] TESS, 2004, “Type 510: Closed Circuit Cooling Tower.”

[17] Zweifel G., Dorer V., Koschenz M., and Weber A., 1995, “Building Energy and System Simulation Programs: Model Development, Coupling and Integration.”

[18] Baltimore Aircoil Company, “Closed Circuit Cooling Towers.”

[19] TESS, 2005, Hybrid Geothermal Heat Pumps at Fort Polk , Louisiana: Final Report to Oak Ridge National Laboratory for Subcontract #4000034426.

[20] Yang H., Cui P., and Fang Z., 2010, “Vertical-borehole ground-coupled heat pumps: A review of models and systems,” Applied Energy, **87**(1), pp. 16–27.

[21] Ingersoll L. R., and Plass H. J., 1948, “Theory of the Ground Pipe Heat Source for the Heat Pump,” Heating, Piping & Air Conditioning, (July), pp. 119–122.

[22] Ingersoll L. R., Zobel O. J., and Ingersoll A. C., 1954, Heat Conduction with Engineering, McGraw-Hill, New York.

[23] Zeng H. Y., Diao N. R., and Fang Z. H., 2002, “A finite line-source model for boreholes in geothermal heat exchangers,” Heat Transfer Asian Research, **31**(7), pp. 558–567.

[24] Zeng H., Diao N., and Fang Z. H., 2003, “Heat transfer analysis of boreholes in vertical ground heat exchangers,” International Journal of Heat and Mass Transfer, **46**(23), pp. 4467–4481.

[25] Bandos T. V., Montero Á., Fernández E., Santander J. L. G., Isidro J. M., Pérez J., Córdoba P. J. F. De, and Urchueguía J. F., 2009, “Finite line-source model for borehole heat exchangers: effect of vertical temperature variations,” Geothermics, **38**(2), pp. 263–270.

[26] Carslaw H. S., and Jaeger J. C., 1959, Conduction of Heat in Solids, Oxford University Press, London.

[27] Deerman J. D., and Kavanaugh S. P., 1991, “Simulation of Vertical U-Tube Ground-Coupled Heat Pump Systems Using the Cylindrical Heat Source Solution,” ASHRAE Transactions, **97**(1), pp. 287–295.

[28] Dobson M. K., O'Neal D. L., and Aldred W., 1995, "Modified Analytical Method for Simulating Cyclic Operation of Vertical U-Tube Ground-Coupled Heat Pumps," Proceedings of the 1995 ASME/JSME/JSES International Solar energy Conference, Maui, HI, pp. 69–76.

[29] Eskilson P., 1987, "Thermal Analysis of Heat Extraction Boreholes," Department of Mathematical Physics University of Lund, Sweden.

[30] Yavuzturk C., and Spitler J. D., 1999, "A Short Time Step Response Factor Model for Vertical Ground Loop Heat Exchangers," ASHRAE Transactions, **105**(2), pp. 475–485.

[31] Young T. R. A. Y., 2001, "Development, Verification and Design Analysis of the Borehole Fluid Thermal Mass Model for Approximating Short Term Borehole Thermal Response," Oklahoma State University.

[32] Bandyopadhyay G., Kulkarni M., and Mann M., 2008, "A New Approach to Modeling Ground Heat Exchangers in the Initiai Phase of Heat-Fiux Build Up," ASHRAE Transactions, **114**(2), pp. 428–439.

[33] Bandyopadhyay G., Gosnold W., and Mann M., 2008, "Analytical and semi-analytical solutions for short-time transient response of ground heat exchangers," Energy and Buildings, **40**(10), pp. 1816–1824.

[34] Bernier M. A., Pinel P., Labib R., and Paillot R., 2004, "A multiple load aggregation algorithm for annual hourly simulations of GCHP systems," HVAC&R Research, **10**(4), pp. 471–488.

[35] Mei V. C., and Fischer S. K., 1984, A Theoretical and Experimental Analysis of Vertical, Concentric-Tube Ground-Coupled Heat Exchangers, Oak Ridge Tennessee.

[36] Mei V. C., and Baxter V. D., 1986, "Performance of a Ground-Coupled Heat Pump with Multiple Dissimilar U-Tube Coils in Series," ASHRAE Transactions, **92**(2), pp. 30–42.

[37] Bi Y., Chen L., and Wu C., 2002, "Ground Heat Exchanger Temperature Distribution Analysis and Experimental Verification," Applied Thermal Engineering, **22**(2), pp. 183–189.

[38] Rottmayer S. P., 1997, "Simulation of Ground Coupled Vertical U-Tube Heat Exchangers," University of Wisconsin - Madison.

[39] Muraya N. K., 1994, "Numerical Modeling of the Transient Thermal Interference of Vertical U-tube Heat Exchangers," Texas A&M University.

[40] Muraya N. K., O'Neal D. L., and Heffington W. M., 1996, "Thermal Interference of Adjacent Legs in a Vertical U-Tube Heat Exchanger for a Ground-Coupled Heat Pump," ASHRAE Transactions, **102**(2), pp. 12–21.

[41] Kohl T., and Hopkirk R. J., 1995, "FRACTure - A Simulation Code for Forced Fluid Flow and Transport in Fractured, Porous Rock," Geothermics, **24**(3), pp. 333–343.

[42] Kohl T., Brenni R., and Eugster W., 2002, "System performance of a deep borehole heat exchanger," Geothermics, **31**(6), pp. 687–708.

[43] Signorelli S., Kohl T., and Rybach L., 2004, "Sustainability of production from borehole heat exchanger fields," Twenty-ninth Workshop on Geothermal Reservoir Engineering, Stanford University, Stanford, CA, January 26-28,2004, Stanford, CA.

[44] Al-Khoury R., Bonnier P. G., and Brinkgreve R. B. J., 2005, "Efficient finite element formulation for geothermal heating systems. Part I: steady state," International Journal for Numerical Methods in Engineering, **63**(7), pp. 988–1013.

[45] Cui P., Yang H., and Fang Z., 2008, "Numerical analysis and experimental validation of heat transfer in ground heat exchangers in alternative operation modes," Energy and Buildings, **40**(6), pp. 1060–1066.

[46] Hellström G., 1989, Duct Ground Heat Storage Model: Manual for Computer Code, Department of Mathematical Physics University of Lund, Sweden.

[47] Shonder J. A., Baxter V., Thornton J. W., and Hughes P. J., 1999, "A New Comparison of Vertical Ground Heat Exchanger Design Methods for Residential Applications," ASHRAE Transactions, **105**(2), pp. 1179–1188.

[48] Thornton J. W., McDowell T. P., and Hughes P. J., 1997, "Comparison of Practical Vertical Ground Heat Exchanger Sizing Methods to a Fort Polk Data/Model Benchmark," ASHRAE Transactions, **104**(1).

[49] Thornton J. W., McDowell T. P., Shonder J. A., Hughes P. J., Pahud D., and Hellstr G. A. J., 1997, "Residential Vertical Geothermal Heat Pump System Models: Calibration to Data," ASHRAE Transactions, **104**(1).

[50] Partenay V., Riederer P., Salque T., and Wurtz E., 2011, "The influence of the borehole short-time response on ground source heat pump system efficiency," Energy and Buildings, **43**(6), pp. 1280–1287.

[51] Spitler J. D., Cullin J., Bernier M. A., Kummert M., Cui P., Liu X., Lee E., and Fisher D., 2009, "Preliminary Intermodel Comparison of Ground Heat Exchanger Simulation Models," Proceedings of 11th International Conference on Thermal Energy Storage; Effstock 2009, Stockholm, Sweden, June 14-17.

[52] Shonder J. A., Hughes P. J., and Thornton J. W., 1998, "Using Calibrated Engineering Models to Predict Energy Savings in Large-Scale Geothermal Heat Pump Projects," ASHRAE Transactions: Symposia, pp. 944–954.

[53] Kavanaugh S. P., and Rafferty K., 1997, Ground Source Heat Pumps: Design of Geothermal Systems for Commercial and Institutional Buildings, American Society of Heating, Refrigerating and Air-Conditioning Engineers, Inc., Atlanta, GA.

[54] ASHRAE, 2009, ASHRAE handbook of fundamentals, Atlanta: American Society of Heating, Air-Conditioning and Refrigeration Engineers, Inc., Atlanta.

[55] Duffie J. A., and Beckman W. A., 2006, Solar Engineering of Thermal Processes, John Wiley & Sons.

[56] Rushing A. S., Kneifel J. D., and Lippiatt B. C., 2011, Energy Price Indices and Discount Factors for Life-Cycle Cost Analysis – 2011.

[57] Energy Center of Wisconsin, 2011, Hybrid Ground-Source Heat Pump Installations: Experiences, Improvements and Tools.

[58] R.S. Means Company, 2007, Mechanical Cost Data, R.S. Means Co.

[59] ASHRAE, 2011, 2011 ASHRAE Handbook - HVAC Applications.

[60] Yavuzturk C., and Spitler J. D., 2001, "Field Validation of a Short Time Step Model for Vertical Ground-Loop Heat Exchangers," ASHRAE Transactions, **107**(1), pp. 617–625.

[61] Xu X., and Spitler J., 2006, "Modeling of vertical ground loop heat exchangers with variable convective resistance and thermal mass of the fluid," Proceedings of the 10th International Conference on Thermal Energy Storage. Ecostock.

[62] Gentry J. E., Spitler J. D., Fisher D. E., and Xu X., 2006, "Simulation of Hybrid Ground Source Heat Pump Systems and Experimental Validation," 7th International Conference on System Simulation in Buildings, Liège, Belgium, December 11-13, 2006, Liege, Belgium, pp. 1–24.

[63] Hern S. A., 2004, Design of an Experimental Facility, Oklahoma State University.

[64] Sound Geothermal Corporation, 2006, "Formation Thermal Conductivity Test and Data Analysis."

[65] Witte H. J. L., 2013, "Error analysis of thermal response tests," Applied Energy.

[66] Geothermal Resource Technologies Inc., 2003, Formation Thermal Conductivity Test and Data Analysis.

[67] Rowan T., 1990, "Functional Stability Analysis of Numerical Algorithms," University of Texas at Austin.

[68] Jones D., Perttunen C., and Stuckman B., 1993, "Lipschitzian Optimization without the Lipschitz Constant," Journal of Optimization Theory and Application, **79**(1), pp. 157–181.

[69] Singer S., and Nelder J., 2009, "Nelder-Mead Algorithm," Scholarpedia, **4**(2), p. 2928.

[70] Finkel D. E., and Kelley C. T., 2004, Convergence analysis of the direct algorithm.

[71] Gablonsky J. M., 2001, DIRECT Version 2.0 User Guide. Technical Report CRSC-TR01-08., Raleigh, NC.

[72] Energy Center of Wisconsin, 2013, "Go Hybrid with HyGCHP."

[73] NREL, 2009, "National Solar Radiation Data Base, 1961-1990: Typical Meteorological Year 2."

[74] NREL, 2009, "National Solar Radiation Data Base, 1991-2005 Update."

[75] CDH Energy Corp. and Thermal Energy Systems Specialists (TESS), 2000, Development of Equivalent Full Load Heating and Cooling Hours for GCHPs Applied in Various Building Types and Locations, Final Report, ASHRAE 1120-TRP.

[76] Devroye L., 1986, Non-Uniform Random Variate Generation, Springer-Verlag, New York City.

[77] IPCC 2007, 2007, Climate Change 2007: The Physical Science Basis. Contribution of Working Group I to the Fourth Assessment Report of the Intergovernmental Panel on Climate Change., Cambridge University Press, Cambridge, UK and New York, NY.

[78] Yavuzturk C., and Spitler J. D., 2000, "Comparative Study of Operating and Control Strategies for Hybrid Ground-Source Heat Pump Systems Using a Short Time Step Simulation Model," ASHRAE Transactions, **106**(2), pp. 192–209.

[79] Yi M., Hongxing Y., and Zhaohong F., 2008, "Study on hybrid ground-coupled heat pump systems," Energy and Buildings, **40**(11), pp. 2028–2036.

[80] Fan R., Jiang Y., Yao Y., and Ma Z., 2008, "Theoretical study on the performance of an integrated ground-source heat pump system in a whole year," Energy, **33**(11), pp. 1671–1679.

[81] Pahud D., 2000, "Central solar heating plants with seasonal duct storage and short-term water storage: design guidelines obtained by dynamic system simulations," Solar Energy, **69**(6), pp. 495–509.

[82] McDowell T. P., and Thornton J. W., 2008, "SIMULATION AND MODEL CALIBRATION OF A LARGE-SCALE SOLAR SEASONAL STORAGE SYSTEM," SimBuild 2008, Third National Conference of IBPSA-USA, Berkeley, CA, pp. 174–181.

[83] Wong B., Snijders A., and McClung L., 2006, "Recent Inter-seasonal Underground Thermal Energy Storage Applications in Canada," 2006 IEEE EIC Climate Change Conference, pp. 1–7.

[84] Yavuzturk C., and Spitler J. D., 2000, "Comparative Study to Investigate Operating and Control Strategies for Hybrid Ground Source Heat Pump Systems Using a Short Time-step Simulation Model," ASHRAE Transactions, **106**(2), pp. 192–209.

[85] Jinggang W., Xiaoxia G., Zhenjiang Y., and Fang L., 2009, "Study of Operating Control Strategies for Hybrid Ground Source Heat Pump System with Supplemental Cooling Tower," 2009 IITA International Conference on Services Science, Management and Engineering, IEEE, pp. 507–510.

[86] Pardo N., Montero Á., Martos J., and Urchueguía J. F., 2010, "Optimization of hybrid – ground coupled and air source – heat pump systems in combination with thermal storage," Applied Thermal Engineering, **30**(8-9), pp. 1073–1077.

[87] Nellis G. F., and Klein S. A., 2008, Heat Transfer, Cambridge University Press.

[88] Baechler M. C., Willimanson J., Gilbride T., Cole P., Hefty M., and Love P. M., 2010, Guide to Determining Climate Regions by County.

[89] 2009, "Residential Prescriptive Requirements: 2009 International Energy Conservation Code."

[90] Kavanaugh S., 2008, "A 12-Step Method for Heat-Pump Design," ASHRAE Transactions.

[91] Kavanaugh S., 2010, "Ground Source Heat Pump System Designer, GshpCalc Version 5.0."

[92] Oklahoma State University, 2007, "GLHEPRO 4.0 for Windows Users' Guide."

[93] Cui P., Yang H., and Fang Z., 2007, "The Simulation Model and Design Optimization of Ground Source Heat Pump Systems," HKIE Transactions, **14**(1), pp. 1–5.

[94] Zeng H. Y., Diao N. R., and Fang Z. H., 2003, "Efficiency of vertical geothermal heat exchangers in ground source heat pump systems," Journal of Thermal Science, **12**(1), pp. 77 – 81.

[95] Energy Center of Wisconsin, 2013, "Go hybrid with HyGCHP."

[96] Klein S. A., 2012, "Engineering Equation Solver."

[97] TESS, 2004, "Type 557: Vertical Ground Heat Exchanger."

[98] Yavuzturk C., Chiasson A. D., and Nydahl J. E., 2009, "Simulation Model for Ground Loop Heat Exchangers," ASHRAE Transactions.

[99] US DOE EERE, 2013, "EnergyPlus Energy Simulation Software."

[100] 2013, "eQuest."

[101] 2013, "TRNSYS."

[102] Henderson H., Huang Y., and Parker D., 1999, "Residential equipment part-load curves for use in DOE-2," LBL Report, (February).

[103] Klein S., and Nellis G., 2011, Thermodynamics, Cambridge University Press, Cambridge, UK.

[104] Kelley C. T., 1999, Iterative Methods for Optimization, SIAM, Philadelphia.